COMBUSTION NOISE INVESTIGATION

D. C. Mathews, N. F. Rekos, Jr. and R. T. Nagel

FEBRUARY 1977

FINAL REPORT

Prepared for

DDC

U.S. DEPARTMENT OF TRANSPORTATION
FEDERAL AVIATION ADMINISTRATION
Systems Research & Development Service
Washington, D.C. 20590

APR 8 1977

D

NOTICE

Technical Report

1. Report No. FAA-RD-77-	2. Government Accession No.	3. Recipient's Catalog No.

4. Title and Subtitle	5. Report Date
COMBUSTION NOISE INVESTIGATION	February 1977
	6. Performing Organization Code

7. Author(s)	8. Performing Organization Report No.
D. C. Mathews, N. F. Rekos, Jr. and R. T. Nagel	PWA-5478

9. Performing Organization Name and Address	10. Work Unit No. (TRAIS)
Pratt & Whitney Aircraft Group United Technologies Corporation East Hartford, Connecticut 06108	
	11. Contract or Grant No. DOT-FA75WA-3663
	13. Type of Report and Period Covered

12. Sponsoring Agency Name and Address	
U. S. Department of Transportation Federal Aviation Administration Systems Research and Development Service Washington, D. C. 20591	Final Report
	14. Sponsoring Agency Code ARD-550

15. Supplementary Notes

16. Abstract

Improved methods for predicting both direct and indirect combustion noise from aircraft engines are developed and experimentally evaluated by conducting rig experiments and by comparing with data from several full scale engines. Comparison of predictions with full scale engine data indicate that direct combustion noise is the dominant source for the P&WA engines investigated.

The direct combustion noise prediction system includes expressions for acoustic power level, peak frequency and full-scale engine acoustic transmission loss due to combustor/duct coupling and turbine attenuation. These expressions are derived in terms of readily available performance and geometry parameters from the burner and turbine. New parameters introduced by the prediction system include the effects of fuel nozzle number and burner length. Predictions are shown to be in good agreement with data obtained from component rig tests on several JT8D type burner configurations (including single and multiple fuel nozzle, conventional and low emission designs). In addition, when transmission losses are accounted for, the predictions are also shown to be in good agreement with observed combustion noise levels and peak frequencies from four P&WA turbofan engines (i.e. the JT8D-109, JT9D-7A, JT9D-70 and the prototype JT10D). Predicted combustion noise directivity patterns and spectra shapes are determined empirically, using the data from both the rig tests and these four engines.

Results from the analytical and experimental combustion noise investigations are used to identify combustion noise reduction methods obtainable through modifications in burner design and/or performance parameters.

17. Key Words	18. Distribution Statement
Acoustics Combustion Noise Aircraft Noise Reduction Core Engine Noise Core Noise	Document is available to the U.S. public through the National Technical Information Service, Springfield, Virginia 22161.

| 19. Security Classif. (of this report)	20. Security Classif. (of this page)	21. No. of Pages	22. Price
Unclassified	Unclassified	204	

Form DOT F 1700.7 (8-72)   Reproduction of completed page authorized

METRIC CONVERSION FACTORS

Approximate Conversions to Metric Measures

Symbol	When You Know	Multiply by	To Find	Symbol
	LENGTH			
in	inches	*2.5	centimeters	cm
ft	feet	30	centimeters	cm
yd	yards	0.9	meters	m
mi	miles	1.6	kilometers	km
	AREA			
in²	square inches	6.5	square centimeters	cm²
ft²	square feet	0.09	square meters	m²
yd²	square yards	0.8	square meters	m²
mi²	square miles	2.6	square kilometers	km²
	acres	0.4	hectares	ha
	MASS (weight)			
oz	ounces	28	grams	g
lb	pounds	0.45	kilograms	kg
	short tons (2000 lb)	0.9	tonnes	t
	VOLUME			
tsp	teaspoons	5	milliliters	ml
Tbsp	tablespoons	15	milliliters	ml
fl oz	fluid ounces	30	milliliters	ml
c	cups	0.24	liters	l
pt	pints	0.47	liters	l
qt	quarts	0.95	liters	l
gal	gallons	3.8	liters	l
ft³	cubic feet	0.03	cubic meters	m³
yd³	cubic yards	0.76	cubic meters	m³
	TEMPERATURE (exact)			
°F	Fahrenheit temperature	5/9 (after subtracting 32)	Celsius temperature	°C

Approximate Conversions from Metric Measures

Symbol	When You Know	Multiply by	To Find	Symbol
	LENGTH			
mm	millimeters	0.04	inches	in
cm	centimeters	0.4	inches	in
m	meters	3.3	feet	ft
m	meters	1.1	yards	yd
km	kilometers	0.6	miles	mi
	AREA			
cm²	square centimeters	0.16	square inches	in²
m²	square meters	1.2	square yards	yd²
km²	square kilometers	0.4	square miles	mi²
ha	hectares (10,000 m²)	2.5	acres	
	MASS (weight)			
g	grams	0.035	ounces	oz
kg	kilograms	2.2	pounds	lb
t	tonnes (1000 kg)	1.1	short tons	
	VOLUME			
ml	milliliters	0.03	fluid ounces	fl oz
l	liters	2.1	pints	pt
l	liters	1.06	quarts	qt
l	liters	0.26	gallons	gal
m³	cubic meters	35	cubic feet	ft³
m³	cubic meters	1.3	cubic yards	yd³
	TEMPERATURE (exact)			
°C	Celsius temperature	9/5 (then add 32)	Fahrenheit temperature	°F

°F   -40   0   32   98.6   160   200   212
°C   -40   -20   0   20   37   40   60   80   100

*1 in = 2.54 (exactly). For other exact conversions and more detailed tables, see NBS Misc. Publ. 286. Units of Weights and Measures. Price $2.25. SD Catalog No. C13.10:286.

TABLE OF CONTENTS

TABLE OF CONTENTS (Cont'J)   Page

TABLE OF CONTENTS (Cont'd)

LIST OF ILLUSTRATIONS

LIST OF ILLUSTRATIONS (Cont'd)

LIST OF ILLUSTRATIONS (Cont'd)

LIST OF ILLUSTRATIONS (Cont'd)

LIST OF ILLUSTRATIONS (Cont'd)

LIST OF ILLUSTRATIONS (Cont'd)

LIST OF ILLUSTRATIONS (Cont'd)

LIST OF ILLUSTRATIONS (Cont'd)

LIST OF ILLUSTRATIONS (Cont'd)

LIST OF TABLES

LIST OF TABLES (Cont'd)

SUMMARY

The major objectives of the current FAA Combustion Noise Investigation (Contract No. DOT-FA75WA-3663) were to:

- Develop prediction procedures for both direct and indirect combustion noise that are applicable to conventional and low emissions burners (both annular and can-type) of the type designed by P&WA.

- Experimentally evaluate and improve these procedures by conducting appropriate rig tests and by comparing with data from full scale engines.

- Determine the dominant combustion noise mechanism (i.e., direct or indirect) for typical turbofan engines.

- Compare results with previous FAA data and predictions.

- Identify combustion noise reduction methods for future low emissions burners and engines under development.

An improved direct combustion noise prediction system was developed, in which expressions for acoustic power levels, peak frequencies, and turbine transmission losses were derived in terms of readily available performance and geometry parameters from the burner and turbine. New parameters introduced by the prediction system include the effects of fuel nozzle number and burner length. Predictions were found to be in good agreement with data obtained from component rig tests on six JT8D type burners, including four conventional burners with both single and multiple fuel nozzles; and two low emissions burners, one with an aerating fuel nozzle, and the other a two-stage burner for low NO_x emissions. The independent effects of fuel nozzle number, burner inlet temperature, pressure, flow parameter and fuel-air ratio were determined from these tests and found to be in excellent agreement with predictions.

To evaluate and improve the existing P&WA indirect combustion noise prediction model, dynamic temperature data at the exit of a JT8D burner were obtained, from which the temperature "hot-spot" amplitudes and length scales were determined and correlated in terms of burner operating parameters. It is the amplitude and size of these hot-spots, as they pass through the pressure drop of the turbine, that determine the characteristics of indirect combustion noise.

Predictions of both direct and indirect combustion noise were compared to combustion noise data from a full-scale JT8D-109 engine. From these comparisons, it was demonstrated that direct combustion noise (rather than indirect) is the dominant source for this engine.

Further comparisons of the new direct combustion noise predictions with data from four P&WA turbofan engines revealed that when turbine transmission losses are accounted for, all of the data from these engines and from the JT8D burner rig tests fit the direct combustion noise predictions with a standard deviation of 1.9 dB. In addition, the observed differences

in peak frequencies between engines (i.e., 280 Hz for the JT9D-7, 315 Hz for the JT9D-70, 450 Hz for the JT8D-109 and 500 Hz from the JT10D) were accurately predicted by the analytically developed peak frequency model. Predicted combustion noise directivity patterns and spectra shapes were obtained empirically, using measured data from the JT8D rig tests and from the above four P&WA turbofan engines.

When the combustion noise power levels measured from P&WA rigs and engines were compared to predictions reported by G. E. under previous contract to the FAA, significant differences were observed. The P&WA and G. E. predicted combustion noise directivity patterns were found to be in good agreement. Although the G. E. spectra are predicted to peak at 400 Hz for all engines, and while the P&WA procedure accounts for differences between engines, the predicted spectral shapes from both procedures are similar.

Results of the current analytical and experimental investigation were used to identify methods for reducing combustion noise from typical aircraft engines. Combustion noise reductions can be obtained by geometry and/or performance modifications as summarized below:

- Increase the number of fuel injection sources in the burner

- Increase the burner cross-sectional area in the reaction region

- Decrease the circumferential extent over which acoustic pressures are correlated at the combustor/turbine interface

- Stage the combustion process

- Decrease the burner inlet pressure

- Increase the burner inlet temperature

- Decrease the burner flow parameter (i.e., throughflow velocities)

- Decrease the burner fuel-air ratio

- Increase the turbine pressure ratio

It will only be through noise/cycle optimization studies that changes in performance parameters can be defined that will reduce combustion noise without sacrificing engine performance, durability, economy and pollutant emissions.

2

1.0 INTRODUCTION

1.1 BACKGROUND

Since the introduction of jet powerplants for commercial airplanes in the late 1950's, there has been a continuing effort by both industry and government agencies to develop the technology to design quieter propulsion systems. While the initial turbojets were jet noise dominated, the introduction of JT3D and JT8D low bypass ratio turbofans to the commercial fleet in the early 1960's gave relief in jet noise at takeoff powers, but introduced problems with fan noise at approach. The high bypass ratio engines introduced later in the 1960's such as the JT9D and CF6, incorporated advanced noise reduction design features which, together with acoustically treated nacelles, provided a further major reduction in aircraft noise.

The major in-flight noise sources from modern subsonic aircraft incorporating turbofan engines include fan noise, combustion noise, turbine noise, jet noise, and airframe noise as illustrated in Figure 1.1-1. The relative levels of these noise components are different depending on the basic engine type, its growth status, bypass ratio, effectiveness of acoustic treatment and noise reduction design features.. The importance of combustion noise relative to other noise sources depends on the particular engine being considered. The following discussion will first consider existing engines, and then advanced engines.
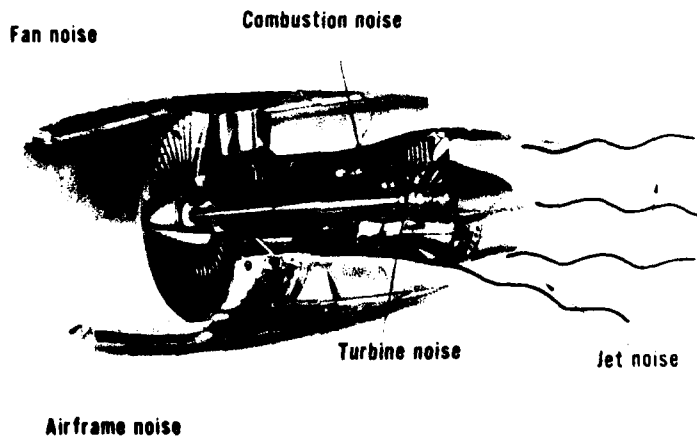
Figure 1.1-1   Aircraft/Engine Noise Sources

Several examples of the relative noise component levels for engines used in today's fleet are shown in Figures 1.1-2 through 1.1-4. These engines include the JT8D-15 (Figure 1.1-2), which is near the top of its growth capability; the JT9D-7 (Figure 1.1-3) installed in short duct nacelles; and the JT9D-70 growth engine in a long duct nacelle (Figure 1.1-4).

3
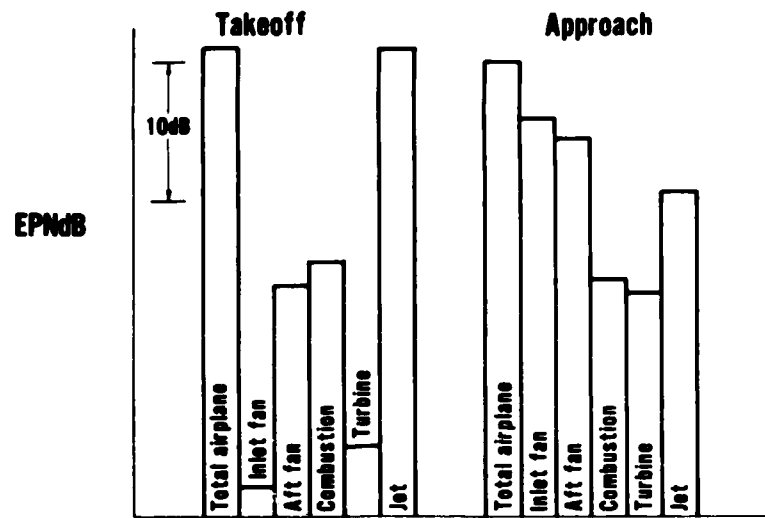
Figure 1.1-2   Noise Component Analysis for JT8D-15 Engine In Narrow-Bodied Aircraft
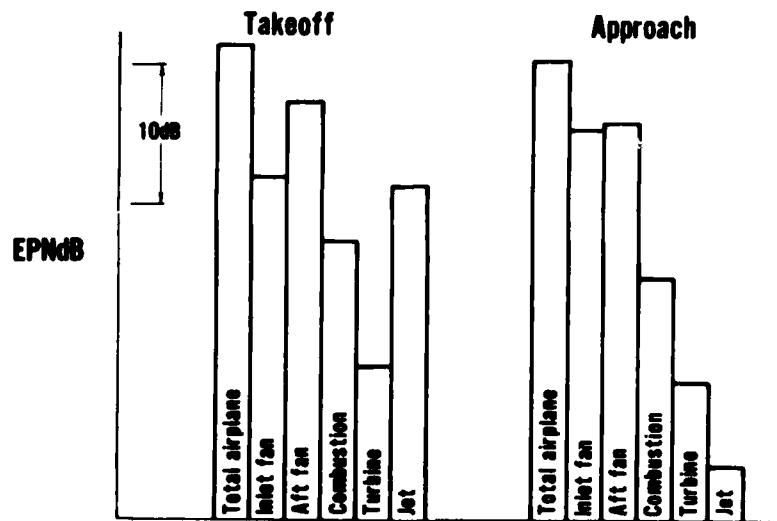
Figure 1.1-3   Noise Component Analysis for JT9D-7F Engine In Wide-Bodied Aircraft
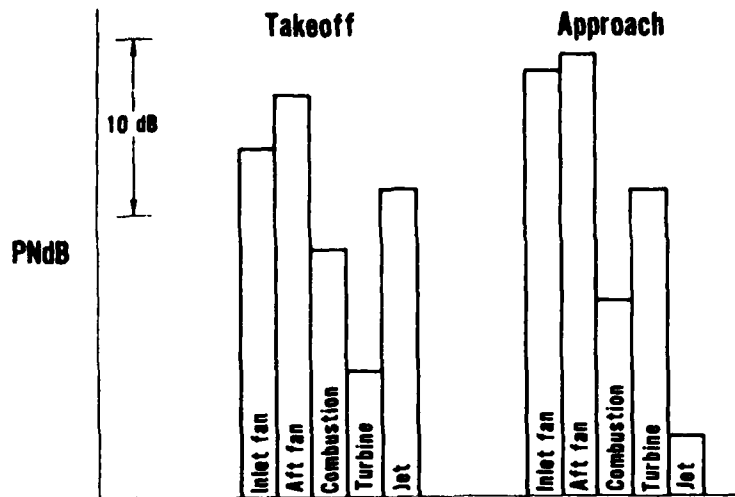
Figure 1.1-4   Noise Component Analysis for JT9D-70 Engine In Wide-Bodied Aircraft

The in-flight noise levels from the above engines are seen to be controlled by fan and jet noise components. Although the noise from aircraft powered by these engines meet existing federal noise regulations, more restrictive rules could require that noise from the fan and jet be reduced to the point where combustion noise reduction may be required.

In addition, anticipated emissions rules have led to burner designs that are quite different than those in current production. The impact of these design changes on combustion noise were explored under this contract, but needs to be defined further for other low emissions burners currently under development.

Examples of near term advanced P&WA engines which are expected to have combustion noise problems are the refan derivatives of the JT8D engine. These engines are an outgrowth of the NASA Refan Program. The JT8D-209 engine has been considered for use in the DC-9 and 727 aircraft and has predicted noise component levels as shown in Figure 1.1-5. Jet noise levels shown in this figure reflect the use of a forced mixer. Combustion noise at approach is higher than the jet noise. At the cutback and takeoff conditions, combustion noise is seen to be a major contributor to the total engine noise signature. In this engine, and particularly in growth versions of this engine, combustion noise reduction may be required to meet current noise regulations. More restrictive rules may require even more significant reductions in combustion noise from these engines. It was in view of this potential problem that measurements of combustion noise in the current investigation were concentrated on the JT8D burners and engine. An indication

of the influence of combustion noise on aircraft total noise for the JT8D-209 engine in a narrow-bodied aircraft is shown in Figure 1.1-6. At the cutback condition, for example, it may be seen that a 4 dB reduction in combustion noise results in a one dB reduction in aircraft total noise, and that an 8 dB increase in combustion noise would cause the total noise to increase by 4 dB. Some of the combustion noise reduction features defined in this investigation may well be applicable to future versions of the JT8D-200 series engines.
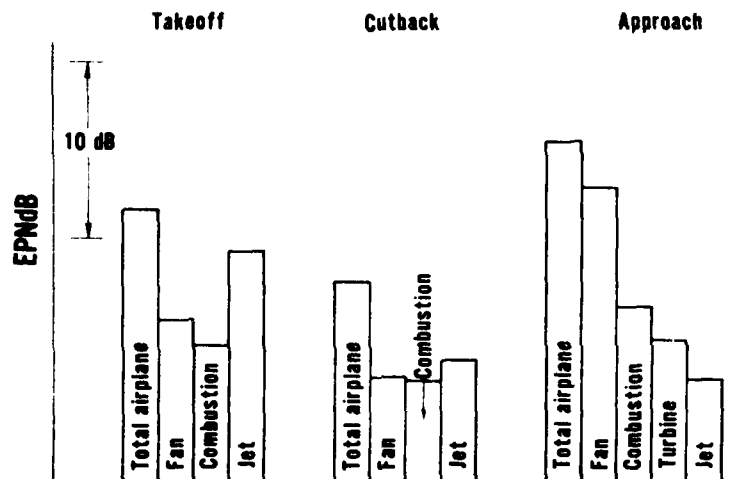
Figure 1.1-5   *Noise Component Analysis for JT8D-209 Engine In Narrow-Bodied Aircraft*
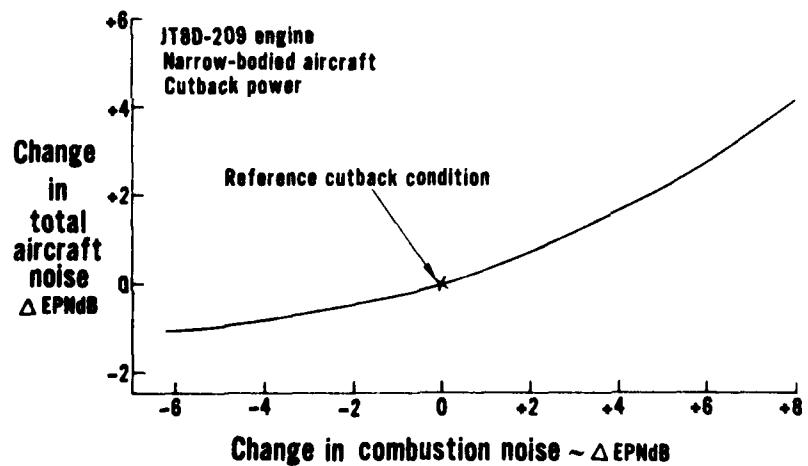
Figure 1.1-6   *Influence of Combustion Noise On Aircraft Total Noise*

6

1.2   DISCUSSION OF COMBUSTION NOISE PREDICTION STATUS

At the inception of this contract, it was generally believed that the dominant sources of what was commonly referred to as "core engine" noise[1] were associated with the combustion process[2, 3, 4, 5, 6] Recent studies[7] at Pratt & Whitney Aircraft, conducted on a JT8D-109 turbofan engine with a forced mixer installed to reduce jet noise, demonstrated (using signal cross-correlation techniques) that, over a wide range of engine operating conditions, a substantial portion of the low frequency noise measured in the farfield of the engine is generated by the combustor

Combustion noise is either of the "direct" type (i.e., resulting directly from the unsteady combustion) or of the "indirect type[8,9] which results from the convection of burner generated temperature fluctuations through the large pressure drop across the turbine. Although several procedures have been published for predicting levels of both types of noise, those for direct combustion noise are empirical in nature and have not adequately accounted for observed differences in noise levels and peak frequencies from different burner geometries. The procedures for predicting indirect combustion noise, in contrast, are purely theoretical in nature, but have not been experimentally evaluated. As a result, it has been very difficult to assess the importance of indirect, relative to direct combustion noise sources.

As part of an earlier FAA Core Engine Noise Control Program, contracted with the General Electric Company[2], burner rig tests were conducted to measure and evaluate combustion noise on burners designed for G. E. engines. Because of design philosophy differences between P&WA engine burners and the burners investigated in the earlier FAA core noise program, there was a need for specialized investigation of P&WA burner designs. Further, it was desired to determine whether the P&WA design changes being evaluated to meet emissions constraints would cause the combustion noise to change. Finally, there was a need to identify combustion noise reduction features that would be applicable to advanced P&WA low emissions burner designs and also to optimize the noise/emissions tradeoff.

Another area which must be considered in the prediction of combustion noise levels from actual engines is the transmission loss that occurs between the combustor and the engine farfield. Very little currently is known regarding the magnitude of these losses, but published estimates range from very small values to losses in excess of 40 decibels

As discussed above, several shortcomings exist in current procedures for predicting direct and indirect combustion noise levels, frequencies and transmission losses. It was these shortcomings, together with the need to investigate the effects of low emissions design features and the effects of differences in burner design criteria between various engine manufacurers, that motivated the current combustion noise investigation.

1.3   PROGRAM DESCRIPTION AND DOCUMENTATION

The current program, which was accomplished in two phases (the second of which contained four tasks) was aimed at developing both direct and indirect combustion noise prediction methods for P&WA's conventional and low emissions burners (both annular and can-type) and to experimentally evaluate and improve these models by conducting appropriate rig tests and by comparing with data from full scale engines. The major sections of this report are keyed to the Phase and Task titles, as described below:

● Phase I   Direct Combustion Noise   Section 2.0

● Phase II, Task I   Indirect Combustion Noise   Section 3.0

● Phase II, Task II - Engine Combustion Noise Investigation   Section 4.0

● Phase II, Task III   Comparison with Previous FAA Data   Section 5.0
                        and Predictions

● Phase II, Task IV   Combustion Noise Reduction   Section 6.0

● Conclusions   Section 7.0

A summary of the information reported in each major section is described in the following paragraphs.

Section 2.0 - Analytical models are developed for the prediction of direct combustion noise power levels and peak frequencies. A noise test program conducted on six P&WA JT8D type burners, including conventional and low emissions designs is described. The data from these tests are utilized to obtain a detailed verification of the analytical models. In addition, an investigation is described that was aimed at determining the feasibility of using optical techniques as a method for diagnosing potential combustion noise problems during the early burner development stages (details in Appendix C).

Section 3.0   A summary is presented of the existing P&WA indirect combustion noise prediction system, and a test program and apparatus is described (details in Appendix D) for obtaining detailed verification of the indirect combustion noise mechanism. Measurements of the dynamic temperature characteristics at the exit of a JT8D burner are presented, which are required as inputs to the P&WA indirect combustion noise prediction system. Correlations of these JT8D "hot-spot" characteristics are derived in terms of known burner operating parameters. These correlations are required in Section 4.0 to predict indirect combustion noise for the JT8D-109 engine.

8

Section 4.0 — Internal and farfield combustion noise data are presented for four P&WA turbofan engines. The internal data are used to demonstrate that combustion noise is the dominant source of core engine noise. In addition, the prediction systems for direct and indirect combustion noise, described in the preceding sections, are evaluated by comparing predicted values with these measured data. The dominant combustion noise mechanism is identified. Next an analytical model is presented for predicting the combustion noise transmission losses that occur across the turbine. This model is evaluated by comparing data from isolated burner rigs with combustion noise data from full scale engines. Finally, a summary is presented of the combustion noise prediction model, a sample application is discussed, and the parameters are identified that control combustion noise.

Section 5.0 — Combustion noise data from the JT8D burner component tests, and from four P&WA engines are compared to G.E. data and predictions obtained during the FAA Core Engine Noise Control Program[2]. Comparisons of combustion noise spectra, directivity patterns, and overall power levels are presented.

Section 6.0 — The combustion noise data and prediction system discussed in the preceding sections are utilized to identify combustion noise reduction methods for future low emissions engines. In addition, emissions data are presented for three of the conventional and low emissions JT8D type burners described in Section 2.0 and for the JT9D-7 engine. Finally, the optimization of the combustion noise/emissions tradeoff is discussed.

2.0 DIRECT COMBUSTION NOISE

2.1   BACKGROUND AND INTRODUCTION

Direct combustion noise, within the context of this report, is defined as the noise reaching a farfield observer that is generated directly by the unsteady turbulent combustion in a reacting region. Although many procedures for predicting direct combustion noise levels have been proposed in the literature and are summarized in recent surveys published by Strahle[10], Motsinger[11] and Huff[12], most methods are empirical and apply primarily to noise generated by open flames. In addition, the methods suggested for actual combustors fail to properly predict differences in noise levels from different conventional burner geometries, and none are capable of predicting the effects of low emissions burner design features on direct combustion noise characteristics.

Although much work has been directed toward the prediction of combustion noise levels, no procedure is currently available that explains the observed differences in combustion noise peak frequency from different burner geometries. As shown in Section 4.2, these frequencies, although nearly invarient for a given burner when operated over a wide range of conditions, have been observed to range between 280 Hz to 500 Hz, depending on the burner geometry.

To address these several shortcomings that exist in the current procedures for predicting combustion noise levels and peak frequencies, an improved procedure has been developed and is presented in this section, together with experimental verification of the method using rig data from both conventional and low emissions burner designs.

Elements of Direct Combustion Noise Prediction System

The development of the prediction system was divided into three parts; the formulation of analytical models for peak frequency and acoustic power level; the verification of these models; and the development of empirical spectra and directivity patterns. The elements of the prediction system are summarized briefly below and described in the remainder of this section.

1.   Peak Frequency Model   An expression for peak frequency is derived in this section and experimentally verified using farfield combustion noise data from conventional and low emissions burner rigs and from full scale engines (Section 4.0).

2.   Acoustic Power Level Model   Starting with the solution to the nonconvective wave equation presented by Strahale[10] for the farfield sound from open flames, an expression is derived for the acoustic power levels generated by engine type combustors, in terms of burner geometry and performance parameters. Variations in power level predicted by each term in the expression are verified independently using farfield combustion noise data from burner rigs (Section 2.3) and full scale engines (Section 4.0).

10

3. Combustion Noise Directivity — The combustion noise directivity pattern used in the prediction system is obtained empirically from farfield engine noise data. This is presented in Section 4.8.

4. Combustion Noise Spectral Shape — Although direct combustion noise peak frequencies vary with burner geometry, and are predicted by the peak frequency model, the spectral shape is determined empirically from JT8D burner rig data (Section 2.3) and verified using the engine data presented in Section 4.8.

Much of the work performed under the current contract in the area of direct combustion noise is summarized by Mathews and Rekos in Reference 13.

2.2   ANALYTICAL MODEL DEVELOPMENT

Representation of Reaction Region in a Burner

The reaction region inside a typical burner is approximated as shown in Figure 2.2-1. The fuel flow, w_f, is introduced through one or more fuel nozzles and the total airflow, w_{a_b}, is divided between that needed for the reactions, w_{a_r}, and that used as dilution air. The reaction length, L_r, is defined as the length of the region in which all the fuel is totally burned. In the actual reaction region, burning takes place in a highly turbulent, recirculating flow environment. Since an exact representation of this flow is not available, the reaction region is approximated by a region within which the flow thermodynamic properties are assumed to be spatially homogeneous. The reaction region, which will vary in size as the burner operating condition is changed, is also assumed to contain a fuel and air mixture that results in stoichiometric burning throughout. Thus, the following relationship exists between the reaction air and fuel flow rates:

$$w_{a_r} = \frac{w_f}{F_{ST}} \tag{1}$$

where F_{ST} is the stoichiometric fuel-air ratio. Remaining parameters required in the subsequent analytical model development include the burner fuel-air ratio, defined as

$$F_b = \frac{w_f}{w_{ab}} \tag{2}$$

the burner cross-sectional area, A_b, and burner length, L_b. With these definitions and assumptions regarding the reaction region, the analytical models for combustion noise peak frequency and acoustic power level may now be presented.

AIRFLOW INTO REACTION   TOTAL BURNER AIRFLOW, Wa$_b$
REGION, Wa$_r$

BURNER LINER

DILUTION AIR

STOICHIOMETRIC,
HOMOGENEOUS   CROSS-SECTIONAL AREA, A$_b$
REACTION REGION

TURBINE INLET

FUEL
FLOW

—REACTION LENGTH, L$_r$—

—BURNER LENGTH, L$_b$—
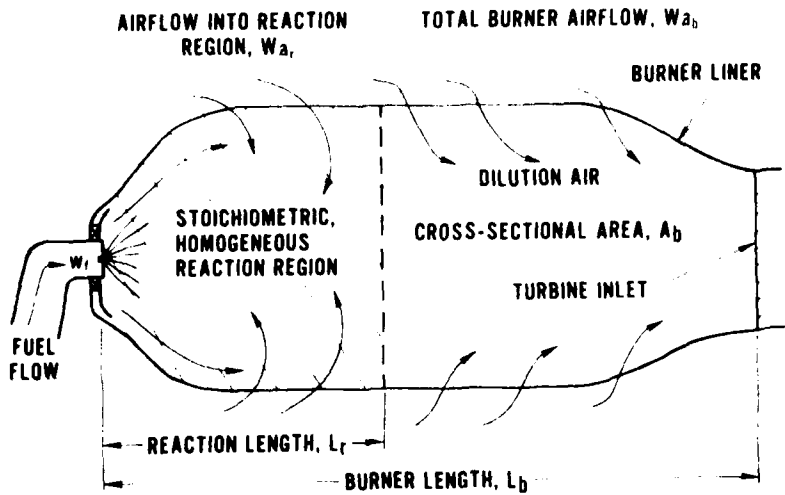
Figure 2.2-1   Representation of Reaction Region In a Burner

2.2.1   Peak Frequency Model

Since the chemistry within the reaction region of a given burner is assumed to
be invarient over all operating conditions (i.e., stoichiometric) the associated re-
action times are also assumed to be independent of the burner operating condi-
tion, and therefore invarient for a specific burner. If we characterize the burning
process by a typical reaction time scale, τ_r, then the peak frequency of combus-
tion noise (denoted by f_c) generated by these reactions should be inversely pro-
portional to the value of τ_r (e.g., shorter reaction times result in higher frequen-
cies). This may be expressed as follows:

$$f_c = \frac{C_1}{\tau_r} \qquad (3)$$

where C_1 is a constant, having the same value for all burners, and τ_r, as discussed
above, may be different for different burners but is not a function of operating
condition for a specific burner geometry. Thus the frequency predicted by Eq.
(3) is a function only of burner geometry and not of burner performance. The
validity of the assumptions leading to Eq. (3) is supported by the ovservations
of several investigators (References 1 through 5, 7) that for a specified burner, the
peak frequency of combustion generated noise remains essentially unchanged over
wide ranges of operating conditions. In addition, the observed peak frequencies
from different designs have been noted to vary from about 280 Hz to 500 Hz,
depending only on burner geometry.

12

A expression for the reaction time, τ_r, appearing in Eq. (3), is derived next. Since all reactions occur within the length L_r (defined in Figure 2.2-1), then a measure of the average time for these reactions to occur would be

$$\tau_r = \frac{L_r}{U_r} \qquad (4)$$

where U_r is the mean flow velocity through the reacting region. The reaction time given in Eq. (4) is the average time that the air and fuel reside in the reaction region. A typical value of this residence time was calculated for several actual combustors to be about .002 seconds, which is consistent with observed combustion noise frequencies in the 300 to 500 Hz range. The frequency, f_c, may now be expressed as

$$f_c = C_1 \frac{U_r}{L_r} \qquad (5)$$

The value of U_r at any operating condition can be described in terms of known parameters. Applying conservation of mass in the reaction region,

$$U_r = \frac{R \, w_{a_r} \, T_{ST}}{p_b \, A_b} \qquad (6)$$

where w_a is given by Eq. (1) p_b is the burner pressure, T_{ST} is the stoichiometric temperature, and R is the gas constant. Since burner liner pressure drops are usually quite small, the burner pressure, p_b, can be approximated by the burner inlet total pressure, p_{t_4}. In addition, from the energy equation, the stoichiometric temperature is

$$T_{ST} = T_{t4} (1 + \frac{H_f \, F_{ST}}{c_p \, T_{t4}}) \qquad (7)$$

Realizing that the second term in the brackets of Eq. (7) is much larger than unity for typical values of T_{t_4}, Eq. (5) may now be written

$$f_c = C_1 \frac{R H_f}{c_p \, A_b} \frac{w_f}{p_{t_4} L_r} \qquad (8)$$

13

Since, as shown earlier, f_c is not a function of burner operation, the last term in Eq. (8) must be a constant. Consider, then, a "reference" operating condition which is chosen as the design point for the burner (usually near the aircraft take-off condition). The peak frequency from Eq. (8) may now be written

$$f_c = C_1 \ \frac{RH_f}{c_p A_b} \left(\frac{w_f}{P_{t_4} L_r} \right)_{ref} \qquad (9)$$

It is next assumed that at the reference (or design) condition, the design philosophy for a given type of burner (e.g., can-type, annular, etc.) is such that the reaction length is a constant fraction of the burner length (i.e., longer burners of a given type have proportionally longer reaction regions, etc.). Thus,

$$(L_r)_{ref} = K_1 L_b \qquad (10)$$

where K_1 is a function only of burner type. Substituting Eq. (10) into (9) yields the final expression for combustion noise peak frequency

$$f_c = K_f \ \frac{RH_f}{c_p} \left(\frac{w_f}{P_{t_4}} \right)_{ref} \frac{1}{A_b L_b} \qquad (11)$$

where the proportionality constant K_f is given by

$$K_f = \frac{C_1}{K_1} \qquad (12)$$

and is dependent only on burner type (e.g. can-type, annular etc.).

It is interesting to note that for a given ratio of fuel flow to burner pressure at the reference condition, the frequencies predicted by Eq. (11) are inversely proportional to the burner volume, $A_b L_b$. Thus, for example, if engine design constraints resulted in a requirement for a shorter burner, keeping burner type and all other parameters constant, higher combustion noise frequencies should be expected.

The validity of Eq. (11) is demonstrated in Section 4.0, where the value of K_f is shown to be about 8 for several can-type burners and 3 for annular burners.

2.2.2 Acoustic Power Level Model

Published theoretical studies of combustion noise deal primarily with open turbulent flames. The theory developed by Chiu and Summerfield[14] represents a complete solution to the convected wave equation and expresses the farfield noise intensity as a sum of six terms, the relative magnitudes of which are highly dependent on flame characteristics and can be obtained only from carefully conducted experiments using sophisticated instrumentation techniques[15]. A simpler, approximate approach was adopted by Strahle [10], where convection terms were ignored. In typical aircraft type combustors, the axial flow Mach numbers through the reaction region are quite low, so the approach of Strahle appears to be adequate for this case. The Strahle model results in an expression for farfield noise from an open flame (source assumed to be compact) in terms of the volume integral of the time derivative of the heat release rate (volumetric) in the combustion region, i.e.,

$$p'(r, t) = \frac{\gamma - 1}{4\pi r c_\infty^2} \int_{V(\vec{r}_o)} \frac{\partial}{\partial t} \dot{Q}(\vec{r}_o, t - \frac{r}{c_\infty}) \, dV(\vec{r}_o) \qquad (13)$$

where r is the distance from the center of the reaction region to the observation point in the farfield, $\vec{r}_o$ is the vector from the center of the reaction region to the volume element, $dV(\vec{r}_o)$, and $\dot{Q}$ is the volumetric heat release rate.

If the source is correlated over a known volume, then $\partial\dot{Q}/\partial t$ is the same at all points within this volume and Eq. (13) can be written

$$p'(r, t) = \frac{\gamma - 1}{4\pi r c_\infty^2} \left(\frac{\partial \dot{Q}}{\partial t} \right)_{t - \frac{r}{c_\infty}} V_{corr} \qquad (14)$$

where V_{corr} is the volume of the correlated reaction region producing the noise. The acoustic power level from this source may be written

$$P = \frac{<p'^2>}{\rho_\infty c_\infty} (4\pi r^2) \qquad (15)$$

Upon substituting (14) into (15), the power becomes

$$P = \frac{(\gamma - 1)^2}{4\pi \rho_\infty c_\infty^5} < \left(\frac{\partial \dot{Q}}{\partial t} \right)^2 > V_{corr}^2 \qquad (16)$$

Consider now an array of N such sources, each independent and uncorrelated with all others. Then the total power from these sources is

$$P_{tot} = N \frac{(\gamma - 1)^2}{4\pi \rho_\infty c_\infty^5} < \left(\frac{\partial \dot{Q}}{\partial t}\right)^2 > V_{corr}^2 \qquad (17)$$

Considering the noise producing fluctuations in $\dot{Q}$ at the peak frequency of radiated noise, f_c, the mean square term in Eq. (17) can be represented as follows:

$$< \left(\frac{\partial \dot{Q}}{\partial t}\right)^2 > \propto f_c^2 < \dot{Q}'^2 > \qquad (18)$$

where $<\dot{Q}'^2>$ is the mean square amplitude of the fluctuations in $\dot{Q}$. The total power can now be written as

$$P_{tot} \propto \frac{(\gamma - 1)^2}{4\pi \rho_\infty c_\infty^5} N f_c^2 V_{corr}^2 < \dot{Q}'^2 > \qquad (19)$$

Eq. (19) is applicable to noise from open flames. Strahle[3] has derived the following expression, which relates the noise from a ducted source to that from an open source:

$$P_{duct} = \frac{P_{open}}{R_w} \qquad (20)$$

where R_w is given in Reference (3) as a function of frequency and the acoustic impedances of the burner liner walls and exit plane. Therefore, using Eqs. (19) and (20), the expression for combustion noise from N ducted sources in an engine burner may be written as:

$$P_{comb} \propto \frac{1}{R_w} \frac{(\gamma - 1)^2}{4\pi \rho_\infty c_\infty^5} N f_c^2 V_{corr}^2 < \dot{Q}'^2 > \qquad (21)$$

It is next assumed that in an actual combustor, the correlation volume, V_{corr}, is represented by the volume of the reaction region downstream of each fuel nozzle. Thus, the number of sources, N, is equal to the total number of fuel nozzles, N_f, in a given combustor and the correlation volume may be written as

$$V_{corr} = \frac{A_b L_r}{N_f} \qquad (22)$$

The combustion noise acoustic power is then

$$P_{comb} \propto \left[\frac{1}{R_w} \frac{(\gamma - 1)^2}{4\pi \rho_\infty c_\infty^5} \frac{1}{N_f} f_c^2 A_b^2 L_r^2 <\dot{Q}'^2> \right] \qquad (23)$$

From the general expression for peak frequency (i.e., from Eqs. (5), (6) and (7)), f_c maybe written as

$$f_c \propto \frac{R w_{ab} T_{t4}}{P_{t4} A_b L_r} \frac{F_b}{F_{ST}} \left(1 + \frac{H_f F_{ST}}{c_p T_{t4}} \right) \qquad (24)$$

Substituting Eq. (24) into (23) and rearranging in terms of independent burner performance and geometry parameters yields

$$P_{comb} \propto \left[\frac{(\gamma - 1)^2 R^2}{R_w 4\pi \rho_\infty c_\infty^5 F_{ST}^2} \frac{1}{N_f} A_b^2 P_{t4}^2 \left(\frac{w_{ab} \sqrt{T_{t4}}}{P_{t4} A_b} \right)^4 \right.$$

$$\left. \left(1 + \frac{H_f F_{ST}}{c_p T_{t4}} \right)^2 F_b^2 \left(\frac{<\dot{Q}'^2> A_b^2}{w_{ab}^2} \right) \right] \qquad (25)$$

The last term in Eq. (25) contains the mean fluctuation in volumetric heat release rate. It is assumed that this term is constant, i.e.,

$$\dot{Q}' \propto \frac{w_{ab}}{A_b} \qquad (26)$$

which requires that the fluctuating heat release rate (per unit volume) be proportional to the mean airflow (per unit area) through the burner. The validity of this assumption is examined in Section 2.4 where predictions from Eq. (25), using this assumption, are shown to agree with experimental data. Substituting Eq. (26) into (25) and combining all constant terms, yields the final expression for the combustion noise acoustic power.

$$P_{comb} = K_2 \left[\frac{1}{N_f} A_b^2 P_{t4}^2 \left(\frac{w_{ab} \sqrt{T_{t4}}}{P_{t4} A_b} \right)^4 \left(1 + \frac{H_f F_{ST}}{c_p T_{t4}} \right)^2 F_b^2 \right] \qquad (27)$$

where the proportionality constant K_2 may be a function of the fuel and oxidizer type, burner liner and exit impedances, and details of the burner geometry that

17

have not been accounted for specifically in the analysis. The value of this constant must be determined by experiment. The next two terms in Eq. (27) contain burner geometry information, including the predicted result that the combustion noise power is inversely proportional to the number of fuel injection sources (fuel nozzles) in the burner. The final four terms in Eq. (27) involve four independent burner performance parameters (i.e., the burner pressure, p_{t_4}, burner flow parameter, normalized burner inlet temperature, and the burner fuel-air ratio, F_b). Other performance parameters may be expressed in terms of these four independent parameters.

The acoustic power level, or OAPWL (in decibels) obtained from Eq. (27) may be written as

$$OAPWL = 10 \log \left[\frac{1}{N_f} A_b^2 p_{t_4}^2 \left(\frac{w_{ab} \sqrt{T_{t4}}}{p_{t_4} A_b} \right)^4 \left(1 + \frac{H_f F_{ST}}{c_p T_{t4}} \right)^2 F_b^2 \right]$$

$$+ K_3 \sim dB \quad (\text{ref. } 10^{-12} \text{ watts}) \tag{28}$$

where $K_3 = 10 \log K_3$, and must be determined from experiment. A detailed, term-by-term experimental verification of the predictions from Eq. (28) is presented in Section 2.4, where K_3 is shown to equal 131.3 for conventional burner designs, and 130.0 for an advanced low emissions burner design.

2.3   JT8D BURNER RIG TEST PROGRAM

The main objectives of the JT8D burner rig test program were to identify the important characteristics of direct combustion noise and to aid in the evaluation of the direct combustion noise analytical models presented in Section 2.2. The test program was conducted using six JT8D type burner configurations at the P&WA outdoor combustion noise facility. Descriptions of the various burners, the combustion noise facility and JT8D burner rig are presented in this section, together with a description of the test conditions, and a summary of internal and farfield noise test results. While the data presented in this section deal only with the internal and farfield acoustic test program results, other specialized test programs were conducted on selected burners (see Table 2.3-1), and are discussed in other sections of this report. Internal burner turbulence characteristics were obtained for three JT8D type burners (Table 2.3-1) and are discussed in Appendix A. Internal dynamic temperature characteristics, including "hot-spot" amplitudes and length scales for one JT8D-17 burner, were obtained in support of the indirect combustion noise investigation and are discussed in detail in Section 3.0.

18

TABLE 2.3-1

JT8D BURNER RIG TEST PROGRAM

Burner Configuration	Far-Field	Internal Kulites	Cold Flow Turbulence	Hot Spots QRTC'S
1. JT8D-17 Production	√	√	√	√
2. JT8D-17 Aerating (Pressure Atomizing Primary only)	√	√		
3. JT8D-17 Aerating (Aerating Secondary Only)	√	√	√	
4. JT8D-9 Production	√	√		
5. J52 Production (4 Fuel Nozzles)	√	√		
6. JT8D Vorbix (Advanced Low Emission Design)	√	√	√	

2.3.1 Burner Configurations

The following six JT8D type burner were selected to be tested at P&WA's outdoor combustion noise test facility (referred to as X-410 stand):

1. JT8D-17 production

2. JT8D-17 aerating (pressure atomizing fuel nozzle)

3. JT8D-17 aerating (aerating fuel nozzle)

4. JT8D-9 production

5. J52 production

6. JT8D-vorbix

The production JT8D-17 burner was selected as the baseline JT8D configuration. Testing of the JT8D-17 aerating burner permitted an investigation of the effect of fuel nozzle type (pressure atomizing versus aerating) on combustion noise. The J52 burner with four fuel nozzles was tested to evaluate the effect of multiple fuel nozzles on combustion noise. With the exception of fuel nozzle number, this burner is similar (length, diameter, etc.) to the single fuel nozzle JT8D burners. The advanced low emissions design JT8D-vorbix burner, a two-stage combustor, was selected to compare with conventional JT8D burner test results.

A photograph of the production JT8D-17 (baseline configuration for the JT8D burner tests) is presented in Figure 2.3-1, together with a photograph of the pressure atomizing fuel nozzle used with this burner.
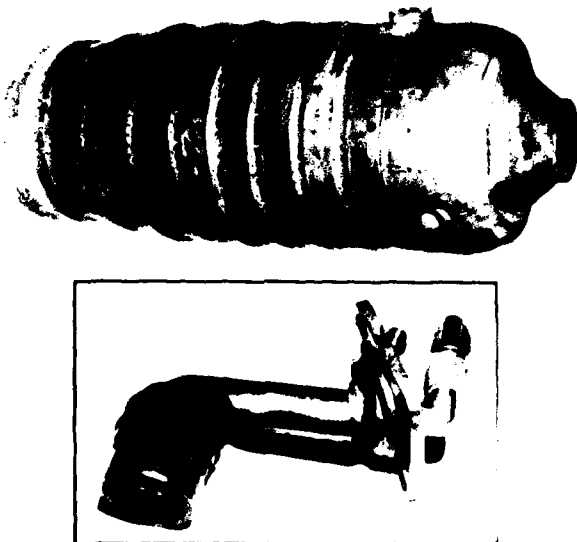
Figure 2.3-1   Production JT8D-17 Burner and Fuel Nozzle

A photograph of the JT8D-17 aerating burner with its aerating fuel nozzle is shown in Figure 2.3-2. The aerating fuel nozzle used for the noise tests at X-410 stand utilizes a pressure atomizing primary and a concentric aerating type secondary fuel system. By conducting noise tests separately on each fuel system, the effects of differences between aerating and pressure atomizing fuel nozzles could be determined without changing the burner geometry. The incorporation of this larger fuel nozzle required additional air to be introduced through the front of the burner, making it necessary for selected aft combustion holes to be reduced in area (relative to the JT8D-17 production burner) in order to maintain a constant total airflow through the burner.

20
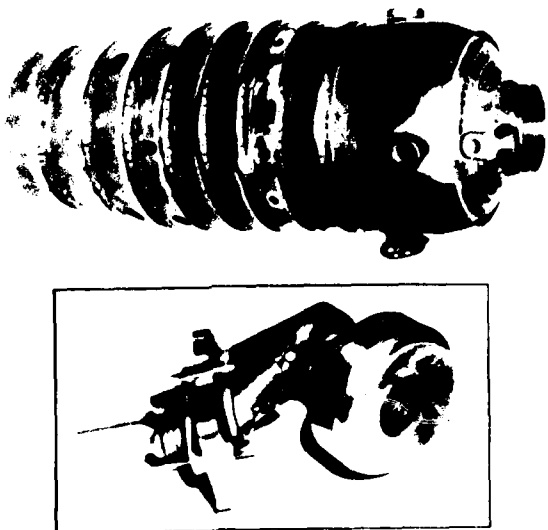
Figure 2.3-2   Low Emission Design JT8D-17 Aerating Burner and Fuel Nozzle

Photographs of the JT8D-9 burner with a pressure atomizing nozzle, and the J52 burner with its four manifolded fuel nozzles are shown in Figure 2.3-3 and 2.3-4, respectively.
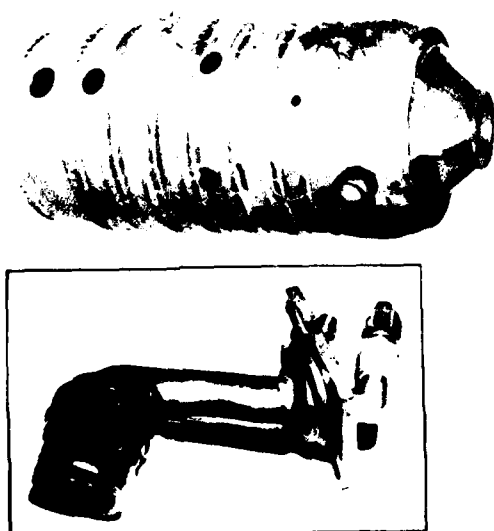
Figure 2.3-3   Production JT8D-9 Burner and Fuel Nozzle
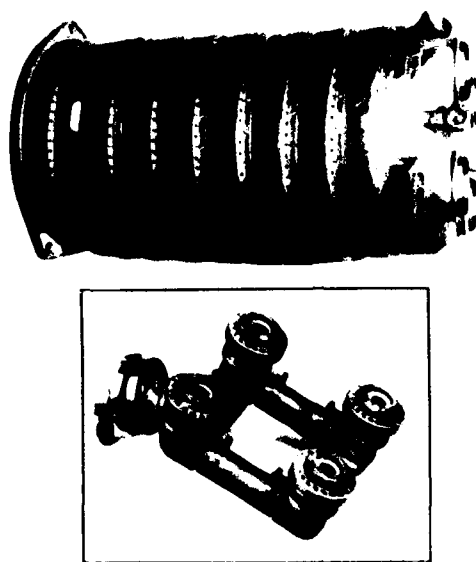
Figure 2.3-4   Production J52 Burner With Four Fuel Nozzles

The JT8D-vorbix burner is shown in Figure 2.3-5. The vorbix burner is an advanced low emissions design incorporating a two-stage fuel system. For low power operation, the fuel is introduced only into the pilot stage shown in Figure 2.3-6. At higher power conditions, additional fuel is injected through four pressure atomizing nozzles downstream of the pilot region, where the combustion air is introduced into this secondary combustion zone in the form of swirling high velocity jets.
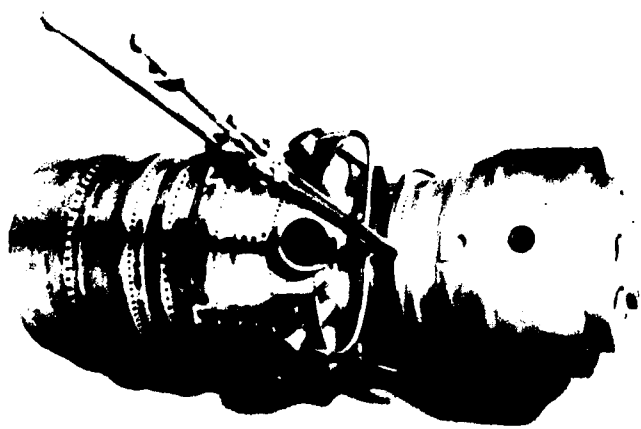
Figure 2.3-5   Advanced Low Emissions Design JT8D Vorbix Burner

22
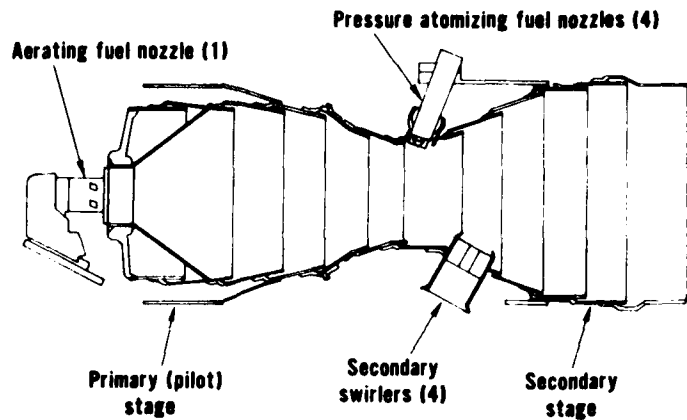
Figure 2.3-6   Two Stage JT8D Vorbix Burner

2.3.2   Outdoor Combustion Noise Test Facility

Noise and performance data for each JT8D type burner were obtained at X-410
stand, which is a facility constructed specifically for combustion noise investiga-
tions (see Figures 2.3-7 and 2.3-8). Combustion air is provided to the test burner
by two compressors. The air may be preheated to the desired burner inlet tempera-
ture by the heater burner mounted upstream of the test burner.
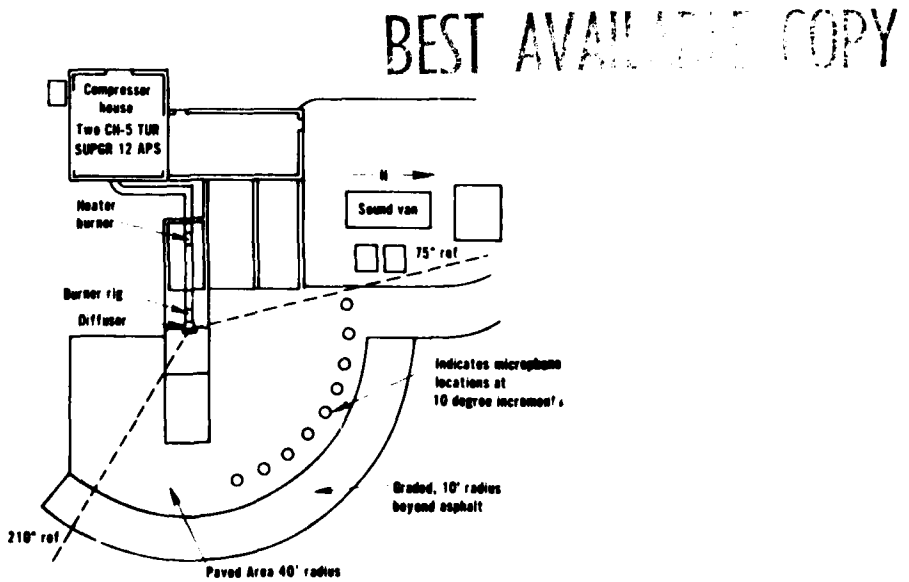
Figure 2.3-7   P&WA Outdoor Combustion Noise Facility, X-410 Stand

23

Figure 2.3-8   P&WA Outdoor Combustion Noise Facility, X-410 Stand

Farfield microphones were located at a radial distance of 35 feet from the JT8D burner rig exit at 10 degree increments between 80 and 160 degrees to the inlet axis. Noise data were obtained using microphones located ½-inch above a hard asphalt surface. A typical microphone installation is shown in Figure 2.3-9. Noise measurements obtained in this manner are free of low frequency spectral distortion caused by phase difference between direct and reflected sound waves. Six dB were subtracted from the measured noise levels to obtain an estimate of free-field levels.
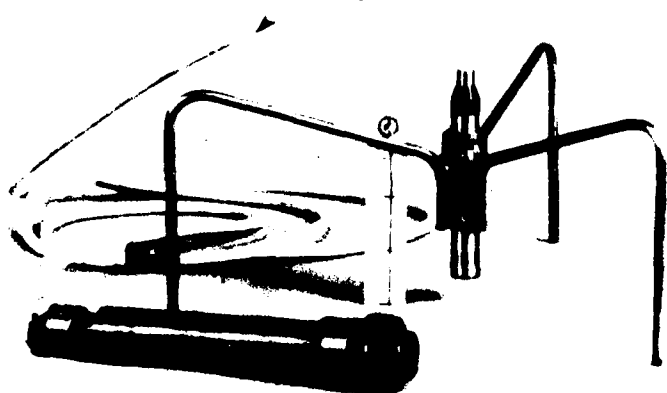
Figure 2.3-9   Farfield Microphone Installation At X-410 Stand

Ground plane farfield noise measurements were recorded in the range of 50 Hz to
10,000 Hz (low frequency noise from 50 Hz to 1000 Hz was the range of interest)
on a 14-channel magnetic tape recording - reproducing system (PI recorder) in the
FM mode providing flat response to 13 kHz. Amplification of the noise signal, before
recording, was made through two auxilliary 10 dB amplifiers and a standard P&WA
signal Amplifier and Attenuation box. A Hewlett Packard digital spectral analyzer
was utilized, in addition to the PI recording system, to obtain on-line spectral in-
formation.

2.3.3   JT8D Burner Rig

Each JT8D type burner was mounted in the rig shown in Figures 2.3-10 and
2.3-11. The rig simulated a 40 degree (one-ninth) annular segment of an actual
engine burner case, since only one can was being tested. At the burner exit loca-
tion, an annular-to-round transition section and a round diffuser were added to
minimize jet noise by maintaining jet velocities below 500 ft/sec at all operating
conditions. A close-up photograph of the rig with a JT8D burner installed is pre-
sented in Figure 2.3-12. A schematic of the burner rig showing the locations of
the JT8D burner and the various pressure and temperature probes and two water-
cooled Kulite transducers is presented in Figure 2.3-13.
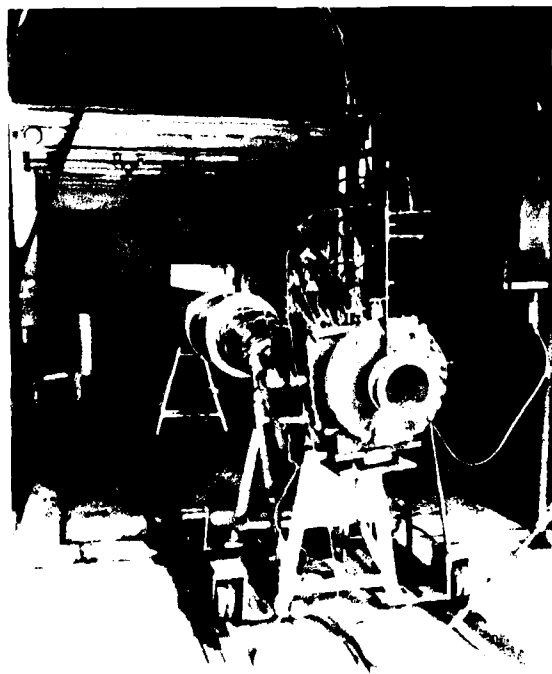
Figure 2.3-10   JT8D Burner Rig At X-410 Stand

25
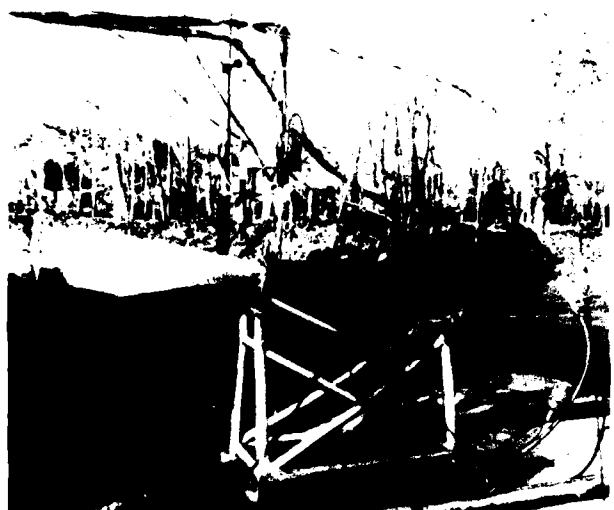
Figure 2.3-11   JT8D Burner Rig At X-410 Stand
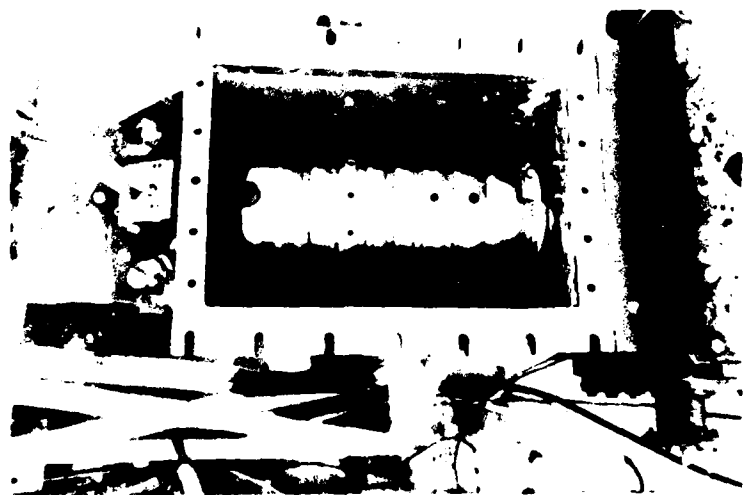
Figure 2.3-12   JT8D-17 Aerating Burner Can Installed In Burner Rig At X-410 Stand
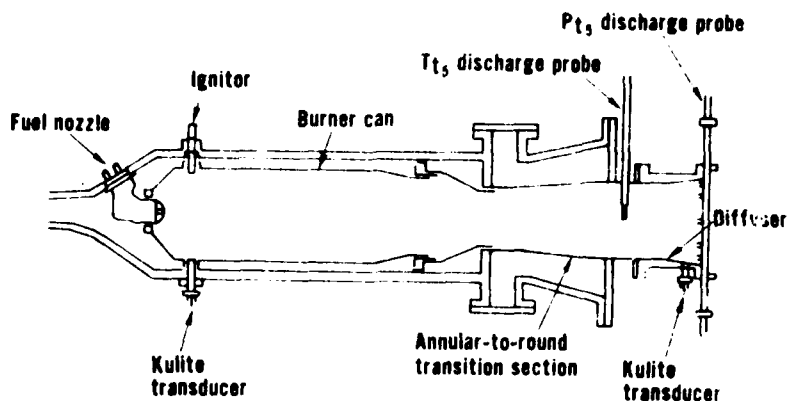
Figure 2.3-13 Schematic of JT8D Burner Rig

2.3.4 Test Conditions

Eighteen test conditions were selected for each burner to investigate the effect of independent variations in inlet temperature, fuel-air ratio, and burner flow parameter on combustion noise. All burner performance variables can be related to these three independent parameters and the burner pressure. Since the JT8D burner rig exhausts to atmosphere, burner pressures were limited to values which resulted in non-contaminating levels of jet noise. This limit precluded study of the effect of pressure on combustion noise generation. The eighteen point test matrix used in the program is shown in Figure 2.3-14 and includes simulated engine idle, approach, climb and takeoff conditions together with fourteen (14) off-design burner operating conditions were selected to determine the effects on noise of independent variations in the above parameters. The simulation is exact except for burner pressure levels, limited as discussed above.
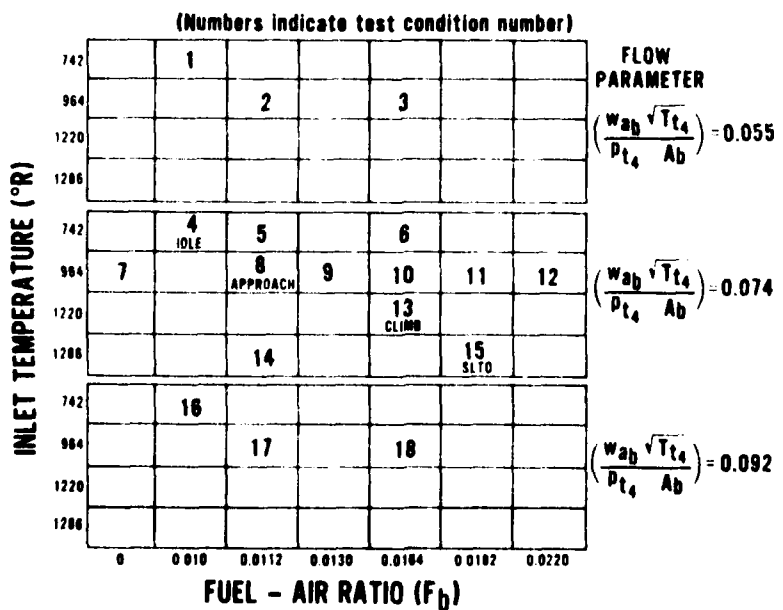
Figure 2.3-14 JT8D Burner Rig Test Matrix

An additional nine test conditions were run on the low emissions JT8D - vorbix burner to allow investigation of various primary/secondary fuel splits. Figure 2.3-15 shows the test matrix for this burner, where it may be seen that the fuel split ranged from 100% primary fuel at low fuel/air ratios to 20% primary/80% secondary at the simulated takeoff condition.

(Numbers represent primary/secondary fuel split)

INLET TEMPERATURE (°R) vs FUEL – AIR RATIO (F_b)

FLOW PARAMETER

$$\left(\frac{W_{ab}\sqrt{T_{t_4}}}{P_{t_4}\,A_b}\right) = 0.055$$

$$\left(\frac{W_{ab}\sqrt{T_{t_4}}}{P_{t_4}\,A_b}\right) = 0.074$$

$$\left(\frac{W_{ab}\sqrt{T_{t_4}}}{P_{t_4}\,A_b}\right) = 0.092$$
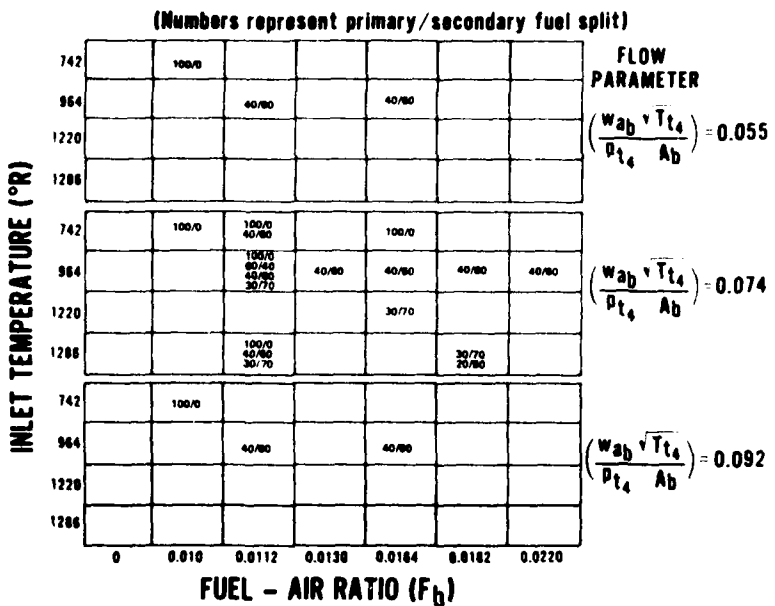
Figure 2.3-15   JT8D Vorbix Burner Test Matrix

2.3.5 Discussion of Farfield Noise Data

Sample measured spectra, power level spectra, and directivity characteristics for each of the six JT8D type burner configurations will be presented in this section. The farfield noise data will be presented in three sub-sections. First, typical noise characteristics from the following five burners will be presented:

1.   JT8D-17 Production Burner

2.   JT8D-17 Aerating Burner (Pressure Atomizing Fuel Nozzle)

3.   JT8D-17 Aerating Burner (Aerating Fuel Nozzle)

4.   JT8D-9 Production Burner

5.   J52 Production Burner (4 fuel nozzles)

Because of the JT8D-vorbix burners' unique geometry and performance characteristics, acoustic spectral and directivity characteristics will be discussed separately in the second sub-section. Finally, the combustion noise power level results, including key performance information for all six burner configurations, will be presented and discussed in the final sub-section.

28

2.3.5.1 Conventional and Aerating Burner Noise Characteristics

The data analysis technique used in determining the combustion noise characteristics of each burner consisted of:

1. The computation of acoustic power level (PWL) spectra for each test condition by numerically integrating the measured SPL spectra over all farfield angles and subtracting 6 dB for free-field simulation.

2. The determination of a generalized combustion noise spectrum for each burner, utilizing computed PWL spectra and measured SPL spectra.

3. The determination of combustion noise directivity characteristics by overlaying the generalized combustion noise spectra on the measured SPL spectra at each angle.

4. The determination of overall acoustic power levels for each test condition by integration of the generalized combustion noise power spectra.

This data analysis procedure is illustrated using the JT8D-9 burner data as an example in the following discussion.

Spectral Characteristics - One-third octave SPL spectra were obtained at all angles for each test condition. Samples of the farfield 1/3 octave band noise spectra at four angles for the JT8D-9 burner are presented in Figure 2.3-16 at the simulated takeoff condition. This example is typical and clearly shows both the combustion noise (centered around 500 Hz) and a low frequency peak near 100 Hz that has been attributed to a rig resonance phenomenon. As discussed in Appendix B, it was possible to spectrally separate the 100 Hz noise from the combustion noise, resulting in uncontaminated definitions of combustion noise.
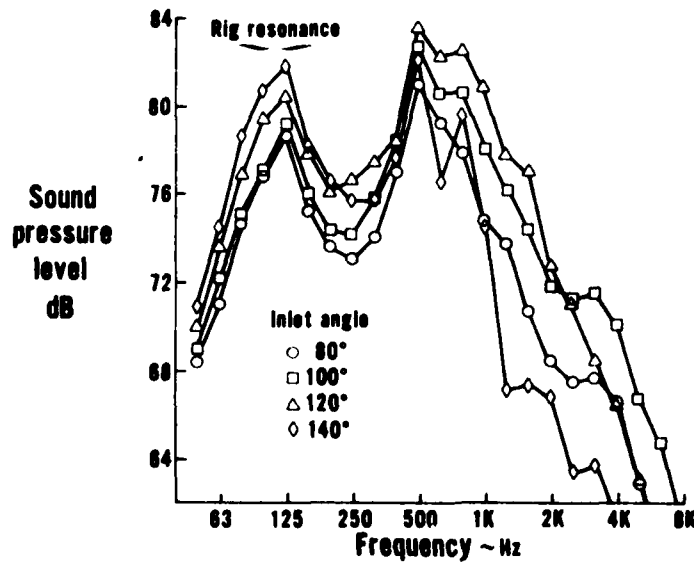
Figure 2.3-16 Typical SPL Spectra for JT8D-9 Burner, Simulated Engine Takeoff Condition

29

The measured 1/3 octave band SPL spectra were numerically integrated over all angles to obtain the power level spectra for each burner and test condition. A typical one-third octave PWL spectra, including the rig resonance spectral peak, is shown in Figure 2.3-17 for the same JT8D-9 burner and operating condition as portrayed in Figure 2.3-16. All acoustic power levels are presented in dB referenced to 10^{-12} watts. An analysis of individual SPL spectra at various angles, together with a separate analysis of PWL spectra obtained for the JT8D-9 burner at all operating conditions revealed no appreciable spectral shape variations with either farfield angle or burner operating condition. These analyses resulted in the generalized JT8D-9 combustion noise spectra shape shown in Figure 2.3-18. This spectra is in good agreement with all SPL and PWL spectra for the JT8D-9 burner. Integrating this spectra shape over frequency results in an OASPL or OAPWL that is 6.5 dB higher than the respective peak SPL or PWL, as indicated in Figure 2.3-18.
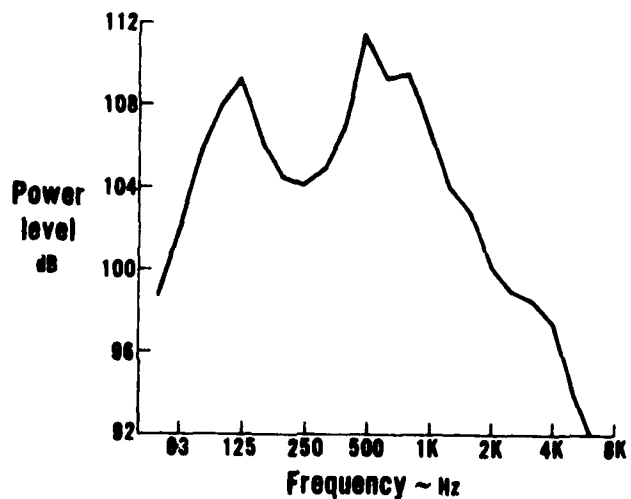
Figure 2.3-17 Typical Power Level Spectra for JT8D-9 Burner, Simulated Engine Takeoff Condition
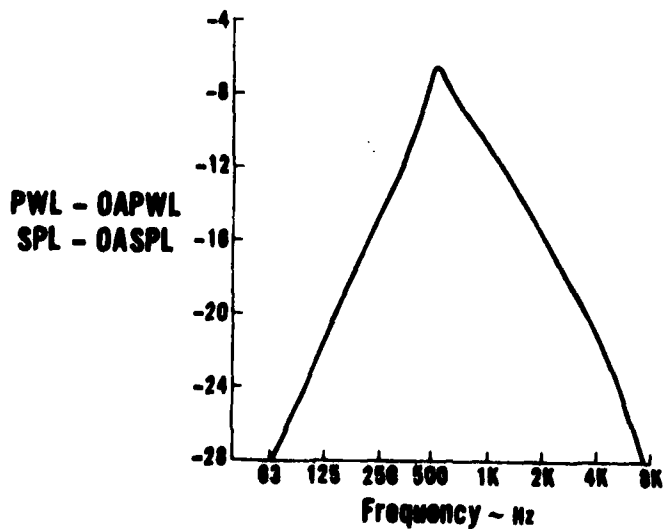
Figure 2.3-18 Combustion Noise PWL and SPL Spectrum for JT8D-9 Burner

30

Figures 2.3-19, 2.3-20 and 2.3-21 represent simulated engine approach, climb and takeoff conditions, respectively, for the JT8D-9 burner, and show the agreement between measured PWL spectra and the combustion noise spectra shape from Figure 2.3-18.
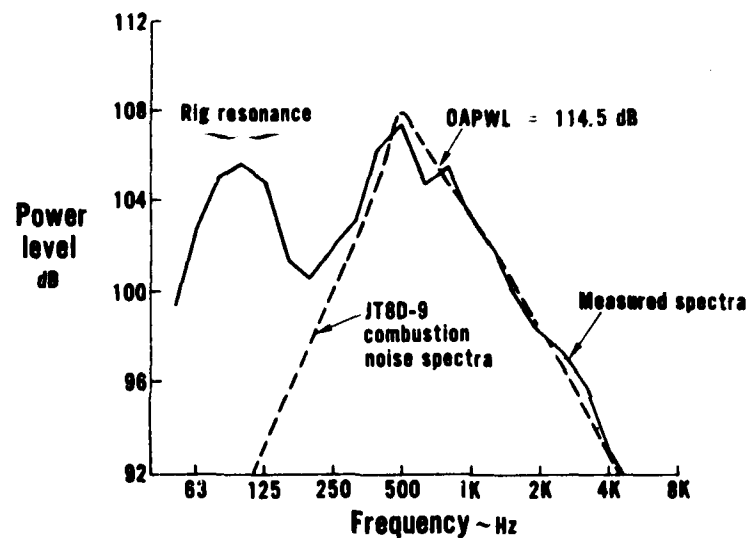
Figure 2.3-19   JT8D-9 Combustion Noise Spectra, Simulated Approach Condition
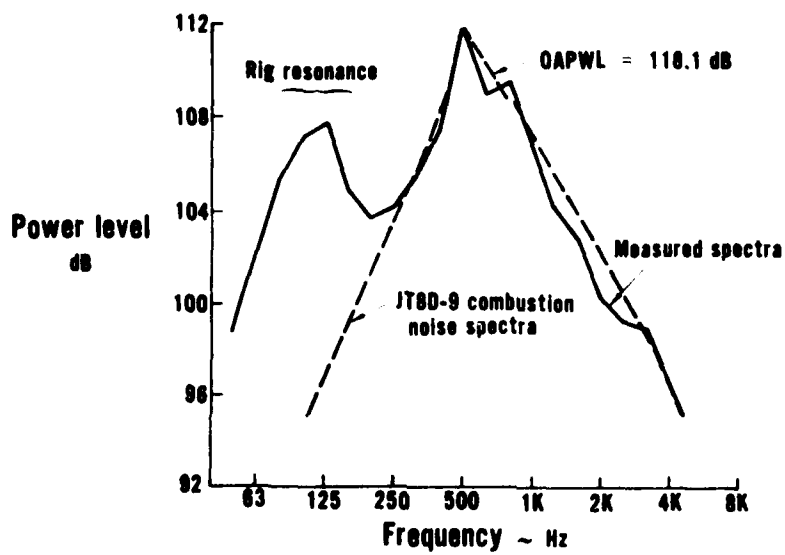
Figure 2.3-20   JT8D-9 Combustion Noise Spectra, Simulated Climb Condition

31
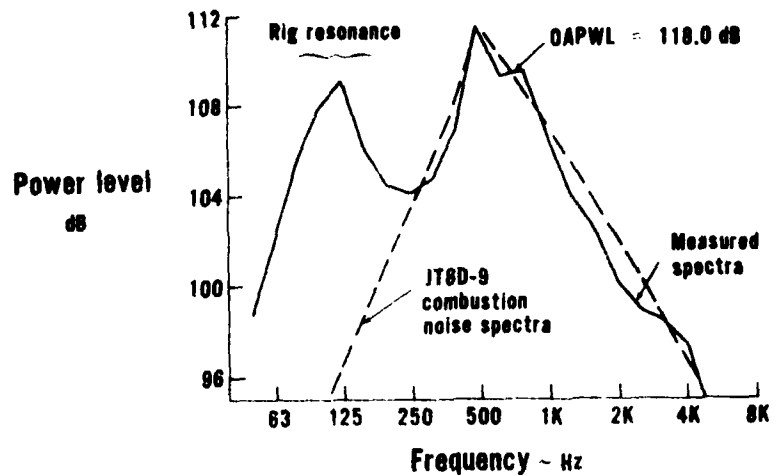
Figure 2.3-21 JT8D-9 Combustion Noise Spectra, Simulated Takeoff Condition

The above data analysis procedure, shown specifically for the JT8D-9 burner, was also applied to each of the remaining burner configurations except the vorbix, which will be presented in the following sub-section. The combustion noise spectra were found to be quite similar, and a generalized combustion noise spectra for all five burners was defined and is presented in Figure 2.3-22.
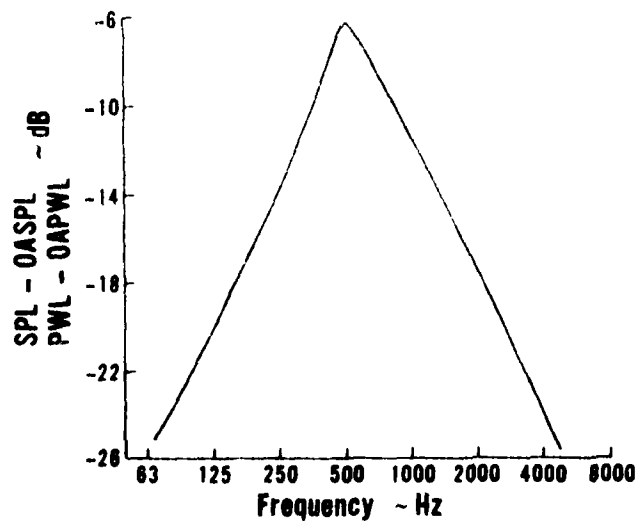
Figure 2.3-22 Generalized Combustion Noise Spectra for JT8D Type Burners, Except Vorbix

32

The overall combustion noise sound power levels (OAPWL) for all burners were obtained by overlaying the combustion noise spectra shape (in a manner shown in Figures 2.3-19 through 2.3-21) on the measured PWL spectra. This procedure eliminated the contribution from the low frequency resonance noise.

Power level spectra from the five burners at the simulated takeoff condition are shown in Figure 2.3-23. The combustion noise from these single and multiple fuel nozzle burners peaks around the same frequency (500 Hz). Another observation from Figure 2.3-23 is that the J52 burner with four fuel nozzles exhibits a combustion noise spectra that is nearly 4 to 6 dB lower than those from the single fuel nozzle burners This result supports predictions from the direct combustion noise model (Section 2.2) and are discussed further in Section 2.4.

The low frequency resonance noise level for the JT8D-17 aerating burner operating with an aerating fuel nozzle appears significantly higher than that from the other burners and is believed to have been caused by a feedback mechanism between the resonance noise and the low pressure fuel injection system of the aerating nozzle. Appendix B discusses this phenomenon in more detail.
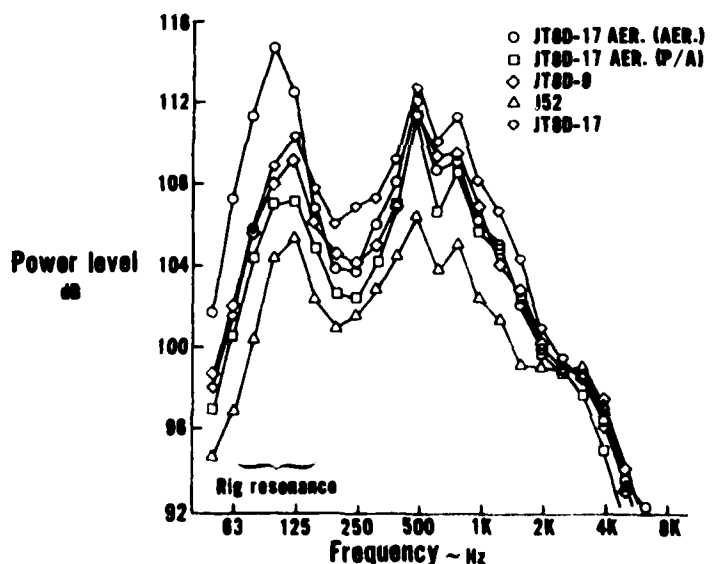
Figure 2.3-23   Power Level Spectra From Several Burners, Simulated Engine Takeoff Condition

Directivity Characteristics   Directivity characteristics from each burner were obtained by overlaying the general combustion noise spectra shape (Figure 2.3-22) on the measured farfield SPL spectra, typical examples of which are shown in Figures 2.3-24 through 2.3-26 at three farfield locations. The resulting OASPL levels obtained at each angle were then plotted versus angle from the inlet axis, examples of which are shown in Figure 2.3-27. The directivities are seen to be

33

quite flat. It was found that all burners tested at X-410 stand resulted in very similar directivity patterns at a given operating condition, and that variations in the pattern shapes appeared as the operating condition was varied. These variations were systematic and consisted of a steepening of the directivities at the rearward angles with increases in either the rig exit velocity or exit temperature. This can be attributed to shear layer refraction effects (Morse and Ingard[16]) where the degree of forward bending of a sound wave originally directed toward the 180 degree location increases approximately in proportion to the sum of the local sonic velocity (or exit temperature) and exit jet velocity, $C_j + V_j$. The measured directivity patterns from all JT8D type burners can be represented quite accurately by the four normalized patterns depicted in Figure 2.3-28 where each pattern is applicable to any of the burners operating in the prescribed range of $C_j + V_j$.
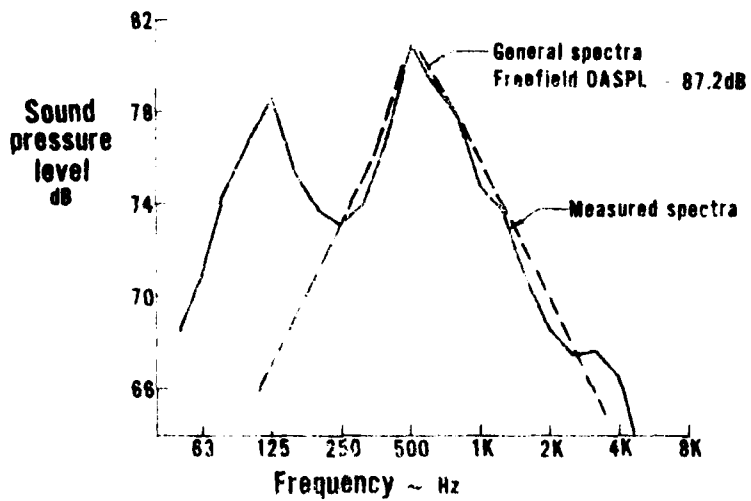
Figure 2.3-24 Typical SPL Spectra With General Combustion Noise Spectra Overlayed, Simulated Takeoff Condition, JT8D-9 Burner, 80° Microphone
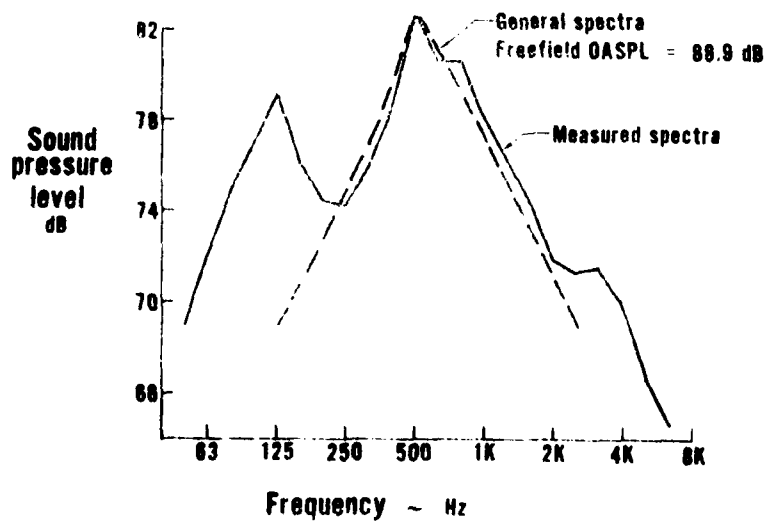
Figure 2.3-25 Typical SPL Spectra With General Combustion Noise Spectra Overlayed, Simulated Takeoff Condition, JT8D-9 Burner, 100° Microphone

34
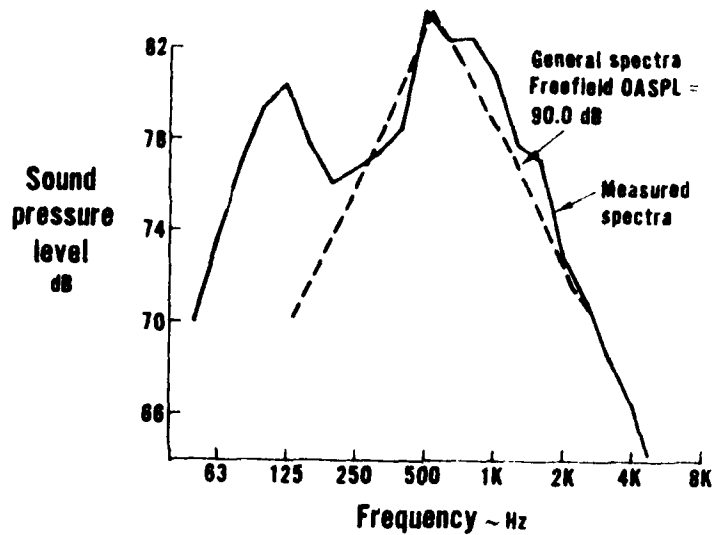
Figure 2.3-26 Typical SPL Spectra With General Combustion Noise Spectra Overlayed,
Simulated Takeoff Condition, JT8D-9 Burner, 120° Microphone
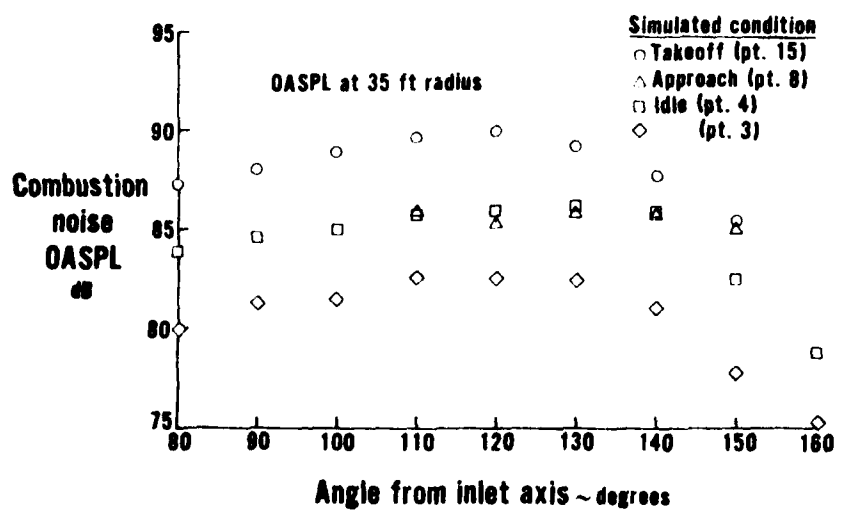
Figure 2.3-27 JT8D-9 Burner Rig Directivity Characteristics

OASPL at 35 foot radius, freefield
OAPWL in dB (ref. 10⁻¹² watts)

OASPL ~
OAPWL
dB

$0 < Cj + Vj < 2200$
$2200 < Cj + Vj < 2400$
$2400 < Cj + Vj < 2600$
$2600 < Cj + Vj < 2800$

Angle from inlet axis ~ degrees
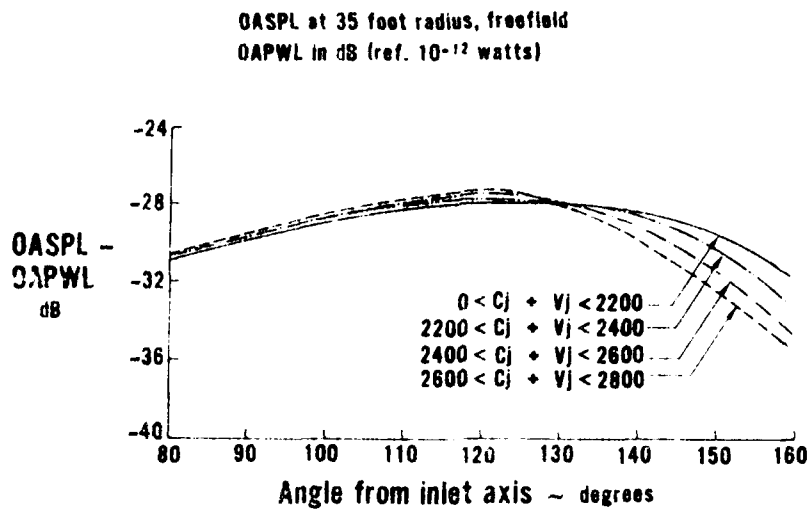
Figure 2.3-28   Normalized Combustion Noise Directivities From JT8D Burner Rig Tests

It should also be noted that directivities are theoretically predicted[16] to be a strong function of the ratio of acoustic wavelength to exit diameter. For large values of this ratio, very flat directivity patterns are predicted. This is the case for the rig data shown in this report, where the ratio of acoustic wavelength (at 500 Hz) to exit diameter is typically about ten. For actual engine configurations, the exhaust nozzle diameter is much larger and the directivity patterns are correspondingly steeper as indicated in Section 4.0.

2.3.5.2   JT8D Vorbix Low Emissions Burner Noise Characteristics

Spectral Characteristics — Several typical measured farfield spectra from the vorbix burner operating with 100% primary fuel are presented in Figure 2.3-29, for the simulated aircraft approach power condition. The acoustic power level (PWL) spectra for this condition, obtained by numerical integration of SPL spectra over all angles, is presented in Figure 2.3-30. PWL spectra shapes from all conditions with 100% primary (pilot) burning were similar and agreed well with the generalized spectra from the other JT8D type burners reported in the preceding section. The general combustion noise spectra shape for JT8D-type burners shown in Figure 2.3-22, has therefore been used to represent the combustion noise from the vorbix burner when 100% of the fuel flows through the primary nozzle. This general combustion noise spectra shape is compared in Figure 2.3-30 to the PWL spectra obtained from the measured data at the 100% primary burning condition discussed above.
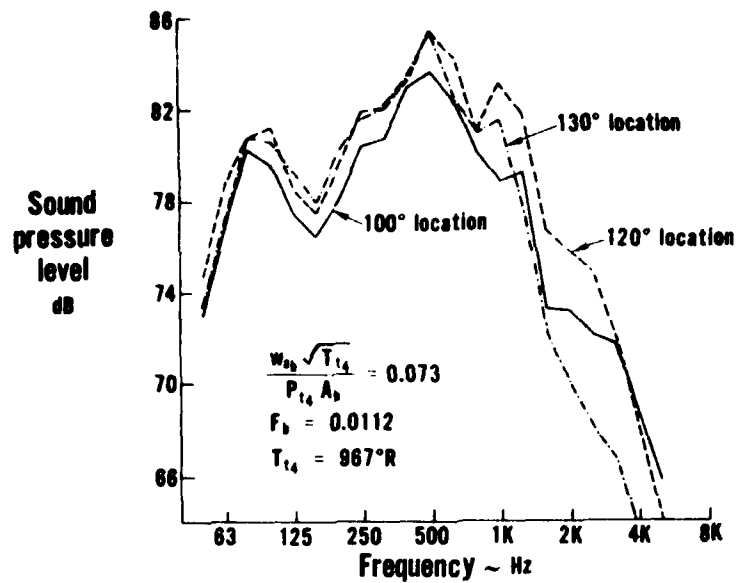
Figure 2.3-29   Typical JT8D-Vorbix SPL Spectra, Simulated Engine Approach Condition
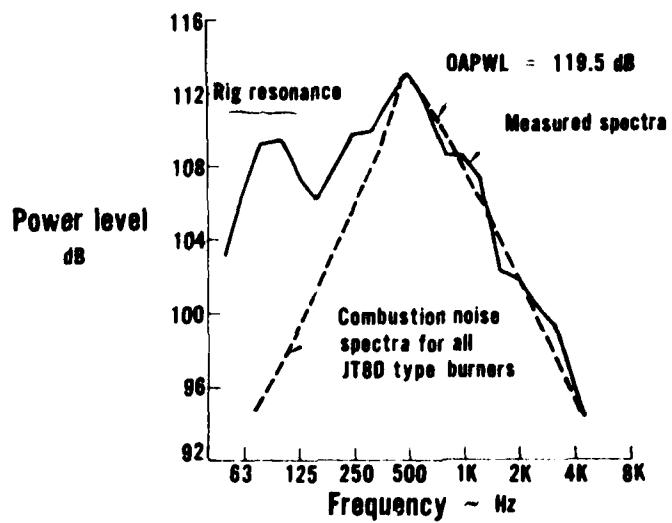
Figure 2.3-30   JT8D-Vorbix Combustion Noise PWL Spectra, Simulated Engine Approach Condition

37

When fuel was injected into the secondary burning region of the vorbix burner, a 1000 Hz peak became evident in the measured JT8D-vorbix spectra. The PWL spectra from several simulated approach conditions (with different primary/secondary fuel splits) are shown in Figure 2.3-31. It is evident that the 1000 Hz noise increases somewhat as the proportion of the total fuel entering the secondary burning region increases. Correspondingly, the 500 Hz combustion noise levels (which are always dominant) decreased as the proportion of fuel to the secondary burning zone was increased. These trends are representative of all the data involving fuel split variations. The generalized spectra shape for the 1000 Hz combustion noise, shown in Figure 2.3-32, was selected following a detailed analysis of the experimental data.
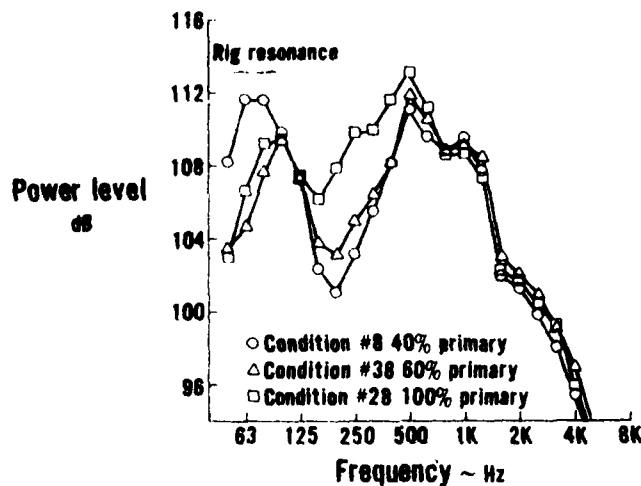
Figure 2.3-31 JT8D-Vorbix Power Level Spectra for Several Primary/Secondary Fuel Splits, Simulated Approach Condition
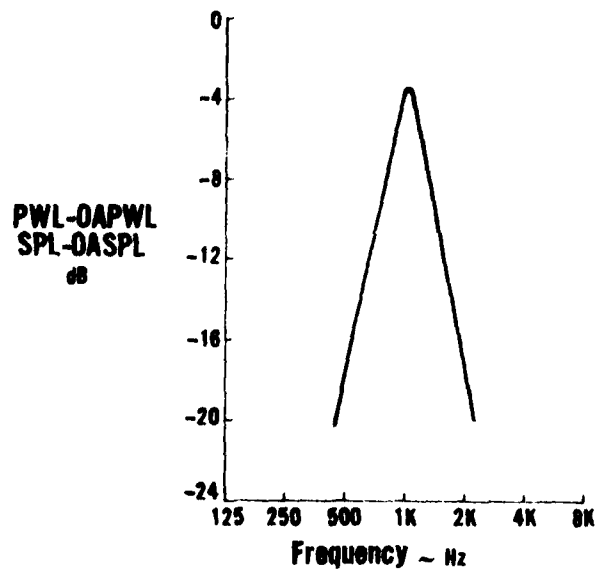
Figure 2.3-32 1000 Hz Combustion Noise Spectra for JT8D-Vorbix Burner

38

Combustion noise spectra shapes (centered at both 500 Hz and 1000 Hz) were combined (as illustrated in Figure 2.3-33) with the measured PWL spectra to obtain overall combustion noise power levels (OAPWL) for every test condition.
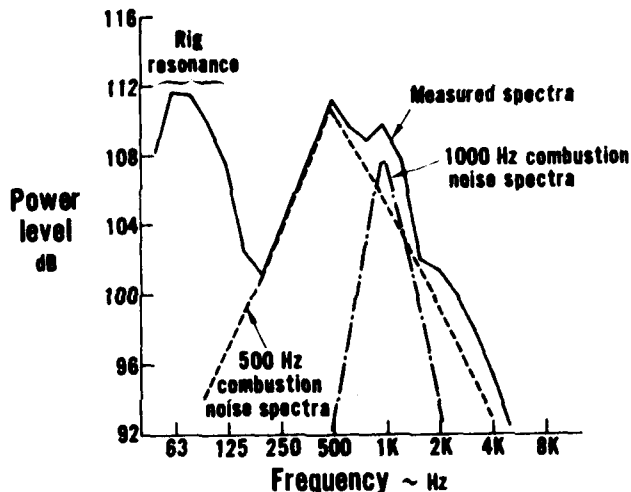
Figure 2.3-33   Power Level Spectra for JT8D-Vorbix Burner At Simulated Approach Condition. 40% Primary, 60% Secondary Fuel Split

Directivity Characteristics — The directivity characteristics of the vorbix were quite similar to those from the other five burners, and are adequately represented by the four patterns presented in Figure 2.3-28.

2.3.5.3   Discussion of Performance and Acoustic Power Levels

The total combustion noise power levels and key performance information for all six JT8D type burners are presented in Tables 2.3-2 through 2.3-7. Although the results presented in these tables will be used in more detail in Section 2.4 for verification of the combustion noise power level model, the following observations may be made from the OAPWL data:

1.   The noise levels from the J52 burner (Table 2.3-6) are approximately 6 dB lower than the levels from the single fuel nozzle burners.

2.   Through the use of a statistical method using a 95% confidence criteria, it was found that combustion noise power levels were not affected by the JT8D-17 aerating burner geometry modifications (Tables 2.3-2 and 2.3-3).

39

3. The results of tests run on the JT8D-17 aerating burner operating separately with two different fuel nozzles (shown in Tables 2.3-3 and 2.3-4) revealed, through the use of the same statistical methods, that the low emissions aerating fuel nozzle did not result in noise differences relative to the conventional pressure atomizing fuel nozzle.

4. The two-stage, advanced low emissions JT8D-vorbix combustion noise levels (Table 2.3-7) are an average of 1.3 dB below the noise levels from the JT8D-17 production burner. In fact, the acoustic power levels from the vorbix burner were found to be in better agreement with those from the single fuel nozzle burners than with those from the J52 burner with four fuel nozzles. This appears to be the case even when the vorbix is operating with a majority of the fuel flowing through the four secondary fuel nozzles. A possible explanation of this result is that the four secondary burning regions are not independent sources of noise, and that the heat release fluctuations in these regions are correlated with, and possibly caused by, the fluctuations in the single upstream primary burning zone.

5. The JT8D-vorbix combustion noise levels (Table 2.3-7) do not vary more than about 2 dB as a function of primary/secondary fuel-split for a given value of fuel-air ratio, flow parameter and inlet temperature.

TABLE 2.3-2

PERFORMANCE AND OAPWL'S FOR JT8D-17 PRODUCTION BURNER

Test Condition	T_{t_4} (°R)	P_{t_4} (psia)	W_{fuel} (lbm/hr)	W_{a_b} (lbm/sec)	F_b	$\dfrac{W_{a_b}\sqrt{T_{t_4}}}{P_{t_4}\,A_b}$	OAPWL (dB)
1	755	15.51	38.8	1.082	.0100	.0560	110.7
2	969	15.82	39.1	.965	.0113	.0555	111.3
3	966	15.82	57.6	.993	.0161	.0570	112.8
4	781	16.70	55.5	1.533	.0101	.0750	117.3
5	783	16.75	62.4	1.533	.0113	.0718	119.4
6	784	16.85	91.8	1.481	.0172	.0721	122.1
7	968	16.64	0	1.413	0	.0772	Cold Flow
8	967	16.34	53.7	1.333	.0112	.0743	118.3
9	972	16.80	63.2	1.381	.0127	.0750	119.3
10	967	16.80	79.6	1.335	.0166	.0723	120.5
11	966	16.74	89.4	1.358	.0183	.0738	121.4
12	961	16.85	108.8	1.376	.0220	.0740	123.1
13	1220	16.73	71.8	1.196	.0167	.0731	119.3
14	1292	16.71	47.6	1.195	.0111	.0753	118.5
15	1295	16.70	77.3	1.172	.0183	.0738	118.9
16	713	17.91	76.0	2.102	.0100	.0916	122.0
17	964	18.10	72.9	1.832	.0111	.0918	122.7
18	964	18.24	110.1	1.856	.0165	.0923	124.0

TABLE 2.3-3

PERFORMANCE AND OAPWL's FOR JT8D-17
AERATING BURNER (P/A FUEL NOZZLE)

Test Condition	T_{t_4} (°R)	P_{t_4} (psia)	w_{fuel} (lbm/hr)	w_{a_b} (lbm/sec)	F_b	$\dfrac{w_{a_b}\sqrt{T_{t_4}}}{P_{t_4}\,A_b}$	OAPWL (dB)
1	774	15.74	39.34	1.095	.0100	.0566	110.7
2	967	15.80	39.36	.977	.0112	.0562	111.4
3	959	15.80	56.3	.977	.0160	.0560	113.1
4	779	16.79	55.7	1.561	.0099	.0759	118.5
5	779	16.77	62.7	1.561	.0112	.0760	118.7
6	778	16.83	91.5	1.535	.0166	.0744	121.5
7	970	16.54	0	1.366	0	.0752	Cold Flow
8	969	16.71	55.4	1.360	.0113	.0741	119.4
9	963	16.72	63.7	1.360	.0130	.0733	119.3
10	963	16.80	80.7	1.370	.0164	.0740	119.9
11	963	16.80	89.4	1.368	.0183	.0739	120.5
12	967	16.87	108.5	1.365	.0221	.0736	122.7
13	1237	16.64	71.1	1.206	.0164	.0745	117.9
14	1291	16.79	55.1	1.182	.0130	.0740	117.9
15	1287	16.76	69.3	1.177	.0164	.0737	116.9
16	799	18.07	74.0	2.050	.0100	.0938	123.0
17	968	18.04	73.6	1.798	.0114	.0907	123.0
18	964	18.38	109.7	1.858	.0164	.0918	125.1

TABLE 2.3-4

PERFORMANCE AND OAPWL'S FOR JT8D-17
AERATING BURNER (AERATING FUEL NOZZLE)

Test Condition	T_{t_4} (°R)	P_{t_4} (psia)	w_{fuel} (lbm/hr)	w_{a_b} (lbm/sec)	F_b	$\dfrac{w_{a_b}\sqrt{T_{t_4}}}{P_{t_4}\,A_b}$	OAPWL (dB)
1	744	15.71	39.6	1.099	.0100	.0558	110.8
2	959	15.66	38.8	.962	.0112	.0556	113.0
3	963	15.63	56.4	.963	.0163	.0558	113.5
4	774	16.70	55.4	1.545	.0100	.0753	119.6
5	784	16.73	62.6	1.550	.0112	.0759	120.6
6	801	16.91	92.1	1.553	.0165	.0760	123.0
7	963	16.46	0	1.353	0	.0745	Cold Flow
8	963	16.68	55.2	1.372	.0112	.0746	118.8
9	967	16.61	62.8	1.342	.0130	.0735	119.6
10	961	16.69	80.0	1.345	.0165	.0731	120.9
11	963	16.70	88.2	1.347	.0182	.0732	121.1
12	963	16.77	106.8	1.351	.0220	.0731	121.0
13	1220	16.47	69.4	1.182	.0163	.0733	117.9
14	1279	16.84	46.9	1.168	.0112	.0725	116.2
15	1284	16.93	77.8	1.185	.0182	.0733	117.6
16	796	18.01	73.6	2.046	.0100	.0937	124.3
17	964	17.91	73.6	1.831	.0112	.0928	123.3
18	964	18.13	108.7	1.834	.0165	.0918	125.8

TABLE 2.3-5

PERFORMANCE AND OAPWL'S FOR JT8D-9 PRODUCTION BURNER

Test Condition	T_{t_4} (°R)	P_{t_4} (psia)	w_{fuel} (lbm/hr)	w_{a_b} (lbm/sec)	F_b	$\dfrac{w_{a_b}\sqrt{T_{t_4}}}{P_{t_4} A_b}$	OAPWL (dB)
1	753	15.54	38.5	1.081	.0099	.0558	108.4
2	964	15.71	38.6	.948	.0113	.0548	108.3
3	964	15.75	57.2	.967	.0164	.0558	110.6
4	765	16.38	54.8	1.533	.0099	.0757	114.2
5	793	16.44	61.6	1.538	.0111	.0770	115.5
6	799	16.50	90.5	1.500	.0168	.0752	119.1
7	965	16.31	0	1.362	0	.0759	Cold Flow
8	965	16.47	54.6	1.365	.0111	.0753	114.5
9	962	16.40	62.1	1.344	.0128	.0743	115.8
10	964	16.50	79.6	1.363	.0162	.0750	118.5
11	964	16.50	88.2	1.347	.0182	.0741	119.1
12	963	16.56	106.9	1.352	.0220	.0741	120.5
13	1231	16.52	70.6	1.194	.0164	.0742	118.1
14	1284	16.39	53.9	1.162	.0129	.0743	115.3
15	1284	16.52	76.4	1.165	.0182	.0739	118.0
16	787	17.54	72.1	1.994	.0100	.0933	121.0
17	963	17.45	70.6	1.770	.0111	.0920	120.7
18	961	17.53	104..0	1.757	.0164	.0909	122.5

TABLE 2.3-6

PERFORMANCE AND OAPWL'S FOR J52 PRODUCTION BURNER

Test Condition	T_{t_4} (°R)	p_{t_4} (psia)	w_{fuel} (lbm/hr)	w_{a_b} (lbm/sec)	F_b	$\dfrac{w_{a_b}\sqrt{T_{t_4}}}{p_{t_4} A_b}$	OAPWL (dB)
1	777	15.85	39.5	1.087	.0101	.0559	109.2
2	964	15.82	38.9	.969	.0111	.0556	110.9
3	963	15.86	57.2	.975	.0163	.0558	110.1
4	774	16.56	55.1	1.534	.0100	.0754	113.3
5	774	16.57	61.8	1.526	.0113	.0749	114.8
6	778	16.72	90.7	1.540	.0164	.0751	116.1
7	963	16.38	0	1.351	0	.0745	Cold Flow
8	962	16.38	53.6	1.328	.0112	.0736	114.0
9	965	16.38	62.9	1.340	.0130	.0743	113.7
10	963	16.63	80.0	1.323	.0168	.0722	114.5
11	962	16.48	87.4	1.334	.0182	.0734	115.7
12	960	16.71	107.6	1.330	.0225	.0721	117.5
13	1224	16.45	70.4	1.201	.0163	.0747	112.9
14	1279	16.60	54.8	1.177	.0129	.0742	111.8
15	1283	16.68	77.3	1.194	.0180	.0750	113.3
16	784	17.86	74.7	2.048	.0101	.0939	118.7
17	964	17.49	71.3	1.751	.0113	.0909	118.1
18	961	17.69	105.6	1.782	.0170	.0913	120.5

TABLE 2.3-7

PERFORMANCE AND OAPWL'S FOR JT8D VORBIX BURNER

Test Condition	T_{t_4} (°R)	P_{t_4} (psia)	w_{fuel} (lbm/hr)	Percent Primary Fuel (%)	Percent Secondary Fuel (%)	w_{a_b} (lbr. /c)	Fuel/Air Ratio	Flow Parameter	OAPWL's dB (ref. 10^{-12} watts) 500 Hz	1000 Hz	Total
1	764	15.96	39.7	100	0	1.094	.0101	.0554	114.6	105.6	115.1
2	969	15.96	39.7	40	60	.973	.0113	.0555	112.3	107.0	114.3
3	963	16.00	56.9	40	60	.987	.0160	.0560	115.3	110.5	116.5
4	769	17.10	55.5	100	0	1.554	.0099	.0737	120.1	111.6	120.7
5	801	17.13	62.6	40	60	1.553	.0112	.0750	118.9	112.1	119.7
25	772	17.11	62.0	100	0	1.538	.0112	.0730	121.1	111.3	121.5
6	772	17.19	91.2	100	0	1.542	.0164	.0728	123.5	115.9	124.2
7	962	16.78	Cold Flow	–	–	1.268	–	.0685	Cold Flow	–	–
8	963	17.01	54.6	40	60	1.362	.0111	.0726	116.8	110.9	117.8
28	967	17.04	55.0	100	0	1.366	.0112	.0729	119.5	None	119.5
38	961	17.08	54.9	60	40	1.375	.0111	.0730	117.5	109.9	118.2
48	969	16.99	54.9	30	70	1.366	.0112	.0732	116.5	110.3	117.4
9	963	17.04	63.3	40	60	1.366	.0129	.0728	117.9	112.1	118.9
10	965	17.25	80.9	40	60	1.379	.0163	.0726	119.5	114.9	120.8
11	963	17.26	89.9	40	60	1.362	.0183	.0716	120.3	116.3	121.8
12	965	17.34	108.4	40	60	1.374	.0219	.0720	121.2	118.7	123.1
13	1219	17.00	71.0	30	70	1.201	.0164	.0721	117.6	114.0	119.2
14	1294	17.01	47.2	40	60	1.174	.0112	.0726	115.0	109.7	116.1
24	1284	17.03	47.2	100	0	1.169	.0112	.0719	116.8	None	116.8
34	1286	16.98	47.3	30	70	1.172	.0112	.0724	114.7	110.3	116.0
55	1288	17.34	78.8	20	80	1.199	.0183	.0725	119.7	114.0	120.7
15	1286	17.38	78.8	30	70	1.205	.0182	.0727	118.6	113.9	119.9
16	779	18.92	76.8	100	0	2.051	.0104	.0885	124.7	114.0	125.1
17	965	18.43	73.5	40	60	1.806	.0113	.0890	121.9	113.1	122.4
18	964	18.73	107.8	40	60	1.828	.0164	.0886	123.2	114.9	123.8

2.3.6 Discussion of Internal Dynamic Pressure Data

Dynamic pressure measurements were obtained at two internal locations (ignitor and rig diffuser exit) for all J^8D type burners tested at X-410 stand. The purpose of these measurements was to obtain the relationship between acoustic power levels calculated from these measurements and those obtained from farfield noise data. This section presents internal data from two typical burner configurations (i.e., the JT8D-9 and the J52). Several internal spectra from both locations are presented and compared to measured farfield spectra at the same conditions. Acoustic power levels were calculated from the internal diffuser exit data (assuming only plane waves are present) and are compared to the corresponding farfield acoustic power levels.

2.3.6.1 Internal Spectra

Water-cooled Kulite (Model CQL-080-25) dynamic pressure transducers were mounted in two locations in the JT8D burners and rig as shown in Figure 2.3-13. Samples of the JT8D-9 measured spectra from these locations are shown in Figures 2.3-34 and 2.3-35 for the simulated approach and climb conditions, respectively. The low frequency peak at 100 to 125 Hz noted in the ignitor spectra is due to burner rig resonance as discussed in Appendix B and does not affect the combustion noise centered at 500 Hz. The dynamic pressure fluctuations (at 500 Hz) from the ignitor location was typically found to be 2 to 6 dB higher than at the diffuser location as shown in Figure 2.3-36.
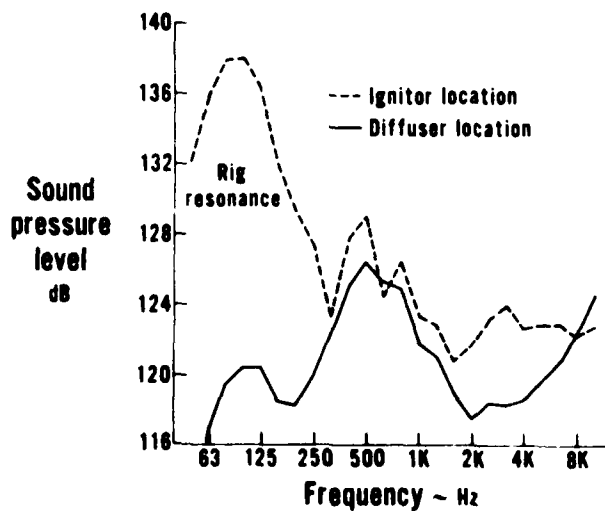
Figure 2.3-34   *Internal SPL Spectra From the JT8D-9 Burner, Simulated Approach Condition*

47
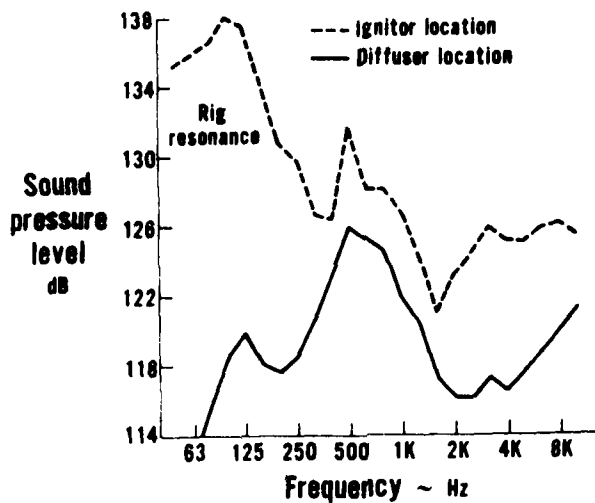
Figure 2.3-35   Internal SPL Spectra From the JT8D-9 Burner, Simulated Climb Condition
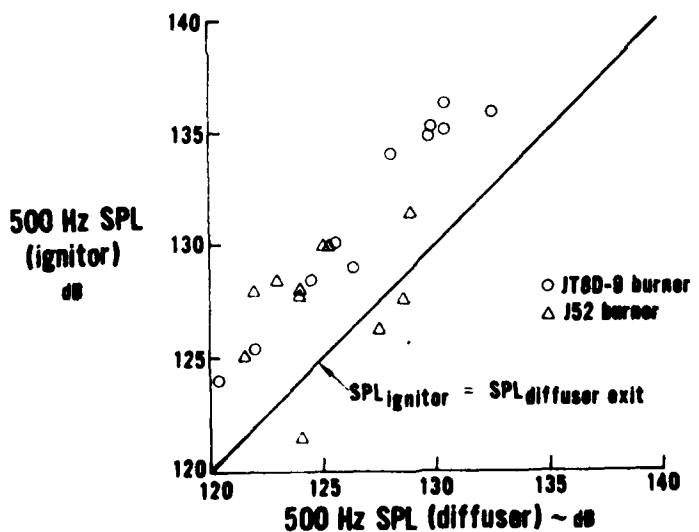
Figure 2.3-36   Comparison of 500 Hz SPL Levels From Two Internal Locations

Several internal 1/3 octave band SPL spectra from the diffuser exit Kulite are presented in Figure 2.3-37. The combustion noise spectra shape characteristics are seen to be similar for all test conditions and, as shown in Figures 2.3-38 and 2.3-39, the internal spectra are in good agreement with the generalized farfield JT8D combustion noise spectra shape presented in Figure 2.3-22.

48

Figure 2.3-37   Internal JT8D-9 SPL Spectra, Diffuser Location

Figure 2.3-38   Comparison of Internal and Farfield Spectra, JT8D-9 Burner, Simulated Approach Condition

49
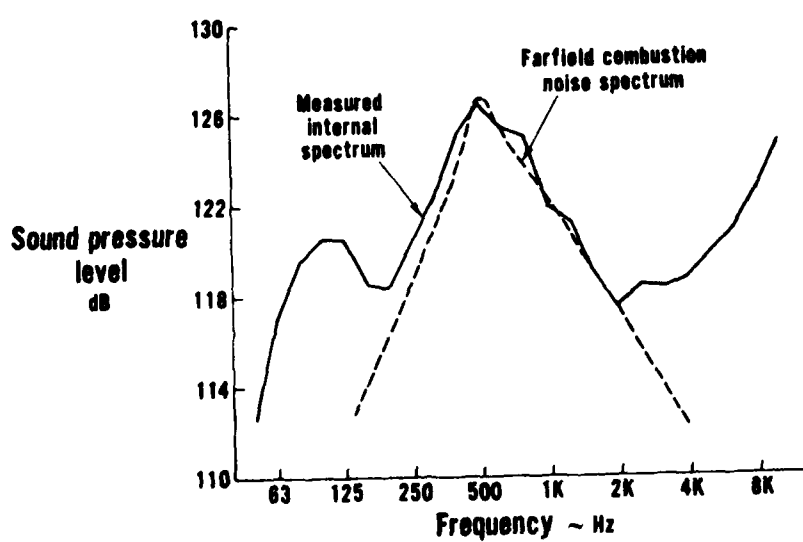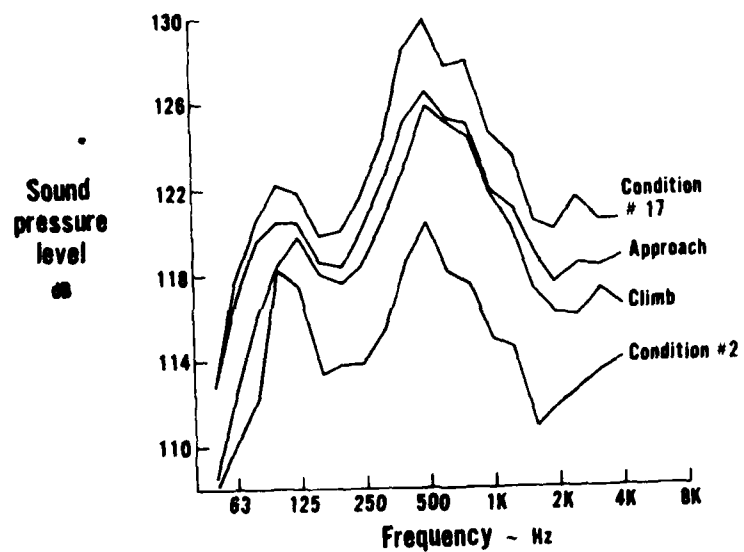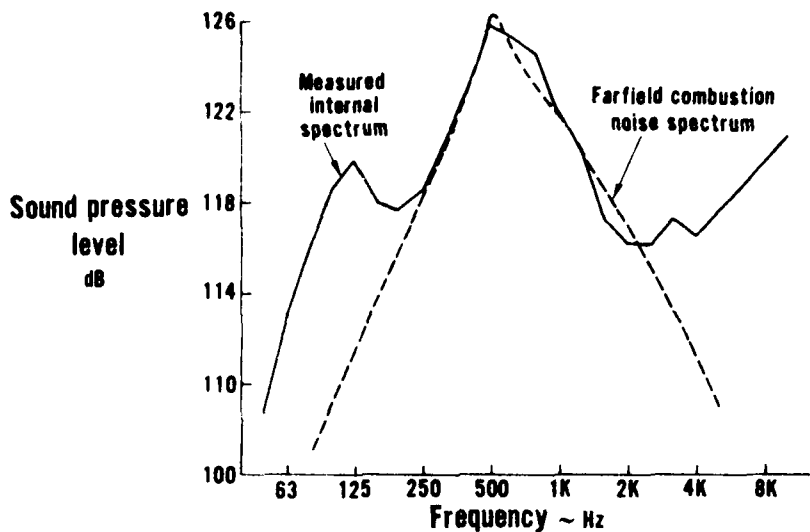
Figure 2.3-39   Comparison of Internal and Farfield Spectra, JT8D-9 Burner, Simulated Climb Condition

2.3.6.2   Internal Acoustic Power Levels

Although both internal measurement locations are considered to be in the near field of the combustion noise source, acoustic power levels were calculated from the spectra measured at the diffuser exit location, where it is assumed that the acoustic energy is carried only in the plane wave mode. Because of the low Mach numbers at the rig exit, convection effects can be ignored and the acoustic power may be represented by

$$P = \frac{<p'^2>}{\rho_5 c_5} A_5 \qquad (29)$$

where subscript 5 refers to conditions at the burner rig exit location. The overall acoustic power level (in dB relative to 10^{-12} watts) may be calculated from Equation (29) by using the spectra shape of Figure 2.3-22 and integrating over frequency. This is expressed in terms of the SPL at 500 Hz as follows:

$$OAPWL = SPL_{500Hz} + 10 \log A_5 + 10 \log\left(\frac{\sqrt{T_{t_5}}}{P_{t_5}}\right) - 27.5 \quad (30)$$

in dB relative to 10^{-12} watts.

50

The internal OAPWL's, calculated from Equation (30) are compared in Figures 2.3-40 and 2.3-41 to the farfield OAPWL's for the JT8D-9 and J52 burners, respectively. The internal OAPWL's appear to be an average of about 2 dB higher than the farfield values. This difference may possibly be attributed to the fact that the diffuser exit location is in the near field of the source. An alternative explanation may be that the rig exit transmission coefficient is slightly less than unity. It is concluded that a reasonable estimate of combustion noise OAPWL's may be obtained from internal measurements at the combustor rig exit. This result is used in the development of a turbine transmission loss model in Section 4.6.
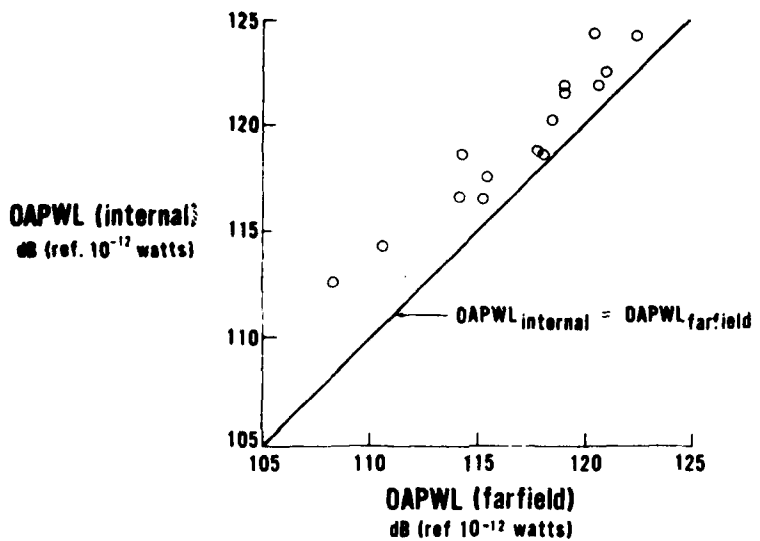
Figure 2.3-40   Comparison of Internal and Farfield Power Levels for JT8D-9 Burner
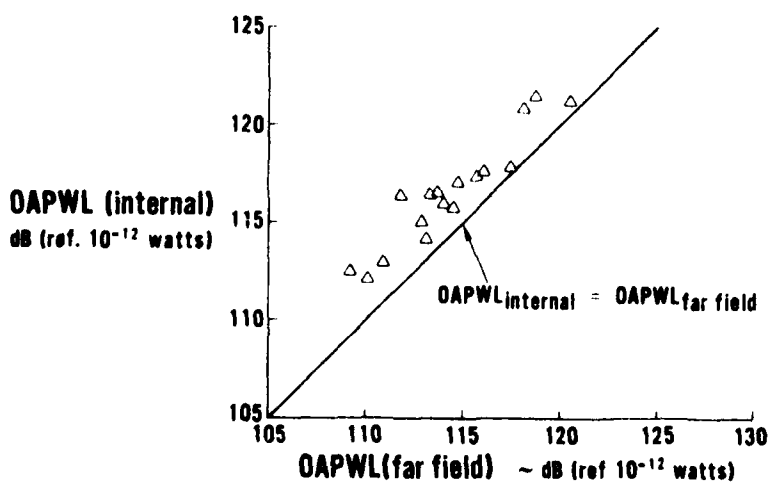
Figure 2.3-41   Comparison of Internal and Farfield Power Levels for J52 Burner

51

2.4 EXPERIMENTAL VERIFICATION OF ACOUSTIC POWER LEVEL MODEL

The predicted combustion noise OAPWL, as expressed by Eq. (28), is verified in the following discussion by comparing the predicted variation due to each term in the equation with the measured variation, using the combustion noise data discussed in the preceding section.

2.4.1 Effect of Fuel-Air Ratio

Figure 2.4-1 presents combustion noise power levels from the isolated JT8D-9 burner as a function only of the burner fuel-air ratio, F_b. Both the burner flow parameter and inlet temperature were held constant for this evaluation. Since, however the burner pressure could not be controlled independently while still obtaining desired values of the other parameters, the acoustic power levels in Figure 2.4-1 have been normalized by the predicted influence of burner pressure. During the testing, the burner pressures varied only from 15.5 to 17.5 psia over the entire range of operation, with the effect that the normalization is almost inconsequential. The slope of the data shown in Figure 2.4-1 is seen to be in excellent agreement with the predicted influence of fuel-air ratio given in Eq. (28), where noise levels increase with the square of F_b.
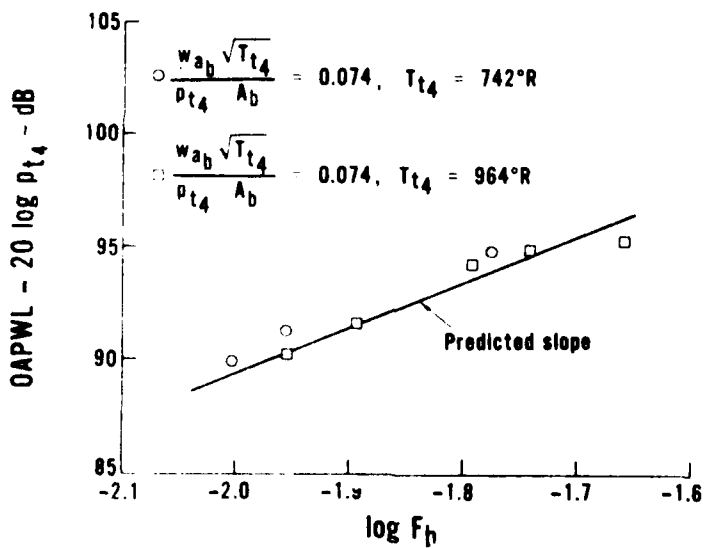
Figure 2.4-1 Effect of Fuel-Air Ratio Variations On Combustion Noise Levels, JT8D-9 Burner

2.4.2 Effect of Burner Flow Parameter

The independent effects of burner flow parameter on combustion noise from the JT8D-9 burner are shown in Figure 2.4-2 for two cases of constant fuel-air ratio and inlet temperature. Again, the predicted dependence on flow parameter, from Eq. (28) is in good agreement with the slopes of both data sets.

52
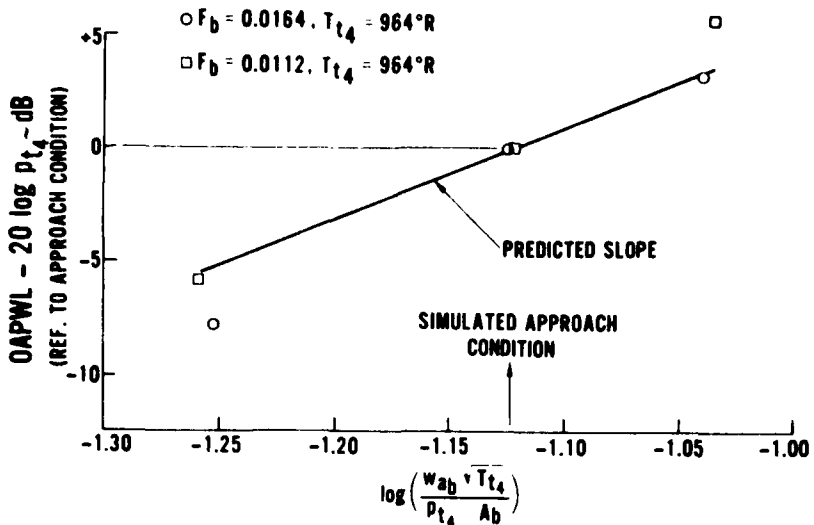
Figure 2.4-2   *Effect of Burner Flow Parameter On Combustion Noise Levels, JT8D-9 Burner*

2.4.3   Effect of Burner Inlet Temperature

Figure 2.4-3 shows the independent effects of burner inlet temperature on combustion noise from the three JT8D production type burners, where fuel-air ratio and flow parameters were held constant. For standard jet fuel, the value of $H_f F_{ST}/c_p$ is taken to be $4500°R$. Although the experimental temperature varied only from 742 to $1220°R$, the noise trends shown in Figure 2.4-3 are in good agreement with the slopes predicted by Eq. (28). It should be noted that as the burner inlet temperature is increased, keeping all other parameters constant, the combustion noise levels decrease.
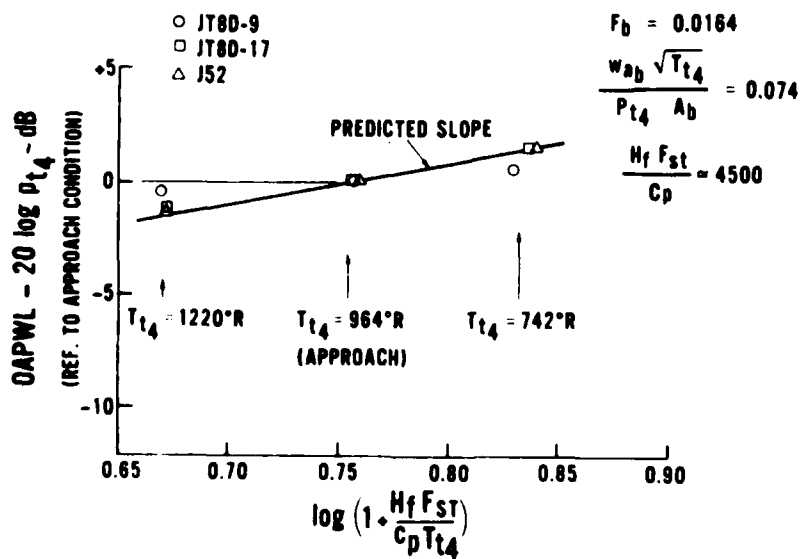
Figure 2.4-3   *Effect of Burner Inlet Temperature On Combustion Noise Levels*

53

2.4.4   Effect of Number of Fuel Nozzles

To verify the predicted effect of the number of fuel nozzles on combustion noise, the J52 four fuel nozzle burner was tested. Since this burner has the same cross-sectional area and length as the single fuel nozzle burners, Eq. (28) predicts that, at a given burner operating condition, the J52 burner should be 6 decibels quieter than the single fuel nozzle JT8D-17 burner. A comparison of combustion noise levels from the J52 and the JT8D-17 burners is shown in Figure 2.4-4, where the noise is plotted as a function of the entire parameter of Eq. (28), except the term involving the number of fuel nozzles. The data from both burners are in agreement with the predicted slope from Eq. (28) and the expected 6 dB difference due the number of fuel nozzles is evident.
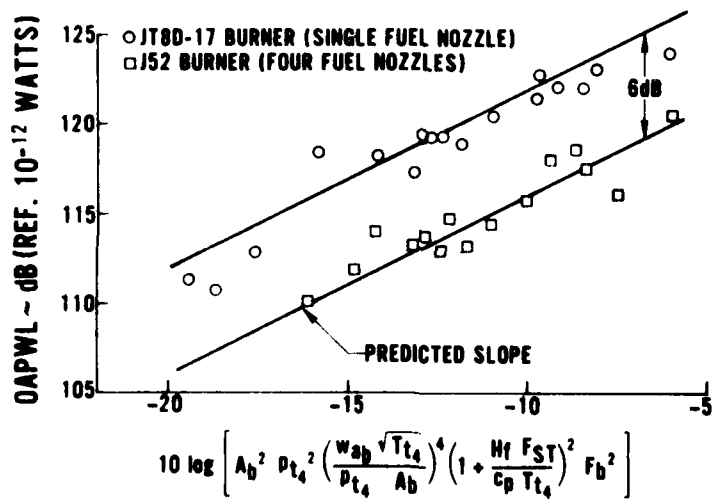
Figure 2.4-4   Combustion Noise Level Differences Due to Number of Fuel Nozzles

When the predicted influence of fuel nozzle number is taken into account, the data shown in Figure 2.4-4 collapse as shown in Figure 2.4-5. Here, the slope of the combustion noise correlation shown by the solid line is in excellent agreement with the predictions of Eq. (28).

54

$$10 \log \left[\frac{1}{N_f} A_b^2 P_{t_4}^2 \left(\frac{w_{ab} \sqrt{T_{t_4}}}{P_{t_4} A_b} \right)^4 \left(1 + \frac{H_f F_{ST}}{C_p T_{t_4}} \right)^2 F_b^2 \right]$$
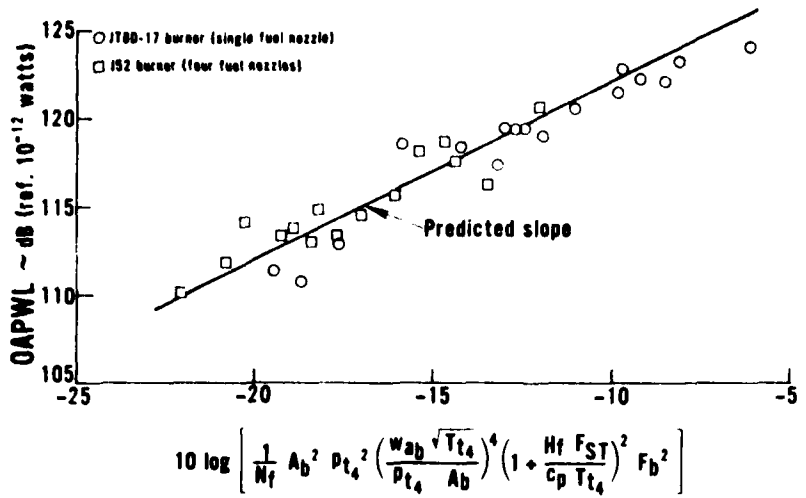
Figure 2.4-5   Combustion Noise Correlation, Including Effect of Fuel Nozzle Number

2.4.5   Effect of Burner Pressure

The direct combustion noise acoustic power level model developed in the Section 2.2.2 states that direct combustion noise levels are proportional to burner pressure raised to a power of two. The JT8D rig test program conducted at X-410 burner noise facility was aimed at evaluating the independent effect of all key combustion noise prediction terms, except the burner pressure. Two methods of examining the validity of the pressure term are possible, however. The first method involves a comparison of internally measured noise spectra from several JT8D type burners operated separately at low pressure (X-410 stand) and at high pressures inside full scale engines. The independent effect of burner pressure is examined by comparing the rig and engine internal dynamic pressure data at constant values of burner inlet temperature, flow parameter and fuel/air ratio. Two typical cases (where both internal rig and engine spectra were available) are presented in this section. The second method for evaluating the predicted pressure term involves the use of farfield engine noise data. This evaluation is discussed in Section 4.3 using the data from four P&WA engines presented in Section 4.2.

Measured spectra at the ignitor location inside a production JT8D-17 burner operating in the JT8D rig and also inside a full scale JT8D-17 engine are presented in Figure 2.4-6. The spectra from both tests are representative of a typical engine idle power condition. The combustion noise levels (500 Hz peak frequency) recorded inside the low pressure burner rig are nearly 10 dB lower than those recorded inside the full scale engine. When the measured sound pressure levels from both tests are normalized by the predicted effect of burner pressure, the two spectra collapse quite well in the combustion noise frequency range, as shown in Figure 2.4-7. The lack of agreement at low frequencies is due to the rig resonance phenomenon (see Appendix B) experienced in rig tests at X-410 stand. Inspection

55

of similar SPL spectra at other engine operating conditions for this burner indicated
that the predicted effect of burner pressure on combustion noise is valid over a
wide range of burner pressures.
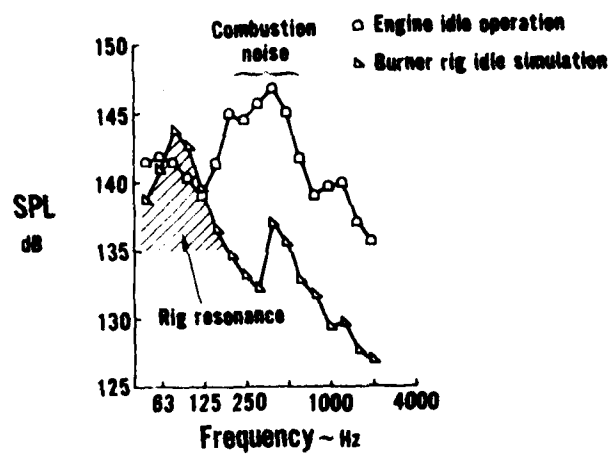
Figure 2.4-6   Comparison of Internal Burner Noise Spectra for JT8D-17 Burner, Full
Scale Engine Vs. Burner Rig Operation
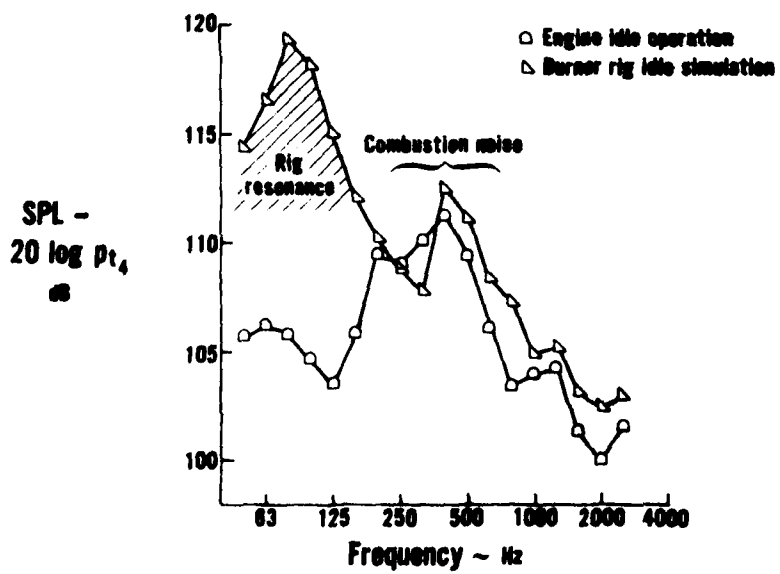
Figure 2.4-7   Effect of Burner Pressure On Internal Combustion Noise Levels From a
Production JT8D-17 Burner

56

Measured spectra from a J52 burner, tested both at X-410 stand and inside a full scale J52 engine are presented in Figure 2.4-8. Both spectra were recorded at a takeoff performance condition and show a difference of nearly 25 dB between the rig and engine internal combustion noise levels. When the measured sound pressure levels from both tests were normalized by the predicted effect of burner pressure, the collapse presented in Figure 2.4-9 was obtained. In the combustion noise frequency range, the normalized levels agree quite well.

The two examples shown in Figures 2.4-6 through 2.4-9 indicate conclusively that the predicted effects of pressure are correct for the various burners investigated. Similar results have been obtained at other operating conditions and for other burners, including the JT8D-9 burner design.
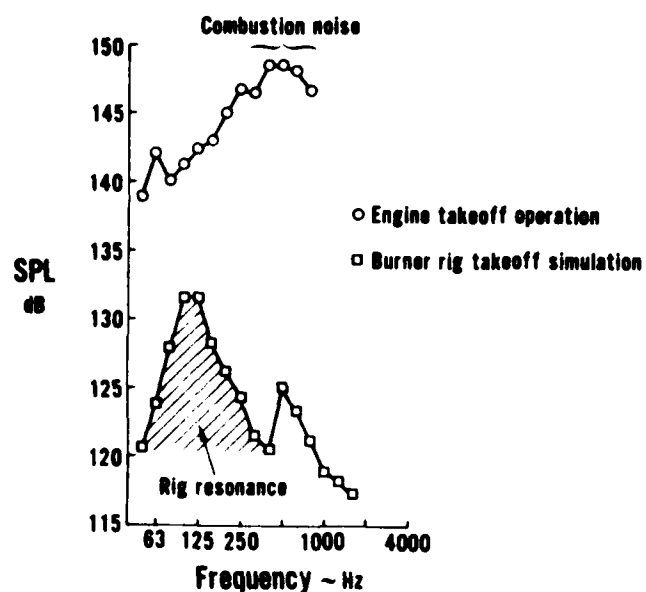
Figure 2.4-8 Comparison of Internal Burner Noise Spectra for J52 Burner, Full Scale Engine vs. Burner Rig Operation
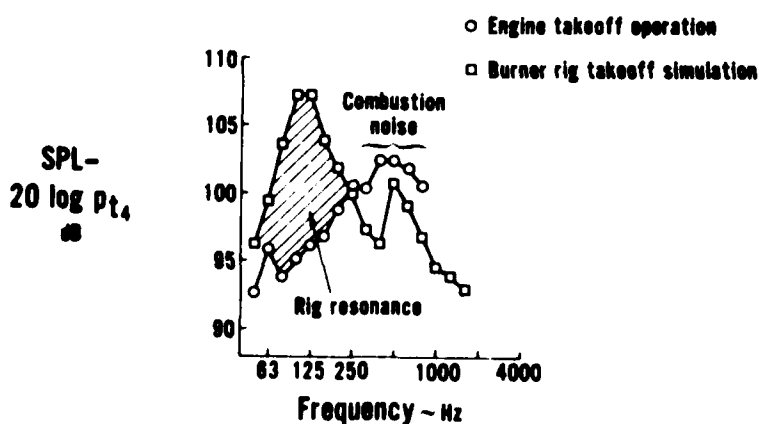
Figure 2.4-9 Effect of Burner Pressure On Internal Combustion Noise Levels From a J52 Burner

57

2.4.6 Direct Combustion Noise Acoustic Power Level Correlations

2.4.6.1 Conventional and Aerating JT8D Type Burners

In the preceding discussion, the predictions from the direct combustion noise power level model, Eq. (28), were verified using experimental data from several JT8D type burners. However, the value of the constant, K_3, in this expression needs to be determined. A least squares fit of all of the data from the five contional and aerating JT8D type burners, to Eq. (28), resulted in a value of 131.3 for K_3 as shown in Figure 2.4-10. The correlation shown in this figure is expressed by

$$
\text{OAPWL} = 10 \log \left[\frac{1}{N_f} A_b^2 p_{t_4}^2 \left(\frac{w_{a_b} \sqrt{T_{t_4}}}{p_{t_4} A_b} \right)^4 \right.
$$

$$
\left. \left(1 + \frac{H_f F_{ST}}{c_p T_{t_4}} \right)^2 F_b^2 \right] + 131.3 \sim \text{dB (ref. } 10^{-12} \text{ watts)} \quad (31)
$$

An indication of the accuracy of this correlation was obtained by calculating the standard deviation of all the data about the mean correlation line through the data. This standard deviation was found to be 1.8 dB.
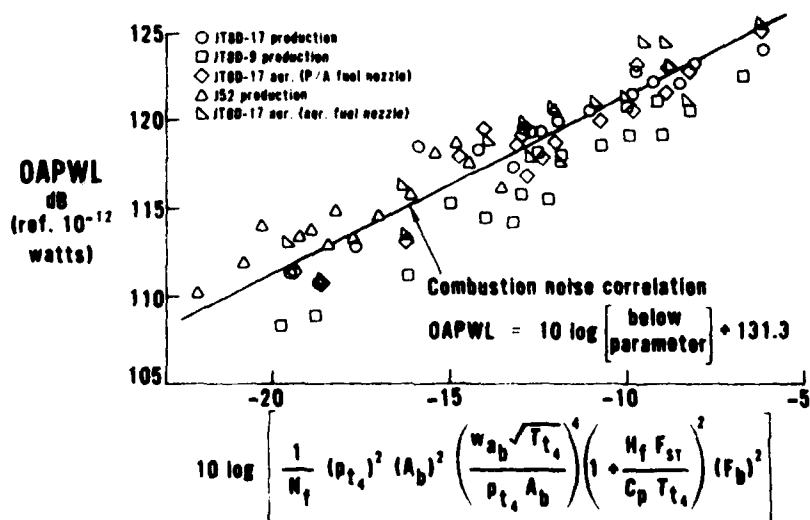
Figure 2.4-10 Combustion Noise Correlation for Conventional and Aerating Burners

58

2.4.6.2 Advanced Low Emissions JT8D-Vorbix Burner

As mentioned in Section 2.3.5, the combustion noise power levels from the two-stage, low emission JT8D-vorbix burner (Table 2.3-7) were found to be somewhat lower than the levels from the JT8D-17 production burner. The data from the vorbix burner were found to be in good agreement with predictions of Eq. (28) when the constant K_3 was equal to 130 dB. This is shown in Figure 2.4-11 where the correlation line for the vorbix burner is given by

$$
\text{OAPWL} = 10 \log \left[\frac{1}{N_f} A_b^2 P_{t_4}^2 \left(\frac{w_{ab}\sqrt{T_{t_4}}}{P_{t_4} A_b} \right)^4 \right.
$$

$$
\left. \left(1 + \frac{H_f F_{ST}}{c_p T_{t_4}} \right)^2 F_b^2 \right] + 130 \sim \text{dB (ref. } 10^{-12} \text{ watts)} \qquad (32)
$$

The standard deviation of the vorbix data around this correlation is 0.99 dB. Although the vorbix burner contained one primary fuel nozzle and four downstream secondary fuel nozzles, the noise levels from this burner were in better agreement with levels from the single fuel nozzle burners than with those from the four nozzle J52 burner. It was suggested in Section 2.3 that the heat release rate fluctuations in the secondary burning regions were related to the fluctuations in the primary zone, and therefore could not be considered as independent sources of noise. For this reason, the correlation given by Equation (32), and shown in Figure 2.4-11, uses $N_f = 1$ instead of $N_f = 5$.

$$
10 \log \left[\frac{1}{N_f} P_{t_4}^2 A_b^2 \left(\frac{w_{ab}\sqrt{T_{t_4}}}{P_{t_4} A_b} \right)^4 \left(1 + \frac{H_f F_{ST}}{c_p T_{t_4}} \right)^2 F_b^2 \right]
$$
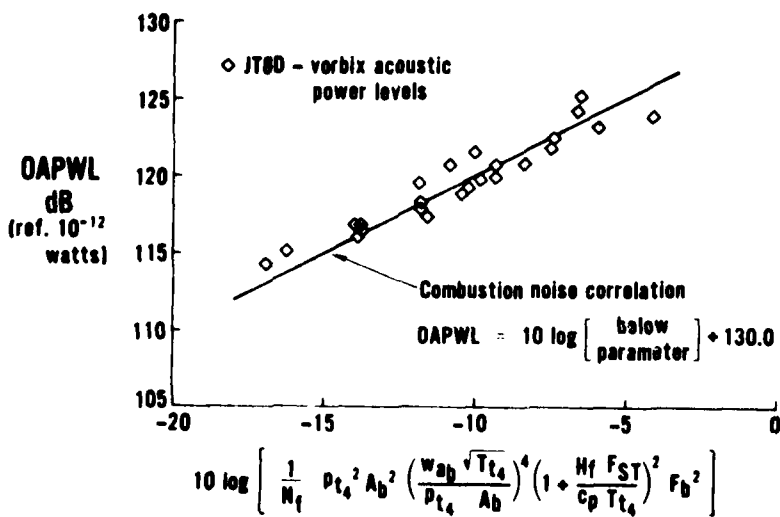
Figure 2.4-11   Combustion Noise Correlation for Low Emissions JT8D - Vorbix Burner

2.5 INVESTIGATION OF OPTICAL TECHNIQUES

The general wave equation for the sound field resulting from heat addition to a medium contains several right hand side source terms[16]. There is general agreement that the dominant source term for direct combustion noise is proportional to the time rate of change of the fluctuating heat release rate. It has been found by several investigators that the heat release rate is related to the light intensity of certain combustion emission bands such as CH, C₂ and OH. By collecting light from the burning zone, optically filtering to pass one of these radiation bands, and collecting the result with a photo-multiplier tube (PMT), a fluctuating electric signal may be obtained. The mean value would be proportional to the average heat release rate, and the fluctuations result from the unsteady combustion. By electrically differentiating this signal with respect to time, a voltage would be obtained which is directly proportional to the combustion noise source. This correspondence has been demonstrated[17] for open flames by cross-correlating the differentiated light signal with a microphone in the farfield. Excellent correlation of the random signals was obtained when the differentiated light signal was delayed by the acoustic transit time to the farfield.

There exists a need for similar experiments for confined flames such as exist in typical aircraft engine burners. The prime motivation for these experiments is that they would allow diagnostic measurements of the combustion noise source term to be obtained during the course of burner development programs conducted on conventional burner test rigs and conventional test facilities. In these facilities, meaningful acoustic measurements are difficult to obtain because of the confinement of the burner flow and acoustic fields by the rig and facility.

Accordingly, as part of the current contract effort, the use of optical methods was explored as a means of defining the radiated power by measuring the cause (heat release rate fluctuations) rather than the effect, i.e., the acoustic pressure in the farfield of the burner. A program was executed to checkout optical instrumentation suitable for incorporation in systems for burner noise source measurement. An open blowtorch flame was used to check operation of the equipment. Following these tests, and analysis was made of the special requirements of optical sensors and signal processing networks needed to evaluate the combustion noise source strength in burner rigs and engines. An account of this investigation, which indicates the feasibility of using optical methods for determining burner noise source characteristics is given in Appendix C and is discussed below.

The propagating acoustic energy of combustion generated noise, because of its low frequency content, is carried primarily in the plane wave mode. For a center frequency on the order of 400 to 500 Hz, its characteristic wavelength in a burner is on the order of 4 feet, whereas the burning region is typically less than a foot long. Therefore, it follows that the source can be considered compact. Under these conditions, a procedure was evolved (Appendix C) to calibrate the light sensor output in terms of radiated noise. A single light sensor is sufficient to predict the radiated noise in the compact case. If the source is not compact, more than one sensor is required, and the technique for calibrating the system becomes much more complex.

3.0 INDIRECT COMBUSTION NOISE

3.1 BACKGROUND

In a typical modern aircraft engine, the flow from the burner into the turbine may contain fluctuations in temperature and axial velocity. The source of these inhomogeneities is the unsteadiness of the combustion process in the burner. When a temperature "hot-spot" passes through the large pressure changes associated with the turbine a compensating pressure perturbation is generated. The resulting acoustic signal generated downstream of the burner is highly dependent upon the amplitude and length scales of the temperature fluctuations originating in the burner, and is therefore termed "indirect combustion noise".

In the remainder of this section a brief summary is presented (Section 3.2) of various prediction models described in the literature. A description of a test rig and plan to study indirect combustion noise is also presented in Section 3.3 with additional details contained in Appendix D. Dynamic temperature data obtained at the JT8D-17 burner exit are presented in Section 3.4, followed by a discussion of how these dynamic temperature characteristics were correlated with burner operating parameters to obtain the inputs required for the use of the P&WA indirect combustion noise prediction model.

3.2 DISCUSSION OF PREDICTION MODELS

The indirect combustion noise mechanism may be more easily visualized by considering the schematic illustration shown in Figure 3.1-1. This figure illustrates the generation of hot-spots and their convection through the turbine blade rows, together with the resulting acoustic signal. The governing parameters include the amplitude and length scales of the hot-spots and the amplitude of the pressure drop through which the hot-spots convect.
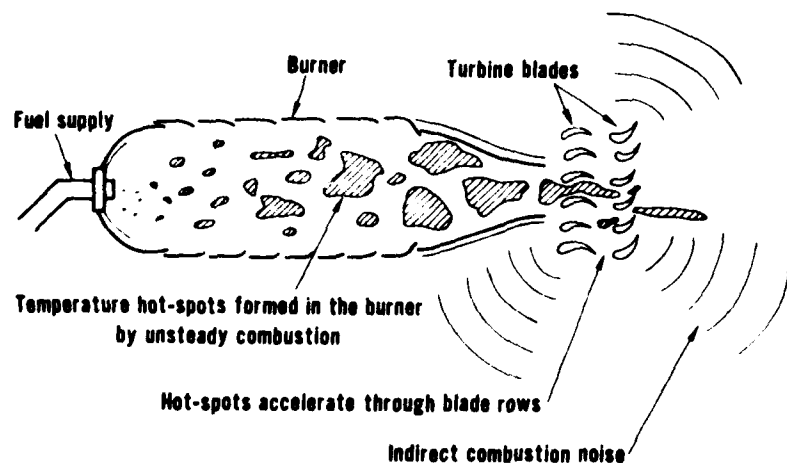
Figure 3.1-1 Schematic Diagram of the Indirect Combustion Noise Generation Process

61

A recent paper by Dils[18] has shown that significant fluctuations in temperature occur in the flow leaving the combustion chamber of modern aircraft engines. Since significant temperature fluctuations have been found to exist, the concept of indirect combustion noise became a possible explanation for the observed core engine noise.

A brief review of several approaches that model indirect combustion noise is presented in the following paragraphs.

Cumpsty-Marble Model - Cumpsty and Marble[19] have modeled the subject noise mechanism by Fourier analyzing an assumed temperature pulse and calculating the interaction of each Fourier temperature component with the discontinuity (i.e., ΔP, ΔV, etc.) created by a given turbine blade row. An actuator disc assumption was applied to each blade row and results were obtained from the solution of the following four equations:

1) Conservation of mass

2) Conservation of energy

3) Conservation of entropy

4) Kutta condition applied at the blade trailing edge

The temperature hot-spots were assumed to be perfectly correlated over the extent of the burner can exit. In general, Cumpsty and Marble predicted that small fluctuations in the temperature of the gas entering the pressure drop of a turbine produce significant amounts of noise. Their results are applicable to cases where the pressure drop is achieved by turning of the flow through vanes (e.g., as in a turbine) as opposed to flow acceleration through an axial nozzle.

Flowcs-Williams/Howe Model - Flowcs-Williams and Howe[20] considered low Mach number steady flow containing discrete temperature inhomogeneities convecting through a duct contraction. They refer to the dominant noise radiation term as "acoustic bremsstrahlung" (which translates as acoustic brake radiation). This refers to the differential acceleration through the nozzle of regions with differing density, and the associated acoustic pulse. A limitation of this analysis, if applied to real engines, is that the hot-spot is assumed to be fully correlated across the duct. In reality, this is not the case, as discussed in Section 3.4. The analysis gives an expression for the acoustic perturbation pressure which shows the acoustic signal strength increasing with increases in either area change across the contraction, density ratio (hot slug/cold gas), or mean flow pressure drop across the contraction.

P&WA Indirect Combustion Noise Prediction Model - The P&WA indirect combustion noise prediction model, presented by Pickett in Reference 8, utilizes an actuator disc assumption applied to each turbine blade or vane row. The following five equations are solved (subject to steady and unsteady jump conditions applied across the actuator disc) as the basis for the P&WA indirect combustion noise model.

62

1. Conservation of mass

2. Conservation of mementum

3. Conservation of energy

4. Equation of state

5. Second law of thermodynamics

Radiated noise intensity was found to depend on the change in pressure across the blade or vane row, and the amplitude and transverse correlation length scales of the hot-spots. Axial correlation length scales, together with the axial convection velocity, determine the frequency of noise generated.

Because the P&WA procedure allows the influence to be determined of the correlation length scales on indirect combustion noise levels and frequencies, and since, as mentioned above, this influence is large, the P&WA procedure was chosen for use in the current investigation (Section 4.4). The P&WA prediction model has been programmed for the IBM 360 computer. The required input includes turbine geometry and steady state performance information, together with the amplitude and correlation length scales (axial, radial and circumferential) of the hot-spots entering the turbine.

3.3 PROGRAM FOR EXPERIMENTAL VERIFICATION OF INDIRECT COMBUSTION NOISE MECHANISMS AND PREDICTIONS

Although several investigators have made attempts to predict indirect combustion noise, very little has been done to experimentally verify the existing prediction methods. This is largely due to:

1. The problem of distinguishing indirect combustion noise from direct combustion noise and other noise sources in a full scale engine.

2. The difficulties of simulating indirect combustion noise mechanisms in model tests. These difficulties arise from the problems associated with generating a temperature discontinuity in the flow upstream of a constriction, without also generating unwanted pressure and velocity perturbations.

A definite need therefore exists to verify both the existence of the indirect combustion noise mechanism and the accuracy of the methods used to predict the characteristics of this noise, so that its importance in full scale engines can be assessed. As part of the present investigation, an experimental rig was designed and built and a test program was defined and was to be run for the purpose of obtaining this verification. However, as the dominance of direct combustion noise became more apparent (see Section 4.5) during the course of the contract, the program was redirected so that additional work was performed in the area of direct combustion noise, and the indirect combustion noise verification tests were not conducted.

Details of the experimental rig and proposed test program description are given in Appendix D.

3.4   JT8D BURNER RIG MEASUREMENTS OF DYNAMIC TEMPERATURE

One objective of the combustion noise rig testing program at X-410 stand was to determine the dynamic temperature characteristics inside, and at the exit of a JT8D-type burner. The purpose of these measurements was to provide the inputs required to use the existing P&WA indirect combustion noise prediction model (summarized in Section 3.2) for the prediction of indirect combustion noise for the JT8D engine. The analysis of the thermodynamic data and the discussion of the results is addressed in this section. The use of these data to determine the required prediction inputs is discussed in Section 3.5.

3.4.1   Rig, Instrumentation and Data Acquisition

Measurements were made with sixteen quick-response thermocouple (QRTC) sensors located at two axial locations in the JT8D-17 production burner. The subject burner and instrumentation within the JT8D burner rig at X-410 stand is schematically shown in Figures 3.4-1 and 3.4-2. Four probes were installed, each having four temperature sensors. The sensors were standard .003 inch diameter thermocouples of platinum/platinum-10% rhodium (type S). The sensors were spaced evenly on the probes, 0.6 inches apart. These thermocouples and the associated frequency compensating electronics are similar to those developed and used by Dils[18] to make similar measurements of dynamic temperatures.

The characteristics of the temperature fluctuations leaving the burner and passing through the turbine pressure drop are required for prediction of indirect combustion noise. For this reason, three of the probes were mounted at the burner exit and the remaining probe was installed inside the burner nine inches from the fuel nozzle face; a short distance upstream from the dilution holes in the burner liner (see Figure 3.4-2).
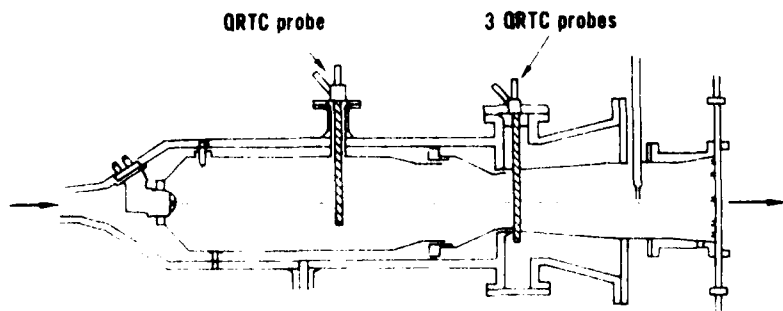
Figure 3.4-1   QRTC Probe Installation At X-410 Stand

Upstream location

Burner exit location
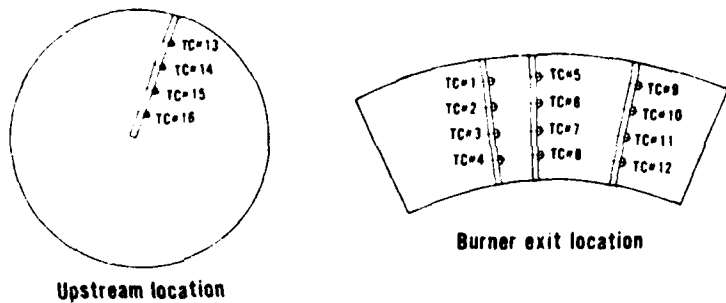
Figure 3.4-2   Cross Sectional Views of QRTC Probe Installation At X-410 Stand

Data were obtained and analyzed from a seven point test matrix that included independent variations in flow parameter, fuel-air ratio, and inlet temperature. The simulated approach power condition was represented in each of these independent variations.

The thermocouple signals were recorded on a Precision Instrument 2100 tape recorder and played back through a compensator circuit which adjusted the response of the system to be constant over the frequency range capability of the thermocouple system (i.e., 1 to 1000 Hz). This range includes the fluctuations of interest for combustion noise. The data was reduced in the form of auto-correlation, cross-correlation and spectral plots. In addition, root-mean-square (RMS) fluctuating temperature levels were obtained.

3.4.2   Test Results

The simulated approach condition was selected for the most detailed analysis because it was represented in each performance variation and also because it represents a condition where noise is of some concern. Thermocouples 3, 5, 6, 7, 8 and 11, shown in Figure 3.4-2, were selected for use in calculating the hot-spot characteristics at the burner exit. These thermocouples define both the radial and circumferential characteristics of the fluctuating temperature field. At the upstream location, sensors 13 through 16 were used to calculate the average RMS temperatures at this location. The temperature fluctuations in this region were found to increase from low RMS values at the center of the burner to high values at the outer wall. Turbulence measurements in this area (Appendix A) suggest unusual flow patterns and recirculation zones which could possibly explain the large variations in temperature fluctuations at the upstream location. At the burner exit, the burning is completed and the fluctuating temperature distribution is more uniform. The measured RMS temperature fluctuations appear to be generally lower than those observed by Dils[18]. The remainder of this section concentrates only on the data at the burner exit location.

65

3.4.2.1 RMS Fluctuating Temperatures

The variation of RMS temperature fluctuations with flow parameter (constant inlet temperature and fuel-air ratio) is plotted in Figure 3.4-3. The levels are seen to be essentially independent of the burner flow parameter.
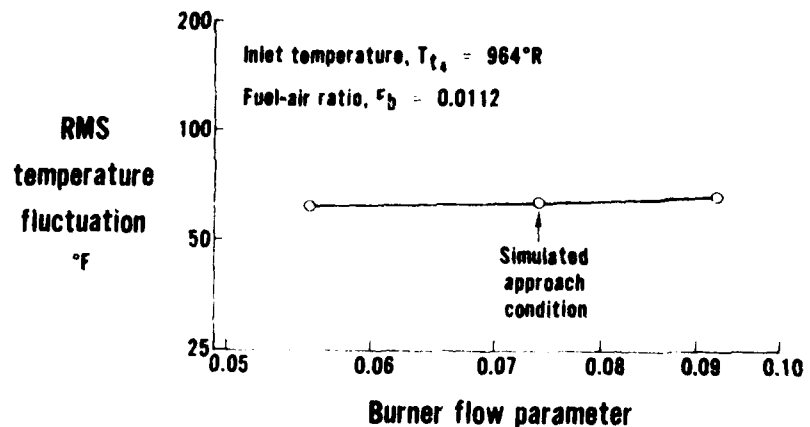
Figure 3.4-3   Variation of RMS Fluctuating Temperature With Flow Parameter At the Burner Exit

Figure 3.4-4 illustrates RMS temperature variations with fuel-air ratio at constant values of inlet temperature and flow parameter. The temperature fluctuations increase almost linearly with an increase of this parameter. This dependence is reasonable, since the higher heat release rates associated with higher fuel-air ratios should result in more unsteadiness.
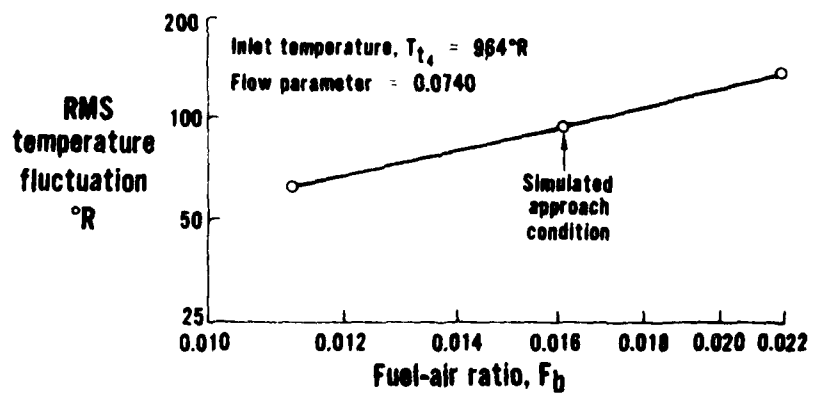
Figure 3.4-4   Variation of RMS Fluctuating Temperature With Fuel-Air Ratio At the Burner Exit

Figure 3.4-5 shows that RMS temperature fluctuations are not a strong function of inlet temperature, T_{t_4}. A change of only a few degrees RMS temperature occurs despite changes of inlet temperature from approximately 700° R to nearly 1300° R. Figures 3.4-? through 3.4-5 indicate that fluctuating temperatures are rather insensitive to flow parameter and inlet temperature, but are quite dependent upon the fuel-air ratio.
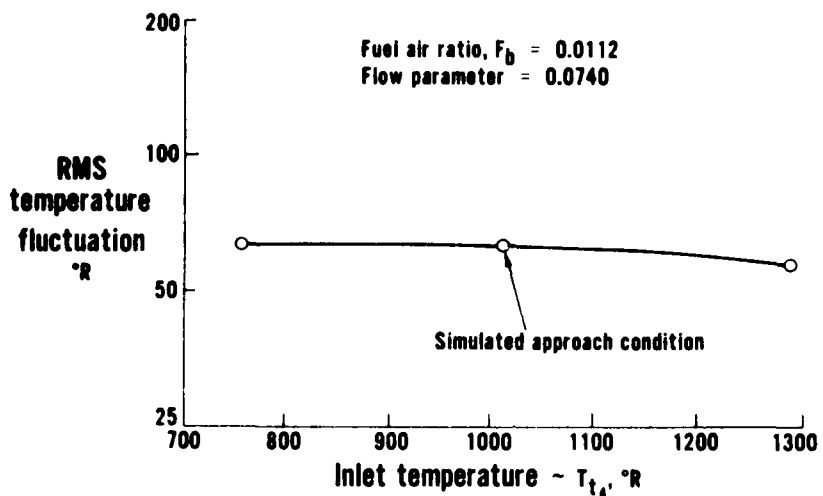
Figure 3.4-5   Variation of RMS Fluctuating Temperature With Inlet Temperature At the Burner Exit

3.4.2.2   Spectral Characteristics of Fluctuating Temperature

This section deals with the spectral analysis of the frequency compensated thermocouple signals at various JT8D-17 burner exit locations and test conditions. Figure 3.4-6 compares spectra at the simulated approach condition obtained at three circumferential locations of the same radius at the burner exit. The three spectra are nearly identical, each peaking at 500 Hz on a one-third octave band basis. A similar comparison of spectra in the circumferential direction obtained from the thermocouples 1, 5, and 9 at a different radial position showed very similar results.

Although no appreciable spectral change appears circumferentially, Figure 3.4-7 shows that changes occur in the radial direction. These spectra demonstrate a clear increase in fluctuations when traversing radially outward from thermocouple 8 to thermocouple 5. The shape of the spectra of Figure 3.4-7 are similar to those of Figure 3.4-6, peaking in the 500 Hz range.

67
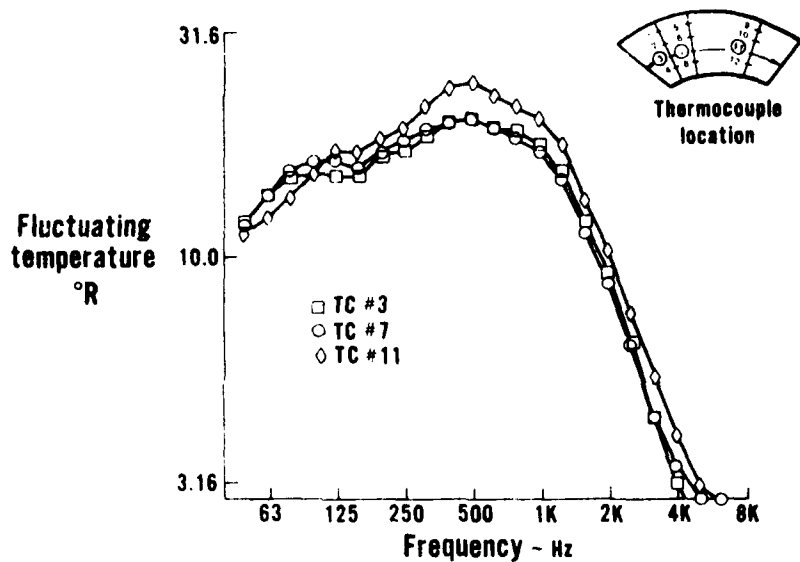
Figure 3.4-6   *Spectral Variation In the Circumferential Direction At the Burner Exit, Approach Condition*
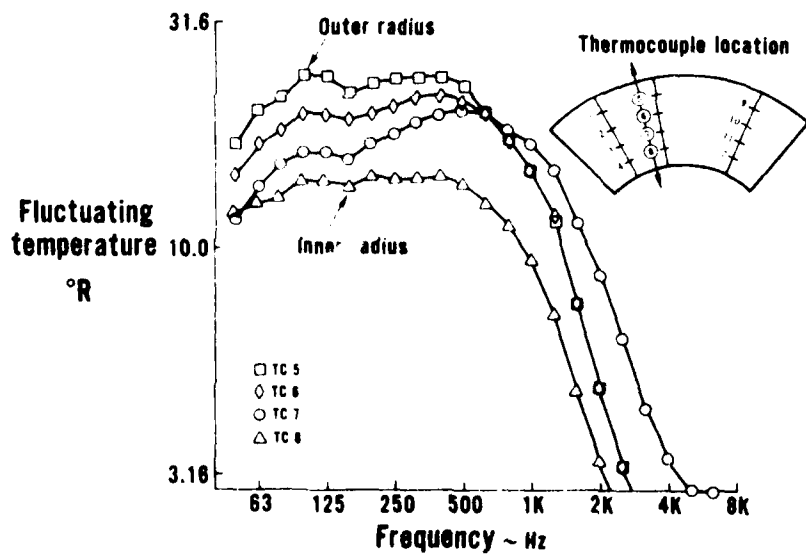
Figure 3 4-7   *Spectral Variation In the Radial Direction At the Burner Exit, Approach Condition*

The independent variation of spectral characteristics with different performance parameters is considered next. Figure 3.4-8 shows a comparison of three spectra measured near the center of the burner exit for three different values of flow

68

parameter (constant inlet temperature and fuel-air ratio). These spectra are nearly identical. Thus, in addition to the RMS fluctuations being insensitive to changes in flow parameter, the spectral distribution also appears to be insensitive to these variations.
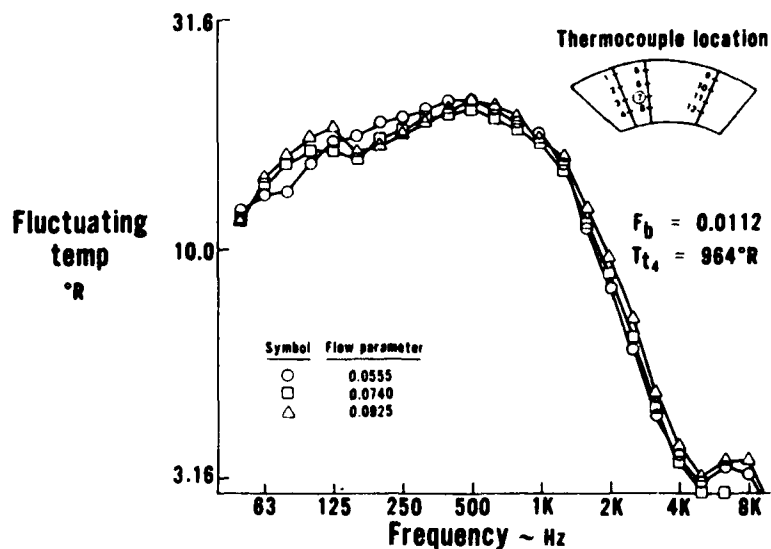
Figure 3.4-8   Variation of Fluctuating Temperature Spectra With Flow Parameter At the Burner Exit

Figure 3.4-9 shows spectra measured at constant flow parameter and inlet temperature, but three different fuel-air ratios. From Figure 3.4-4 it was shown that the RMS temperature increases with fuel-air ratio. Figure 3.4-9 shows that this increase is very uniform over all frequencies.
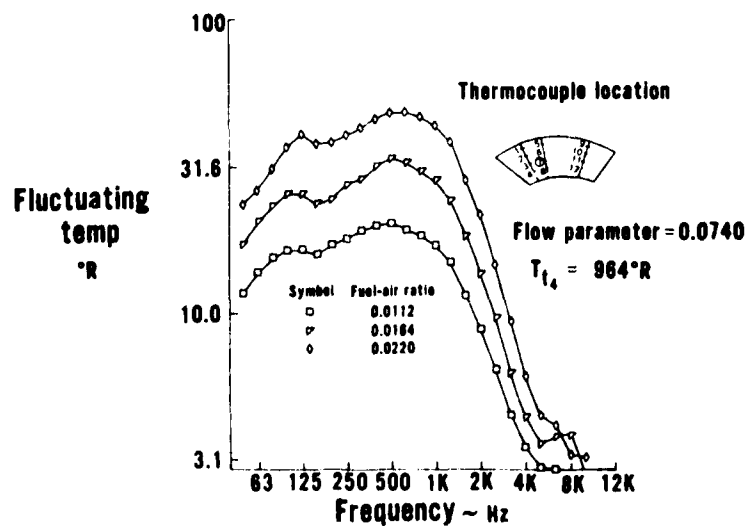
Figure 3.4-9   Variation of Fluctuating Temperature Spectra With Fuel-Air Ratio At the Burner Exit

The independent effects of inlet temperature is shown in Figure 3.4-10. Some small differences exist but the variation is only a few degrees, and is once again nearly constant for all freque.icies. Although a trend toward lower fluctuations is observed with increasing inlet temperature, the variation is quite small.

The analysis of spectra at all measurement locations and test conditions suggest a nearly constant spectral shape which peaks at about 500Hz, and decays sharply after 1000 Hz.
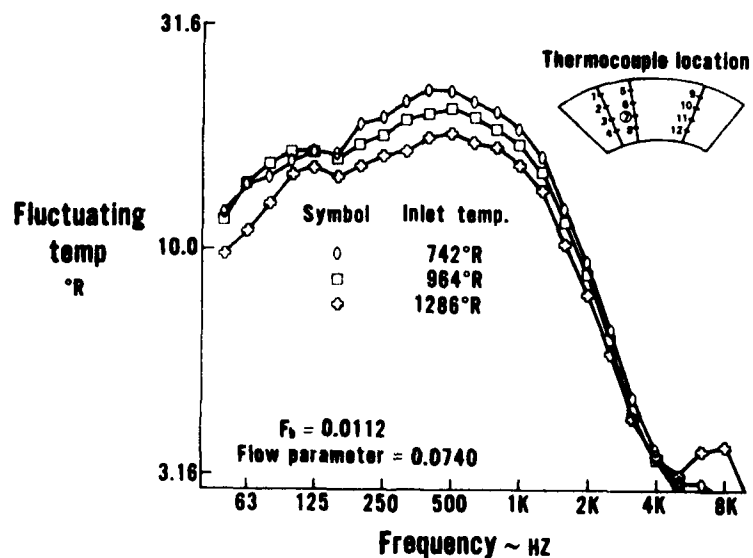
Figure 3.4-10 Variation of Fluctuating Temperature Spectra With Inlet Temperature At the Burner Exit

3.4.2.3   Correlation Length Scales

A significant number of signal auto and cross correlations of the temperature data were required to allow calculation of the axial and transverse correlation length scales of the hot-spots at the JT8D-17 combustor exit plane. Figure 3.4-11 illustrates the manner in which the axial correlation lengths of the hot-spots were calculated from the auto correlations of the thermocouple signals. Since the normalized correlation function follows a Gaussian distribution, the integral time scale, τ, is defined to be the time increment at which the function assumes the value of $1/e$. Multiplication of this time scale by the convection velocity in the axial direction provides the axial length of the correlated temperature region.
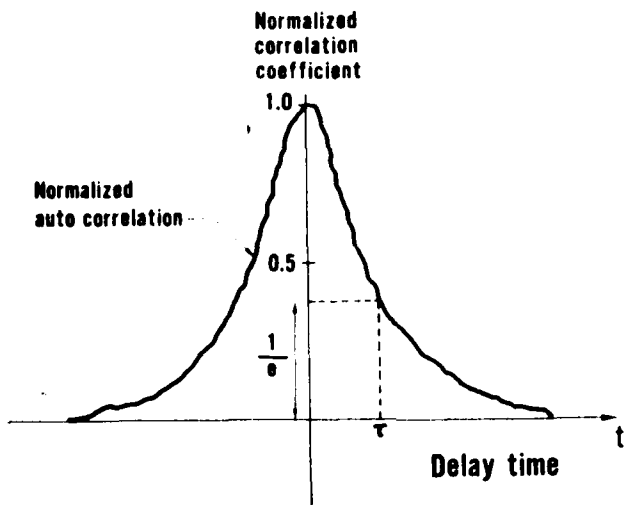
Figure 3.4-11 Determination of Hot-Spot Correlation Length Scales In the Axial Direction

Calculations of the hot-spot length scales in the radial and circumferential directions are performed in a different manner. These calculations require signal cross-correlation coefficients between two spacially separated thermocouples, in addition to the auto-correlation. Figure 3.4-12 illustrates the relationship between the auto-correlation of the signal from thermocouple number 8 (T.C. #8) and the normalized cross-correlation functions obtained by cross-correlating the signal from thermocouple number 8 with other thermocouples in the radial direction. Each function shown on Figure 3.4-12 is symetrical and peaks at zero delay time indicating a lack of skewness of the hot-spots as they convect through the burner exit.
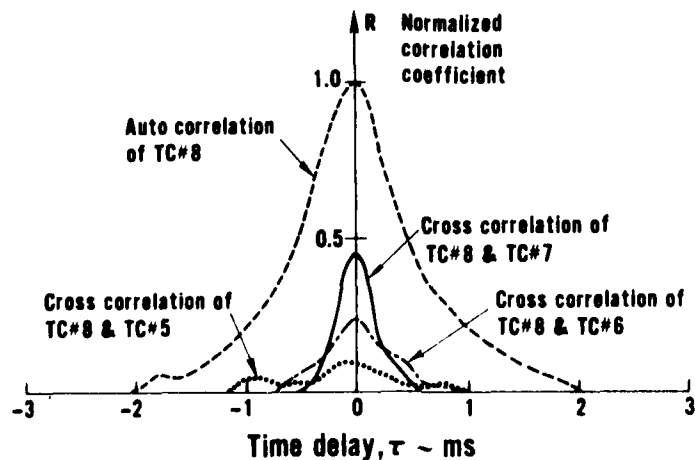
Figure 3.4-12 Relationship of Correlation Data In Radial Direction, Simulated Approach Condition

71

The transverse hot-spot length scales are determined by plotting the peak correlation coefficients of Figure 3.4-12 as a function of separation distance as shown in Figure 3.4-13. From the Gaussian distribution shown in Figure 3.4-13, the correlation length scales are found in a manner similar to that used to determine the axial length scales. The procedure illustrated in Figures 3.4-12 and 3.4-13 was used for calculation of length scales in both the radial and circumferential directions.
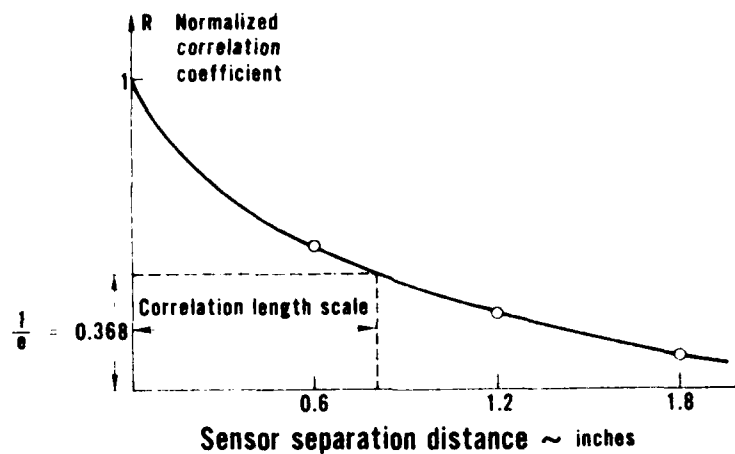
Figure 3.4-13   Determination of Correlation Length Scales In Radial and Circumferential Direction

Figures 3.4-14 through 3.4-16 are plots of the correlation length scales versus the three independent performance parameters. The correlation length in the axial direction is always the longest, and the correlation length in the radial direction is always the shortest. The overall variation of correlation length is not large. Figure 3.4-14 indicates an increase in the length scales in all directions when the flow parameter is increased. Very little variation occurs with changing fuel-air ratio, as shown in Figure 3.4-15, and a slight decrease in correlation lengths occur with increasing inlet temperature as shown in Figure 3.4-16. Throughout the range of operating conditions, the correlation length scales at the burner exit were between 0.60 and 2.5 inches. The most erratic variation occurred in the circumferential direction. Typically, the correlated regions at the burner exit were approximately 2.5 inches long in the axial direction, 0.75 inches in the radial direction and 1.75 inches in the circumferential direction.
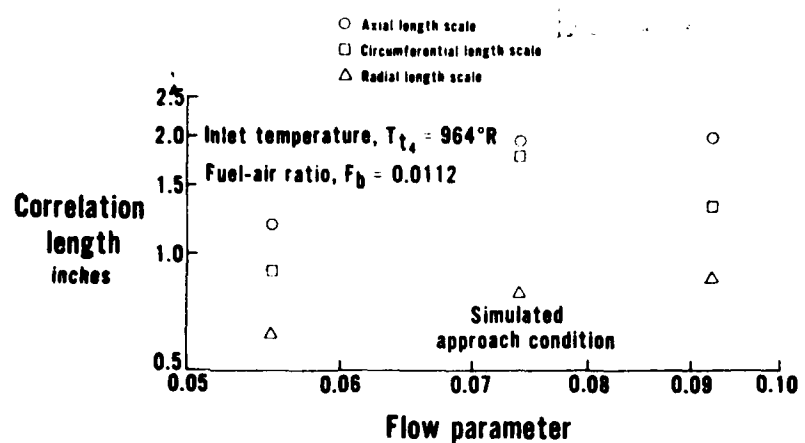
Figure 3.4-14   Variation of Hot-Spot Length Scales With Flow Parameter
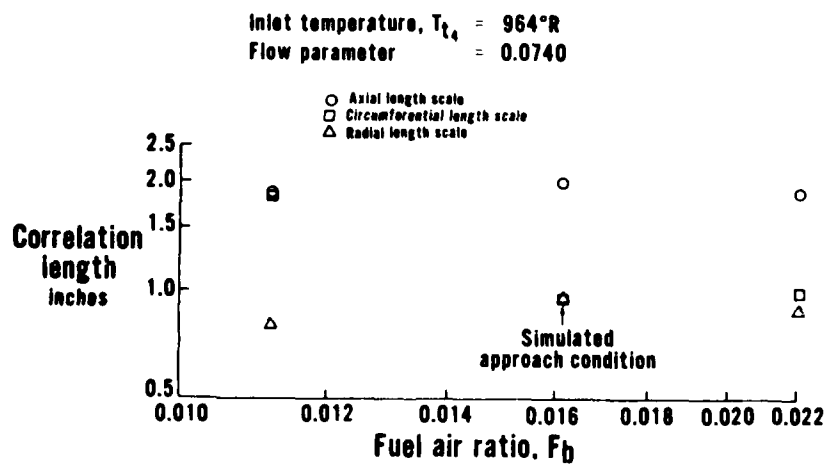
Figure 3.4-15   Variation of Hot-Spot Length Scales With Fuel-Air Ratio

Figure 3.4-16   Variation of Hot-Spot Length Scales With Inlet Temperature

73
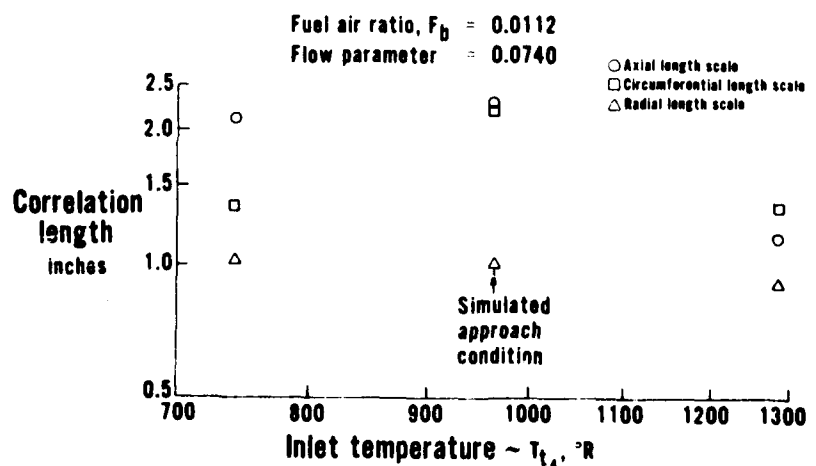
3.5 CORRELATIONS OF JT8D HOT-SPOT CHARACTERISTICS

The P&WA indirect combustion noise model indicates that acoustic signals associated with unsteady temperatures convecting through the turbine are highly dependent on the amplitude and correlation length scales of the fluctuations. The model requires these amplitudes in degrees RMS and length scales (in all three directions) as input, in addition to pertinent turbine performance information. The required turbine performance information is frequently available for a specific engine, but details of the temperature inhomogeneities convecting from the burner to the turbine are not generally known. For this reason the results of the dynamic temperature measurements discussed in Section 3.4 were correlated with burner performance data to determine a set of empirical equations that describe the temperature inhomogeneities at the burner exit in terms of independent burner operating parameters. These correlations are presented in this section.

3.5.1 RMS Fluctuating Temperatures

It was shown in Section 3.4 that RMS fluctuating temperatures at the exit of the JT8D-17 production burner were essentially independent of burner flow parameter and inlet temperature and depend primarily upon the fuel-air ratio, F_b. Figure 3.5-1 indicates that RMS temperatures are linearly dependent upon fuel-air ratio. This direct proportionality results in the following relationship

$$T_{RMS} = 5900 \, F_b \sim {}^\circ R \tag{33}$$

where T_{RMS} is the RMS fluctuating temperature of the hot-spot in degrees Rankine. The fuel-air ratio is approximately proportional to the temperature rise across the burner, i.e.,

$$F_b \sim \frac{c_p \, (T_{t_5} - T_{t_4})}{H_f} \tag{34}$$
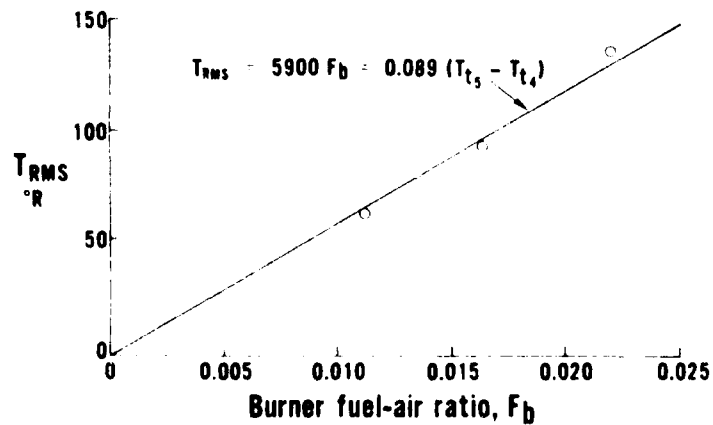
Figure 3.5-1 *Correlation of Hot-Spot RMS Temperature Fluctuations At the Exit of the JT8D-17 Burner*

Using typical values of c_p and fuel heating value, H_f, the relationship between temperature fluctuations and burner temperature rise may be written as

$$T_{RMS} = 0.089 \, (T_{t_5} - T_{t_4}) \tag{35}$$

The RMS temperature fluctuations are, therefore, equal to approximately 9% of the temperature rise across the burner. Although the current rig tests were conducted at constant pressure, similar measurements in high pressure rig[21] and in full scale engines[1] do not indicate that the burner pressure exerts a strong influence on the dynamic temperature characteristics at the burner exit.

3.5.2 Dynamic Temperature Spectrum

The spectral shape of the fluctuating temperature was found in Section 3.4 to be nearly constant for all performance conditions, and always peaked near 500 Hz. Figure 3.5-2 shows the suggested fluctuating temperature spectrum which represents an average of those measured.
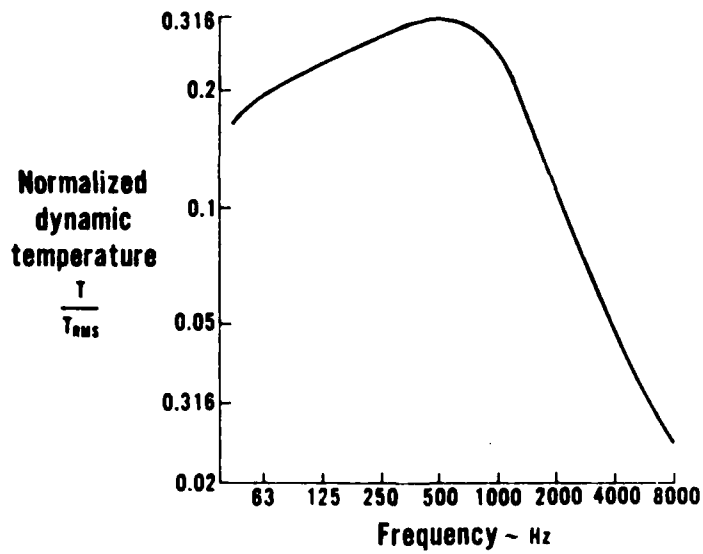
Figure 3.5-2 One-Third Octave Spectrum for Temperature Fluctuations At the Exit of the JTSD-17 Burner

3.5.3 Correlation Length Scales

It was also found in Section 3.4 that correlation length scales were independent of burner inlet temperature and fuel-air ratio, but were approximately proportional to the burner flow parameter. A plot of correlation length scales versus flow parameter is shown in Figure 3.5-3, together with the lines of proportionality which

75

best fit the data. The direct proportionality of L_x with flow parameter is not surprising since the finding of constant peak frequency requires such a relationship. The resulting equations which govern the hot-spot correlation lengths for the JT8D-17 burner, as determined from Figure 3.5-3, are:

$$L_x = 22.2 \frac{w_{a_b} \sqrt{T_{t_4}}}{p_{t_4} A_b}$$

$$L_\theta = 17.5 \frac{w_{a_b} \sqrt{T_{t_4}}}{p_{t_4} A_b} \tag{36}$$

$$L_R = 10.0 \frac{w_{a_b} \sqrt{T_{t_4}}}{p_{t_4} A_b}$$

where the correlation lengths are given in inches.
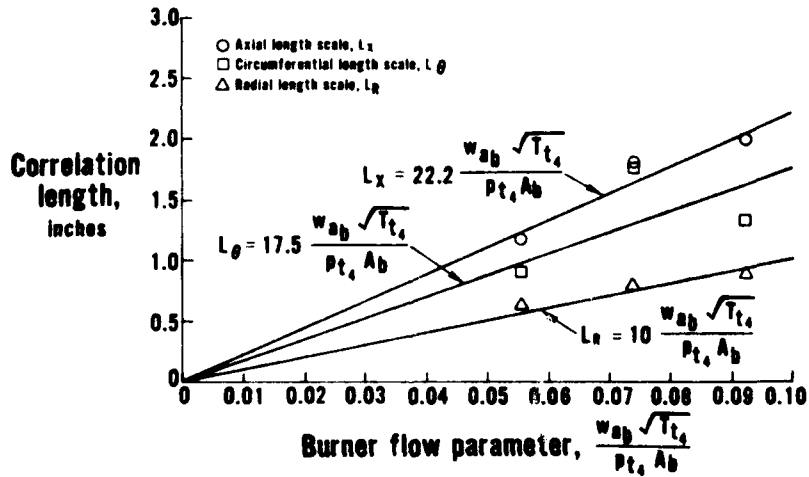
Figure 3.5-3 *Correlation of Hot-Spot Length Scales At Exit of the JT8D-17 Burner*

These correlations were used to define the correlation length scales and the RMS amplitude of the temperature fluctuations for the JT8D-109 engine so that predictions of indirect combustion noise could be made. These predictions are discussed in Section 4.4, where an evaluation of the importance of indirect combustion noise is discussed for the JT8D-109 engine.

4.0 ENGINE COMBUSTION NOISE INVESTIGATION

In this section, internal dynamic pressure and farfield combustion noise data are presented for four P&WA turbofan engines. These engines (i.e., JT8D-109, JT9D-7A, JT9D-70 and prototype JT10D) include both low and high bypass ratio designs with annular and can-type burners, together with P&WA's most advanced prototype high bypass ratio engine. The internal data is used to demonstrate that combustion noise is the dominant source of core engine noise. In addition, the prediction systems for direct and indirect combustion noise, described in the preceding sections, are evaluated by comparing with the farfield data, and the dominant combustion noise mechanism is identified. Next, an analytical model is presented for predicting the combustion noise transmission losses that occur across the turbine. This model is evaluated by comparing data from isolated burner rigs with combustion noise data from full scale engines.

Finally, a summary of the final combustion noise prediction model is presented, a sample application is discussed, and the parameters that control combustion noise are identified.

4.1   DESCRIPTION OF P&WA ENGINES AND NOISE TEST FACILITY

The four P&WA engines discussed in this section were tested at P&WA's X-314 outdoor noise test stand, shown in Figure 4.1-1 and described in Reference 22. Noise measurements at this test stand may be obtained using either elevated or ground plane microphones. Since combustion noise occurs primarily at frequencies below several thousand Hz, ground plane microphones mounted 1/2-inch above a hard asphalt surface were used, which eliminate spectral distortions due to ground reflection effects. Freefield definitions were obtained from the measured data by subtracting 6.0 dB from the measured spectra. An illustration of the test stand, showing the microphone locations is presented in Figure 4.1-2.
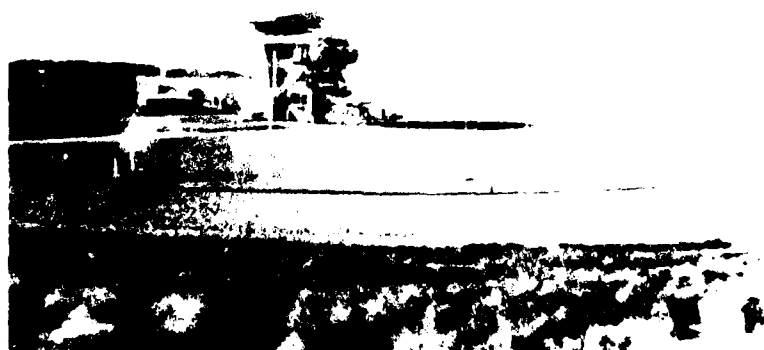
Figure 4.1-1   P&WA Outdoor Engine Noise Test Facility

	Microphone data	
	Ground level	Elevated
No. of microphones	7	20
Height (ft)	—	16 (at engine ₵)
Field surface	Asphalt	Crushed stone
Radial distance from engine (ft)	150	150
Spacing (deg)	10	5 and 10
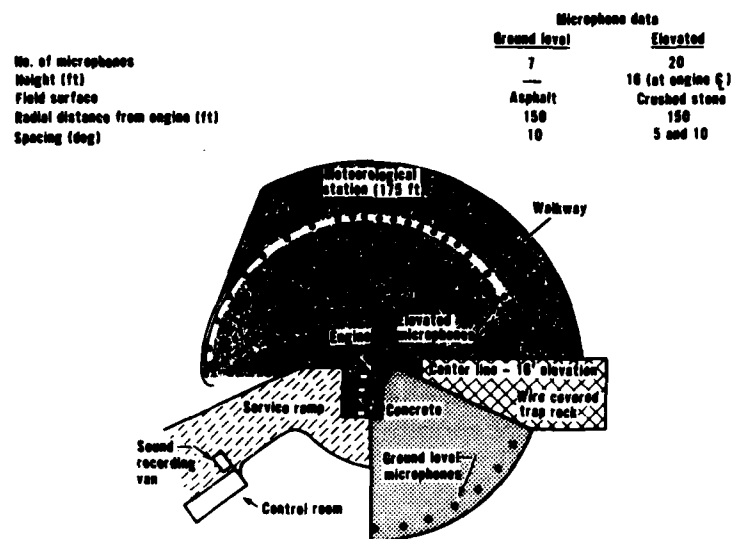
Figure 4.1-2   X-314 Outdoor Noise Stand

The JT8D-109 engine is shown in Figure 4.1-3 installed at X-314 test stand.
This engine was configured with a forced mixer which mixes the high velocity
primary airflow with the slower velocity fan airflow, thereby reducing the jet
noise levels and enabling a clear combustion noise definition to be obtained
over a large range of thrust levels. The JT8D-109 engine contains nine separate
burner cans (identical to the JT8D-9 burner tested in separate rig tests), one of
which is shown in Figure 4.1-4.
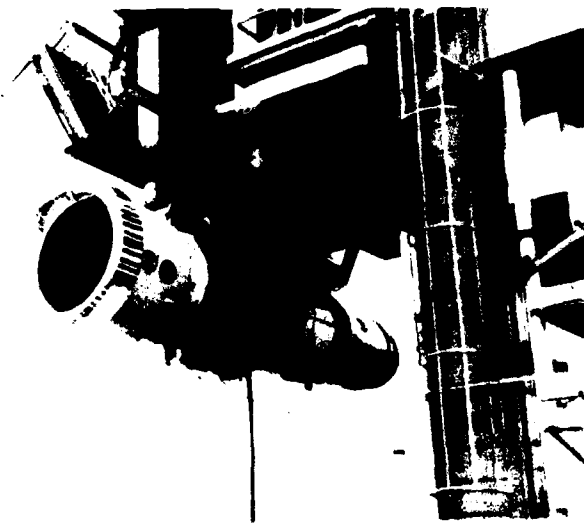
Figure 4.1-3   JT8D-109 Mounted At X-314 Stand

78

Pressure atomizing
fuel nozzle (1 per can)

Turbine
entrance
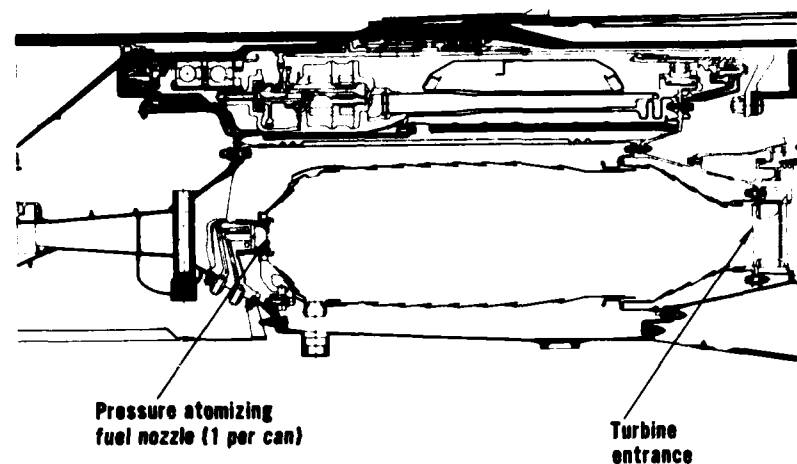
Figure 4.1-4   Cross-Section of JT8D-109 Burner

The JT9D-7A engine is shown in Figure 4.1-5 mounted at X-314 test stand.
This engine has an annular type burner with 20 fuel nozzles, as shown in
Figure 4.1-6.
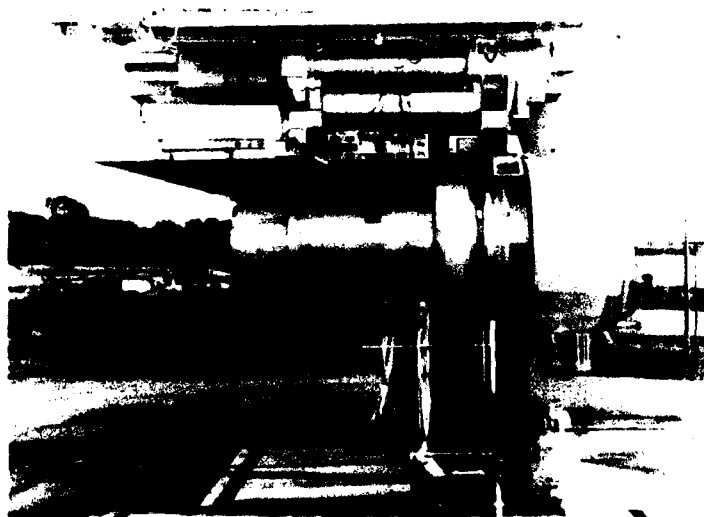
Figure 4.1-5   JT9D-7A Mounted At X-314 Stand

79

Pressure atomizing fuel nozzles (20)

Turbine entrance
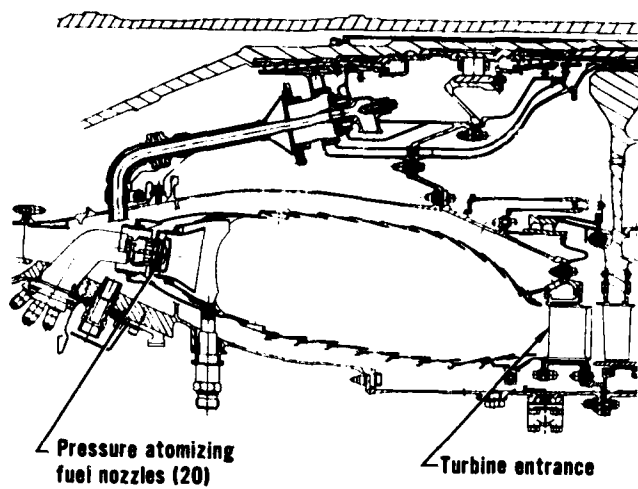
Figure 4.1-6   Cross-Section of JT9D-7A Burner

The JT9D-70 engine is shown in Figure 4.1-7 mounted at X-314 stand. This engine incorporates an annular type burner, also with 20 fuel nozzles. A sketch of the JT9D-70 burner with its bulkhead front end is presented in Figure 4.1-8. This burner is somewhat shorter than the JT9D-7A burner.
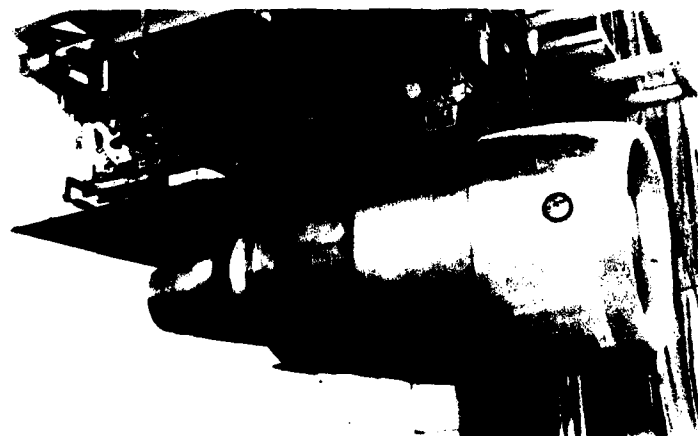
Figure 4.1-7   JT9D-70 Mounted At X-314 Stand
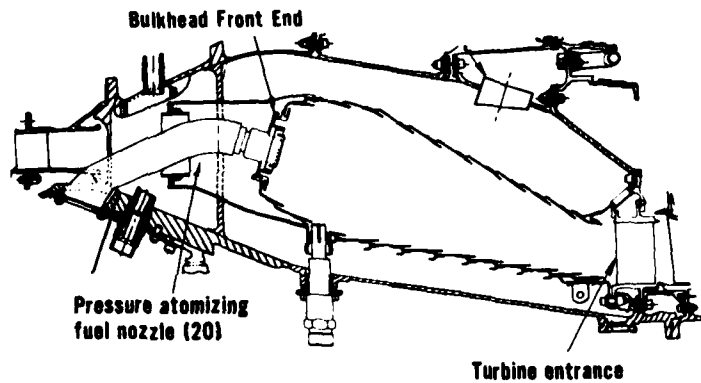
Figure 4.1-8   Cross-Section of JT9D-70 Burner

The JT10D (prototype) engine is shown in Figure 4.1-9 mounted at X-314 test stand. The test configuration included a treated fan inlet, and fan exit flow diverter ducts, the purpose of which were to isolate the combustion noise from other engine noise sources. The JT10D-prototype burner, shown in Figure 4.1-10 is annular and contains 12 primary and 36 secondary fuel nozzles. The fuel and air are premixed and prevaporized prior to entering the burning region.
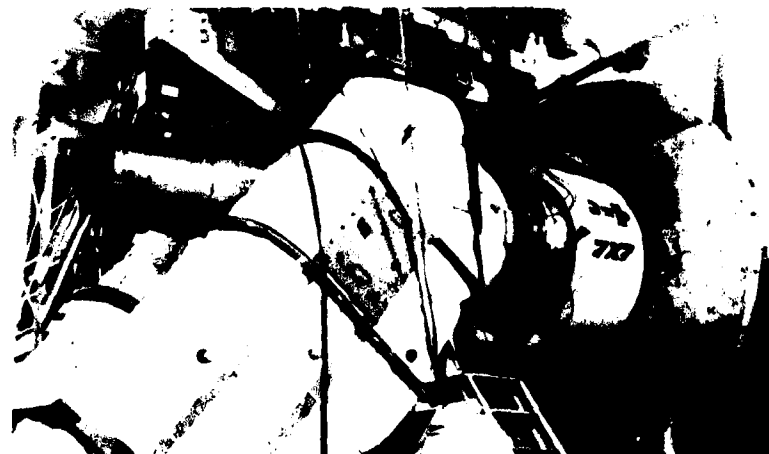
Figure 4.1-9   JT10D Prototype Engine Mounted At X-314 Stand

81
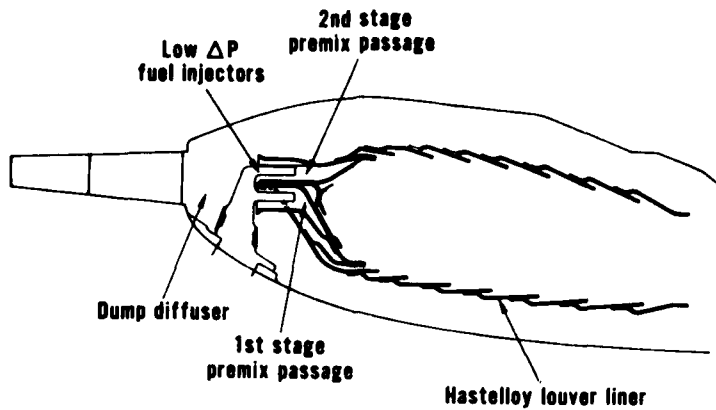
Figure 4.1-10   JT10D Premix Burner

4.2   SUMMARY OF ENGINE COMBUSTION NOISE DATA

Combustion noise characteristics (including combustion noise spectra,
directivities and overall acoustic power levels) from farfield measurements are
presented in this section for the P&WA JT8D-109, JT9D-7A, JT9D-70 and
prototype JT10D engines. These farfield noise characteristics were determined
after the jet noise spectra for each engine were defined for each condition and
angle and subtracted from the total low frequency noise spectra. Internal
dynamic pressure data from two engines (JT8D-109 and JT9D-7A) recorded
inside the burners and at selected locations downstream in the exhaust ducts
are also presented. The internal dynamic pressure measurements from the
JT8D-109 engine were recorded simultaneously with farfield signals. Results
from cross-correlations of internal and farfield signals are also discussed, which
show that the combustor is the source of low frequency core noise.

4.2.1   Farfield Noise Characteristics

4.2.1.1   JT8D-109 Engine

Figure 4.2-1 shows several farfield measured spectra, typical of those used to
define the combustion noise characteristics of the JT8D-109 engine. The nor-
malized 1/3-octave band combustion noise spectra shape, derived by examina-
tion of many measured spectra, is shown in Figure 4.2-2 and is centered around
the 400 Hz 1/3 octave band. This spectra shape was found to change very little
with either angular location or engine speed. This combustion noise spectrum
shape was next combined with both the predicted jet noise and the measured
spectra to define the level of combustion noise, an example of which is shown
in Figure 4.2-3. Combustion noise levels were determined in this manner for
each farfield angular location and engine test condition. From the combustion
noise levels at each angle, a general normalized directivity pattern was derived
for the JT8D-109 engine and is presented in Figure 4.2-4.

82
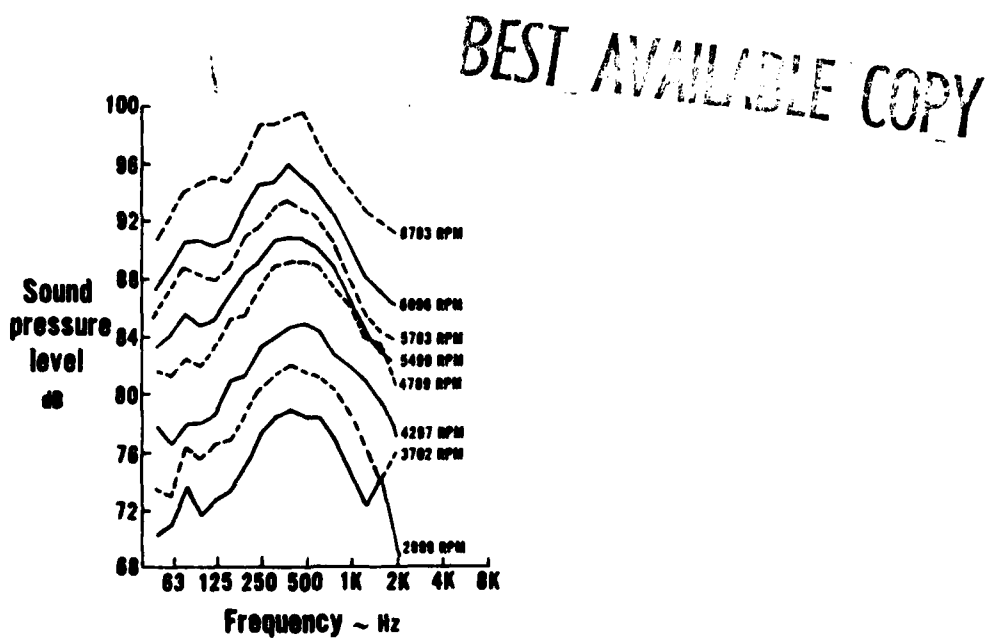
Figure 4.2-1 Typical Measured Spectra for the JT8D-109 Engine, 120° Farfield Location, 150 foot radius
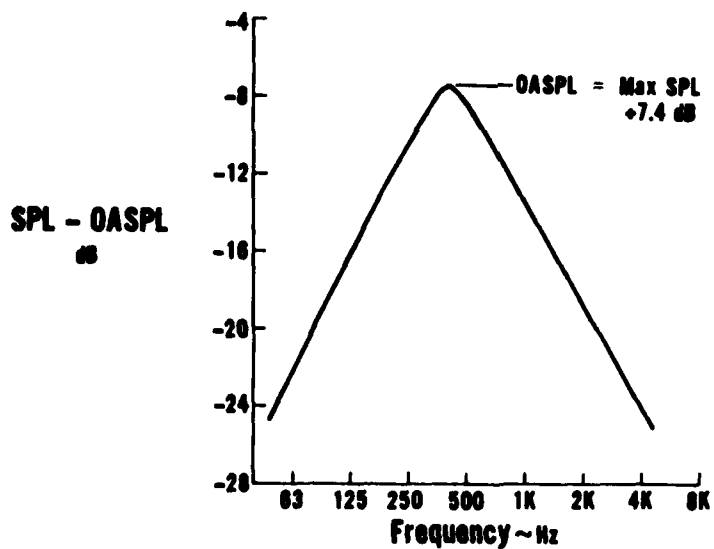
Figure 4.2-2 JT8D-109 Combustion Noise Spectral Definition

83
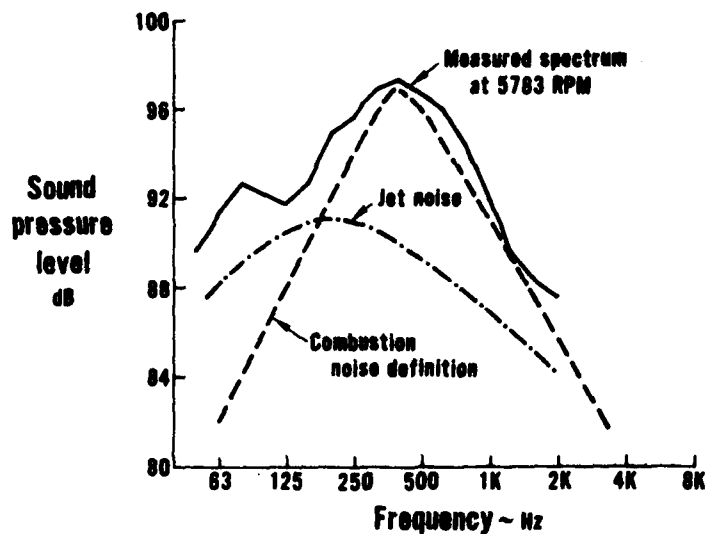
Figure 4.2-3   JT8D-109 Combustion Noise Spectral Definition Compared to Measured Data, 120° Farfield Location, 150 Foot Radius
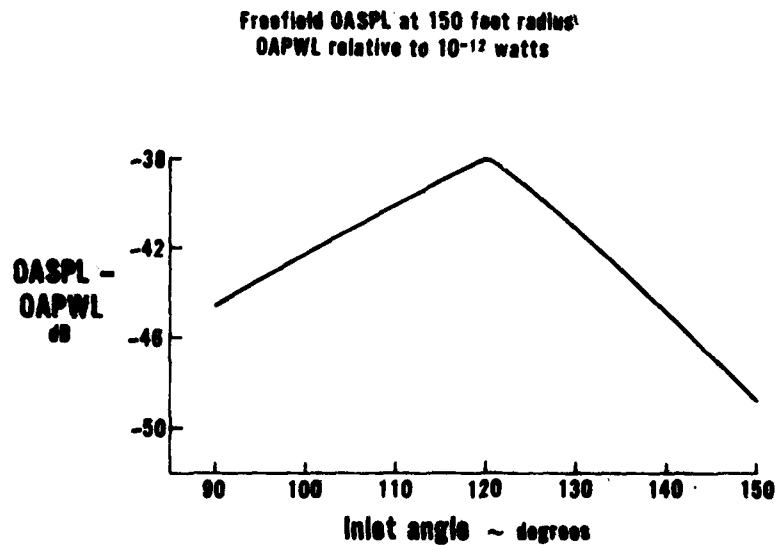
Figure 4.2-4   JT8D-109 Combustion Noise Directivity

The acoustic power levels (OAPWL) at each engine test condition were determined by numerically integrating the combustion noise over all frequencies and farfield angles (using the spectral and directivity characteristics of Figures 4.2-2 and 4.2-4) and are presented in Table 2.4-1.

84

TABLE 4.2-1

JT8D-109 COMBUSTION NOISE POWER LEVELS

Engine RPM (N_1)	Combustion Noise OAPWL (ref 10^{-12} watts) dB
2999	123.6
3702	126.6
4297	129.1
4789	131.8
5199	133.6
5499	135.1
5783	136.8
6096	138.9
6414	141.6
6798	142.6
7427	144.2
7669	145.4

4.2.1.2   JT9D-7A Engine

Typical farfield measured spectra at several JT9D-7A engine test conditions
are shown in Figure 4.2-5 for the 120 degree measurement location. The com-
bustion noise spectra shape was defined after examination of many measured
spectra, primarily at the low engine speed conditions where the jet noise levels
were low. Figure 4.2-6, shows the resulting JT9D-7A combustion noise spectral
definition. The peak frequency was consistently between the 250 and 315 Hz
1/3 octave bands.
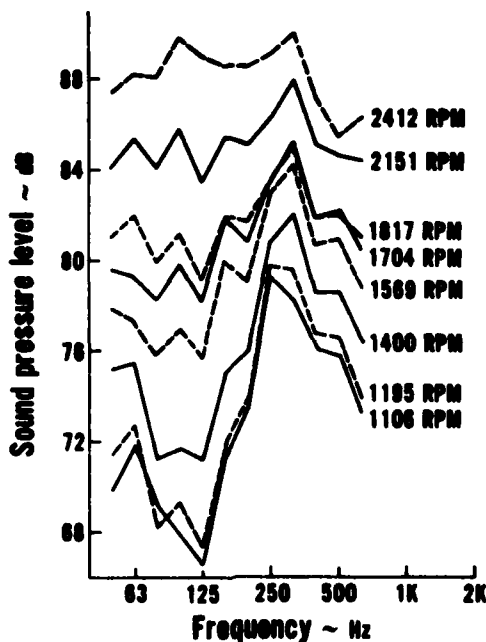
Figure 4.2-5   *Typical Measured Spectra for the JT9D-7A Engine, 120° Farfield Location,*
150 Foot Radius
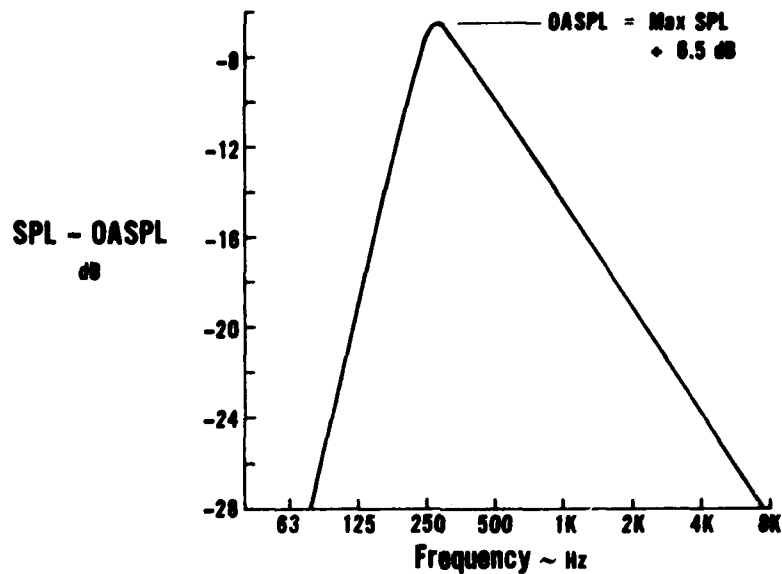
Figure 4.2-6   JT9D-7A Combustion Noise Spectral Definition

In a manner similar to that used for the JT8D-109, the combustion noise
spectral definition was used in conjunction with jet noise predictions to deter-
mine the combustion noise levels for each farfield location and engine condi-
tion as illustrated in Figure 4.2-7. These levels were then used to identify the
combustion noise directivity characteristics for the JT9D-7A engine, which are
shown in Figure 4.2-8. The directivity pattern was observed to narrow as the
engine RPM increased and therefore three directivities are shown. These direc-
tivities correspond to RPM's equal to or below 1400, between 1400 and 2100,
and equal to or greater than 2100. One likely explanation for this change in
directivity is the differences in the refraction of acoustic waves that occur
with increases in primary exit velocity or temperature. This trend has been
noted previously in the directivity patterns from the JT8D component burner
tests at X-410 Stand (Section 2.3.5).

Acoustic OAPWL's at each engine test condition were determined by
numerically integrating the combustion noise over all frequencies and farfield
angles and are tabulated in Table 4.2-2.

86
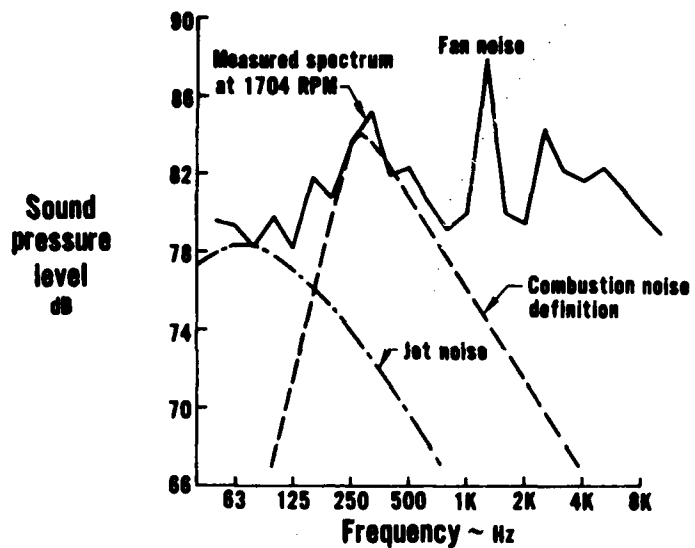
Figure 4.2-7   JT9D-7A Combustion Noise Spectral Definition Compared to Measured Data, 120° Farfield Location, 150 Foot Radius
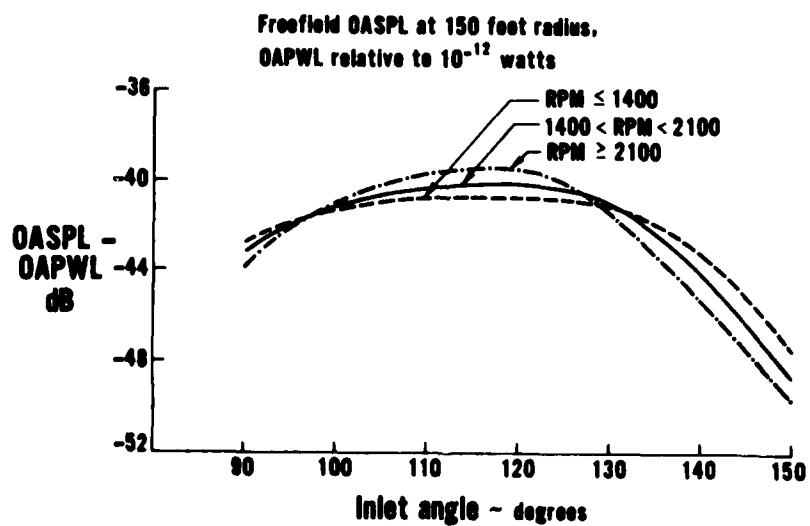
Figure 4.2-8   JT9D-7A Combustion Noise Directivity

TABLE 4.2-2

JT9D-7A COMBUSTION NOISE POWER LEVELS

Engine RPM (N_1)	Combustion Noise OAPWL (ref 10^{-12} watts) dB
1106	125.8
1195	127.0
1400	128.4
1569	130.0
1704	130.6
1817	131.1
2151	132.7
2412	133.9

4.2.1.3   JT9D-70 Engine

Measured spectra from the 120 degree farfield location are presented in Figure 4.2-9 for three JT9D-70 engine test conditions. The combustion noise is clearly visible in the measured spectra only at these low engine speeds. Figure 4.2-10 shows the derived combustion noise spectral definition which was found to change very little with farfield location or engine speed. The combustion noise peak frequency was between the 315 and 400 Hz 1/3 octave bands.
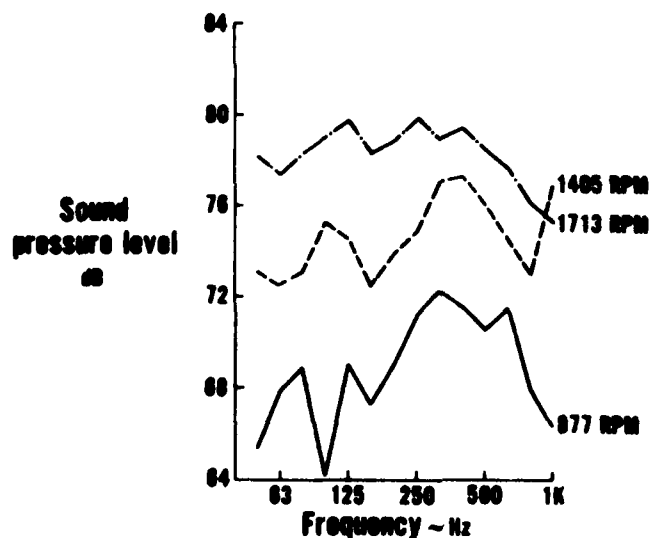
Figure 4.2-9   *Typical Measured Spectra for the JT9D-70 Engine, 120° Farfield Location, 150 Foot Radius*

88
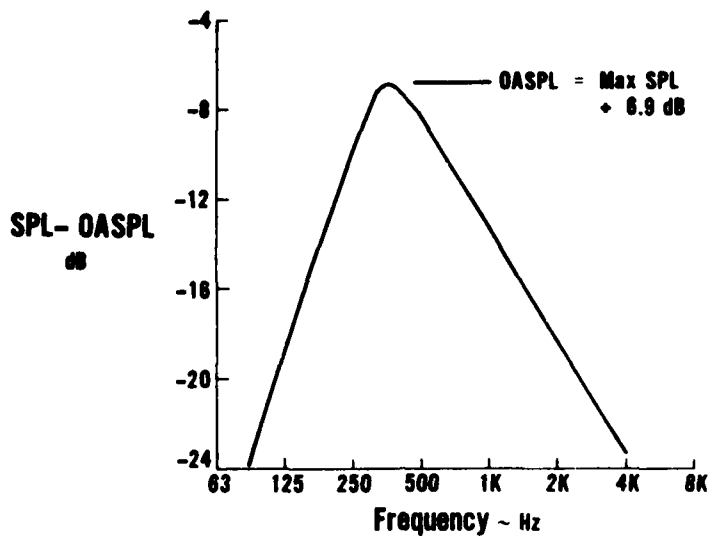
Figure 4.2-10   JT9D-70 Combustion Noise Spectral Definition

The combustion noise spectral definition together with the jet noise predictions were used to determine the combustion noise levels at all angles. A typical example is shown in Figure 4.2-11. Analysis of the data at angles ranging from 90 to 150 degrees indicated a directivity change with engine test condition. Three directivities were selected to define the farfield noise characteristics as shown in Figure 4.2-12. The changes in directivity are similar to those shown in Figure 4.2-8 for the JT9D-7A engine.
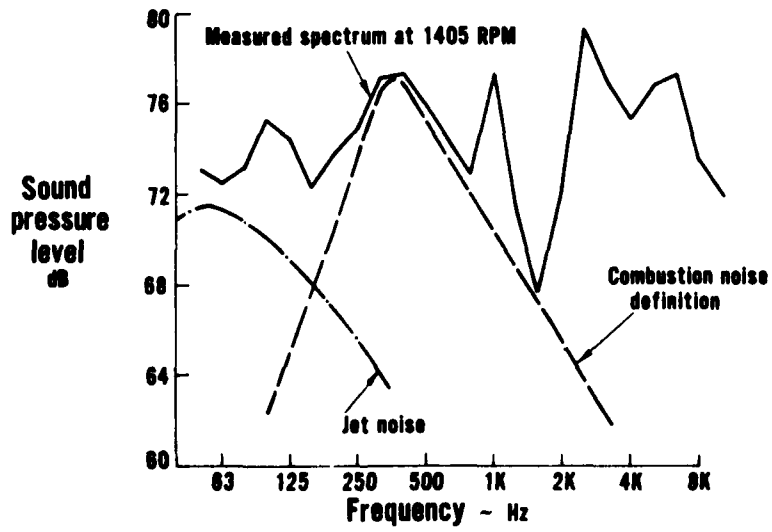
Figure 4.2-11   JT9D-70 Combustion Noise Spectral Definition Compared to Measured Data, 120° Farfield Location, 150 Foot Radius

89

Freefield OASPL at 150 feet radius
OAPWL relative to 10^{-12} watts
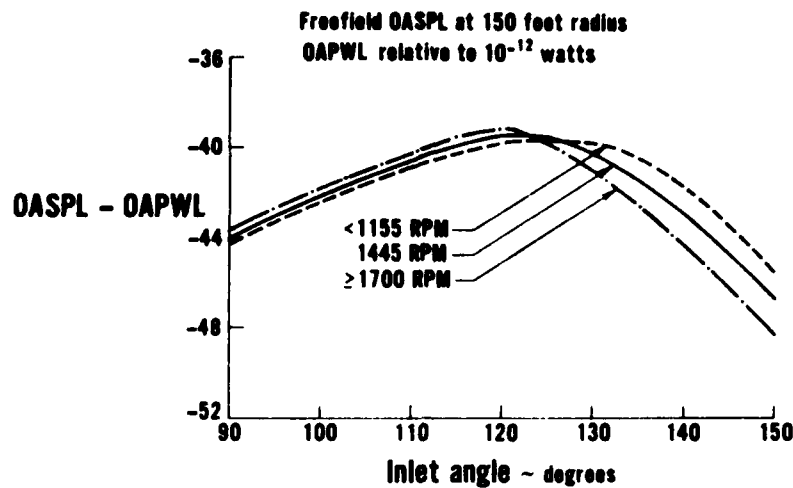
Figure 4.2-12   JT9D-70 Combustion Noise Directivity

OAPWL's were calculated for three low engine thrust conditions by numerically integrating the combustion noise over all frequencies and angles, and are shown in Table 4.2-3.

TABLE 4.2-3

JT9D-70 COMBUSTION NOISE POWER LEVELS

Engine RPM (N_1)	Combustion Noise OAPWL (ref. 10^{-12} watts) dB
877	119.0
1405	123.7
1713	125.1

4.2.1.4   JT10D Prototype Engine

Measured 1/3 octave band spectra at the 120 degree farfield location are presented in Figure 4.2-13 for the JT10D prototype engine at four low power conditions. The 160 Hz peak evident in the spectra is a tone, the frequency of which is related to 1 revolution of the high spool rotor. This tone is unrelated to the combustion process, and was therefore removed in the analysis of the data. The combustion noise spectral definition was obtained from measured data at low engine thrust conditions and is shown in Figure 4.2-14 where the peak frequency is seen to be centered around the 500 Hz 1/3 octave band.

90
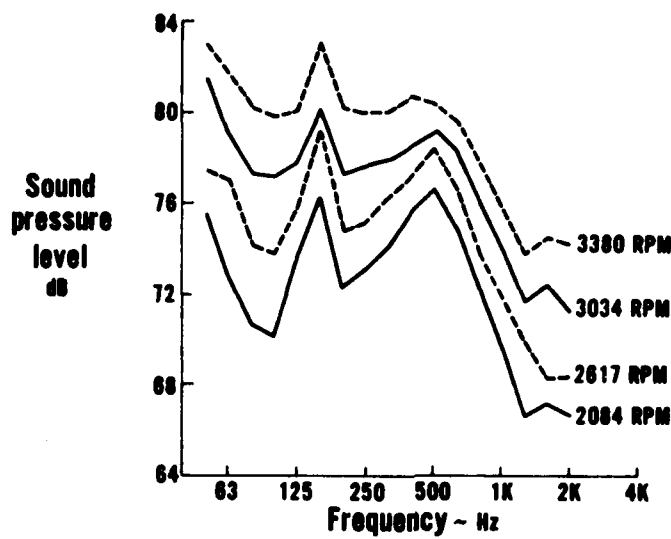
Figure 4.2-13   Typical Measured Spectra for JT10D Prototype Engine, 120° Farfield Location, 150 Foot Radius
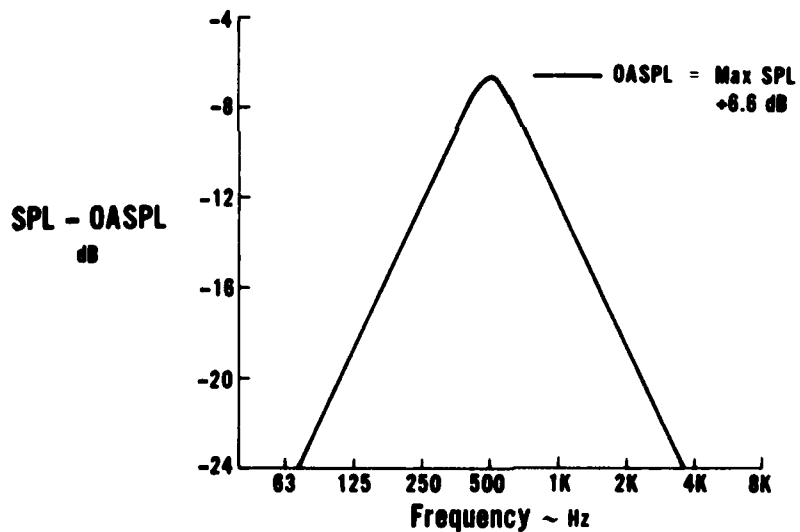
Figure 4.2-14   JT10D Prototype Combustion Noise Spectral Definition

The combustion noise spectral definition, together with jet noise predictions, were used to determine the combustion noise levels at each farfield location and engine test condition, as illustrated in Figure 4.2-15. Figure 4.2-16 shows the directivity pattern obtained from the farfield noise data. The pattern was found to be fairly constant for the four test conditions considered.

91
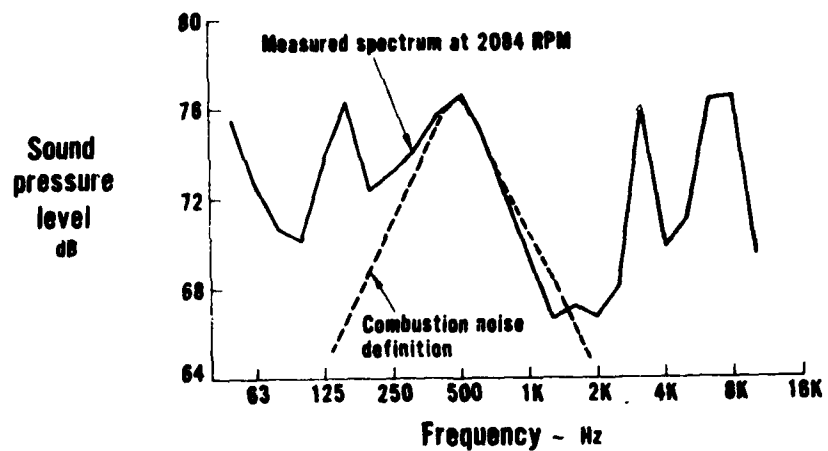
Figure 4.2-15 *JT10D Prototype Combustion Noise Spectral Definition Compared to Measured Data, 120° Farfield Location, 150 Foot Radius*
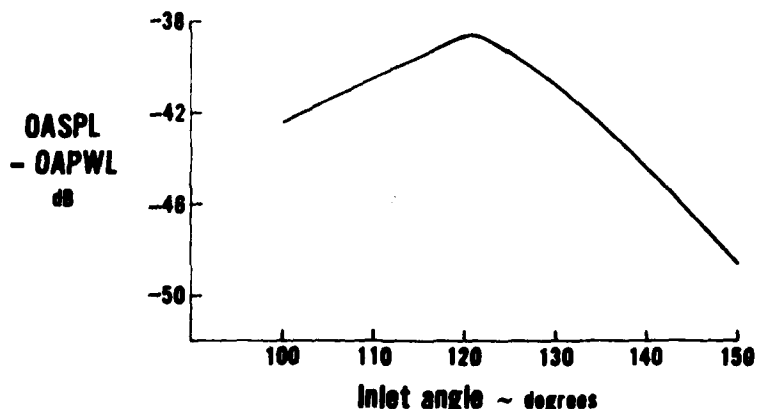
Figure 4.2-16 *JT10D Prototype Combustion Noise Directivity*

OAPWL's were calculated for four engine speeds by numerically integrating the combustion noise over all frequencies and farfield angles and are tabulated in Table 4.2-4.

TABLE 4.2-4

JT10D PROTOTYPE COMBUSTION NOISE POWER LEVELS

Engine RPM (N_1)	Combustion Noise OAPWL (ref. 10^{-12} watts) dB
2084	121.6
2617	122.9
3034	123.7
3380	124.5

92

4.2.2   Internal Dynamic Pressure Data

Internal data from two engines (JT8D-109 and JT9D-7) were obtained inside the burners and at selected locations along the primary flowpath. In this section, a detailed discussion is included of the instrumentation used to measure the internal noise levels, together with a description of the locations of this instrumentation, and several samples of the measured data. Data from both engines will be used in Section 4.7 to evaluate the turbine transmission loss model developed in Section 4.6. The internal JT8D-109 data presented here were recorded simultaneously with farfield signals at the outdoor test facility for use in source location studies using cross-correlation techniques (see Section 4.2.3).

4.2.2.1   Dynamic Pressure Instrumentation

Internal noise measurements were obtained with internal flush mounted Kulite differential pressure transducers (type XCQL-5-200-25D and XSL-11-093-25D) as described below:

1. Transducer type XCQL-5-200-25D is configured for use in a high pressure, high temperature environment (such as in burner).

    a. High pressure applications – The transducer is vented on the measurement side of the pressure sensing diaphragm through a tubing system that is designed to allow the pressure at both sides of the diaphragm to equalize for very low frequency fluctuations (below approximately 25 Hz). The diaphragm then senses the small pressure fluctuations at higher frequencies in the burner. This system (Figure 4.2-17) enables a thin diaphragm, low pressure Kulite to be used in a high pressure environment, while maintaining a flat frequency response above about 25 Hz.

    b. High temperature applications – Transducers installed in hot areas are protected by Kistler water cooled adapters, Model 616M, as shown in Figure 4.2-18.

2. Type XSL-11-093-25D Kulite transducers are used in lower pressure engine environments (i.e., the fan inlet and discharge ducts, turbine exit and tailpipe reas). These transducers are protected from heat by Kistler Model 616M water cooled adapters.
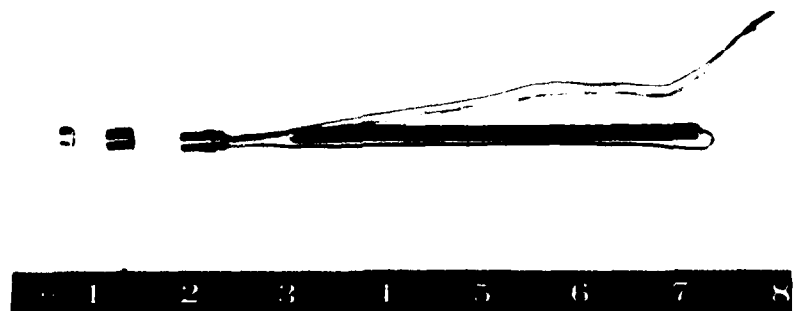
Figure 4.2-17   Kulite Pressure Transducer With Vent Tube

Ⓐ Kulite transducer adapter ass'y   Ⓒ Ignitor probe ass'y
Ⓑ Low pressure applications   Ⓓ High pressure ass'y
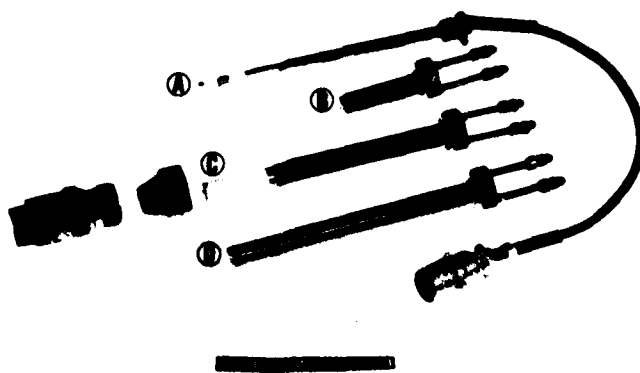
Figure 4.2-18   Typical Water Cooled Kulite Installation

4.2.2.2   JT8D-109 Internal Measurements

Dynamic pressure signals were recorded at seven axial locations inside the
JT8D-109 engine. These locations were selected to enable later source location
studies using cross-correlation techniques. Measured spectra from three locations
in the engine are presented. The test program for this engine included several
performance settings, ranging from idle to takeoff thrust.

The 1/3 octave SPL spectra from the burner igniter Kulite are presented in Figure 4.2-19 for three engine speeds. The peak is centered around 400 to 450 Hz at all speeds, as is the farfield combustion noise. The 1/3 octave spectra measured at the forced mixer location are shown in Figure 4.2-20 at the same engine speeds. As in Figure 4.2-19, a peak appears near 400 to 450 Hz and becomes less visible as the engine RPM increases due to aerodynamic noise contamination. The peak in the spectra is not as clear from the tailpipe data, as shown in Figure 4.2-21. Still, at the lower RPM settings, the combustion noise peak appears to be contributing in the 250 to 800 Hz range.
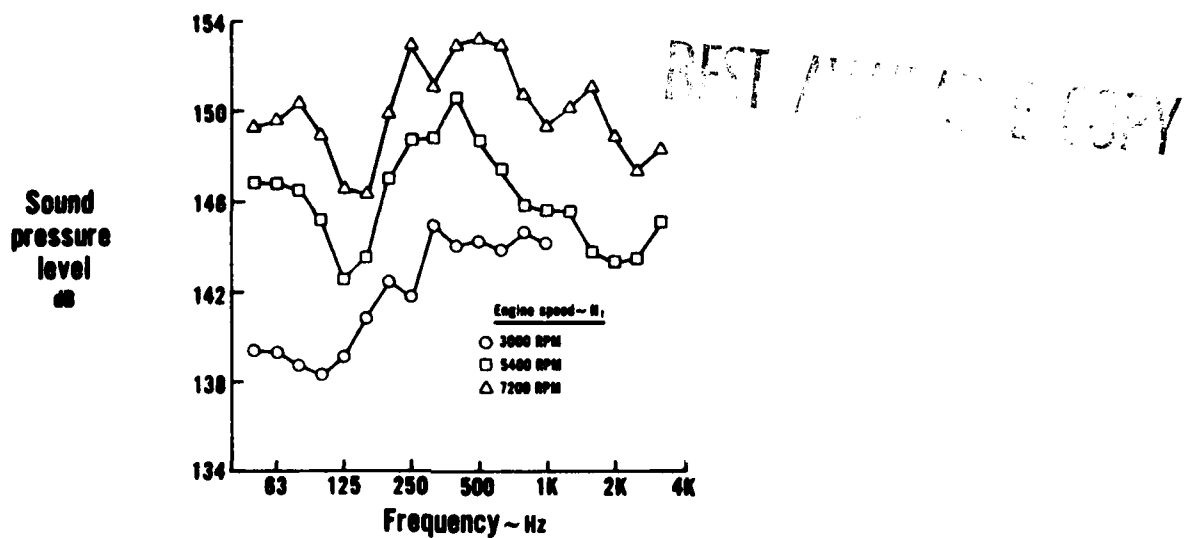
Figure 4.2-19   Internal Kulite Spectra for the JT8D-109, Ignitor Location
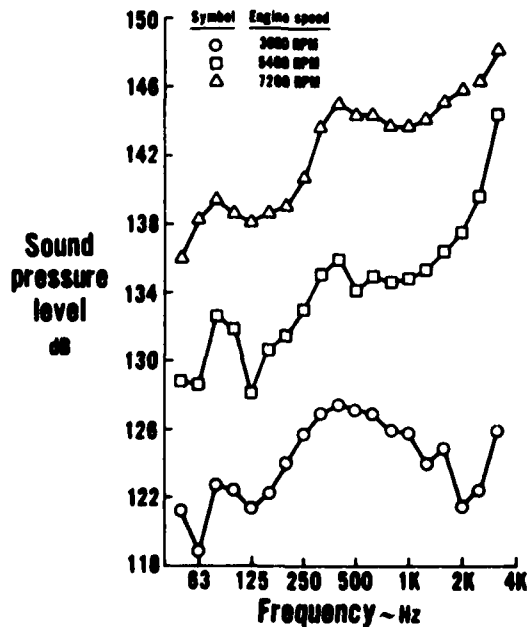
Figure 4.2-20   Internal Kulite Spectra for the JT8D-109, Forced Mixer Location

95
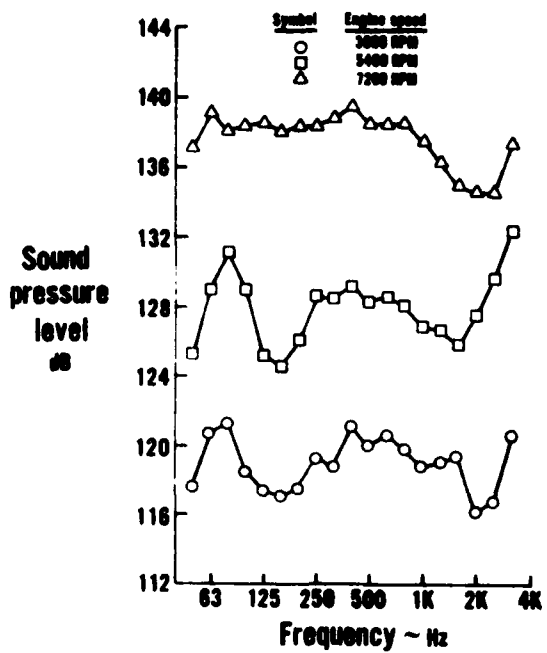
Figure 4.2-21 Internal Kulite Spectra for the JT8D-109, Tailpipe Location

The combustion noise peak SPL levels are shown in Figure 4.2-22 as a function of axial distance from the burner igniter. This figure gives some indication of transmission losses thru the turbine and will be used in Section 4.7 to evaluate the transmission loss model.
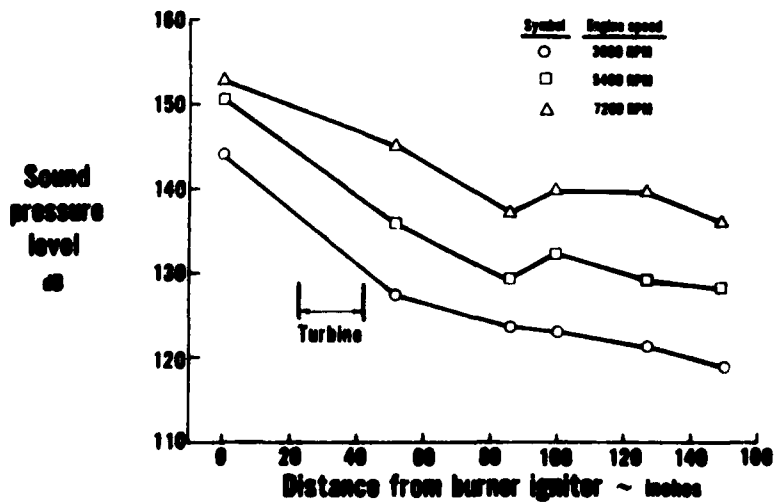
Figure 4.2-22   Max 1/3 Octave SPL level (450 Hz) Inside JT8D-109 Engine

96

4.2.2.3   JT9D Internal Measurements

Internal pressure signals were recorded at four axial locations in the JT9D engine, shown in Figure 4.2-23. The test program included engine power settings varying from low approach to takeoff thrust levels.
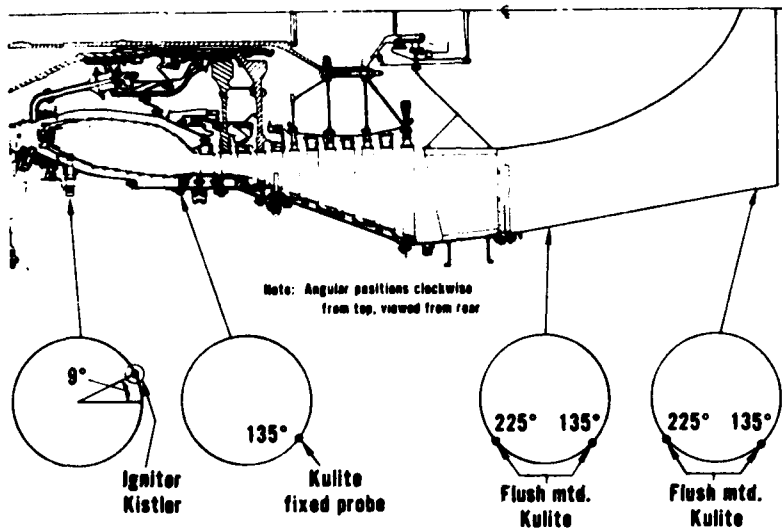
Figure 4.2-23   Internal Transducer Measurement Locations for the JT9D Engine

Although many of the dynamic pressure spectra obtained inside the engine were dominated by high flow noise levels, combustion noise characteristics were visible at selected locations and speeds below 2982 RPM (high approach). The 1/3 octave band SPL spectra inside the burner (Figure 4.2-24) give the clearest indication of the combustion noise spectra shape. Generally, the combustion noise spectra peaked near 315 to 400 Hz, as in the farfield. Aerodynamic noise levels dominated the signals in the two tailpipe locations. Figures 4.2-25 and 4.2-26 shows the 1/3 octave band SPL spectra recorded at the upstream and downstream tailpipe locations.

Maximum sound pressure levels at the combustion noise peak frequency of 315 Hz were obtained from Figures 4.2-24, 4.2-25 and 4.2-26. These values, in some cases, indicate only the maximum possible SPL the combustion noise may have since the aerodynamic noise sometimes dominates. These levels are shown versus the axial distance from the burner ignitor in Figure 4.2-27. Although these SPL levels do not indicate true combustion noise levels, an indication of the magnitude of the turbine attenuation for the JT9D may be obtained.
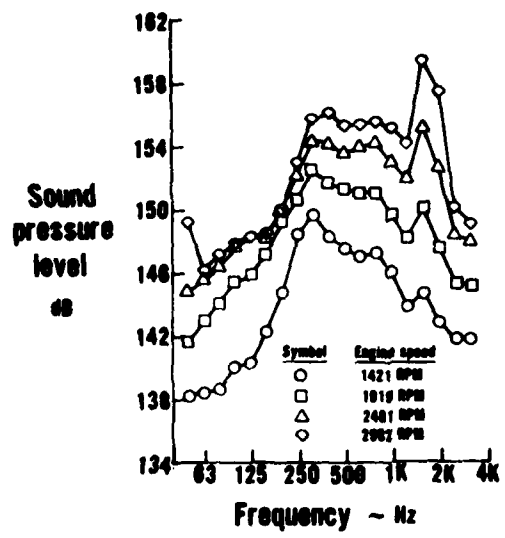
Figure 4.2-24 Internal Kulite Spectra for the JT9D, Burner Location
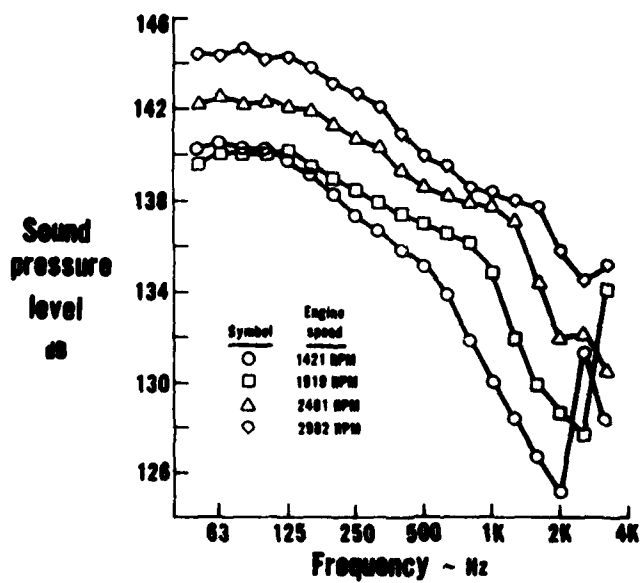
Figure 4.2-25 Internal Kulite Spectra for the JT9D, Tailpipe, Upstream Location
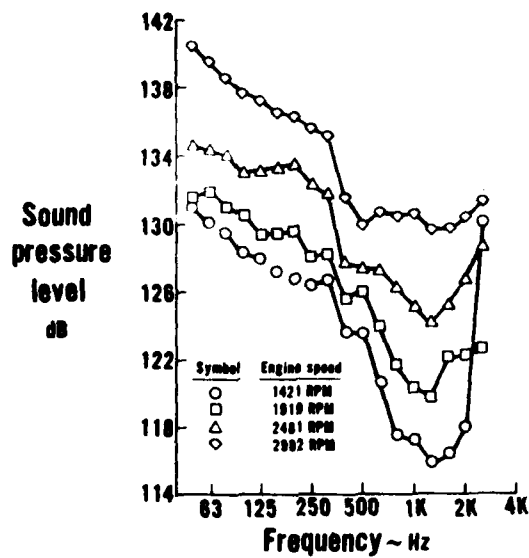
Figure 4.2-26 *Internal Kulite Spectra for the JT9D, Tailpipe, Downstream Location*
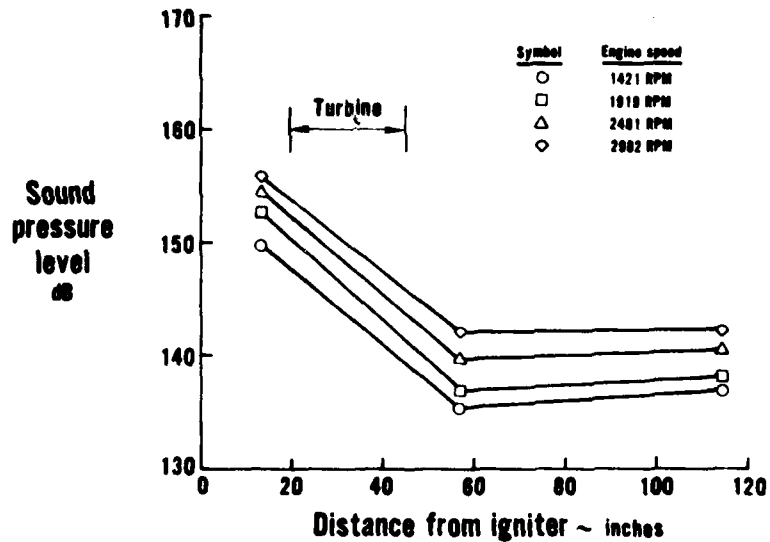
Figure 4.2-27 *Max 1/3 Octave SPL Level (315 Hz) Inside JT9D Engine*

4.2.3 JT8D-109 Cross-Correlation Studies

This section reviews the results of signal cross-correlation studies conducted on the JT8D-109 engine tested at the X-314 outdoor noise test facility. Acoustic pressure signals were recorded simultaneously from an array of farfield ground plane microphones at a radius of 150 ft from the engine centerline and from

several Kulite pressure transducers located inside the engine (i.e., upstream of the burner, inside the burner and in the exhaust duct downstream of the turbine). Cross correlations were performed between each of the internal dynamic pressure signals with the signal from the 120° farfield microphone. The associated time delays were then used to determine and verify that the burner is the primary source of core engine noise.

Kulite pressure transducers were mounted at seven axial locations inside the JT8D-109 engine. Several internally measured spectra were presented in Section 4.2.2. Typical cross-correlation diagrams between the 120° farfield and three internal dynamic pressure signals (aft tailpipe, forward tailpipe and ignitor locations) are shown in Figures 4.2-28, 4.2-29 and 4.2-30, respectively. The large positive cross-correlation peak occurring in Figure 4.2-28 occurs at a time delay (τ) of 136.6 milliseconds, which corresponds precisely to the time for an acoustic wave to travel from the tailpipe Kulite to the 120° farfield location, more than 150 feet away. The large correlation peak in Figure 4.3-30 occurs at a time delay of 143.0 milliseconds, indicating that it takes 6.4 milliseconds longer for the signal to travel from the igniter to the farfield than from the tailpipe to the farfield. In fact, this 6.4 milliseconds was calculated to be the time for an acoustic wave to propagate (at the speed of sound plus the convected speed) from the burner to the tailpipe exit. Figure 4.2-31 shows a summary of the time delays as a function of axial distance from the burner igniter for three different engine speeds and several transducer locations including one upstream of the burner. The slope of the line fitted through the 7200 RPM data (shown in Figure 4.2-31) corresponds closely to the calculated acoustic wave velocity (speed of sound plus convected velocity) of approximately 2450 ft/sec. The slopes indicated by the data from all three speeds are similar, with the relative differences attributable to changes in the acoustic wave propagation speed. In all cases, the signal took longer to get from the burner to the farfield than from any other location. If the noise source was located upstream or downstream of the burner, this would not be the case. These results provide strong evidence that core engine noise is dominated by combustion sources in turbofan engines.
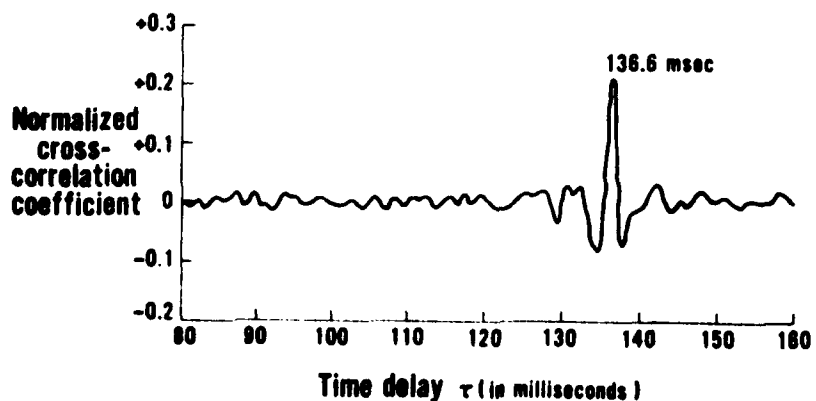
Figure 4.2-28 JT8D-109 Cross-Correlation of Signals Recorded From the Aft Tailpipe and 120° Farfield Locations

100
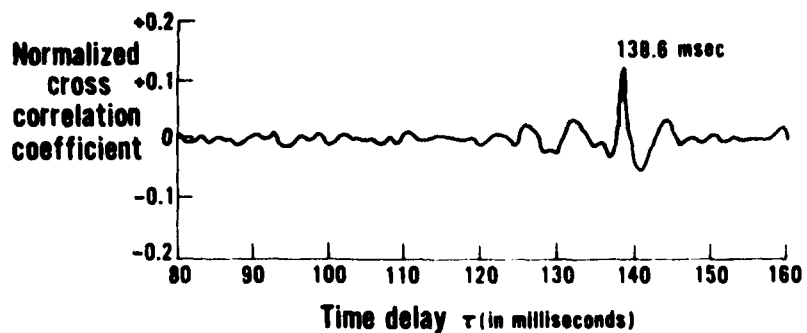
Figure 4.2-29   JT8D-109 Cross-Correlation of Signals Recorded From the Forward Tailpipe Kulite and 120° Farfield Locations
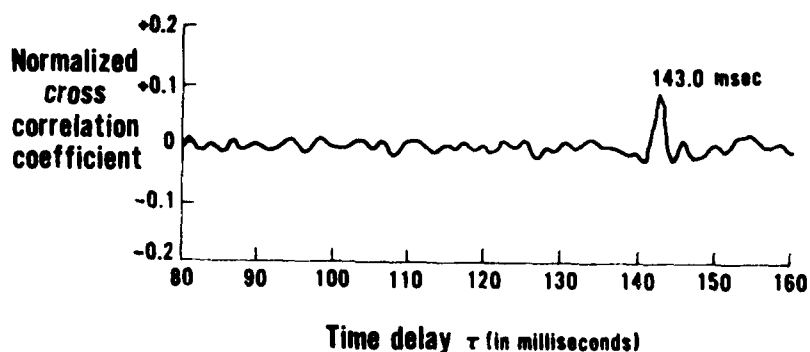
Figure 4 2-30   JT8D-109 Cross-Correlation of Signals Recorded From the Ignitor Kulite and 120° Farfield Locations
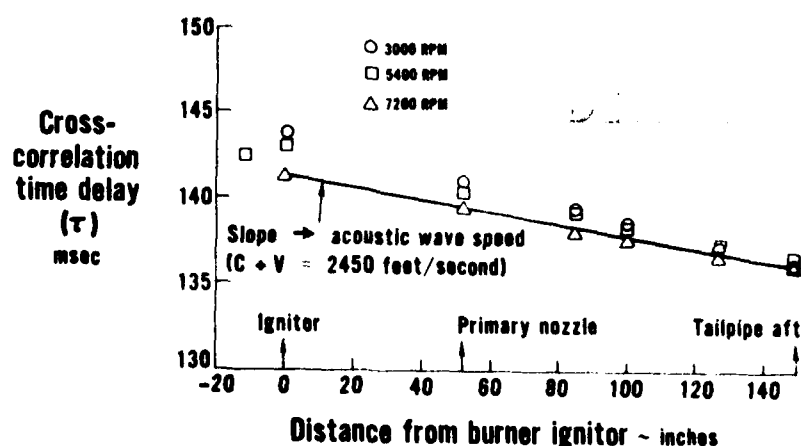
Figure 4.2-31   JT8D-109 Cross-Correlation Time Delays Between Internal Kulites and 120° Farfield Microphones

101

4.3   ENGINE EVALUATION OF DIRECT COMBUSTION NOISE PREDICTION MODELS

In this section, the prediction models developed in Section 2.2 for direct combustion noise peak frequencies and acoustic power levels are evaluated by comparing with the full scale engine noise data discussed in Section 4.2.

4.3.1   Peak Frequency Model

The normalized combustion noise spectral definitions (i.e., SPL levels normalized by OASPL; frequencies normalized by f_c) obtained in Section 4.2 are presented in Figure 4.3-1 for the four P&WA turbofan engines and for the JT8D burner rigs tested at X-410 stand. The characteristics of the combustion noise spectra are summarized below

1. The normalized combustion noise spectra from all four engines are similar, and agree well with the JT8D combustion noise spectra obtained from rig tests.

2. The combustion noise peak frequency, f_c, is different for each engine.

3. For a given engine, the combustion noise peak frequency is essentially constant over the engine operating range, consistent with the results of the JT8D burner component tests, and with the predictions from the peak frequency model.

4. Combustion noise spectral characteristics are independent of farfield location.
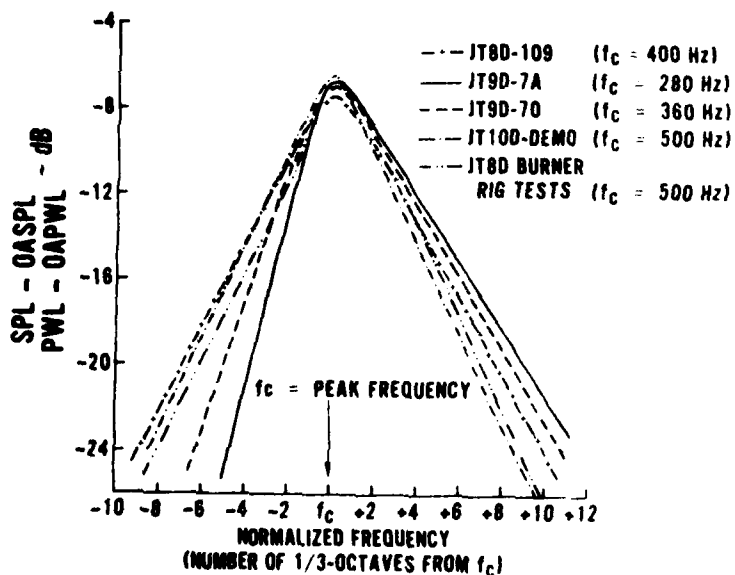
Figure 4.3-1   Normalized Combustion Noise Spectra

102

The expression derived in Section 2.2 for combustion noise peak frequency, Eq. (11), contains a proportionality constant K_f which was stated to be dependent on burner type. Figure 4.3-2 plots the measured values of f_c versus the right hand side of Eq. (11), for both can-type and annular burners, using data from JT8D rig tests and five turbofan engines. The data for can-type burners are seen to fall along one line, and data for annular burners along another, as predicted by the model. Values of the constant K_f are seen to be 8 and 3, respectively, for can-type and annular burners. The trend toward higher frequencies for smaller volume burners is evident for the JT9D-7, JT9D-70 and JT10D-prototype engines. The "ref" condition (or design point) was taken to be takeoff power for the cases shown in Figure 4.3-2.
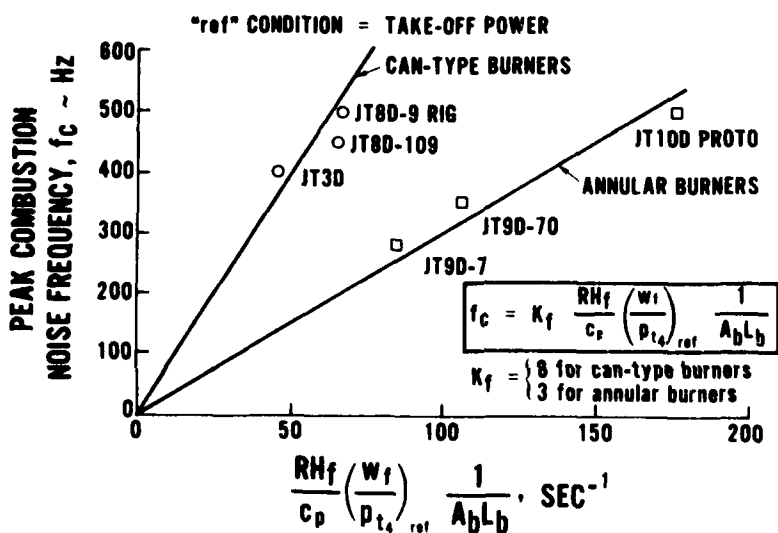
Figure 4.3-2   Combustion Noise Peak Frequency Correlation

4.3.2   Acoustic Power Level Model

The predicted combustion noise OAPWL, as expressed by Eq. (28) in Section 2.2, was verified in Section 2.4 by comparing with rig data from several JT8D type combustors, where the constant, K_3, in Eq. (28) was shown to be equal to 131.3 for conventional and aerating burners, and 130 for the two-stage low emissions vorbix burner. This section provides further verification of the prediction model by comparing the predictions with full scale engine data from four P&WA turbofan engines.

4.3.2.1   Effects of Burner Pressure

Internal dynamic pressures, measured in the burners of both rigs and engines, were used in Section 2.4 to evaluate the predicted dependence of combustion noise on burner pressure. Further verification of the pressure term in Eq. (28)

103

may be obtained by normalizing the engine noise levels by everything but burner pressure (assuming the transmission loss is not a strong function of engine operation and presenting the normalized levels as a function of burner pressure. This is shown in Figure 4.3-3 where the normalized combustion noise power levels from several turbofan engines are seen to increase with the square of burner pressure. as predicted in Eq. (28).
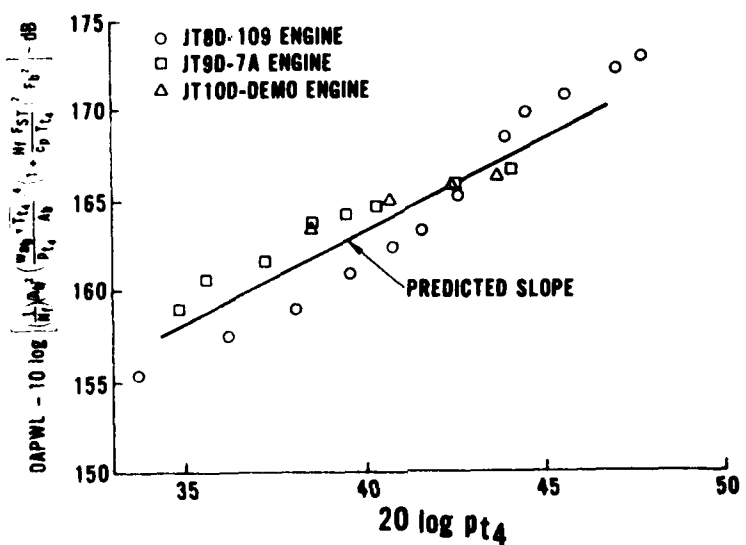
Figure 4.3-3   Effect of Burner Pressure On Combustion Noise Levels

4.3.2.2   Acoustic Power Level Correlation

Combustion noise power levels from the JT8D type combustors (including single fuel nozzle and four fuel nozzle designs) are presented in Figure 4.3-4, together with the results from the four P&WA turbofan engines discussed in Section 4.2. The data are presented as a function of the total power level parameter given in Eq. (28). The correlation line shown is the same as that presented previously in Figure 2.4-10, and is given in Eq. (31). The acoustic power levels from the turbofan engines are seen in Figure 4.3-4 to lie approximately 6 to 10 dB lower than the correlation line and to have the same slope. This difference is probably attributable to the turbine transmission loss. This is discussed in Sections 4.6 and 4.7. The trends of the engine data shown in Figure 4.3-4 provide evidence that engine combustion noise levels are dominated by direct combustion noise sources.

104

$$10 \log \left[\frac{1}{N_f} A_b^2 p_{t_4}^2 \left(\frac{W_{ab} \sqrt{T_{t_4}}}{p_{t_4} A_b} \right)^4 \left(1 + \frac{H_f F_{ST}}{c_p T_{t_4}} \right)^2 F_b^2 \right]$$
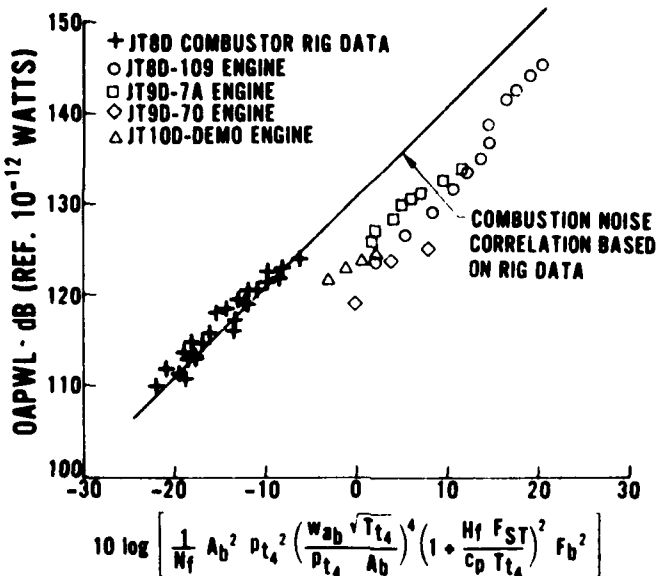
Figure 4.3-4   Comparison of Combustor Rig and Engine Data

4.4   EVALUATION OF THE INDIRECT COMBUSTION NOISE PREDICTION MODEL FOR THE JT8D-109 ENGINE

The direct combustion noise prediction model was evaluated in Section 4.3 by comparing to engine data, and while the predicted levels were higher than the data, the slopes were correctly predicted. In addition, the higher predicted value will be reduced when transmission losses are accounted for. In this section, a similar evaluation will be presented for indirect combustion noise, using the JT8D-109 engine, since this is the only engine for which the necessary hot spot information is available.

In order to determine the importance of indirect combustion noise as a possible source of core engine noise, the P&WA indirect combustion noise prediction model described in Section 3.2 was utilized. The empirical equations given in Section 3.5 for the hot-spot characteristics were used to provide the inputs required to exercise the prediction model for the JT8D-109 engine. The JT8D-109 engine was selected for this comparison because the engine performance and measured core engine noise power levels from low to high engine powers were readily available, and because estimates of the hot-spot characteristics entering the turbine had been measured for a JT8D burner (Section 3.4).

The indirect combustion noise calculation was performed individually across each turbine blade row using the hot-spot characteristics at the burner exit as input to the calculation for the first blade row. Changes in the hot-spot axial length scales across each turbine blade row were calculated (to preserve frequency) and used as input for the following blade row. When the calculation was completed for each blade row, the resulting acoustic power level of indirect combustion noise was obtained by summing the levels from all blade rows.

105

Comparison of the predicted power levels with the JT8D-109 data, discussed
in Section 4.2, is presented in Figure 4.4-1. The range of engine operation
shown includes typical approach, cut-back and takeoff power settings. The
predicted indirect combustion noise levels are 7 to 15 dB lower than the meas-
ured values over the entire range of operation. In addition, the trends of the
predicted power levels do not agree with measurements. It may be seen that
measured combustion noise power levels increase much faster with engine
speed than the predicted indirect combustion noise power levels. Furthermore,
the predicted levels shown in Figure 4.4-1 do not consider turbine transmission
losses, which would make the differences between data and predictions even
larger.
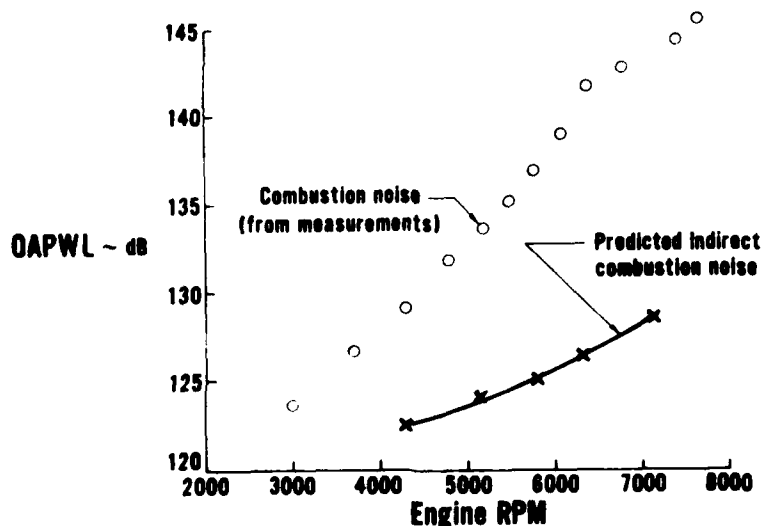
Figure 4.4-1   *Comparison of Measured JT8D-109 Combustion Noise Power Levels With
Predicted Indirect Combustion Noise*

Figure 4.4-2 shows the spectrum shape of measured combustion noise com-
pared to the predicted indirect combustion noise spectrum. The measured
combustion noise spectrum peaks at 400 Hz on a one-third octave band plot,
and is broadband in nature. Although the predicted indirect combustion noise
spectrum has a broadband character, the peak occurs at 1000 Hz, which is con-
siderably higher than that of the measured combustion noise.

Figure 4.4-3 shows a typical measured 1/3 octave band spectrum from the
JT8D-109 engine. Both the predicted jet noise and the predicted indirect com-
bustion noise are also shown on this figure. The peak indirect combustion
noise levels (without considering transmission losses) are 5 to 6 dB below the
measured data and do not represent a significant contribution to the measured
noise.

106
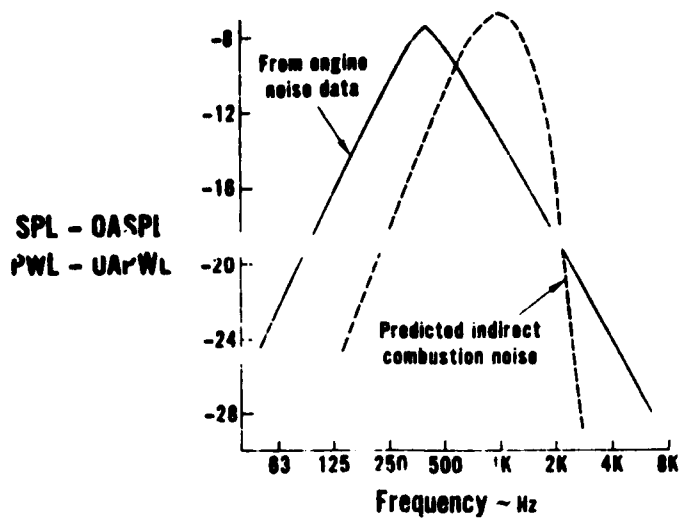
Figure 4.4-2 *Comparison of Normalized Spectra for the JT8D-109 Engine, Measured Vs. Predicted Indirect Combustion Noise*
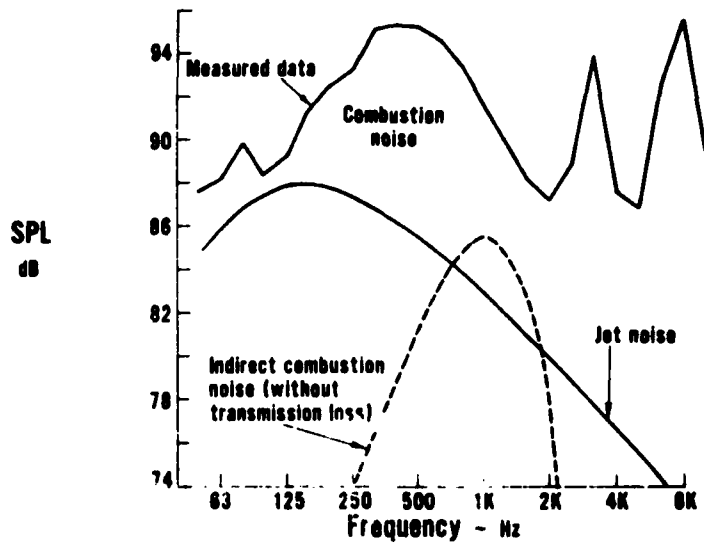
Figure 4.4-3 *Spectral Comparison of Measured Combustion Noise and Predicted Indirect Combustion Noise*

In summary, the results presented above reveal that for the JT8D-109 engine, the predicted indirect combustion noise levels are too low, even when transmission losses are not included. When transmission losses are included the agreement between data and predictions will not improve. Furthermore, the predicted trends (slope) are not in agreement with data and the predicted frequencies are more than twice the observed values.

107

4.5 IDENTIFICATION OF THE DOMINANT COMBUSTION NOISE SOURCE

The purpose of this section is to compare the relative importance of direct and indirect combustion noise in typical aircraft engines, and to identify the dominant noise source, using the prediction models developed herein.

Figure 4.5-1 shows a plot of combustion noise power levels determined from noise measurements on a JT8D-109 engine, together with predictions of both direct and indirect combustion noise. The predicted direct combustion noise is seen to be higher than the indirect combustion noise by 18 to 22 dB when transmission losses are neglected. This result together with the incorrect slope of the indirect combustion noise lead to the conclusion that direct combustion noise, rather than indirect combustion noise, is the dominant source for the JT8D-109 engine.

Similar comparisons for other P&WA engines was not possible because of inadequate dynamic temperature information. However, as shown in Sections 4.3 and 4.7, data from these other engines is well correlated by the direct combustion noise models for both power level and peak frequency, once turbine attenuation is included in the analysis. Therefore it is inferred that for all the engines discussed herein (i.e., JT8D-109, JT9D-7, JT9D-70 and prototype JT10D), direct combustion noise is the dominant source.

In order to demonstrate that direct combustion noise is the dominant source in these other engines, an estimate of the transmission losses that occur through the turbine is required. The formulation of a transmission loss analytical model is discussed in the next section (4.6), followed by an evaluation of this model in Section 4.7.
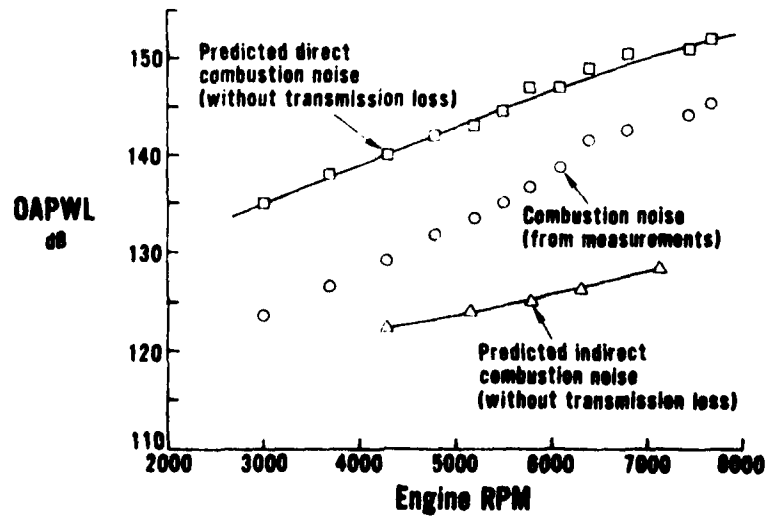
Figure 4.5-1   *Comparison of Measured JT8D-109 Combustion Noise Power Levels With Predicted Direct and Indirect Combustion Noise*

108

4.6 FORMULATION OF TRANSMISSION LOSS MODEL

An analytical model is presented in this section that relates the noise generated by an isolated combustor to that generated by a combustor installed in an engine. This model accounts for the transmission losses associated with combustor/duct coupling at the turbine entrance location and also across the turbine itself. Experimental verification of the model is presented in Section 4.7.

4.6.1 Transmission Loss Due to Combustor/Duct Coupling

The duct at the combustor/turbine interface has a specified outer diameter, D, as shown in Figure 4.6-1a. The area over which the combustion noise pressure fluctuations are correlated at this interface is given by

$$A_{corr} = \frac{L}{\pi D} A_{duct} \tag{37}$$

where L is the circumferential correlation length scale at the interface (shown in Figure 4.6-1a) and A_{duct} is the total cross-sectional area of the annular duct. It is assumed that over the low frequency range of interest, the sound power radiated from an isolated combustor is carried by plane waves in the burner and may be expressed by

$$P_b = \frac{p'_o{}^2}{2 \rho_5 c_5} A_{corr} \tag{38}$$

where p'_o is the acoustic pressure amplitude at the burner exit plane (station 5). This relationship was verified experimentally in Section 2.3.6 where it was shown that for several JT8D type burners, tested separately in a rig at atmospheric pressure, the sound powers calculated from Eq. (38) using the isolated combustor rig exit area as the correlated area, agree quite well with the sound powers obtained from farfield noise measurements.
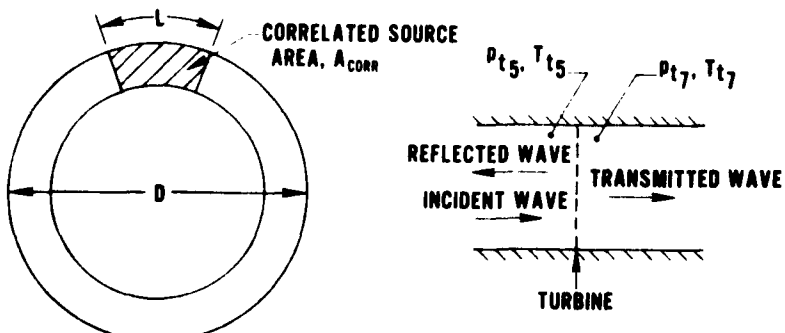
a. DUCT AT COMBUSTOR/   b. REPRESENTATION OF PLANE
    TURBINE INTERFACE   WAVE TRANSMISSION
                            THROUGH TURBINE

Figure 4.6-1   Elements of Combustion Noise Transmission Loss Model

It is next assumed that, when the combustor is installed in an annular duct, the acoustic pressure at the combustor/duct interface has the same amplitude as it would have at the exit of the isolated combustor operating at the same condition. This is equivalent to stating that the acoustic pressure at the interface is independent of any downstream acoustic impedance. The acoustic particle velocity, however, may vary at the combustor exit depending on the downstream installation, resulting in differences in the radiated sound power.

The final assumption deals with the modal distribution of the noise in the duct downstream of the burner. Here, the acoustic energy from each correlated source is assumed to be carried in the duct plane wave mode only. Calculations for several engines indicate that, in the combustion noise frequency range, the higher order modes can be neglected since they decay in the exhaust duct and therefore do not propagate acoustic energy. The acoustic pressure amplitude of the duct plane wave mode is obtained by modeling the circumferential acoustic pressure distribution as a pulse of circumferential length, L, and amplitude, p'_o. The Fourier decomposition of this spatial pulse gives the following expression for the amplitude of the m = o (i.e., plane wave) duct mode:

$$p'_{m=o} = \frac{L}{\pi D} \; p'_o \tag{39}$$

The intensity of the plane wave mode in the duct is then

$$I_{m=o} = \frac{\left(\dfrac{L}{\pi D}\right)^2 p'^2_o}{2 \rho_s c_s} \tag{40}$$

and the acoustic power radiated from the ducted source is

$$P_d = \frac{\left(\dfrac{L}{\pi D}\right)^2 p'^2_o}{2 \rho_s c_s} A_{duct} \tag{41}$$

The transmission loss associated with the combustor/duct coupling can be expressed (in decibels) in terms of the ratio of power generated by the isolated burner to the power generated by the same burner coupled with a duct, i.e.,

$$(T.L.)_d = 10 \log \left(\frac{P_b}{P_d}\right) \tag{42}$$

which from Eqs. (38) and (41) becomes

$$(T.L.)_d = 10 \log \left[\frac{A_{corr}}{(L/\pi D)^2 \; A_{duct}}\right] \tag{43}$$

Substituting Eq. (37) into Eq. (43) yields

$$(T.L.)_d = 10 \log \left[\frac{1}{L/\pi D} \right] \qquad (44)$$

This energy loss occurs as a result of differences in acoustic particle velocity between the two cases of an isolated combustor and the ducted combustor, and is dependent only on the ratio of the correlated source area at the combustor exit to the total duct area at the combustor/turbine interface. Thus, as an example, if the source at the combustor exit is correlated over only 10 percent of the circumference (i.e., $L/\pi D = 0.1$), a 10 dB transmission loss would be predicted using Eq. (44), whereas if the source were correlated over the entire duct, all the energy is in the plane wave mode and there would be no transmission loss. The value of $L/\pi D$ must be measured experimentally or established empirically using experimental data. An empirical estimate of this factor, based on rig and engine data, is presented in Section 4.7.

4.6.2   Turbine Transmission Loss

The transmission loss associated with a plane wave traveling through the turbine is obtained by representing the entire turbine as a surface of discontinuity in characteristic impedance, ρc. This is depicted schematically in Figure 4.6-1b where the length of the turbine is assumed to be small relative to the acoustic wavelength of the incident noise. (For typical engines, the ratio of acoustic wavelength to turbine length is about 4.) It is also assumed that no reflections occur from locations in the tailpipe downstream of the turbine. This assumption appears valid for most engine configurations where noise carried by plane waves at typical combustion noise frequencies is totally transmitted at the exhaust nozzle exit[16]. As the incident acoustic plane wave contacts the turbine, both reflected and transmitted plane waves are developed due to the difference in characteristic impedance across the turbine. If the axial flow through the turbine is neglected (i.e., low axial Mach numbers), the ratio of the incident to the transmitted power can be expressed (from Reference 23) as

$$\frac{P_i}{P_t} = \frac{(1+F)^2}{4F} \qquad (45)$$

where F is the ratio of the upstream characteristics impedence (at station 5) to the downstream (station 7) characteristic impedence. Since the axial Mach numbers are fairly low at both locations, the static pressures and temperatures may be approximated by the more readily available stagnation values and F may be expressed by

$$F = \frac{P_{t5}}{P_{t7}} \sqrt{\frac{T_{t7}}{T_{t5}}} \qquad (46)$$

111

From Eq. (45), the transmission loss across the turbine (in decibels) is

$$(T.L.)_{turb} = 10 \log \left[\frac{(1 + F)^2}{4F} \right] \sim dB \qquad (47)$$

Typical values of F in an actual engine range from 3 to 8, resulting in a transmission loss calculated from Eq. (47) of approximately 1 to 4 decibels.

4.6.3   Total Transmission Loss

The total transmission loss associated with both the combustor/duct coupling and the turbine may be expressed (in decibels) as

$$T.L. = (T.L.)_d + (T.L.)_{turb} \qquad (48)$$

From Eqs. (44) and (47) this becomes

$$T.L. = 10 \log \left[\frac{(1 + F)^2}{4F \, (L/\pi D)} \right] \sim dB \qquad (49)$$

It is interesting to note that for the low frequencies assumed in the analysis, the total transmission loss is independent of frequency. Thus, the noise spectra radiated from isolated combustors should be similar to the noise spectra from combustors installed in engines. This indeed is the case, as was shown in Figure 4.3-1 for the JT8D burner. The predictions of Eq. (49) are evaluated in the following section.

4.7   EVALUATION OF TRANSMISSION LOSS MODEL

In this section, the transmission loss model presented in Section 4.6 is evaluated using two independent techniques. The first method uses a comparison of farfield combustion noise data from rigs and full scale engines, while the second technique involves an examination of internal engine noise data upstream and downstream of the turbines.

4.7.1   Farfield Data Evaluation

The expression for acoustic transmission loss, given in Eq. (49), includes the ratio L/π D which represents the extent to which the acoustic pressures are circumferentially correlated in the engine at the combustor/turbine interface. The value of this ratio was determined empirically in the present study by requiring that the rig and engine data shown previously in Figure 4.3-4 collapse when the engine data has been corrected for the transmission loss. This occurs when it is assumed that the source is correlated over 23 percent of the duct circumference at the combustor/duct interface (i.e., L/π D = .23) for can-type

112

and annular burner installations. The results are shown in Figure 4.7-1, where
the combustion noise correlation is shown by the straight line and may be
written as follows:

$$OAPWL = 10 \log \left[\frac{1}{N_f} A_b^2 P_{t_4}^2 \left(\frac{w_{ab}\sqrt{T_{t4}}}{P_{t_4} A_b} \right)^4 \right.$$

$$\left. \left(1 + \frac{H_f F_{ST}}{c_p T_{t4}} \right)^2 F_b^2 \right] + 131.3 - T.L. \tag{50}$$

where the transmission loss, T.L., is given in Eq. (49) with $L/\pi D = .23$. The rig
data from five conventional and aerating burners and the data from four P&WA
engines fit the prediction of Eq. (50), with a standard deviation of 1.9 dB.
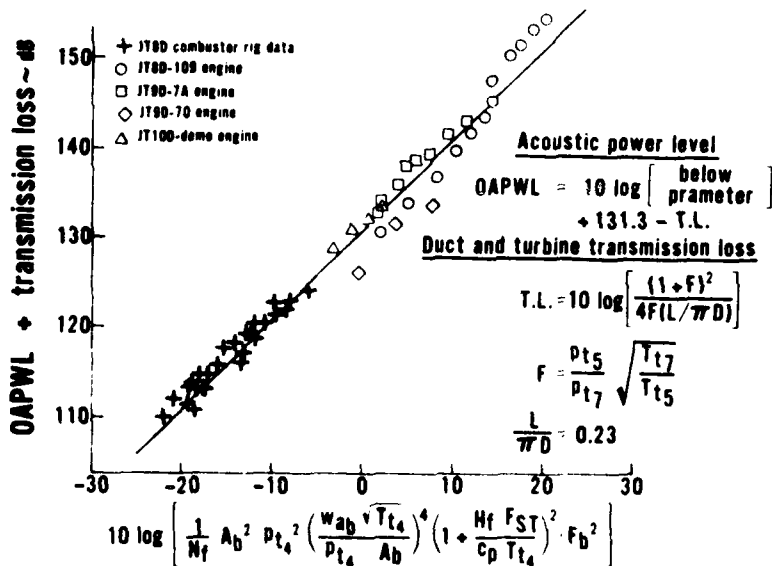
Figure 4.7-1   Combustion Noise Acoustic Power Level Correlation

4.7.2   Internal Engine Dynamic Pressure Data Evaluation

The transmission loss model developed in Section 4.6 is evaluated in the follow-
ing discussion by using internal dynamic pressure data from the JT8D-109
and JT9D engines, which was summarized in Section 4.2.

Maximum sound pressure levels from several locations inside a JT8D-109 en-
gine are presented in Figure 4.7-2 as a function of distance from the burner
igniter. The relative location of the turbine and the predicted transmission
loss are included in this figure. Considering the fact that SPL differences are

113

not a true indication of an acoustic power level loss, and that the internal burner transducer is in the source near field, and also may be contaminated by flow noise, it still appears that the predicted transmission losses are reasonable when compared to the magnitude of the SPL difference across the turbine.
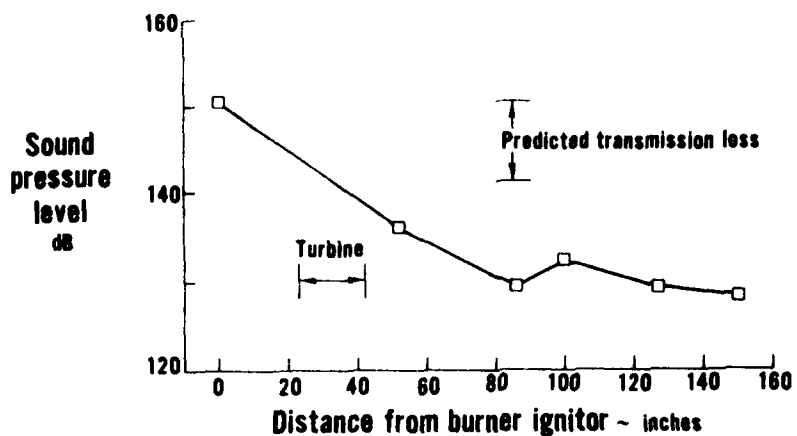
Figure 4.7-2   Max 1/3 Octave SPL Level (450 Hz) Inside JT8D-109 Engine at 5400 RPM

For the JT9D engine, SPL's at the combustion noise peak frequency of 315 Hz from three locations inside the engine are presented in Figure 4.7-3. The agreement between the predicted transmission loss and the differences in SPL across the turbine are in better agreement than for the JT8D-109 discussed earlier and verify, at least to first order, the magnitude of the predicted transmission loss of Eq. (49), with $L/\pi D = .23$.
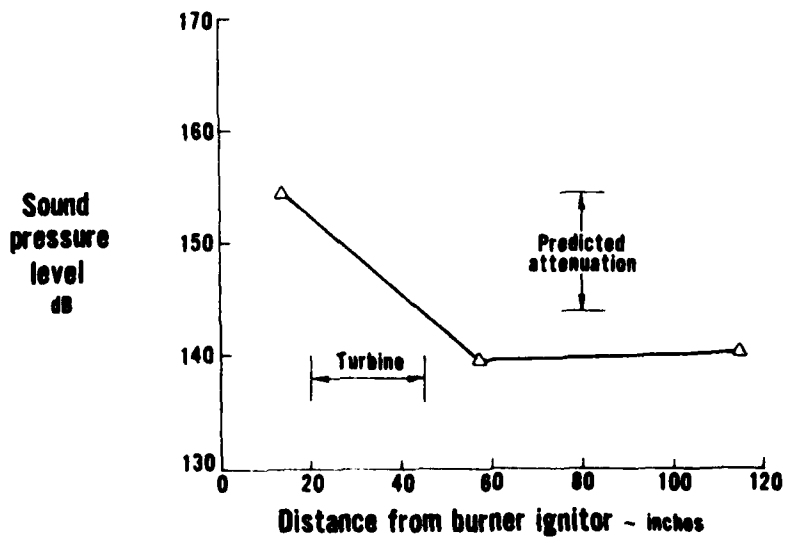
Figure 4.7-3   Max 1/3 Octave SPL Level (315 Hz) Inside JT9D Engine at 2481 RPM

114

4.8   SUMMARY OF ENGINE COMBUSTION NOISE PREDICTION SYSTEM

Based on the analytical and experimental results presented in the preceeding sections, including the apparent dominance of the direct combustion noise mechanism, a procedure was formulated that is applicable to the prediction of combustion noise power levels, directivity patterns, and spectral characteristics. The procedure is summarized in this section.

4.8.1   Combustion Noise Power Levels

4.8.1.1   Conventional and Aerating Type Burners

The prediction of combustion noise power levels from full scale engines must consider both the noise generation and the transmission losses associated with the combustor/duct coupling and the turbine. A relationship was presented in Section 4.7 which meets this requirement and also collapses the noise data from both burner rigs and full scale engines as shown in Figure 4.7-1. For summary purposes, this relationship is rewritten below.

$$\text{OAPWL} = 10 \log \left[\frac{1}{N_f} A_b^2 P_{t_4}^2 \left(\frac{w_{ab} \sqrt{T_{t4}}}{P_{t_4} A_b} \right)^4 \left(1 + \frac{H_f F_{S1}}{c_p T_{t4}} \right)^2 F_b^2 \right] + 131.3 - \text{T.L.} \tag{50}$$

where

$$\text{T.L.} = 10 \log \left[\frac{(1 + F)^2}{4F \ (L/\pi D)} \right] \sim \text{dB} \tag{49}$$

F is the ratio of characteristic impedances across the turbine, given by

$$F = \frac{P_{t_5}}{P_{t_7}} \sqrt{\frac{T_{t7}}{T_{t5}}} \tag{46}$$

and $L/\pi \ D = .23$ (obtained empirically in Section 4.7). The data from five different JT8D burners (rigs) and four P&WA turbofans fit the prediction of Eq. (50), with a standard deviation of 1.9 dB.

4.8.1.2   Two-Staged Vorbix Type Low Emission Burners

Based on the results presented in Section 2.4.6 (Figure 2.4-11), for the JT8D-vorbix burner, it is recommended that for burners of this type, Eq. (50) be used with the constant of 131.3 replaced by a value of 130.0.

4.8.2   Combustion Noise Directivity

Figure 4.8-1 presents normalized combustion noise directivities from the four
P&WA turbofan engines discussed in Section 4.2 The directivity pattern pre-
sented in Figure 4.8-2 is recommended for use in determining the overall sound
pressure level (OASPL) of combustion noise as a function of angle from the in-
let axis. This directivity was established empirically by averaging the character-
istics presented in Figure 4.8-1. Although Figure 4.8-2 applies at a radius of
150 feet from the engine, the values of freefield OASPL at any other distances
may be determined using standard methods. A numerical representation of
this directivity pattern is presented in Table 4.8-1.
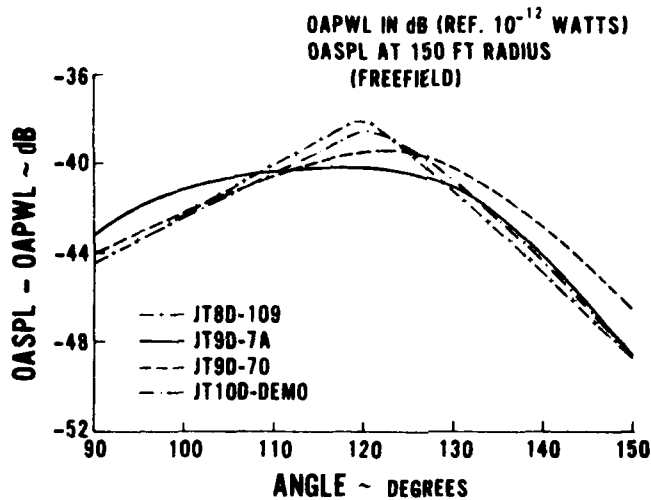
Figure 4.8-1   Engine Directivity Characteristics
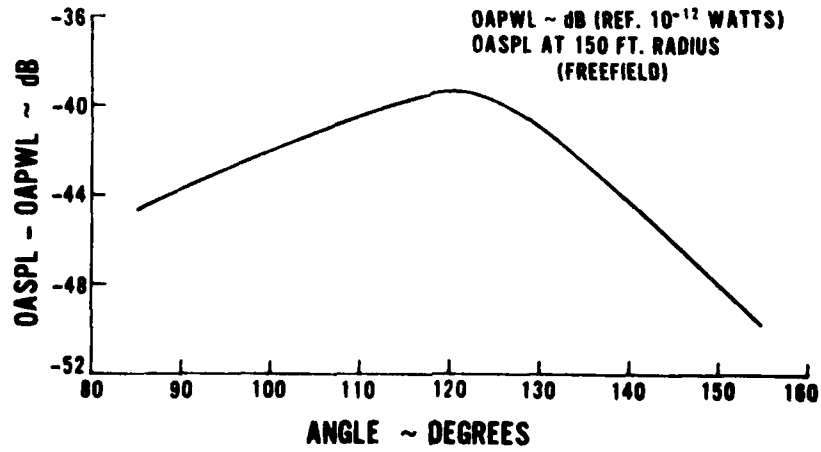
Figure 4.8-2   Generalized Combustion Noise Directivity

TABLE 4.8-1

NORMALIZED COMBUSTION NOISE DIRECTIVITY PATTERN FOR TURBOFAN ENGINES

(Free-Field, 150 Ft. Radius, OAPWL in dB ref. 10^{-12} Watts)

Angle From Inlet Axis ~ Degrees	OASPL – OAPWL ~ dB	Angle From Inlet Axis ~ Degrees	OASPL – OAPWL ~ dB
10	–58.3	90	–43.8
20	–56.5	100	–42.0
30	–54.8	110	–40.4
40	–53.0	120	–39.2
50	–51.1	130	–40.9
60	–49.3	140	–44.3
70	–47.5	150	–48.0
80	–45.7	160	–51.6

4.8.3   Combustion Noise Spectra

Based on an average of the combustion noise spectra from measured rig and engine data presented in Figure 4.3-1, a generalized combustion noise one-third octave spectrum was obtained and is presented in Figure 4.8-3. The maximum SPL from this spectrum is seen to be 6.8 dB below the OASPL. The frequency scale has been normalized in terms of the number of one-third octaves from the peak frequency, f_c. For a given burner, the combustion noise spectrum is the same at all farfield angles and burner operating conditions. The peak frequency of combustion noise is, however, a function of burner geometry. The expression for peak frequency, f_c, is given by

$$f_c = K_f \frac{RH_f}{c_p} \left(\frac{w_f}{p_{t_4}} \right)_{ref} \frac{1}{A_b L_b} \qquad (11)$$

where K_f = 8 for can-type burners and K_f = 3 for annular burners. The reference (or design) condition, denoted by "ref", is taken to be at the engine take-off power condition. The validity of the above expression was demonstrated in Section 4.3.1 (Figure 4.3-2). A numerical representation of the generalized noise spectrum is given in Table 4.8-2.
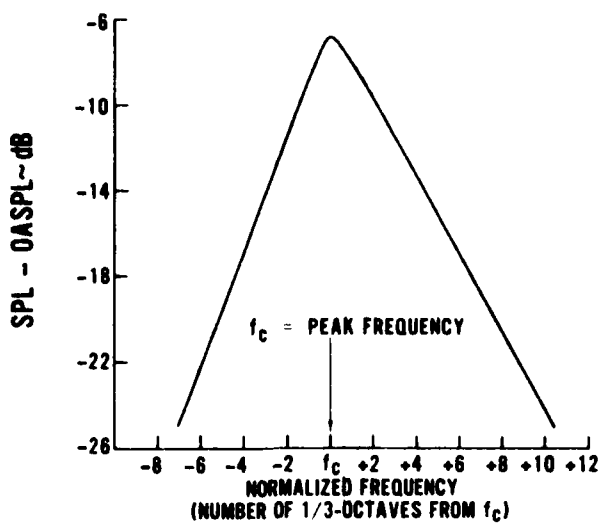
Figure 4.8-3   Generalized Combustion Noise One-Third Octave Spectra

TABLE 4.8-2

GENERALIZED COMBUSTION NOISE SPECTRA

Number of 1/3 Octaves From Peak Freq.	Combustion Noise SPL – OASPL ~ dB	Number of 1/3 Octave From Peak Freq.	Combustion Noise SPL – OASPL ~ dB
-7	-24.7	2	- 9.8
-6	-22.3	3	-11.5
-5	-19.5	4	-13.3
-4	-16.8	5	-15.0
-3	-14.1	6	-16.8
-2	-11.4	7	-18.6
-1	- 8.8	8	-20.5
0	- 6.8	9	-22.4
1	- 8.1	10	-24.3

4.8.4   Sample Application of Prediction System

The use of the combustion noise prediction system is demonstrated in this section for the JT8D-109 engine. All of the steps required to predict the combustion noise spectrum at the 120° farfield microphone location are presented as an example. The predicted combustion noise spectra is then compared with the corresponding measured farfield spectra. The performance and geometry parameters required for making these predictions are presented in Table 4.8-3.

118

TABLE 4.8-3

PERFORMANCE AND GEOMETRY REQUIRED FOR COMBUSTION NOISE PREDICTION SYSTEM
(JT8D-109 ENGINE, 5499 RPM)

$N_f = 9$

$A_b = 307.8 \text{ in}^2$

$L_b = 1.98 \text{ ft}$

$F_b = 0.0128$

$w_{a_b} = 86.0 \text{ lbm/sec}$

$P_{t_4} = 120.5 \text{ psia}$

$P_{t_5} = 110.5 \text{ psia}$

$P_{t_7} = 17.8 \text{ psia}$

$T_{t_4} = 1061°R$

$T_{t_5} = 1904°R$

$T_{t_7} = 1236°R$

$H_f = 18,500 \text{ B/lbm}$

$F_{ST} = 0.068$

$C_p = 0.28 \dfrac{B}{\text{lbm °R}}$

$R = 53.35 \dfrac{\text{ft lbf}}{\text{lbm °R}}$

$$\left(\frac{w_f}{P_{t_4}} \right)_{ref} = 0.01082$$

The following steps were utilized in obtaining the predicted combustion noise at the 120° angle, and 150 ft. radius location for the JT8D-109 engine at 5499 RPM.

1. Utilize Eq. (50) to calculate

   OAPWL + T.L. = 144.8 dB

2. Calculate the transmission loss, T.L., from Eq. (49) where F is given by Eq. (46).

   T.L. = 8.9 dB

3. From steps 1 and 2, determine the OAPWL

   OAPWL = 135.9 dB

4. Utilize Figure 4.8-2 or Table 4.8-1 to determine the free-field OASPL at the 120° location

   OASPL (120°) = OAPWL − 39.2 = 96.7 dB

119

5 Calculate the peak frequency, f_c, from Eq. (11), with $K_f = 8$

$$f_c = 501 \text{ Hz}$$

6. Using the OASPL and peak frequency from steps 4 and 5, construct the free-field, one-third octave spectrum from Figure 4.8-3 or Table 4.8-2.

7. Add 6 dB to the free-field spectrum, for purposes of comparing with data measured with ground plane microphones.

This completes the prediction for the 120 degree location. For other locations, only steps 4, 6 and 7 need to be repeated.

Figure 4.8-4 presents the results of the above prediction compared to the corresponding measured spectrum from the JT8D-109. Also shown is the predicted jet noise spectrum. The comparison of measurement with predictions is seen to be quite good.
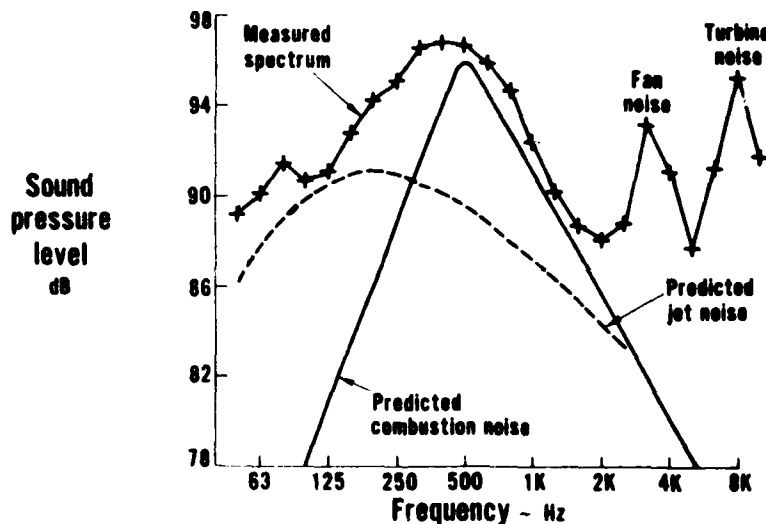
Figure 4.8-4   Measured and Predicted Combustion Noise Spectra for the JT8D-109 Engine Engine, 120°, 150 Ft Radius, 5499 RPM

4.9   IDENTIFICATION OF CONTROLLING PARAMETERS

The combustion noise prediction system presented in the preceding section has identified both geometry and performance variables that control the combustion noise power levels, transmission losses, and spectral peak frequencies. These are summarized in this section.

4.9.1   Acoustic Power Levels

Predicted and measured engine and rig combustion noise power levels from Eq. (50) are:

- Inversely proportional to the number of fuel nozzles.

- Proportional to the square of the burner cross-sectional area, although this parameter appears to the inverse 4th power in the flow parameter term.

- Proportional to the square of burner inlet pressure.

- Proportional to the 4th power of the burner flow parameter.

- Approximately proportional to the inverse square of burner inlet temperature.

- Proportional to the square of burner fuel-air ratio.

- Dependent on the transmission losses associated with the propagation of combustion noise to a farfield observer, as discussed next.

4.9.2   Transmission Losses

The transmission losses predicted by Eq. (49) were found to be:

- Approximately proportional to the ratio of specific impedances across the turbine (i.e., turbine pressure ratio divided by square root of turbine temperature ratio); This typically accounts for approximately 1 to 4 dB attenuation.

- Inversely proportional to the circumferential extent (i.e., $L/\pi D$) over which the acoustic pressures are correlated at the combustor/ turbine interface in the engine. The value of this parameter was empirically determined to be equal to .23 in the present study, which accounts for a 6.3 dB transmission loss.

4.9.3   Peak Frequencies

Predicted and measured combustion noise peak frequencies from Eq. (11) are:

- Proportional to the ratio of fuel flow rate to burner inlet pressure at the design condition, which is taken to be at the engine takeoff power condition.

- Inversely proportional to the burner volume.

121

5.0 COMPARISON WITH PREVIOUS FAA DATA AND PREDICTIONS

Combustion noise data from the JT8D burner component tests at X-410 stand, and from four P&WA full scale engines (i.e., JT8D-109, JT9D-7A, JT9D-70 and JT10D prototype) are compared in this section to General Electric data and predictions obtained under previous FAA Contract (Reference 2). Comparisons of combustion noise spectra, directivity patterns, and overall power levels are presented.

The General Electric acoustic data was obtained using pole mounted microphones which required "ground-dip" corrections to the spectra[2] to obtain estimates of free-field levels. P&WA noise data was obtained using ground plane microphones over a hard surface, which require only a constant adjustment factor of —6 dB at all frequencies for correction to free-field conditions. All General Electric and P&WA results are presented herein as "free-field".

5.1   BURNER RIG COMBUSTION NOISE DATA

In this section, P&WA data from several JT8D type burner configurations, tested separately at X-410 stand, are compared to rig data from two full size annular type burners (i.e., the CF6 and F101) that are reported in Reference 2. Comparisons are also included of the P&WA rig data with G.E.'s suggested correlations for both engine and rig levels. OAPWL's presented in this section are referenced to 10^{-13} watts for comparison with G.E. data and predictions.

5.1.1   Combustion Noise Power Levels

Figures 5.1-1 and 5.1-2 present combustion noise power levels from several P&WA JT8D type burners compared to the suggested G.E. combustion noise correlations for full scale engines and burner rig tests, respectively. The JT8D rig noise levels are roughly 20 dB higher than the G.E. engine correlation as shown in Figure 5.1-1 and, in addition, are scattered by as much as 12 dB at a given value of the correlation parameter. Figure 5.1-2 shows that when the JT8D rig data is presented as a function of the burner exit velocity (suggested by G.E. in reference 2), the data are below the correlation of the CF6 and F101 data by as much as 8.5 dB.

5.1.2   Combustion Noise Directivity

A typical directivity from the P&WA JT8D burner component tests is compared with two sample directivities from the G.E. CF6 burner (for different fuel/air ratios) in Figure 5.1-3. The directivity for the G.E. CF6 burner is significantly steeper than the JT8D. This difference may be attributed to refraction changes due to the differences in rig exit diameters, exit temperatures and exit jet velocities.

122
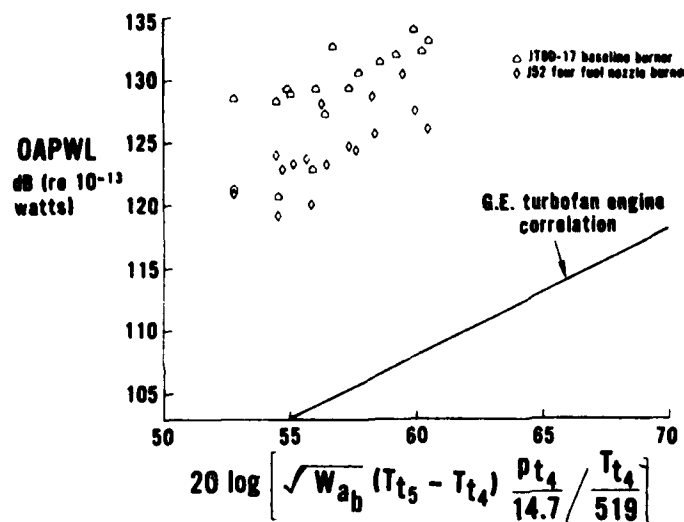
Figure 5.1-1   Comparison of JT8D Burner Component Noise Levels With the Suggested
G.E. Engine Correlation Parameter
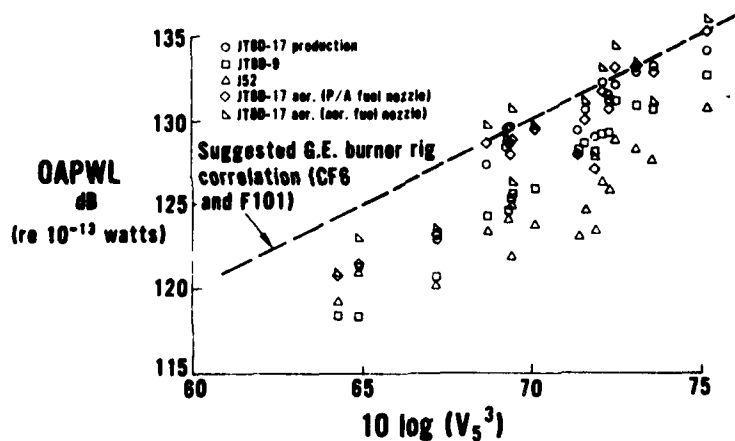
Figure 5.1-2   Comparison of JT8D Burner Component Noise Levels With the Suggested
G.E. Rig Correlation Parameter
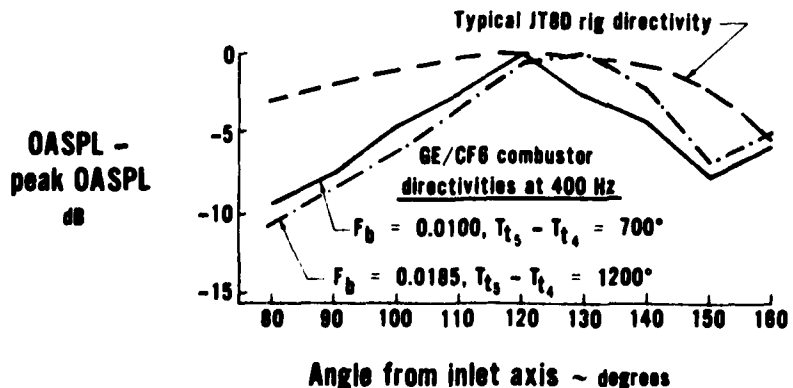
Figure 5.1-3   Comparison of G.E./CF6 and P&WA/JT8D Combustion Noise Directivities
From Rig Data

123

5.1.3 Combustion Noise Spectra

The general combustion noise spectral definition derived from the JT8D burner rig test program is compared to those from the G.E. CF6 and F101 burners in Figures 5.1-4 and 5.1-5, respectively. The general combustion noise spectra shapes are similar for both the G.E. and P&WA burners, although the combustion noise peak frequencies for the G.E. burners are around 280 Hz (similar to the P&WA JT9D annular burner) as compared to 500 Hz for the JT8D can-type burner.
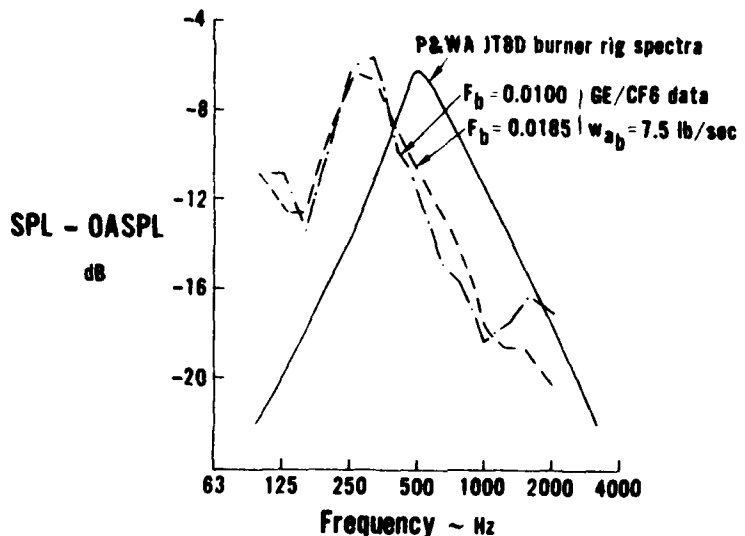
Figure 5.1-4   *Comparison of G.E./CF6 and P&WA/JT8D Combustion Noise Spectra, Component Rig Tests*
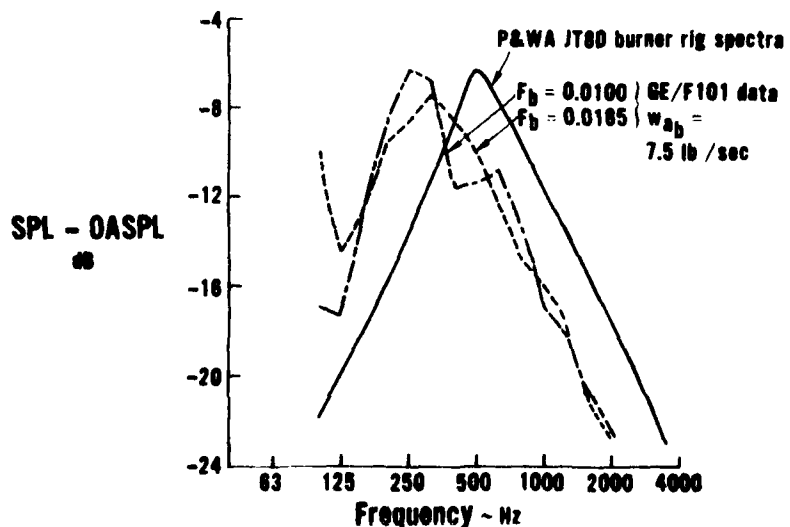
Figure 5.1-5   *Comparison of G.E./F101 and P&WA/JT8D Combustion Noise Spectra, Component Rig Test*

124

5.2 ENGINE COMBUSTION NOISE DATA

In this section data from four P&WA engines tested at X-314 outdoor noise test stand (Section 4.0) are compared to similar G.E. combustion noise data and predictions for turbofan engines.

5.2.1 Combustion Noise Power Levels

Combustion noise power levels from the four P&WA engines are compared in Figure 5.2-1 with the suggested G.E. turbofan prediction system [2]. While the six data points from the G.E. turbofans are in fair agreement with the correlation, the P&WA data differs by as much as +9 dB and −5 dB from the suggested G.E. prediction. The P&WA data in Figure 5.2-1 fit the G.E. turbofan equation to a standard deviation of 6.4 dB.
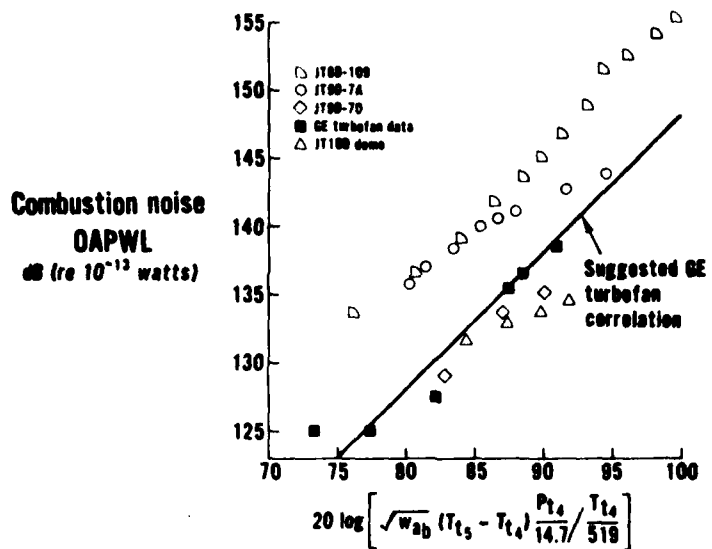
Figure 5.2-1   Comparison of P&WA Engine Test Results Wigh G.E./FAA Turbofan Prediction

5.2.2 Combustion Noise Directivity

The general P&WA directivity pattern, developed from an average of the results from four turbofan engines (Section 4.8) is compared with the predicted G.E. directivity pattern (based on G.E./T64 data) in Figure 5.2-2. The directivity patterns for P&WA and G.E. engines are in good agreement at all angles.

125

OASPL at 150 ft radius, OAPWL ref 10⁻¹³ watts

OASPL -
OAPWL
dB

Angle from inlet axis ~ *degrees*
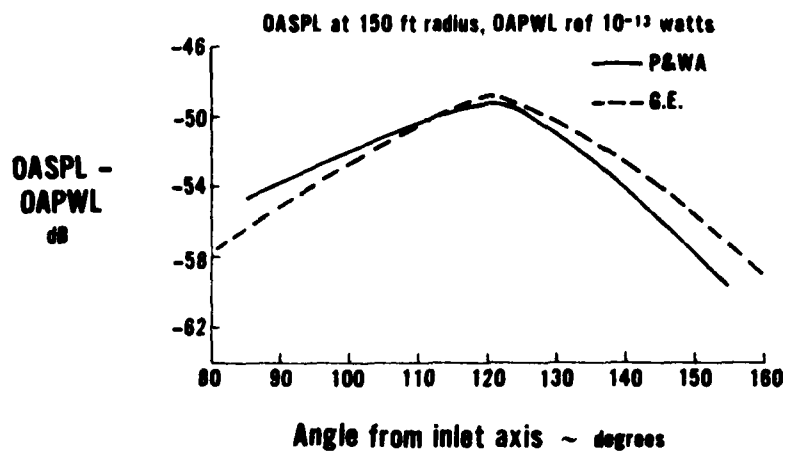
Figure 5.2-2   Comparison of P&WA and G.E. Combustion Noise Directivity Predictions

5.2.3   Combustion Noise Spectra

Figure 5.2-3 shows the combustion noise spectral characteristics for the G.E./
T64 and four P&WA turbofan engines. Although the spectral shapes are quite
similar, the combustion noise peak frequencies vary from about 280 to 500 Hz
on a 1/3 octave band basis. The combustion noise spectra shape characteristics
of both P&WA and G.E. engines are seen to be in good agreement in Figure
5.2-4, when normalized by their respective peak frequencies. For all engines the
combustion noise spectral characteristics were found to be relatively invarient with
engine operation.

SPL - OASPL
dB

Frequency - Hz
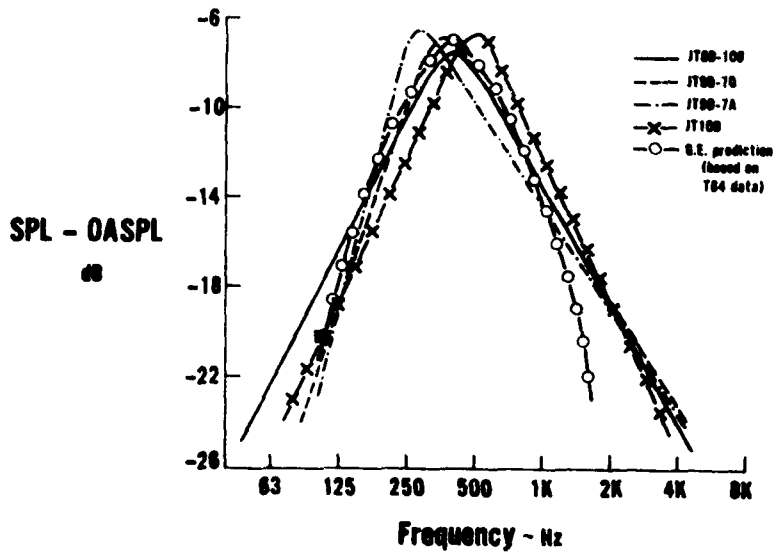
Figure 5.2-3   Combustion Noise Spectra From P&WA and G.E. Turbofan Engines

126
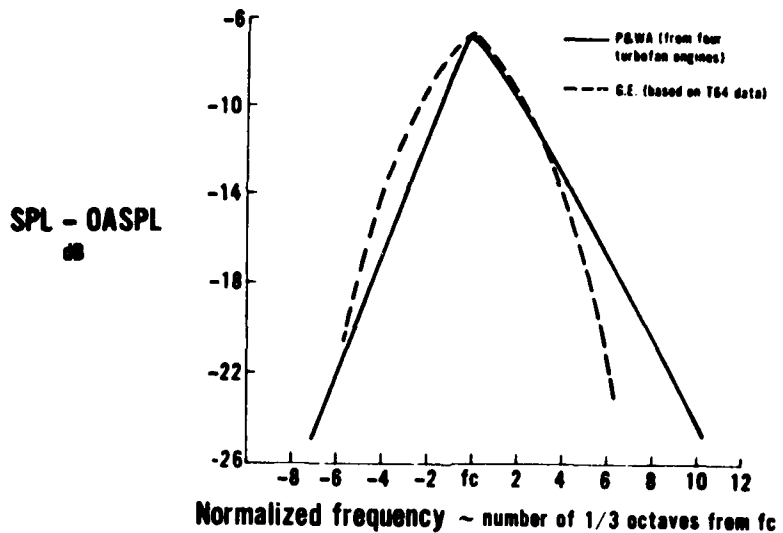
Figure 5.2-4 *Comparison of P&WA and G.E. Combustion Noise Spectra Shape Predictions*

5.3 SUMMARY OF COMPARISONS

The following remarks summarize the results of the comparison of P&WA rig and engine combustion noise data with previous FAA data and predictions presented in Reference 2.

Rig Data and Predictions

- Neither G.E. rig nor engine correlation parameters adequately collapse data from P&WA burner rig tests, on a power level basis.

- The P&WA rig data do not fit the G.E. recommended correlation curves.

- The P&WA rig directivities are flatter than those from G.E. rig tests due to changes in refraction[16] caused primarily by the larger ratio of exit diameter to wavelength associated with the G.E. rig.

- The P&WA and G.E. rig combustion noise spectra are similar in shape, but are centered at different peak frequencies. The magnitude of these differences is consistent with those predicted by the P&WA peak frequency model.

Engine Data and Predictions

- Combustion noise power levels from P&WA turbofan engine data are not in good agreement with the turbofan predictions suggested by G.E. in Reference 2.

- P&WA and G.E. predicted combustion noise directivity patterns are similar.

- P&WA and G.E. engine combustion noise spectra are similar in shape, but are centered at different frequencies.

- The G.E. predicted spectra peaks at 400 Hz for all engines. The P&WA engine spectra peak at frequencies ranging from 280 to 500 Hz depending on the engine burner geometry. These differences are predicted by the P&WA procedure.

6.0 COMBUSTION NOISE REDUCTION

In this section, the combustion noise data and prediction system discussed in the preceding sections are utilized to identify combustion noise reduction methods for future low emissions engines. In addition, emissions data are presented for three of the conventional and low emissions JT8D type burners described in Section 2.0, and for the JT9D-7 engine. Finally, the optimization of the combustion noise/emissions tradeoff is discussed.

6.1 IDENTIFICATION OF NOISE REDUCTION METHODS

In Section 4.9, the parameters that control combustion noise levels were presented. These parameters fall into two categories (i.e., geometry and performance). Some of the parameters affect the generation of combustion noise, while others influence the transmission losses between the combustor and a farfield observer. In this section, methods for reducing the generated noise and increasing the transmission losses for future engines are discussed.

6.1.1 Geometry Modifications

Five possible methods for obtaining reductions through burner geometry modifications have been identified. These are discussed below.

- Measured levels of combustion noise on a four fuel nozzle JT8D type burner (Sections 2.3 and 2.4) were found to be 6 dB lower than those from single fuel nozzle production JT8D burners. This reduction is also predicted by Eq. (50). Additional evidence of this effect is provided by the fact that measured combustion noise levels from a JT3D engine[1] with eight burners (each containing six fuel nozzles) are substantially lower than the levels from the JT8D engines with nine burners (each containing only one fuel nozzle). These predicted and measured results suggest that an effective means of reducing combustion noise would be to increase the number of fuel nozzles in the burner.

- Although the burner cross-sectional area appears to be a power of +2 in the prediction model of Eq. (50), it also appears to the −4 power in the flow parameter term, thus suggesting that increases in the burner cross-sectional area will result in noise reductions by decreasing the velocities through the burner. The extent to which the area may be increased however, may be limited by practical considerations, such as fuel distribution problems in the burner which would require multiple radial fuel nozzles. In addition, if the flow parameter were reduced in this manner, the length of the burner would have to be shortened to maintain the smaller residence times required for low NO_x emissions (If the burner were not shortened, a high residence time would result in increased NO_x pollutant levels.). In addition, the shortened burner could result in pattern factor problems at the turbine first stage.

129

- It also appears that noise reductions can be achieved by reducing the circumferential extent, $L/\pi D$, over which the acoustic pressures are correlated at the combustor/turbine interface. This would serve to increase the transmission losses that occur downstream of the combustor. It has not yet been determined how this may physically be achieved.

- Figure 4.7-1 shows that combustion noise levels from the JT9D-70 engine (with a short, bulkhead front-end burner) are 4 to 5 dB lower than those from the earlier JT9D-7 engine with a significantly different burner design. It is not currently understood how these design changes resulted in the observed noise reduction. More work needs to be done to ascertain the reasons for this reduction.

- The geometry modification associated with the two-stage, advanced low emissions JT8D-vorbix burner resulted in small noise reductions relative to conventional JT8D type burners, as discussed in Section 2.3. This has been reflected in the prediction procedure presented in Section 4.8, and suggests that there is potential for reducing the noise by staging the combustion process.

6.1.2 Performance Modifications

The combustion noise reduction potential associated with cycle (or performance) changes is limited for current engines and for growth derivatives of these engines. For future P&WA engines, however, where cycles will in part be selected by noise considerations, the prediction procedure presented in Section 4.8 indicates that combustion noise may be reduced by any one (or combination) of the following methods:

- Decrease the burner inlet pressure

- Increase the burner inlet temperature (in an actual engine, the inlet pressure and temperature are not independent, but are related through the compressor efficiency.)

- Decrease the burner fuel-air ratio

- Increase the turbine pressure ratio (This appears in the transmission loss term, as part of the ratio of specific impedances across the turbine.)

In past cycle selection studies, the above parameters were dictated by performance requirements alone. However, as a result of the prediction system developed under this contract, it will be possible to include combustion noise considerations in future engine cycle selections. However, it will only be through detailed noise/cycle optimization studies that changes in these parameters can be defined that will reduce noise without sacrificing engine performance, durability, TSFC, and emissions.

130

6.2 COMBUSTION NOISE/EMISSION OPTIMIZATION STUDY

6.2.1 Summary of Emissions Data

Emissions information at several key design operating conditions (idle, approach, climb and takeoff) are supplied in this section for the production JT8D-17 burner, the low emission JT8D-17 aerating nozzle burner, the two-stage advanced low emission JT8D-vorbix burner, and the JT9D-7A engine. All emission data is presented in terms of emission indices (EI) which specify lbm of pollutant per 1000 lbm of fuel. The pollutants discussed here include carbon monoxide (CO), unburned hydrocarbons (THC) and oxides of nitrogen (NO_x).

6.2.1.1 JT8D Conventional and Low Emissions Burners

A summary of emission data obtained for three JT8D type burners tested in high pressure rigs is presented in Table 6.2-1. This information is presented at the simulated idle, approach, climb and takeoff conditions as defined in the 1979 Emissions Regulations. Table 6.2-1 shows clearly that the introduction of the aerating fuel nozzle reduced emission levels of unburned hydrocarbon (THC) and carbon monoxide (CO) at idle and approach conditions. Increases seen in the THC and CO levels from the JT8D-17 aerating burner at climb and takeoff conditions are considered insignificant since idle and approach levels constitute over 90% of the regulated EPAP parameter.

The advanced low emission JT8D-vorbix burner achieved marked improvement in THC and NO_x pollutants over the production JT8D-17 burner. The reduction in THC levels for the vorbix burner was comparable to that achieved with the JT8D-17 aerating burner, while the lower NO_x levels from the vorbix burner at higher powers represented a significant improvement over the production and aerating JT8D-17 burner levels. The reduction achieved in the CO level for the JT8D-17 aerating burner was not duplicated with the JT8D-vorbix burner. As indicated in Table 6.2-1, the vorbix levels were comparable to those from the production JT8D-17 burner.

TABLE 6.2-1

JT8D BURNER EMISSIONS DATA
(FROM HIGH PRESSURE RIGS)

Operating Condition	JT8D-17 Production Emission Index (EI)			JT8D-17 Aerating Emission Index (EI)			JT8D-vorbix Emission Index (EI)		
	THC	CO	NO_x	THC	CO	NO_x	THC	CO	NO_x
Idle	25.5	55.6	2.77	1.75* 20^x	14.52* 7.73^x	3.7.* 3.96^x	43+	52.95+	2.73+
Approach	1.31	12.50	7.40	.24	2.14	9.43	.28+	13.53+	5.20+
Climb	.14	.81	20.30	.23	3.18	22.65	.30	1.97	11.03
SLTO	.06	.53	24.30	.13	1.12	29.23	.10	1.05	14.06

* All secondary fuel (A/R)
x All primary fuel (P/A)
+ 100% pilot

131

6.2.1.2 JT9D Engine

Emissions data from a JT9D-7 engine is presented in Table 6.2-2. The emission indices for THC, CO and NO_x are presented at four key engine operating conditions (i.e., idle, approach, climb, and takeoff). The general trends seen in Table 6.2-2 are toward decreasing CO and THC levels and increasing NO_x levels, when going from idle to takeoff engine conditions.

TABLE 6.2-2

JT9D-7A EMISSIONS DATA
(FROM FULL SCALE ENGINE TESTS)

Operating Condition	Emission Index (EI)		
	THC	CO	NO_x
Idle	29.8	77.0	3.3
Approach	1.0	9.6	8.4
Climb	0.1	0.5	22.9
Takeoff	0.05	0.2	31.5

6.2.2 Noise/Emissions Tradeoff Influence Coefficients

In order to define methods of reducing noise, subject to emissions constraints, it is necessary to establish the noise/emissions tradeoffs in terms of burner operating parameters. A discussion of the effects on noise and emissions of changing the burner flow parameter was presented in Section 6.1.1. In this section, the effect of independent variations in burner fuel-air ratio, inlet temperature and pressure on noise and emission trends is discussed for the JT8D-17 production burner, the JT8D-17 aerating burner and the JT8D-vorbix burner.

While the independent effects on noise due to variations in the above parameters are presented quantitatively by the predictions given in Section 4.8, similar information for emissions was obtained in the form of influence coefficients from available emissions data on the three burners being considered. This information is presented in Tables 6.2-3 through 6.2-5 in the form of emissions influence coefficients, i.e., the percent change in emissions index (EI) associated with a 1% change in the performance parameter. The total effect on a particular pollutant of changing several burner performance parameters can be represented by

$$d\,(EI) = \left[\frac{\partial(EI)}{\partial P_1}\right]_{P_2, P_3} dP_1 + \left[\frac{\partial(EI)}{\partial P_2}\right]_{P_1, P_3} dP_2 + \left[\frac{\partial(EI)}{\partial P_3}\right]_{P_1, P_2} dP_3 + \ldots \qquad (51)$$

where P represents a particular performance parameter and the partial derivatives in this equation represent the emissions index influence coefficients associated with an independent change in the specific performance parameter. Tables 6.2-3 through 6.2-5 show the effects on emissions of an independent parameter change which results in combustion noise reduction. The emission trend information presented in these tables are estimates based upon limited high pressure burner rig test data.

TABLE 6.2-3

EMISSIONS INDEX INFLUENCE COEFFICIENTS FOR FUEL/AIR RATIO DECREASES
(LIMITED TO ±20% VARIATION IN F_h)

Burner	Operating Condition	Effect on Noise	EI Influence Coefficients (%/%)		
			CO	NO_x	THC
JT8D-17	Idle	Decrease	- .3	- .6	+ 1.4
Production	Approach	Decrease	+1.2	0	+ 2.4
	Climb	Decrease	?	+ .5	?
	SLTO	Decrease	?	+1.0	?
JT8D-17	Idle	Decrease	+ .1	- .4	+ 1.7
Aerating	Approach	Decrease	?	0	?
	Climb	Decrease	?	+ .5	?
	SLTO	Decrease	?	+ 1.0	?
JT8D-Vorbix	SLTO	Decrease	+1.5	- .5	?

TABLE 6.2-4

EMISSIONS INDEX INFLUENCE COEFFICIENTS FOR BURNER
INLET TEMPERATURE INCREASES
(LIMITED TO 50°R CHANGES IN T_{t_4})

Burner	Operating Condition	Effect On Noise	EI Influence Coefficients		(%/%)
			CO	NO_x	THC
JT8D-17 Production	Idle	Decrease	-2.0	+3.3	-4.4
JT8D-17 Aerating	Idle	Decrease	-2.8	+2.0	-5.0
JT8D-Vorbix	SLTO	Decrease	-4.1	+2.2	?

133

EMISSIONS INDEX INFLUENCE COEFFICIENTS FOR
BURNER PRESSURE DECREASES
(LIMITED TO +20% VARIATION IN p_{t_4})

| Burner | Operating Condition | Effect On Noise | EI Influence Coefficients | | (%/%) |
			CO	NO_x	THC
JT8D-Vorbix	SLTO	Decrease	+.9	-.4	?

Table 6.2-3 presents the emissions index influence coefficients associated with re-
ductions in burner fuel-air ratio. A decrease in fuel-air (keeping all other parameters
constant) resulted in a predicted decrease in combustion noise levels at all condi-
tions for all burners (Section 4.8). At the approach condition, it is shown that
NO_x levels would not change for either the production or aerating JT8D-17 burn-
ers, while CO and THC levels would increase significantly for the production JT8D-17
burner. The available emission trend information for the JT8D-vorbix burner is for
the takeoff condition only, and shows that a slight reduction in NO_x levels is accom-
panied by an increase in CO levels.

The effect of an increase in burner inlet temperature on combustion noise and
emissions levels is shown in Table 6.2-4 for limited operating conditions. By in-
creasing the burner inlet temperature, a predicted noise reduction is obtained at
all conditions. Idle CO and THC levels are shown to decrease and NO_x levels are
shown to increase for both JT8D-17 type burners. For an increase in inlet tempera-
ture at the takeoff condition, the CO levels from the vorbix burner are shown to
decrease, while NO_x levels increase for this burner.

Data were not available to demonstrate the effect of burner pressure on emission
levels from the JT8D-17 production or aerating burners. The only available informa-
tion on the effects of burner pressure changes on emissions was for the JT8D-vorbix
burner at a takeoff condition, shown in Table 6.2-5. A burner pressure decrease
is predicted (Section 4.8) to result in a combustion noise reduction, while CO
levels will increase and NO_x levels decrease.

The use of tradeoff information such as that presented in Tables 6.2-3 through
6.2-5 for optimizing the noise/emissions tradeoffs are discussed in the following
section.

6.2.3 Optimization of Combustion Noise/Emission Tradeoff

As mentioned previously, there are two basic methods (i.e., geometry modifications and performance changes) by which combustion noise may be reduced. Both methods can result in desirable or undesirable effects on pollutant emissions, and are discussed separately in this section.

6.2.3.1 Optimization Through Geometry Changes

The only burners under this contract for which information on noise, emissions and geometry was available were the JT8D-17 production burner, the low emissions JT8D-17 aerating burner, and the two-stage vorbix advanced low emissions burner. Combustion noise characteristics for these burners, presented in Section 2.3, indicated that virtually no noise benefit will be obtained by utilizing aerating fuel nozzles, and that the reductions in noise associated with the vorbix burner were only modest (i.e., 1 to 2 dB) at all operating points tested (including both design and off-design conditions).

The emissions data for these burners were used to calculate the parameter regulated by the EPA (i.e., EPAP) for each pollutant. The EPAP ratings of the aerating and vorbix burners, relative to the JT8D-17 production burner, are shown in Table 6.2-6, where it can be seen that both the aerating and the vorbix burner produced reductions in THC and NO_x EPAP's. The aerating burner also produced a reduction in CO, but the vorbix burner had higher CO levels.

TABLE 6.2-6

EPAP RATINGS OF JT8D-17 AERATING AND JT8D-VORBIX BURNERS,
RELATIVE TO JT8D-17 PRODUCTION BURNER

Burner	EPAP – EPAP JT8D-17 Production		
	THC	CO	NO_x
JT8D-17 Aerating	-4.26	-12.52	-.26
JT8D- Vorbix	-4.21	+ 3.28	-3.5

The noise and emissions data from these three burners lead to the following conclusions regarding the optimization of the noise/emissions without sacrificing ometry changes:

- The geometry changes associated with the use of aerating, rather than pressure atomizing fuel nozzles resulted in lower emissions without sacrificing noise. These changes, however, do not appear to provide a noise reduction.

135

- The geometry changes associated with the staged vorbix burner result in lower emissions (THC and NO_x) but modest noise reductions.

From the noise, geometry and emission information available to date, it appears that combustion noise cannot be significantly reduced by the incorporation of low emission design features. This observation is based on data from only two low emission burners. Before more definite conclusions can be drawn, additional noise measurements are required on other low emissions burners, including annular type vorbix configurations being considered for engines such as the JT9D.

6.2.3.2 Optimization Through Performance Changes

Tradeoff studies in which performance parameters, such as fuel-air ratio, burner pressure, etc., are varied to minimize noise subject to emissions constraints require knowledge of both the variation in the emissions constituents, and the variation of the combustion noise as functions of these performance parameters. Furthermore, constraints imposed by engine performance (e.g., thrust, fuel consumption, etc.) also need to be included in the tradeoff studies. Because the results of such a tradeoff study will vary, depending on the burner and engine type being considered, general conclusions cannot be made. In this section, a brief description will be given of an approach that could be used to perform noise/emissions tradeoff studies in terms of cycle performance parameters.

The emissions constraints can be defined in terms of the influence coefficients discussed in Section 6.2.2. These coefficients define the effects on emissions of vaiations in the performance parameters, e.g., fuel-air ratio, burner pressure, and burner temperature. The constraints imposed by the engine performance (e.g., thrust) are defined in terms of cycle parameters such as engine pressure ratio, burner fuel-air ratio, etc. Having the emission and cycle constraints defined, application of the calculus of variations would yield a set of performance parameters that would minimize noise while meeting the emissions and engine cycle constraints. A more easily used, but less rigorous alternative to the above approach would be to obtain estimates from Tables 6.2-3 through 6.2-5 of appropriate directions in which the performance parameters could be varied to reduce noise while holding emissions constant (or improving emissions).

136

7.0 CONCLUSIONS

Results from the analytical and experimental combustion noise studies presented in the preceding sections support the following conclusions.

7.1 COMBUSTION NOISE POWER LEVELS

1. Predicted levels of indirect combustion noise for the JT8D-109 engine (using measured dynamic temperature characteristics as input) were 18 to 22 dB lower than those for direct combustion noise. Based on this result, together with the agreement between direct combustion noise predictions and data from four P&WA engines, it is concluded that combustion noise power levels from aircraft type engines are dominated by the "direct" noise mechanisms (resulting directly from the unsteady combustion), rather than by "indirect" combustion noise associated with the convection of burner generated temperature fluctuations through the turbine pressure drop.

2. An improved direct combustion noise prediction procedure has been developed that accurately predicts levels and peak frequencies from both rigs and engines. When the prediction model for transmission losses associated with both the combustor/duct coupling and across the turbine itself are taken into account, the combustion noise levels from both burner rigs and full scale engines fit a single power level prediction equation to a standard deviation of 1.9 dB. This deviation is significantly less than that experienced when the same data is compared with previously reported procedures (i.e., Reference 2).

3. Predicted and measured combustion noise power levels are inversely proportional to the number of fuel nozzles in the burner.

4. Predicted and measured combustion noise power levels increase with both burner pressure and fuel-air ratio to a power of 2, increase with burner flow parameter to a power of 4, and decrease with increasing inlet temperature.

5. Combustion noise characteristics from burners utilizing aerating fuel nozzles for low emissions are not noticeably different than those from burners operating with conventional pressure atomizing fuel nozzles.

6. Combustion noise levels from the two-stage, advanced low emission JT8D-vorbix burner are 1 to 2 dB lower than those from conventional JT8D burners.

7.2 COMBUSTION NOISE TRANSMISSION LOSS

1. Predicted combustion noise transmission losses are dependent only on the ratio of specific acoustic impedances across the turbine and on the combustor/ duct coupling, i.e., the circumferential extent to which the acoustic pressures are correlated at the combustor/turbine interface.

2. From comparisons of rig and engine data, typical transmission losses are approximately 7 to 11 dB. About 6 dB of this loss is associated with the coupling of the combustor with the duct, where the acoustic pressures are not correlated over the entire circumference at the combustor/turbine interface. The remainder of the loss is predicted to be due to the discontinuity in specific acoustic impedances across the turbine.

3. The measured spectra from JT8D burner component rig tests are similar to the combustion noise spectra from full scale engines, verifying the predicted result that turbine transmission losses are not a function of frequency.

7.3 COMBUSTION NOISE SPECTRA

1. Since the spectral shape characteristics of combustion noise are similar for all burners investigated (including both can-type and annular geometries), it is possible to use a single normalized spectrum for general prediction purposes.

2. Expressions have been analytically derived and experimentally verified for the peak frequencies associated with combustion noise from both can-type and annular burners. For a given burner type, this peak frequency is:

   a. Proportional to the ratio of fuel flow to burner pressure at the design condition.

   b. Inversely proportional to the burner volume.

3. For a given burner, the peak frequency of combustion noise (predicted and measured) is independent of burner operating conditions and farfield measurement location.

7.4 COMBUSTION NOISE REDUCTION

Methods have been identified for reducing combustion noise through either design or performance modifications. These methods are presented below.

Geometry Modifications

Without changing the engine cycle, results of the current investigation suggest that combustion noise may be reduced by:

138

- Increasing the number of fuel nozzles (independent burning regions) in the burner.

- Increasing the cross-sectional area of the reacting region.

- Reducing the circumferential extent to which the acoustic pressures are correlated at the combustor/turbine interface.

- Staging the combustion, as in the two-stage, advanced low emissions, JT8D-vorbix burner.

Performance Modifications

Analytical and experimental results also indicate that combustion noise may be reduced by:

- Decreasing the burner inlet pressure

- Increasing the burner inlet temperature

- Decreasing the burner flow parameter (i.e., velocities through reaction region)

- Decreasing the burner fuel-air ratio

- Increasing the turbine pressure ratio

Many of the above performance modifications, if utilized to effect reductions in combustion noise, could result in penalties in engine performance, durability, weight, economy and pollutant emissions. The results of the current investigation will enable combustion noise considerations to be used in the trade-off studies that are a part of the cycle selection process for future engines.

APPENDIX A

SUMMARY OF TURBULENCE MEASUREMENTS IN JT8D-TYPE BURNERS

As part of Phase I of the current contract, cold flow turbulence measurements were made inside a JT8D-17 production burner, a JT8D-17 aerating burner, and a JT8D-vorbix low emissions burner. The primary objective of these tests was to determine the relationship between direct combustion noise and cold flow turbulence characteristics inside the burner. The details of the turbulence and how these details may relate to combustion noise were of prime concern and are discussed in this appendix.

TEST PROGRAM DESCRIPTION

The burner rig at X-410 stand was used to obtain turbulence measurements on the three JT8D-type burners. Although no fuel was burned, the flow parameters (and thus Mach numbers) and inlet temperatures into the burner were set near the aircraft approach condition. More detailed information regarding the operation of X-410 stand was presented in Section 2.3. The flow was provided from the rig through an inlet section to the burner. A hot wire probe was inserted along the center line through the exit diffuser and transition section into the burner as shown schematically in Figure A1. A Disa miniature probe was used with a platinum plated Tungsten sensor. The hot wire sensor was 9 microns in diameter and has a flat frequency response to 15 KHz. A Disa anemometer system was utilized with a RMS voltmeter and a DC voltmeter. Signals from the hot wire were recorded on a Precision Instrument tape recorder for later reduction and analysis.
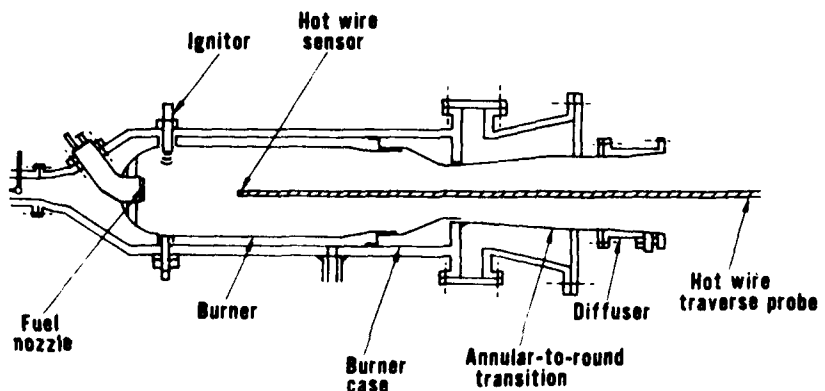
Figure A 1   JT8D Burner Rig and Hot Wire Probe Diagram (X-410 Stand)

The JT8D-17 production and aerating burners are very similar in design with the main difference being the higher mass flow entering the forward section of the aerating burner. The two-stage vorbix burner has a distinct shape with forward and rear reacting regions. In the rear reacting zone there are four swirlers through which approximately 25% of the air passes. These four swirlers are spaced circumferentially every 90 degrees and alternate in swirl direction between clockwise and counterclockwise swirl. Thus, we would expect high fluctuating velocities in the region of these swirlers. The locations along the centerline

141

of each burner where the probes were positioned were 2.5, 5 and 9 inches from the fuel nozzle for the two JT8D-17 type burners and 2.5, 6.5 and 13 inches from the fuel nozzle for the JT8D-vorbix burner. These locations were selected to be within the reaction regions of these burners.

Cold flow turbulence measurements using the hot wire system were obtained at three axial locations in each burner over a range of three performance settings. Flow parameters of approximately 0.055, 0.074 and 0.092 were tested, where the value of 0.074 is approximately the approach condition. In addition to a magnetic tape record of the fluctuating hot wire signal, the RMS fluctuations and the D.C. velocity were obtained at each point.

Because the probe used for the turbulence measurements possessed a single sensor located on the burner centerline, only an approximate idea of the character of the overall cold flow turbulence in the burners was possible. Only components of velocity in the axial direction may be calculated. None-the-less, these measurements should provide valuable knowledge of basic turbulence properties within the reacting region of the JT8D burners that were tested.

DISCUSSION OF RESULTS

The usual technique for representing turbulence information is to express results in terms of "percent turbulence". This value depends upon the local mean velocity measured at the sensor location. Because there exists unusual flow through louvers, dilution holes, swirlers, etc., the measured local mean velocity on the centerline may not necessarily be typical of the mean velocity over the entire cross-sectional area. It was assumed that the measured fluctuations were typical, but that the percent turbulence based upon measured mean velocity was not an accurate indication of the percent turbulence inside the burner. It was therefore decided to present the turbulence directly in terms of the RMS fluctuating velocity.

Figure A2 shows typical levels of RMS fluctuating velocity for each burner at the simulated approach condition (0.074 flow parameter). This figure illustrates the variation of the fluctuation along the burner centerline. The levels for the JT8D-17 burners are in the 20-40 ft/sec range, whereas the turbulence velocities within the vorbix burner increase to about 70 ft/sec in the downstream reaction zone due to the influence of the previously mentioned swirlers.
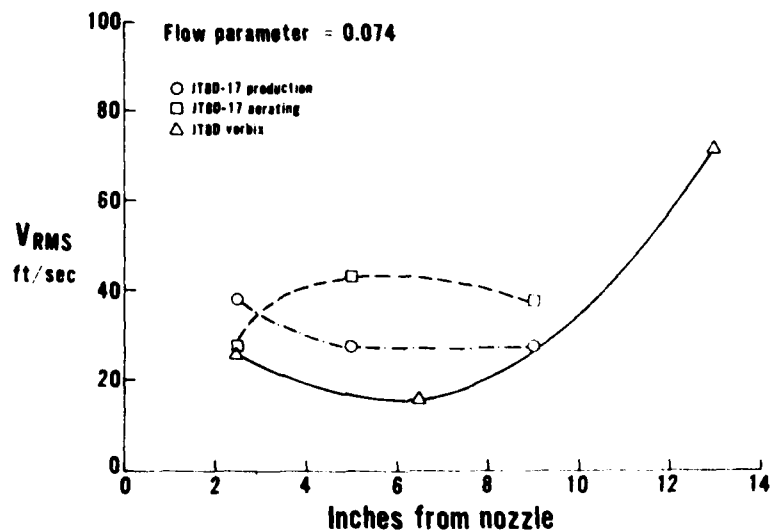
Figure A 2   *Variation of RMS Fluctuating Velocity With Distance From the Nozzle Face*

Figures A3, A4, and A5 show the turbulence 1/3 octave band spectra for the JT8D-17 production, JT8D-17 aerating and vorbix burners, respectively. In all cases the peak frequencies of the turbulence appear to decrease with increasing downstream distance, consistent with the idea of increasing eddy length scales with distance. Spectra from the aerating burner, Figure A4, are quite different from the production burner although the levels of velocity fluctuations are similar. The increased airflow entering the aerating nozzle causes the peak frequency of fluctuation to occur near 6000 Hz at the forward position. As the eddies evolve downstream, their peak frequencies decrease to 125 Hz at a position 9 inches from the fuel nozzle face. Results of spectral measurements inside the vorbix burner are shown in Figure A5. The turbulent velocities tend to decrease in level as the eddies move from the 2.5 inch position to the 6.5 inch position. The decrease in level over this distance reflects the decay of the turbulence in the forward reaction zone. As expected, the spectra from the downstream reaction region is higher in level due to the influence of the swirlers at this location. The fluctuating velocities at the downstream location peak at about 315 Hz and are several times higher in level than at other locations in the burner. The spectra shapes at the other flow parameter settings were similar to those shown in Figures A3, A4 and A5.

Figure A6 shows RMS fluctuating velocity plotted versus the bulk velocity over the range of operation of all three burners. The bulk velocity at any location is proportional to the flow parameter and is calculated from the local mass flow and area. This bulk velocity term is more accurate than the local mean velocity measured by the hot-wire sensor for reasons previously discussed. Figure A6 shows that the RMS fluctuating velocity at the downstream location is roughly proportional to the mean flow through the burner. Although the constant of proportionality changes for other locations, the proportionality relation holds fairly well.
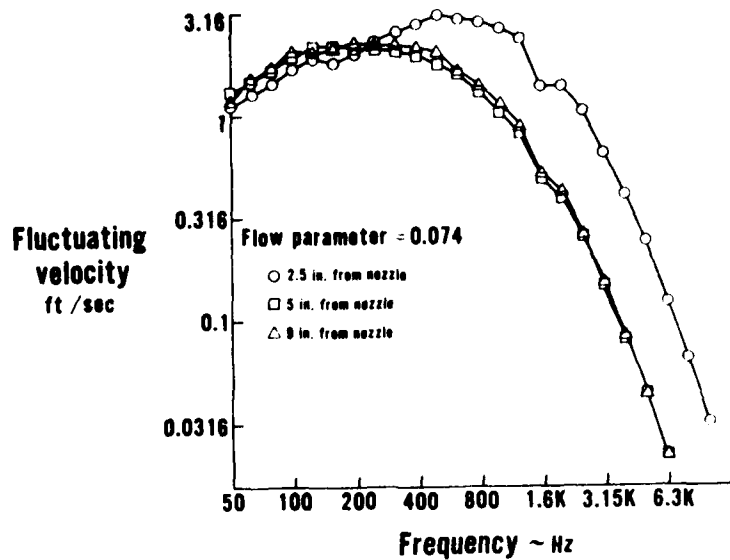
Figure A 3   *Turbulence Spectra Inside the JT8D-17 Production Burner At Approach Condition, Cold Flow*
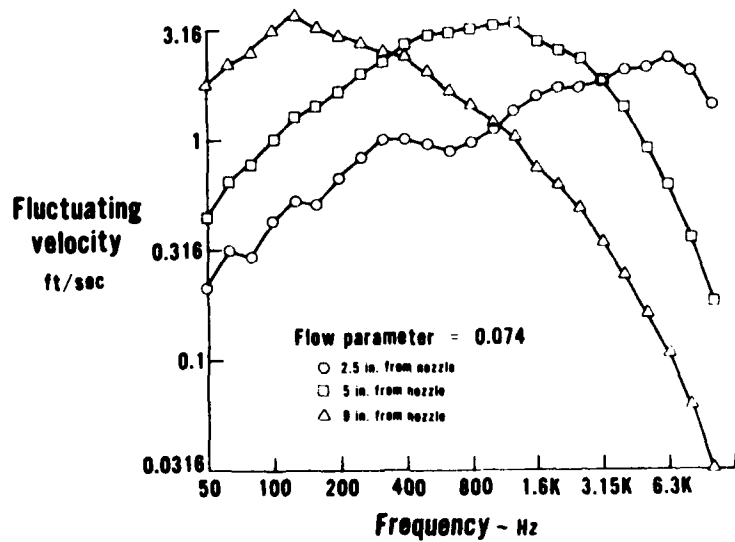
Figure A 4   *Turbulence Spectra Inside the JT8D-17 Aerating Burner At Approach Condition, Cold Flow*

144
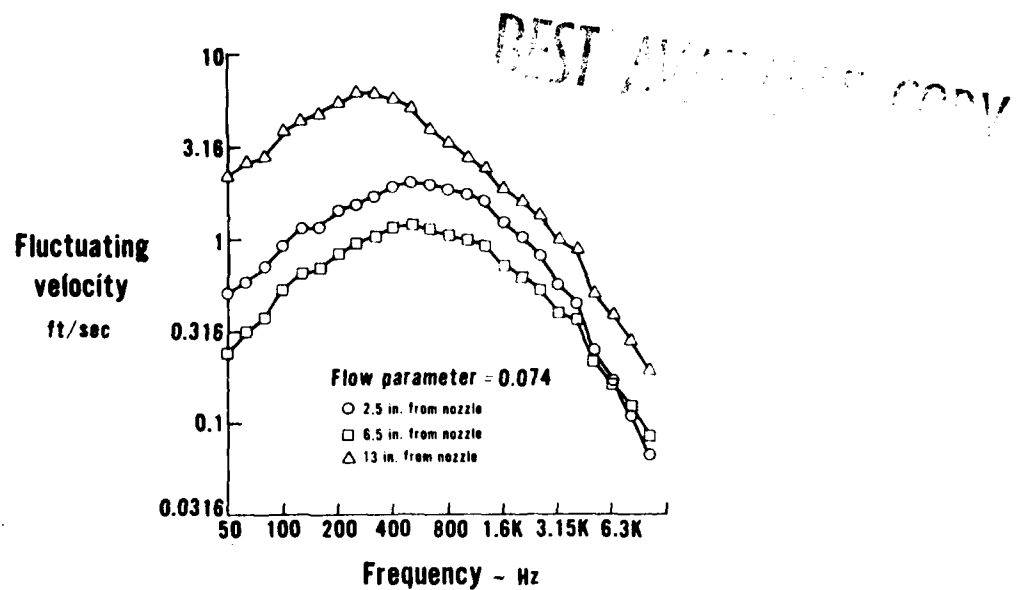
Figure A 5   *Turbulence Spectra Inside the JT8D Vorbix Burner At Approach Condition, Cold Flow*
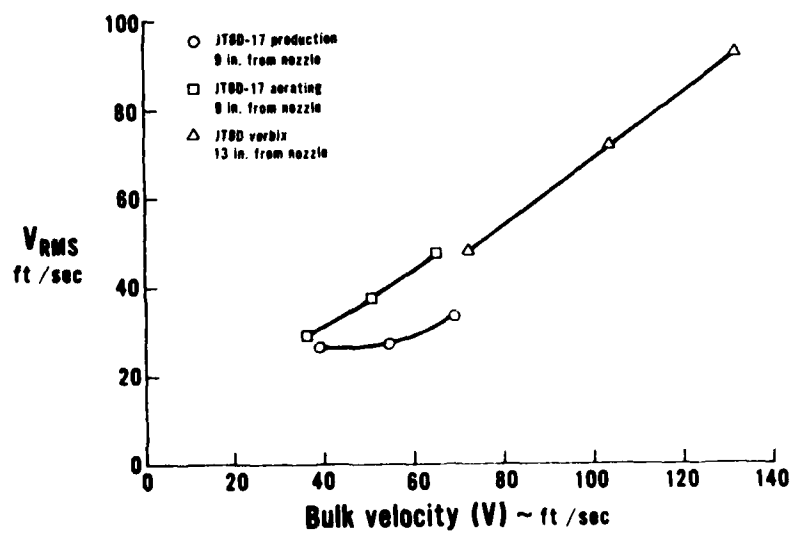
Figure A 6   *RMS Fluctuating Velocity Variation With Bulk Velocity for Three Burners*

145

Another parameter related to frequency is the turbulence length scale. Figure A7 presents the variation of turbulent length scales with flow parameter for the vorbix burner. In general, the length scales of the eddies providing peak fluctuations increase with distance downstream, but remain fairly constant with increasing flow parameter. This implies that the length scales at all locations appear to be controlled more by the geometry than by the flow conditions. At the most rearward position, the length scales are roughly .375 ft. (4.5 inches), suggesting that the turbulent eddy sizes are of the same order of magnitude as the burner can diameter. Similar results were obtained for each of the other two burners tested.
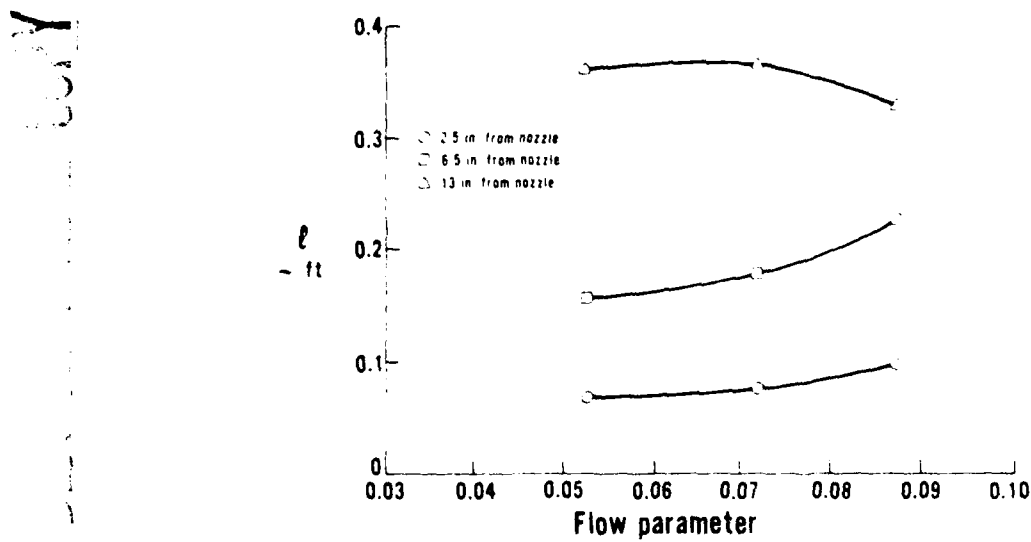
Figure A7   Turbulence Length Scale Variation With Flow Parameter for the JT8D
            Vorbix Burner

CONCLUDING REMARKS

In Section 2.2, an analytical model for direct combustion noise was derived that relates the noise to the fluctuations in heat release rate within the burner. While these fluctuations are probably linked to the turbulence within the reaction region, the characteristics of this hot-flow turbulence are unknown and are most likely highly dependent on the details of the chemical reactions which take place. Therefore, in order to obtain a usable prediction procedure, it was assumed in Section 2.2 that the amplitude of the heat release fluctuations are proportional to the steady mass flux through the burner. This resulted in a prediction procedure that was shown to be in excellent agreement with data from the burners and engines presented in this report. Since the cold flow turbulence characteristics discussed in this Appendix are quite different for the three burners investigated, and since the combustion noise characteristics of these burners were very similar, it is therefore concluded that the cold-flow and hot-flow turbulence characteristics are not strongly correlated, and thus that the generation of direct combustion noise cannot be related to the cold flow turbulence characteristics.

146

APPENDIX B

DISCUSSION OF JT8D RIG RESONANCE PHENOMENON

This appendix reports the efforts performed to define and identify the source of the low frequency noise peak (e.g., 100 to 125 Hz) visible in the measured spectra obtained from JT8D burner rig tests at X-410 stand. It was required that the appearance of this noise in the measured spectra be explained so that an accurate analysis of the actual combustion noise characteristics could be obtained. There were originally thought to be several possible sources of this low frequency noise. Listed below are those which were investigated and are discussed in this section:

1. Jet noise

2. X-410 burner stand and probe noise

3. Actual combustion noise

4. Resonance associated with rig geometry, the frequency of which would be dependent on rig length and temperature

ANALYSIS OF THE LOW FREQUENCY NOISE EVIDENT IN X-410 STAND DATA

Jet noise is a common problem plaguing the analysis of core (combustion) noise in full size engines. The JT8D burner noise rig, diffuser and test conditions were selected to minimize the effects of any jet noise as discussed in Section 2.0. The maximum jet velocity obtained from the burner rig was less than 500 ft/sec and the jet noise SPL level corresponding to this velocity was well below the SPL levels of the low frequency noise.

With regard to the possibility of burner stand or probe noise, three cold flow conditions were run and noise was recorded. Measured spectra from these conditions did not reveal any characteristic low frequency peak near 100 Hz. The highest SPL levels recorded from these cold flow tests were again well below the levels associated with this peak. In addition, the total pressure probe located in the exit plane of the burner rig was removed to determine whether the low frequency noise was caused by this probe. Removal of the probe had no apparent effect on the farfield noise spectra.

Actual combustion noise was also investigated as a possible source of the 100 Hz peak. A literature review of other combustion noise studies did not reveal any mention of a low frequency (i.e., 100 Hz) component to the combustion noise from typical burners. In addition, the combustion noise (near 500 Hz), from tests at X-410 stand (e.g., levels, spectral characteristics and directivity), follow completely different trends than the 100 Hz peak.

The fourth area investigated dealt with a possible longitudinal resonance phenomenon. The resonant frequency of the burner rig may be determined by the speed of sound within the burner rig and the length between the front of the burner and the rig exit plane. If the low frequency peak were due to a resonance, then reducing the length of the burner rig would

increase the peak frequencies according to the following approximate relationship

$$\text{FREQUENCY} \propto \frac{\sqrt{T_{t5}}}{L} \qquad (B1)$$

where L is the length mentioned above and T_{t5} is the burner exit temperature.

During the JT8D-9 burner rig test program the exit diffuser, which is 5.0 inches long, was removed and the simulated approach power condition was rerun. Figure B1 shows the 1/3 octave power level spectra obtained from the simulated approach test condition with and without the diffuser installed. The peak frequency of the resonant spectra increased nearly one 1/3 octave band. This increase in peak frequency can be analytically determined using Equation (B1). With the length of the rig from the face of the fuel nozzle to the exit plane of the diffuser being 37.9 inches, the peak frequency should increase 13.5 percent when the diffuser is removed. This anticipated increase is approximately what is seen in Figure B1.
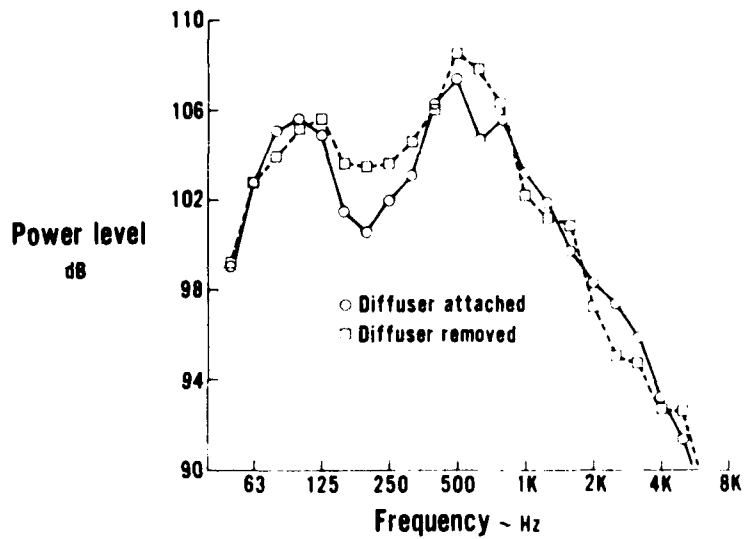
Figure B 1   Effect of Rig Length On Farfield PWL Spectra, JT8D-9 Production Burner

The peak frequencies of the resonance spectra from the JT8D-9 burner are plotted versus the burner exit temperature in Figure B2. The results do not indicate any collapse of the "diffuser removed" condition (square data point) with the remainder of the data. In contrast, when the peak frequencies of the possible resonance spectra were plotted versus $\sqrt{T_{t5}}/L$, a good collapse of all the data resulted as shown in Figure B3. In addition, Figure B3 shows that the data follows a line at the expected slope predicted by Equation (B1).
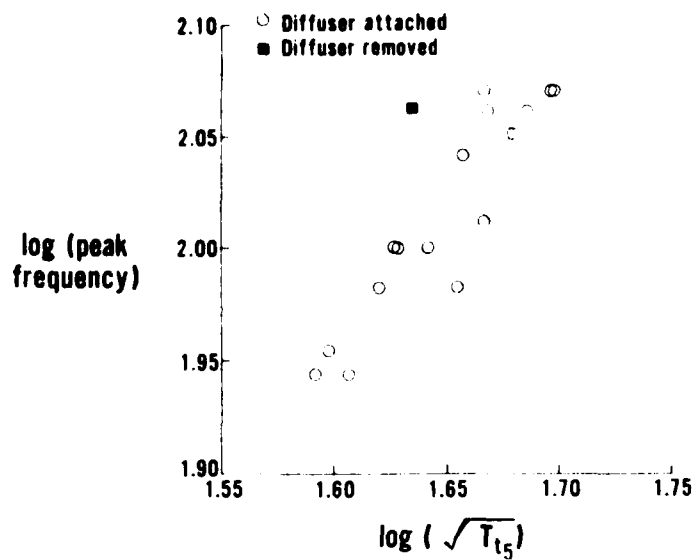
Figure B 2   *Measured Resonance Frequencies, JT8D-9 Burner Rig*
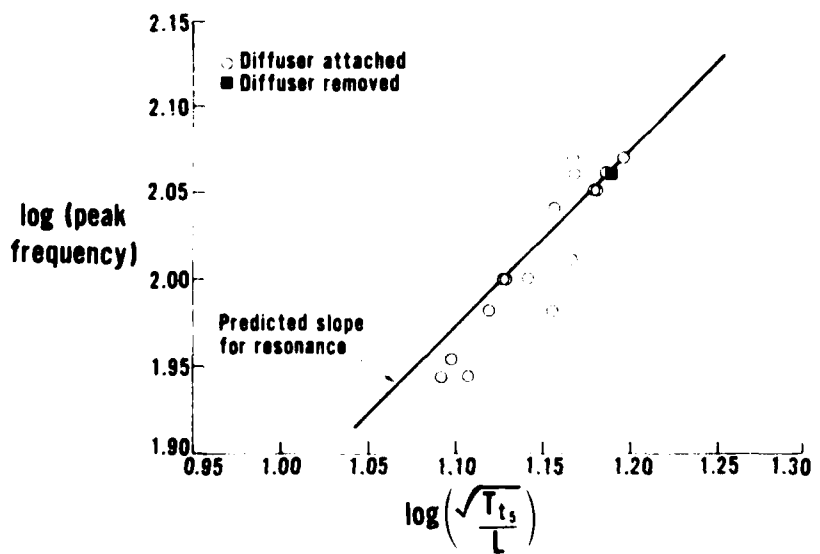
Figure B 3   *Comparison of Predicted and Measured Resonance Frequencies, JT8D-9 Burner Rig*

149

If this low frequency peak is indeed due to resonance. then standing waves should exist, such that the internal pressure fluctuations at this frequency should be a maximum at the front of the burner and a minimum at the rig exit plane, regardless of whether the resonance is of the "organ pipe type" (i.e., quarter-wave length) or of the Helmholtz type. The internal dynamic pressure was analyzed to see if. in fact, standing waves of this sort do exist. The resonance, located in the 100 to 125 Hz region, that was clearly visible in the farfield microphone data is also seen in the spectra from the internal Kulites, as shown in Figure B4. However, the peak SPL levels of the low frequency resonance noise is seen to be nearly 15 dB lower at the rig exit than at the front of the burner, which as mentioned above, would be expected of a resonance phenomenon.
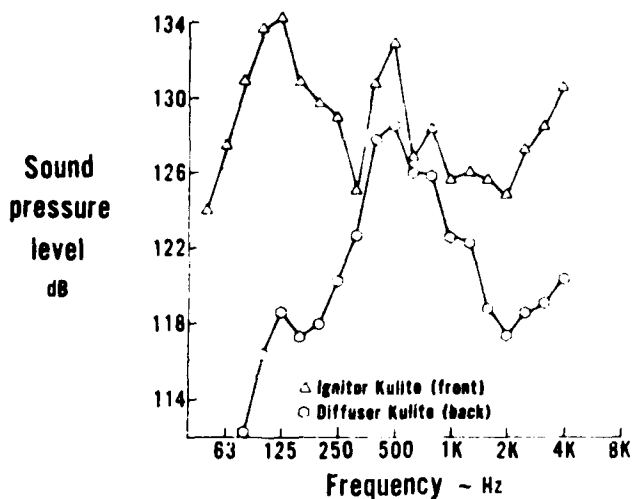
Figure B 4   Internal Burner Rig SPL Spectra At Simulated Approach Condition. JTSD-17 Aerating Burner, P/A Fuel Nozzle

Although these studies have not attempted to account for the effects of axial temperature and velocity gradients occurring within the burner rig. it is believed that sufficient evidence has been found to demonstrate that the low frequency spectra peak (centered at about 100 Hz) is indeed a resonance phenomenon. Fortunately, this resonant spectra does not prohibit an accurate definition of the combustion noise SPL levels and spectral characteristics. In addition, the levels of the pressure fluctuations due to this resonance are not considered to be strong enough to affect the combustion process.

RESONANT NOISE AND FEEDBACK COUPLING WITH FUEL SYSTEMS

Two types of fuel systems were tested on the JT8D-17 aerating burner (i.e., pressure atomizing and aerating types). Although no differences in the combustion noise (500 Hz) levels were observed, substantial difference in the low frequency resonant noise levels were seen. as shown in Figure B5. A brief discussion of the two fuel systems and their sensitivity to acoustic feedback at X-410 burner noise stand is presented in the following paragraphs.

150
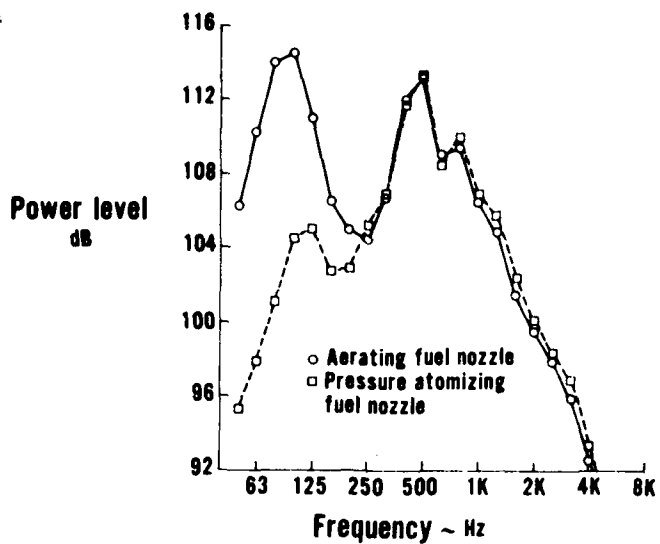
Figure B 5   *Farfield Burner Rig PWL Spectra At Simulated Approach Condition,*
JT8D-17 Aerating Burner

The fuel from the pressure atomizing nozzle is atomized by a large pressure drop across the fuel nozzle. Distribution of the fuel into the burning region is determined by the velocity of the fuel as it exits from the fuel nozzle. This distribution would be essentially insensitive to burner pressure fluctuations, since the fuel pressure drop across the nozzle is quite large compared to the fluctuations in burner pressure.

In contrast, the fuel for the aerating fuel nozzle is atomized by the high velocity air passing over the surface of the fuel. The distribution density of the fuel droplets in the air is dependent upon the instantaneous velocity of the air which entrains the fuel. Any fluctuation in this velocity (such as could be caused by burner pressure fluctuations) as the flow entrains the fuel will cause a similar fluctuation in the distribution of the fuel into the burning region, thus making the aerating system more sensitive to acoustic feedback than the pressure atomizing system.

From the above analysis, it is suggested that the resonance noise present in the X-410 burner noise stand affects the fuel distribution mechanism of the aerating fuel nozzle and results in a coupling (or feedback) between the resonance and the fuel injection system. This coupling is postulated to be responsible for the increased amplitude of the low frequency peak shown in Figure B5 for the aerating fuel nozzle. Fortunately, it does not appear (Figure B5) that this phenomenon affects the combustion noise generated at higher frequencies.

151

APPENDIX C

INVESTIGATION OF OPTICAL TECHNIQUES

INTRODUCTION

The objective of this investigation was to explore the use of optical techniques in providing a prediction of radiated noise by measuring the characteristics of the source function of combustion noise, as distinct from the more usual investigations in which only the result, namely the acoustic pressure field, is the measured variable. The forcing function, or right-hand side of the ordinary acoustic wave equation, under conditions of heat addition contains a term that is proportional to the time rate of change of the fluctuating heat release rate. Among several forcing terms [C1], this one is generally considered to be dominant, although quite recent studies [C2] were directed to exploring the significance of additional contributors that have been suggested [C3] to have comparable importance in cases where the flow velocities are high enough to require use of the convected wave equation.

The advantage of being able to measure the source function (cause) of combustion noise instead of, or in addition to, the acoustic pressure field (result) is evident in situations where meaningful acoustic field measurements are difficult or impossible to perform, for example during rig test programs where burners are being developed, or during performance testing of engines. Additionally, noise produced by unsteady combustion in aircraft gas turbine powerplants is sometimes difficult to measure in the farfield due to the complicated transmission process of burner noise in propagating through the turbine stages and exhaust nozzle and, because of the presence of continuous spectra noise from other powerplant sources such as the fan and exhaust jet. Internal fluctuating pressure measurements have been made with water-cooled transducers penetrating through the burner walls, but these measurements are subject to another set of obscuring factors (e.g. aerodynamic noise) that make interpretation comparably uncertain [C4].

In the assessment of the effects of burner design and operating conditions on noise generation, and in developing burners for reduced combustion noise levels, a system that would define the noise driving function would bypass some of these difficulties by allowing predictions of noise from measurements of the source strength (cause) rather than the farfield pressure. This is the context in which the possibility of using optical methods was suggested as an important topic of investigation in this program. A particularly important application would be in test rigs for burner development programs. Typical burner rig designs are such that combustion noise measurements are difficult to interpret as a result of local flow noise contamination and other complications [C4]. In developing and refining burner designs, a direct measure of the combustion noise source strength would be of value in two ways. First, it would allow an estimate of the farfield noise of an engine incorporating the combustor design, the accuracy of the estimate depending on the calculation of the transmission of the combustion noise through turbine stages and tailpipe. Secondly, and with obviously greater simplicity and reliability, different burner designs could be ranked for their noise reduction capability by simply comparing their measured combustion noise source strengths.

153

APPROACH

Experiments using fluctuations in light emission as a measure of heat release rate fluctuations, and relating these fluctuations to the acoustic farfield pressure of open premixed turbulent flames have been reported in references C2, C5, C6 and C7. The essential features of the process can be described briefly as follows: it has been determined that the steady light emission intensity in a typical emission band, such as CH, C_2 and OH, resulting from the combustion of gaseous hydrocarbon - air mixtures is proportional to the steady heat release rate. In a turbulent flame, the light intensity is observed to fluctuate about a mean value as a result of time variations in the heat release rate. It is assumed that the ratio of the fluctuations in light intensity and heat release rate is numerically equal to the ratio of the corresponding steady-state quantities, and at the relatively low frequencies of interest in combustion noise, this assumption is likely to be quite secure. Therefore, the fluctuations in light intensity can be used as a measure of the heat release rate fluctuations, using the constant of proportionality as determined from measurements of steady light intensity and (measured or calculated) steady heat release rate. As has been described earlier, the primary source term for combustion noise is proportional to the time rate of change of this unsteady heat release rate. Consequently, for a relatively compact burning zone, if the output voltage of an optically filtered photomultiplier cell viewing the flame is supplied to a differentiator circuit, the output signal will be proportional to the instantaneous source strength.

The procedure for evaluating the use of optics as a diagnostic technique required an arrangement where both the source distribution and the acoustic transmission path are simpler than in the geometry of an engine burner system. Such a validation program was formulated using a relatively compact heat-light-sound source, an open turbulent flame, radiating in a uniform pattern to the farfield. A microphone sensing the farfield acoustic pressure signal would provide means of testing the operation of the system in the following simple manner: By cross-correlating the time-differentiated light signal (proportional to acoustic source strength) with the resulting microphone signal, a high value of cross correlations (at a delay time related to the speed of sound and the source-to-microphone distance) would substantiate the basic concepts and indicate that the equipment was performing satisfactorily. Subsequent to this test program, the factors involved in employing these concepts to measure the source strength and from it estimate the radiated noise in an engine burner would be considered in order to indicate the feasibility of using optical methods in engine combustion noise evaluation studies.

TEST PROCEDURE

The optical system elements were selected on the basis of their expected applicability for use in engine burners and special burner test rig programs. The following elements were involved: selectable apertures to control light intensity; selectable optical filters, and a type IP 28-935 photomultiplier tube. This optical system output voltage was processed in a manner to be described below.

Three types of optical bandpass filters were provided in order to examine those emission bands where previous experience in spectroscopic examination of gas turbine combustion

has indicated high emission levels. Filters were provided to pass radiation from the following species:

OH: 3064, 3067, and 3089 Å — maximum radiation when combustion is
       near stoichiometric

CH: 4315 Å – best in excess air

C₂: 5165 Å – best in fuel rich environment

A schematic diagram of the optical sensor elements is shown in Figure C1.
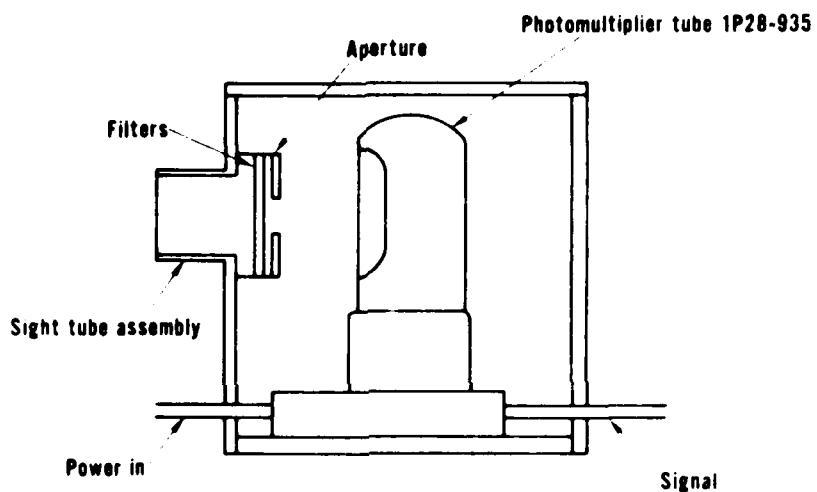
Figure C 1   Diagram of Optical Sensor Elements

A blowtorch was used to provide the source of light and sound. This flame source was selected because of its ready availability, convenience of operation, and because it employs liquid hydrocarbon fuel. Aviation gasoline was employed rather than jet fuel because of its better volatility.

The sound field from the flame source was measured by a standard B&K microphone, preamplifier and power supply system. A schematic diagram showing the arrangement of the flame source, microphone and light sensor is presented in Figure C2.

Figure C3 is an operational circuit diagram for both microphone and photomultiplier tube (PMT) systems, and for cross correlating their output voltages. The microphone system branch elements are standard and required no further description. Several elements are included in the optical system branch, following the PMT, and are described below.

3 ft to 7 ft

Blow torch
light source

1 ft, 2 ft
and 4 ft

B&K 4134
microphone

Photo multiplier
tube

Optical bench
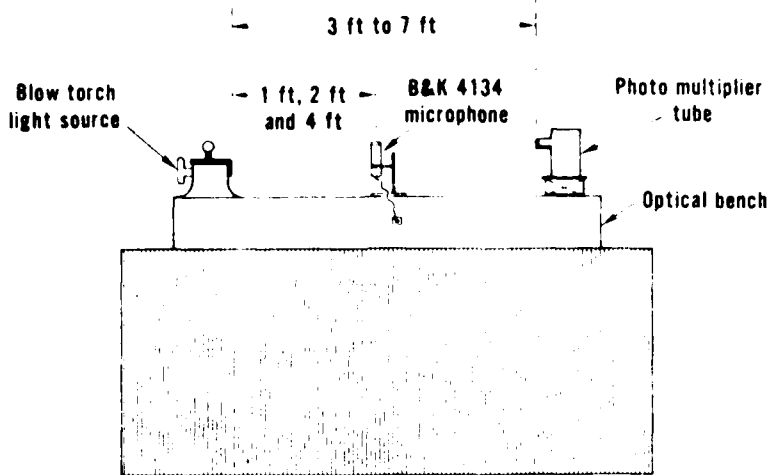
Figure C 2   Optical Test Equipment Arrangement
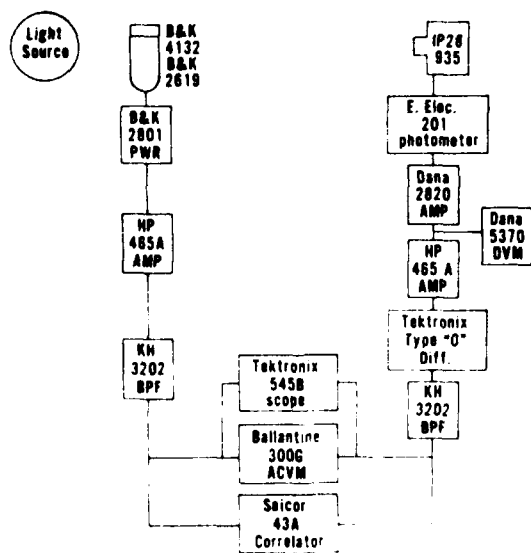
Figure C 3   Optics-Acoustics Circuit Diagram

Immediately following the PMT, a photometer was provided for determining steady light intensity. This element was not used to measure intensity as such, since it was sufficient to have access to the output (both steady and fluctuating components) in units of voltage. In addition to standard elements such as amplifiers, bandpass filters, etc., the most significant circuit elements were as follows: the Dana 5370 Digital Voltmeter used to measure the

156

steady component of the PMT output voltage; the Tektronix type 0 operational amplifier—used to differentiate the fluctuating component of the PMT voltage; Krohn Hite Model 3202 filters in both optical and pressure signal branches—to limit information to the low frequency combustion noise domain; a Ballantine Model 300G true rms voltmeter used to measure the fluctuating output voltage of the microphone and the (differentiated) fluctuating voltage component of the PMT output; and a Saicor 43A correlator—the terminal circuit element used to cross correlate the signals from the acoustic and optics branches.

Two of these elements require additional comment to clarify their essential roles in the measurement system. First, the differentiator is needed in the light circuit because the acoustic source of the microphone signal (and correlated fluctuating light) is not simply proportional to the fluctuating heat (or light) as such, but rather to its time rate of change [C1,C6,C7]. Thus it is desired to correlate the time derivative of the light-proportional voltage (source) with the microphone voltage (receiver).

The Dana Model 5370 D.C. digital voltmeter serves two purposes. For fixed geometry, aperature, optical filter and PMT, it provides a measure of the steady component of the radiated light. But more important than providing the capability of measuring steady light emission, the steady dc voltage is used to calculate how much of the fluctuating signal is due to spurious electrical noise generated by the PMT. A photomultiplier tube has the property that when exposed to completely steady radiation, such as emitted by a battery-supplied light bulb, the output voltage contains a random time-fluctuating signal (noise) as well as a steady component. Therefore, when the PMT is subjected to the light from an unsteady flame, the output voltage (and its derivative) contains two unsteady components. The one of interest is proportional to the unsteady light emission, but the other component which must be accounted for, is a spurious electrical fluctuation that would also be present in viewing a steady flame of the same average intensity. Therefore, if the dc voltage is recorded in a flame test, and if the PMT system has been calibrated with a steady, battery-supplied light source, the purely electrical noise corresponding to the steady component of the flame intensity can be determined from the light bulb calibrations, and appropriate corrections can be made. The nature of these corrections is best described by considering the final measurement stage: cross correlation of the microphone and PMT circuit voltages.

CROSS CORRELATION PROCEDURE

Through use of the Saicor correlator, and applying corrections for the spurious electrical noise in the optical system, values were determined for the normalized cross correlation coefficient relating the source function (derivative of fluctuating light intensity which is proportional to the derivative of the heat release rate) and the response function (sound pressure at the microphone). To simplify notation, the microphone system voltage is designated by $p(t)$ rather than $e_p(t)$—the letter p suggesting acoustic pressure. For the derivative of the voltage proportional to the derivative of the light intensity fluctuation the notation employs $\dot{\ell}(t)$. It is understood that $\dot{\ell}(t)$ applies to the particular optical filter-aperature-PMT and source distance for which the specific correlation measurement is being taken.

The quantity desired as a measure of the degree of correlation between light and sound is the normalized cross correlation coefficient, $R_{\dot{\ell},p}(\tau)$, which is a function of the relative time delay between the instant of generation and the subsequent arrival of the resulting acoustic

wave at the microphone location. In particular, the maximum value of $R'_{\ell,p}(\tau)$, corresponding to the acoustic transit time, is required. Normalization is selected such that perfect correlation is indicated by max $R = 1$.

The function defined by the following expression satisfies these conditions:

$$R'_{\ell,p}(\tau) = \frac{\displaystyle\lim_{T \to \infty} \frac{1}{T} \int_0^T \dot{\ell}(t)\, p\,(t+\tau)\, dt}{\left[\displaystyle\lim_{T \to \infty} \frac{1}{T} \int_0^T \dot{\ell}^2(t)\, dt\right]^{1/2} \left[\displaystyle\lim_{T \to \infty} \frac{1}{T} \int_0^T p^2(t)\, dt\right]^{1/2}} \tag{C1}$$

The quantity in the numerator is the unnormalized light-sound correlation, and is generated as a continuous function of the slowly varying delay time, τ, with a finite integration time, T, selected such that a good approximation to the limiting process is secured. The factors in the denominator are recognizable as (by standard definition) the root-mean-square measures of the differentiated light intensity $\dot{\ell}(t)$ and the pressure variation, $p(t)$. They are measured by the true rms voltmeter mentioned previously. (The prime symbol on R designates a normalized quantity.) Therefore Eq.(C1) can be written more compactly as

$$R'_{\ell,p}(\tau) = \frac{1}{\dot{\ell}_{rms}\, p_{rms}} \lim_{T \to \infty} \frac{1}{T} \int_0^T \dot{\ell}(t)\, p\,(t+\tau)\, dt \tag{C2}$$

If, in fact, voltages $\dot{\ell}$ and p were directly available, the measurement procedure description would be complete and the results of performing these measurements could be presented without further discussion. However, because of the presence of significant electrical system noise in the light circuit voltage, $\dot{\ell}(t)$, is actually not available directly at the measurement terminals, as distinct from $p(t)$. Instead, the output of the optical system consists of a superposition of the desired $\dot{\ell}(t)$ and "noise", denoted by $n(t)$. This noise is a well known characteristic of photomultiplier tubes, and is generated along with a dc voltage when the system is exposed to a perfectly steady illumination. Since this electrical noise is a function, determined by calibration, of the mean (dc) light intensity, this relation can be suggested by modifying the electrical noise symbol into the form $n_L(t)$. More significantly since $n_L(t)$ depends only on the steady light intensity, the electrical noise and the voltage proportional to the fluctuating (differentiated) light are completely uncorrelated. This is,

$$R_{n,\dot{\ell}}(\tau) = \lim_{T \to \infty} \frac{1}{T} \int_0^T \dot{\ell}(t)\, n_L\,(t+\tau)\, dt \tag{C3a}$$

$$\equiv 0 \text{ for all } \tau.$$

Obviously, the pressure and electrical noise signals are also uncorrelated, i.e.,

$$R_{n,p} \equiv 0 \tag{C3b}$$

With these relations established, it is easy to determine the result of cross correlating the microphone pressure signal with the voltage that is supplied at the end of the optics system branch. Let this optics branch voltage be denoted by $e(t)$, where $e(t)$ is the (uncorrelated) sum of the voltage proportional to the fluctuating light intensity derivative, $\dot{\ell}(t)$, and electrical noise, $n_L(t)$, i.e.,

$$e(t) = \dot{\ell}(t) + n_L(t) \tag{C4}$$

The pressure-optical system voltage (unnormalized) correlation function that the Saicor will generate is specified by:

$$R_{e,p}(\tau) = \lim \frac{1}{T} \int_o^T e(t)\, p\,(t+\tau)\, dt$$

$$= \lim \frac{1}{T} \int_o^T \left[\dot{\ell}(t) + n_L(t) \right] p\,(t+\tau)\, dt$$

$$= \lim \frac{1}{T} \int_o^T \dot{\ell}(t)\, p\,(t+\tau)\, dt + \lim \frac{1}{T} \int_o^T n_L(t)\, p\,(t+\tau)\, at$$

Which reduces simply to

$$R_{e,p}(\tau) = \lim \frac{1}{T} \int_o^T \dot{\ell}(t)\, p\,(t+\tau) \tag{C5}$$

since the second term, the noise-pressure cross correlation, vanishes because the integrand factors are uncorrelated.

By comparing Eqs. (C5) and (C1) it is evident that identical unnormalized cross correlations result regardless of the strength of the contaminating noise signal, i.e.,

$$R_{e,p}(\tau) = R_{\dot{\ell},p}(\tau)$$

To obtain the normalized function, Eq.(C1), the output of the correlator, Re, p must be divided by the product of the rms levels of $p(t)$ and $\dot{\ell}(t)$, not by the product of p_{rms} and e_{rms}.

It remains only to determine the rms value of the light component of the noise-contaminated signal, $e(t)$.

159

By definition,

$$\dot{\ell}_{rms} = \left[\lim \frac{1}{T} \int_0^T \dot{\ell}^2 \, (t) \, dt \right]^{1/2}$$

Also, by Eq.(C4), and the definition of rms value:

$$e_{rms} = \sqrt{\dot{\ell}_{rms}^2 + n_{Lrms}^2} \qquad (C6)$$

Solving Eq.(C6) for the required rms value of the uncontaminated signal, $\dot{\ell}_{rms}$ gives

$$\dot{\ell}_{rms} = \sqrt{e_{rms}^2 - n_{Lrms}^2} \qquad (C7)$$

Thus the appropriate normalization factor, $\dot{\ell}_{rms}$, that will give unity cross correlation between light and sound under hypothetically perfect correlation is determined from the simple formula Eq.(C7).

In Eq.(C7), e_{rms} is measured by the true rms voltmeter. To find n_{Lrms} the value of the steady component of light, L, is read on the Dana dc digital voltmeter. This value is used to enter the calibration curve of n_{Lrms} versus L which was obtained by calibrating the optical system with a flicker-free light bulb source.

Therefore, the final result can be expressed in terms of measured or operationally defined quantities as follows:

$$R'_{\dot{\ell}, p}(\tau) = \frac{1}{P_{rms}\sqrt{e_{rms}^2 - n_{Lrms}^2}} \lim_{T \to \infty} \frac{1}{T} \int_0^T e(t) \, p(t + \tau) \, dt. \qquad (C8)$$

TEST RESULTS

Tests were conducted with the blowtorch, microphone, and PMT arranged as shown in Figure C2. Microphone distances of 1 and 2 feet were employed, with the PMT located at 40 inches from the flame source, in the tests employing 5176Å, 4319Å, and 3080Å filters. The aperture was run wide open. Two additional types of experiments were conducted. In the first, no optical filter was used, allowing the PMT to respond to the entire visible line and broadband radiation. In these tests it was more convenient to reduce the light intensity to an acceptable range for the PMT by moving the PMT farther away (from 40 inches to 90 inches) from the light source rather than by installing a restricting aperture. The second additional test omitted the microphone but employed two separate optical systems, one incorporating a 3080Å filter and the other using a 5176Å filter.

This test was conducted to obtain preliminary information about the correlation between radiation from the open flame in different optical bands, or regions of differing fuel-air ratio.

Table C1 summarizes the results of the optical-acoustic cross correlation checkout test program, listing the peak normalized cross correlation value, along with the optical filter wavelength and torch to microphone distance.

TABLE C1

SUMMARY OF OPTICAL-ACOUSTIC CHECKOUT
TEST PARAMETERS AND RESULTS

Test	Optical Filter Wavelength Å	Torch to Microphone Distance (feet)	Max. Correlation $R'_{\ell, p}$
1	5176	1	0.31
2	5176	2	0.29
3	4319	1	0.42
4	4319	2	0.34
5	3080	1	0.45
6	None	2	0.53
7	None	4	0.52

The peak cross correlations, occurring at time delays for the acoustic wave transit time, ranged from about 0.3 to 0.5, and are considered indicative of a high degree of causality between light fluctuations (assumed to be perfectly correlated with heat release rate fluctuations) and the resulting acoustic pressure fluctuations. For example, in carefully conducted experiments in an anechoic chamber, using a controlled premixed gaseous hydrocarbon-air turbulent flame, having a flame brush completely visible to the PMT, Plett[C8] indicates a corresponding figure of 0.75. The tests reported in this appendix were made to give an early warning of possible component and systems malfunction. Neither the acoustic or light propagation were "clean". Multiple acoustic reflections could occur to produce at the microphone a signal that was contaminated thereby and was not a true measure of the direct wave from the combustion zone to microphone. Furthermore, the aspirator tube of the flame source, which enclosed a significant portion of the combustion zone could be expected to modify both sound generation and propagation and obviously prevented the PMT from viewing the complete region of light emission. For these reasons the 0.3 to 0.5 range of peak cross correlations obtained here are considered to provide sufficient substantiation that the instrumentation was free of any first order operating problems. As a matter of information, the correlograms from which the tabulated peak values were obtained are presented in Figures C4 through C10.

Correlation of p(t) & İ (t)
5176 Å filter
Light — 12 in — p(t) — 28 in — İ(t)

R = 31.4%
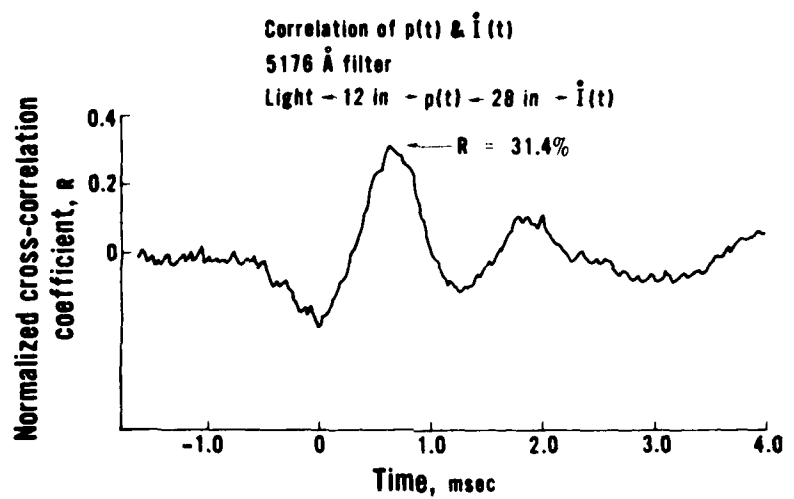
Figure C 4   *Optical-Acoustic Signal Correlogram*

Correlation of p(t) & İ(t)
5176 Å filter
Light — 24 in → p(t) ← 16 in → İ(t)

R = 28.7%
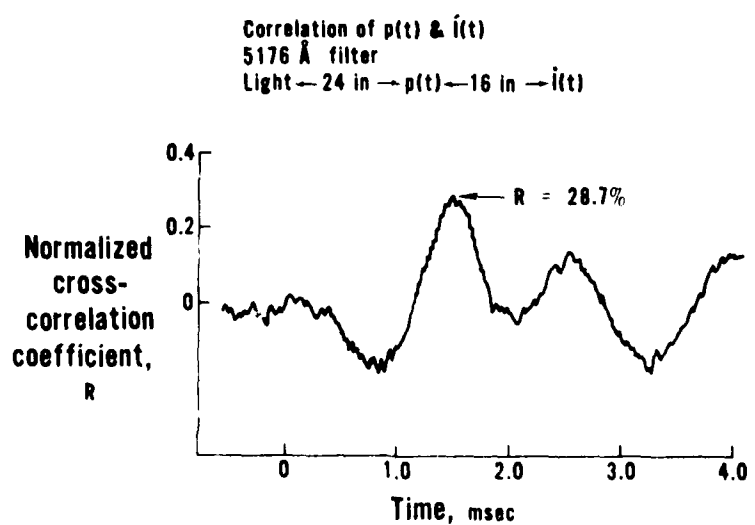
Figure C 5   *Optical-Acoustic Signal Correlogram*

Correlation of p(t) & İ(t)
4319 Å filter
Light—12 in —p(t)—28 in —İ(t)

Normalized
cross-correlation
coefficient,
R

R = 42.4%

-1.0   0   1.0   2.0   3.0   4.0

Time, msec
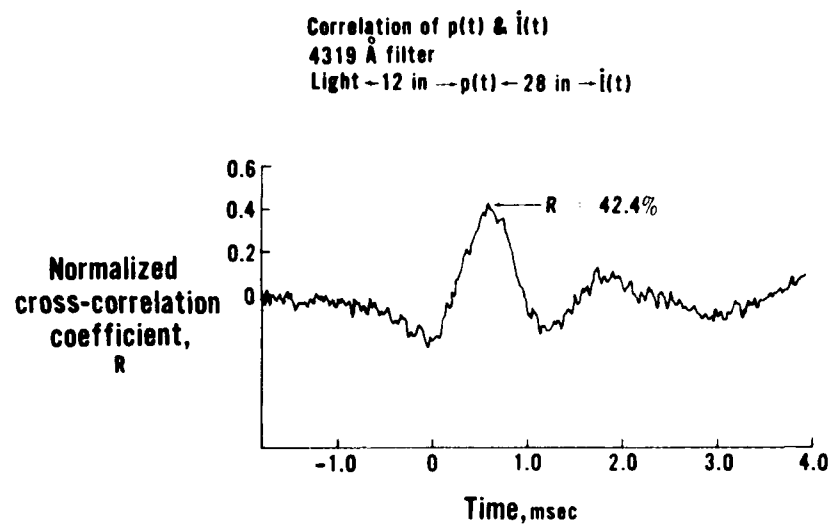
Figure C 6   Optical-Acoustic Signal Correlogram

Correlation of p(t) & İ(t)
4319 Å filter
Light—24 in —p(t)—16 in — İ(t)

Normalized
cross-correlation
coefficient,
R

R = 34.4%

0   1.0   2.0   3.0

Time, msec
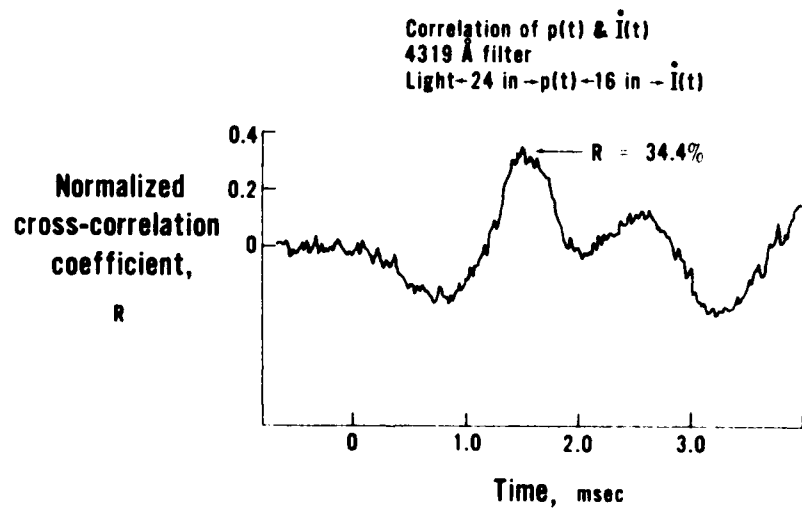
Figure C 7   Optical-Acoustic Signal Correlogram

163

Correlation of p(t) & İ(t)
3080 Å filter
Light–12in–p(t)–18 in –İ(t)

Normalized cross-correlation coefficient, R

R   44.7%

Time, ~ msec
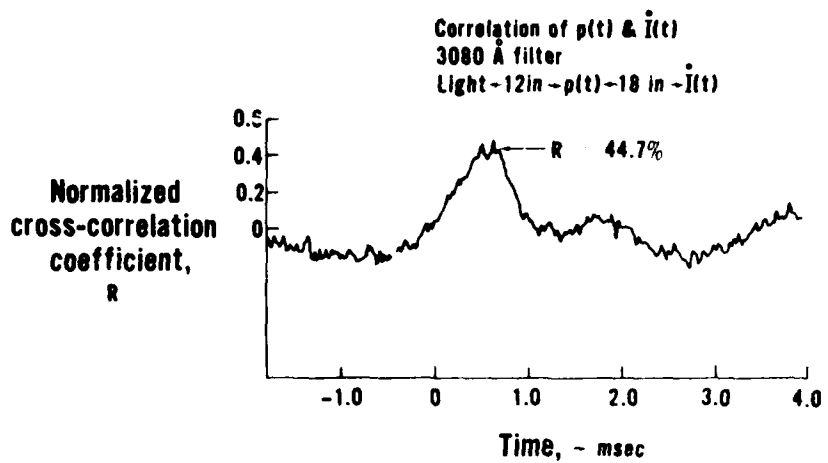
Figure C 8   Optical-Acoustic Signal Correlogram

Correlation of p(t) & İ(t)
No filter
Light–2 ft–p(t)–5.5 ft–İ(t)

Normalized cross-correlation coefficient, R

R = 52.9%

Time, msec
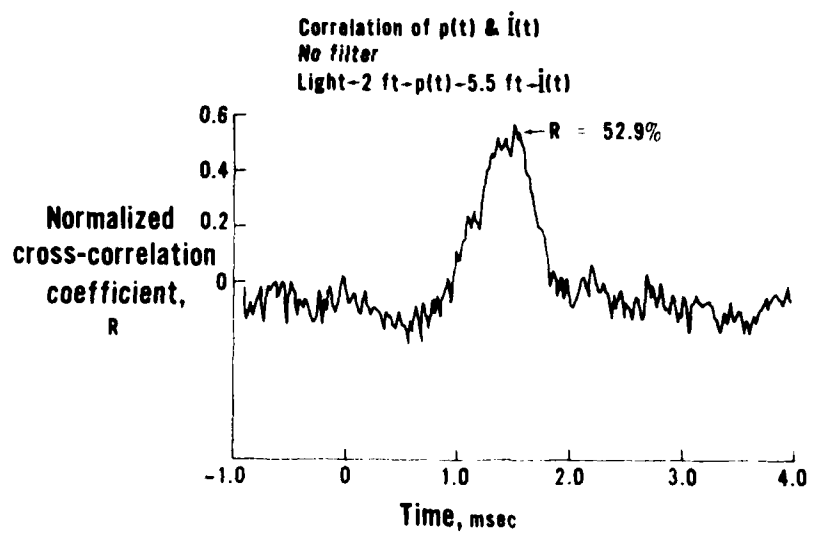
Figure C 9   Optical-Acoustic Signal Correlogram

164

Correlation of p(t) & i(t)
No filter
Light–4 ft–p(t)–3.5 ft – i(t)
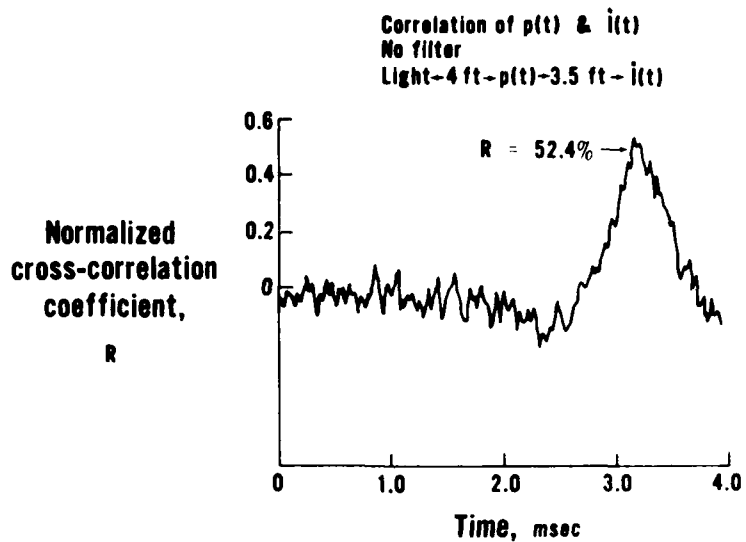
Figure C 10   Optical-Acoustic Signal Correlogram

It should be noted (Table C1) that the highest values of normalized peak correlation were obtained when no optical filter was employed in the light sensing circuit. The correlograms for this case are shown in Figures C9 and C10. Previously reported test results seem to have been restricted to cases in which filters were used. Although it was not possible to explore further for an explanation of this result, it suggests that efforts to apply optical methods to burner rig environments, should include the provision for sensing the total radiated light.

Another interesting result was obtained from the cross correlation of the light fluctuation in two different emission bands. For this test two separate optical systems were used, one incorporating a 3080Å filter, and the other using a 5176Å filter. No microphone was used, the differentiator was bypassed, and the light bulb steady source calibration of each system for electrical noise was also conducted with the differentiator bypassed.

Figure C11 shows the auto correlation functions of each optical circuit and the cross correlogram. A peak normalized cross correlation of 0.83 was achieved. This highly correlated radiation in two bands, each of which is most responsive to different fuel-air ratios suggests that a high degree of synchronons heat release fluctuation exists throughout the flame region.

The high interband radiation correlation, together with the result that the best light-sound correlation was obtained by viewing the entire optical spectrum, suggests that heat and light fluctuations were highly correlated over the flame region and that the best indicator of overall heat release fluctuations is obtained without the use of any optical filter in the light-sensing circuit. Thus, the basic operation of the system was validated, and the tests provided encouragement for extending the technique to evaluate confined burner noise, particularly using unfiltered optical radiation.

165
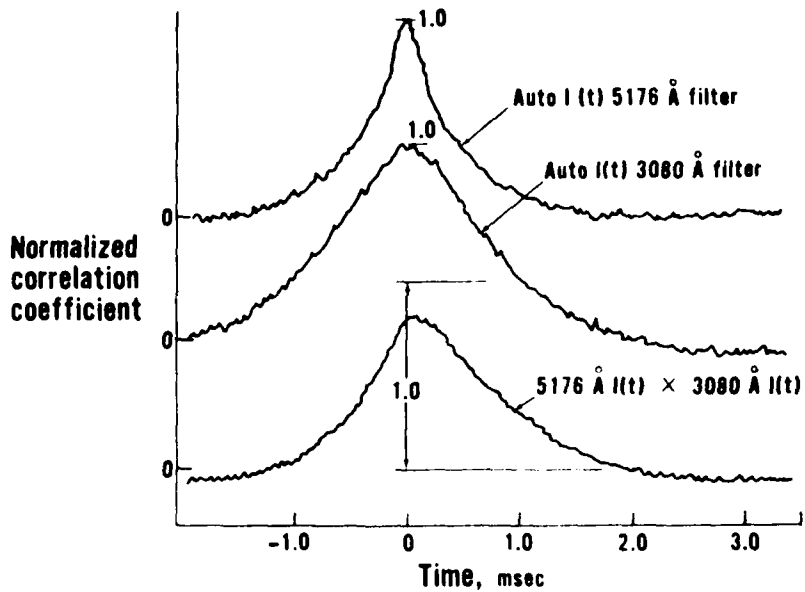
Figure C 11   Correlation of Different Optical Band Signals

EXTENSION TO COMBUSTION NOISE SOURCE MEASUREMENT

Having demonstrated by light-sound cross correlation tests that the optical sensing and signal processing equipment employed in this program can be used to obtain a measure of the source function for open flames, it remains to examine the requirements for employing these methods in the prediction of noise generated by unsteady combustion within the confines of an engine type burner.

There are two classes of problems that must be addressed to determine the feasibility of optical methods for burner noise source determination. One class concerns such matters as durability of sensing elements, ease of installation and calibration, and allied mechanical and operating characteristics. Evaluation of these properties can only be achieved as a result of experience in actual burner rigs. The other class of problems involves selection of equipment, calibration and the design of experiments to validate the basic concept. These matters should be explored on a simple can type burner rig that incorporates a sufficiently long, simple discharge duct in which reliable acoustic pressure measurements can be made at a considerable distance from the burning zone. The purpose of providing this measurement location is to avoid near field measurement problems associated with transducers placed in the combustor itself.

<u>Heat, Light, and Sound from Compact Flames</u> -- To appreciate the essentials of the relationships, it is helpful to re-examine the open flame case, paying special attention to what a farfield microphone hears and what the photomultiplier tube sees. Modifying the notation of Equation (13) of this report, results in an expression for the pressure, p(t), at the microphone location, with the origin of coordinates taken at the microphone. Let the open flame occupy a volume, V, of fluctuating heat release distribution. In this

166

source volume, a typical volume element, dV, is releasing heat at a rate $\dot{Q}\,(\vec{r}_o,\ t-\frac{r_o}{c})\,dV$. This says that $\dot{Q}$ is a function of position in the source volume, and further that the time, t, when the effect is sensed at the microphone corresponds to emission at the source at the earlier time, $t-\frac{r_o}{c}$ (Differences between the speed of sound in the source volume and from the flame to the farfield are ignored.). Recognizing that the source strength is proportional to the time rate of change of $\dot{Q}$, summing over all elements in the flame region, and subsuming known constants by using α to denote proportionality, the farfield pressure at a point can be written:

$$p(t) \propto \int_V \frac{1}{r_o}\ \frac{\partial}{\partial t}\ \dot{Q}\ (\vec{r}_o,\ t - \frac{r_o}{c})\ dV \qquad (C9)$$

This integral states that the acoustic pressure at any instant is the sum of the contributions of a distribution of sources evaluated at times appropriate to their distances from the receiver (and attenuated by the familiar $\frac{1}{r_o}$ spherical divergence factor).

Consider next what the photocell sees when viewing the flame. Compared to the acoustic transit times, the photocell receives light instantaneously. Therefore, light from all regions in the burning zone is received simultaneously and at the instant, t, that the microphone is responding to earlier heat (and light) emission. If the light emission intensity in a certain optical band is denoted by ℓ, it has been found that ℓ is proportional to heat release rate, the factor of proportionality depending on the equivalence ratio, ϕ. Thus, $\ell = k(\phi)\,\dot{Q}\,dV$ and if the fluctuations are not excessively rapid, by differentiating these results: for the light intensity from an element of

$$\frac{\partial \ell}{\partial t} = \dot{\ell} = k(\phi)\frac{\partial}{\partial t}\ \dot{Q}\,dV\,,$$

combustion volume.

Assuming that the combustion equivalence ratio varies locally in the flame, the photo-multiplier tube will see (neglecting constants for aperture and distance attenuation):

$$\ell(t) = \int_V k\ \left[\phi\,(\vec{r}_o)\right]\ \dot{Q}\ (\vec{r}_o,\ t)\ dV \qquad (C10)$$

and the differentiated light signal will be:

$$\dot{\ell}(t) = \int_V k\ \left[\phi\,(\vec{r}_o)\right]\ \frac{\partial}{\partial t}\ \dot{Q}\ (\vec{r}_o,\ t)\ dV \qquad (C11)$$

At this point it is appropriate to examine the limiting terms of these expressions for the microphone pressure and the differentiated light signal when the assumption is made that the source is compact (i.e., small compared to acoustic wavelength), which is the case for direct combustion noise applications. If the microphone is located in the farfield, then all positions of the flame are at about the same distance, and the transit times are common. Denoting this typical distance by r_{avg}, Eq. (C9) for the pressure becomes

$$p(t) \propto \frac{1}{r_{avg}} \int_V \frac{\partial}{\partial t} \dot{Q} (\vec{r}_o, t - t_{avg}) \, dV \tag{C12}$$

where: $t_{avg} = r_{avg}/c$

If the expression, Eq. (C11), for the differentiated light signal is compared with Equations (C9) and (C12), it is seen that Eq. (C12) for the pressure due to a compact source compares more closely with the light expression then does Eq. (C9) in that the time dependence in both expressions does not depend on specific location in the flame. The time dependence of p is exactly like that of ℓ except that a common value of time shift is involved in the integrand.

There is one complication that should be noted for future reference. Whereas the pressure in Eq. (C12) is just the time derivative of the local heat release rate, the light intensity is proportional to this quantity by a factor $k[\phi (\vec{r}_o)]$ which generally depends on specific location in the flame. The effect of this variation is to make $\ell (t)$ a biased estimator of the source function of the pressure. In the case where the source is highly coherent over a large fraction of the flame volume, a single effective (or mean) value of k could be found by obtaining the ratio of the total radiated steady light to the (calculated or otherwise measured) total steady heat release rate from the flame. This same k_{eff} would then apply to determining the coherent time fluctuation of the volume heat release rate by dividing the fluctuating light intensity by k_{eff}. The data from the open flame experiments previously reported support the concept that the light fluctuations are coherent over different regions of the flame, and suggest that the use of an effective value of k may be used, especially if unfiltered light fluctuations are employed.

Under these assumptions of (a) a compact source and (b) coherent burning fluctuations in the flame volume, the value of k_{eff} can be obtained as described below. Under these assumptions, k will be constant and can be transposed as a factor outside of the integral in Equations (C10) and (C11). Equation C10 can then be used to evaluate k_{eff} by using the ratio of measured steady light intensity to total steady heat release rate, which may be calculated from knowledge of the overall fuel-air ratio of the burning process, i.e.,

$$k_{eff} = \frac{\ell \, steady}{\int_V \dot{Q} \, steady \, dV} = \frac{\ell \, steady}{\dot{Q} \, tot \, steady} \tag{C13}$$

Finally, from (C11) and the above constant,

$$\dot{\ell}(t) = \frac{\ell \, steady}{\dot{Q} \, tot \, steady} \int_V \frac{\partial}{\partial t} \dot{Q} (\vec{r}_o, t) \, dV \tag{C14}$$

Notice that if the steady and fluctuating light intensity components are measured at the same distance from the flame, the constant of proportionality implied by the $\propto$ symbol may be replaced with an equality symbol in expression (C14).

Finally, the acoustic pressure in the farfield can be predicted by substituting Eq. (C14) into Eq. (12), i.e.,

$$p(t) = \frac{1}{r_{avg}} \frac{\dot{Q} \text{ total steady}}{\ell \text{ steady}} \dot{\ell}(t - t \text{ avg}) \qquad (C15)$$

EXTENSION TO ACTUAL BURNERS

The preceding discussion of open, compact flames will now be extended to explain the application of optical techniques to enclosed flames in burners. For the peak frequency range of primary interest (400 - 500 Hz) and for typical burner temperatures, the source region can be considered to be compact. For example, at 500 Hz and 2000° R, the wave length of sound is about 4 ft, whereas the combustion region is on the order of .5 ft. Furthermore, based on the results of the open flame studies discussed previously in this appendix, the combustion region will be taken to be a single coherent source. Finally, at the frequencies under consideration (i.e., 500 Hz) only plane waves can propagate from the burning region towards the burner and engine exits.

Consider next a burner through which the burning process is viewed by a PMT. The following discussion describes the way in which the resulting PMT output can be calibrated to estimate the burner generated noise. The calibration procedure requires the burner to be mounted in the upstream end of a long duct in which a microphone can be placed. The derivation of Eq. (C15) will now be extended to include the case of an enclosed flame.

Let the region of the coordinates be located downstream in the duct, where the pressure is to be measured by a microphone to provide the required calibration between light intensity and sound. Since only plane waves of sound will propagate at the frequencies associated with combustion noise, a particularly simple Green's function or influence coefficient results. Let G denote the plane wave pressure resulting from a unit rate of change of heat release rate per unit source volume, $A dx_o$. G has no r-dependence as in the spherical wave field of open flames, but is simply a constant combination of steady-state thermodynamic quantities.

Thus for a heat source element located at x_o, the pressure at the microphone ($x_o = 0$) is simply:

$$p(o, t) = \dot{G} \frac{\partial}{\partial t} Q(x_o, t - \frac{x_o}{c}) A dx_o$$

where A is the duct area and dx_o is a differential element of length. For a source distribution in the duct, the pressure is

$$p(o, t) = \int G \frac{\partial}{\partial t} \dot{Q}(x_o, t - \frac{x_o}{c}) A dx_o$$

$$= G \int \frac{\partial}{\partial t} \dot{Q}(x_o, t - \frac{x_o}{c}) A dx_o \qquad (C16)$$

169

If, as in the open flame case, the source is compact with respect to acoustic wavelength, and also fluctuates with a high degree of coherence over its extent, the above expression may be simplified to the form

$$p(o, t) = G \frac{\partial}{\partial t} \int \dot{Q} (x_{o \, avg}, t - \frac{x_{o \, avg}}{c}) A dx_o$$

$$= G \frac{\partial}{\partial t} \dot{Q}_{tot} (t - \frac{x_{o \, avg}}{c}). \tag{C17}$$

where $\dot{Q}_{tot}$ is the total fluctuating heat release rate of the combustion process, considered to be emitted at an effective location $x_{o \, avg}$.

Now, the method of evaluating $\frac{\partial \dot{Q}}{\partial t}$ total by optical sensing is exactly the same as was described for the open flame case. With an optical sensor viewing the flame region, an effective light-heat proportionality constant is evaluated from the steady quantities. From equation (C13), this constant is:

$$k_{eff} = \frac{\ell \, steady}{\dot{Q} \, tot \, steady} \tag{C13}$$

$$\text{Then} \quad \frac{\partial}{\partial t} \dot{Q} \, tot = \frac{1}{k_{eff}} \dot{\ell} = \frac{\dot{Q} \, tot \, steady}{\ell \, steady} \dot{\ell}$$

Finally, the fluctuating pressure can be expressed in terms of the fluctuating light intensity derivative:

$$p(o, t) = G \frac{\partial}{\partial t} \dot{Q} \, tot (t - \frac{x_{o \, avg}}{c})$$

$$= G \frac{\dot{Q} \, tot \, steady}{\ell \, steady} \dot{\ell} (t - \frac{x_{o \, avg}}{c}) \tag{C18}$$

Using the measured value of pressure, the value of G can be computed, and the relationship between pressure and light intensity is obtained.

In the above discussion, a method has been proposed for developing and verifying the use of light sensors to predict combustion noise. If the correlation tests indicate success, then internal microphones can be eliminated and the procedure can be used in normal burner development rigs.

170

CONCLUSIONS

1. Checkout tests using a blowtorch for a source of sound and light fluctuations served to validate the satisfactory operation of the instrumentation selected for optical studies of combustion noise.

2. Significant levels of cross correlation between sound and fluctuating light intensity in 3 optical bands were observed, indicating that the basic concept of using light fluctuation as a measure of acoustic source strength is valid.

3. Very high correlation between light fluctuations in different optical radiation bands and the achievement of maximum light-sound cross correlation using wideband (unfiltered) radiation implies that areas within the burning region are highly correlated with each other.

4. A procedure for estimating radiated noise using measured light fluctuations from the combustion source was defined for open flames.

5. A method was defined for extending this procedure to include enclosed flames in burners.

REFERENCES

C1.   Morse, P. M., and Ingard, K. U., "Theoretical Acoustics", McGraw-Hill, 1968, Chapter 7.1, pp 322-325.

C2.   Shafer, H. J., Plett, E. G., and Summerfield, M., "Optical Evaluation of Combustion Noise Source Terms", AIAA Paper No. 76-38, 1976.

C3.   Chiu, H. H., and Summerfield, M., "Theory of Combustion Noise", Acta Astronautica, V1, 1974, pp 967-984.

C4.   Sofrin, T. G., and Riloff, N., Jr., "Experimental Clean Combustor Noise Study", NASA CR 135106, Oct. 1976.

C5.   Price, R. B., Hurle, I. R., and Sugden, T. M., "Optical Studies of the Generation of Noise in Turbulent Flames", 12th Symposium on Combustion, The Combustion Institute, Pittsburgh, 1968.

C6.   Hurle, I. R., Price, R. B., and Sugden, T. M., "Sound Emission From Open Turbulent Premixed Flames", Proc. Roy. Soc., A303, pp 409-427, 1968.

C7.   Shivashankara, B. M., Strahle, W. C., and Handley, J. C., "An Evaluation of Combustion Noise Scaling Laws by an Optical Technique, AIAA Paper No. 74-7, 1974.

C8.   Plett, E. G., Shafer, H. J., and Summerfield, M., "Combustion Noise Source Evaluation" Proceedings, Third Interagency Symposium on University Research in Transportation Noise. University of Utah, Nov. 12-14, 1975.

C9.   Mathews, D. C., and Rekos, N. F., Jr., "Direct Combustion Noise in Turbopropulsion Systems", AIAA Paper No. 76-579, 1976.

C10.   Mador, R. J., and Roberts, R. J., "A Pollutant Emissions Prediction Model for Gas Turbine Combustors", AIAA Paper No. 74-1113.

APPENDIX D

DETAILS OF THE INDIRECT COMBUSTION NOISE HOT—SPOT TEST PROGRAM

As mentioned in Section 3.2, the current contract effort was redirected when it became apparent that direct combustion noise, instead of indirect combustion noise, is the dominant source of core engine noise in turbofan engines. As a result, additional work was conducted in the area of direct combustion noise, and the rig test program to simulate and verify indirect combustion noise was not conducted. This appendix contains a description of the rig, instrumentation, test plan and data reduction and analysis techniques which were to be used in the experimental investigation of indirect combustion noise at P&WA's X-206 test stand.

INDIRECT COMBUSTION NOISE RIG (HOT-SPOT GENERATOR)

After examining several possible methods of generating hot-spot pulses within a mean flow to simulate indirect combustion noise, the design shown in Figures D1 and D2 was selected. This design utilizes two parallel branches of pipe and a three-way ball valve (#1) to switch the flow from one branch to the other. While the cold flow is passing through one branch, the other branch is charged with a slug of hot gas as shown in Figure D1. After the hot gas has been injected into the parallel branch, the three-way valve (#1) is actuated and the flow is switched to the branch containing the hot-spot as shown in Figure D2. This flow then carries the hot-spot to the primary test pipe and to the nozzle where the subject noise is generated. A separate system of valves (#3 and #4), also shown in Figures D1 and D2, is used to inject the hot spot into the rig while the main flow is directed through the other parallel path. During the hot gas injection cycle, shown in Figure D1, valve #2 remains closed to assure a distinct hot region. Before the hot-spot is propelled down the duct, valves #3 and #4 are switched closed to isolate the hot slug, and valve #2 is then opened. The flow is then transferred by valve #1 to the branch containing the hot-spot. Figure #2 illustrates the hot spot moving downstream to the nozzle.
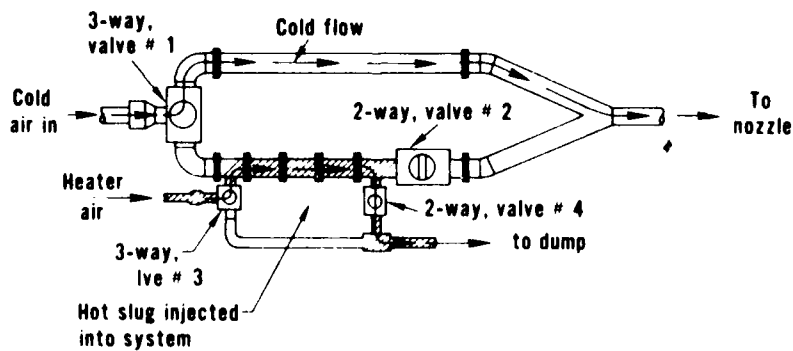

Figure D 1   Hot-Spot Generator Schematic, Hot-Spot Charging Period, Long Hot-Spot Configuration
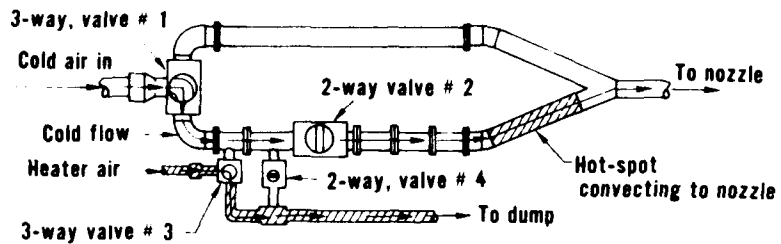
Figure D 2   Hot-Spot Generator Schematic, Hot-Spot Delivery Period, Short Hot-Spot Configuration

The length of the spot may be varied by installing spacer sections in the lower branch. Hot-spots of 5, 10, 15 and 20 inches in length are possible. The velocity of the flow may be regulated by setting the upstream pressure. The temperature of the hot-spot may be regulated by a flow heater. Two nozzles were to be tested with exit diameters of 0.75 and 0.53 inches. The valve operating sequence is controlled by a specially designed timing circuit box shown in Figure D3. This device allows the timing between each valve sequence to be controlled so that smooth operation of the hot-spot generator is assured. Sensors located on the valves, and connected to a visicorder, supply a record of the operation sequence.
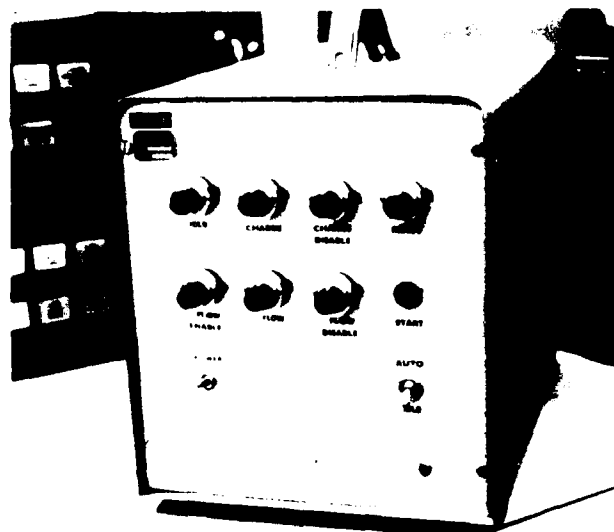
Figure D 3   Electronic Valve-Controller Box for Hot-Spot Generator

With the correct valve operating sequence, this hot-spot generator should provide a flow to the nozzle that contains fluctuations only in the flow temperature. Velocity fluctuations associated with the generation of the hot-spot should not be significant and any noise associated with the valve actuations will precede the subject noise pulse by long times relative to the desired pulse duration. Calculations show that the nozzle size and the hot-spot parameters can be selected to suppress jet noise below the level of predicted indirect combustion noise. Further suppression of the jet noise floor relative to the indirect combustion noise will be achieved by the cyclic injection of hot spots, at the prescribed frequency of about one-per-second, and then signal enhancing the resulting farfield and internal pressure time histories by using periodic sampling, keyed to the injection frequency. This will enhance the deterministic indirect combustion noise pressure history while averaging the random jet noise pressure time history toward zero.

STAND DESCRIPTION

The hot spot generator was installed in P&WA's X-206 stand as shown in Figure D4. X-206 stand consists of an anechoic chamber designed and built for the measurement of noise generated by model jet nozzles. Eleven 0.25 inch B&K farfield microphones are located on a 16 foot radius at 10 degree increments over an arc of 60 through 160 degrees. A schematic of the air supply system to X-206 stand is shown in Figure D5.
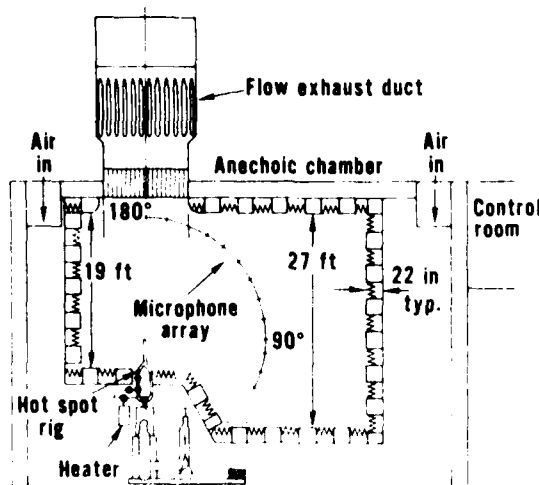

Figure D 4   Installation of Hot Spot Generator In X-206 Stand

175
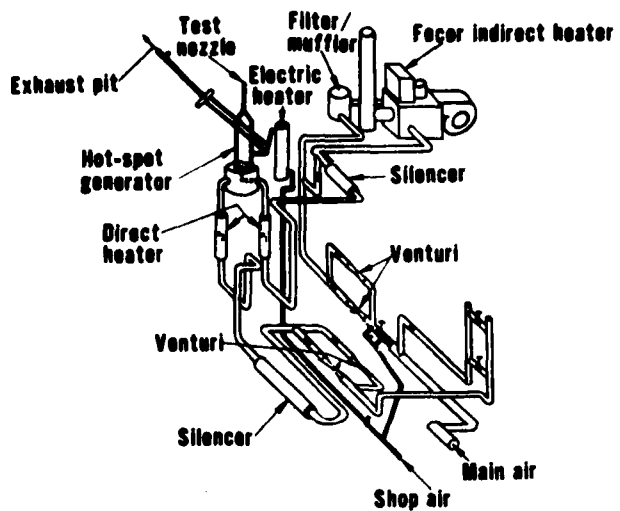
Figure D 5   X-206 Stand Air Supply (Hot-Spot Generator Configuration)

INSTRUMENTATION

The following instrumentation will be used to control and measure indirect combustion noise in the hot-spot rig at X-206 stand.

1.   5-kulite flush mounted pressure transducers

2.   3-quick response thermocouples

3.   1-hot-wire sensor

4.   9-farfield microphones

5.   1 pitot-static probe

6.   oscilliscope camera equipment

7.   required pressure and heat control for rig operation

The placement of the instrumentation within the rig is schematically shown in Figure D6. The motivation for this instrumentation is as follows.

The symmetry of the generated signal will be checked by placing two kulite transducers opposite each other at the same axial location 4.5 inches upstream of the nozzle. The remaining Kulites will be spaced axially at distances of 9, 18 and 27 inches from the nozzle to measure the upstream sound wave generated by the hot-spot as it passes through the nozzle.
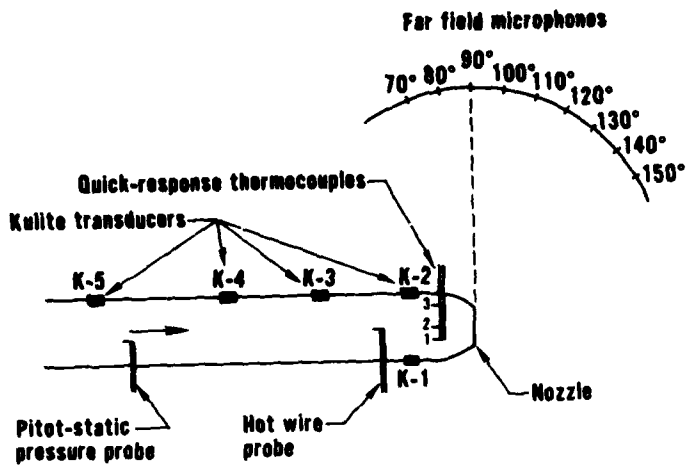
Figure D 6   *Instrumentation Schematic for Indirect Combustion Noise Test*

Just upstream of the nozzle a probe will be mounted which contains three thermocouples. The thermocouples will measure the character of the hot-spot just before it passes through the pressure drop of the nozzle in order to determine both the length and amplitude of the temperature pulse so that the noise mechanism can be properly evaluated and compared to existing theoretical models.

As previously discussed, velocity fluctuations are unwanted in the system. A hot-wire sensor will therefore be placed near the centerline of the duct to measure the amplitude of any velocity fluctuations which accompany the hot spot. Farfield acoustic data will be collected with nine of the existing arc of B&K 0.25 inch condensor microphones at X-206 stand. Signals measured with this array will require signal enhancement to distinguish the indirect combustion noise from the jet noise. A photograph of the hot spot generator installed in X-206 stand is shown in Figure D7. The nozzle and several sensors are clearly visible in this figure.
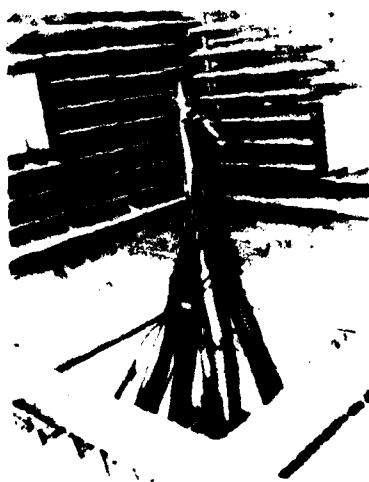

Figure D 7   *Hot-Spot Generator Mounted In X-206 Stand*

177

ON STAND DATA REDUCTION EQUIPMENT

In addition to instrumentation installed directly in the rig, other apparatus is required for on-line monitoring of the experiment. A set-up to photograph oscilloscope traces of the time histories from the various signals is required. The oscilloscope will be set to trigger on the opening of valve #1. The oscilliscope will also have an adjustable delay time incorporated into the system so that particular blocks of time may be examined after the movement of valve #1.

As previously discussed, it is quite possible that indirect combustion noise from the hot-spot may be contaminated by jet noise from the rig. A correlator for signal enhancement will therefore be utilized to separate the repeated portion of the signal (indirect combustion noise) from the random jet noise.

TEST PROGRAM DEFINITION

The testing of the rig will be performed in four phases, which include rig checkout and detailed data acquisition phases. The details of this test plan is contained in the following discussion.

Test Plan, Phase 1

Objective — The Phase 1 objective is to test the rig for valve noise caused by the valve opening and closing and the flow switching processes. It is also necessary to determine the "ambient" noise generated by the rig when no heat is added and no pressure drop exists at the nozzle location. The test matrix for this phase is shown in Figure D8.

Figure D 8   Test Program Matrix, Phases 1, 2, and 3

178

Configuration – The rig will operate with no nozzle and no heat addition. A straight duct termination will be utilized to determine the noise inherent to the rig.

Test Plan, Phase 2

Objective – The objective of this phase is to test the rig for undesirable effects of velocity fluctuations. Despite efforts to achieve a clean flow, velocity perturbations may occur during the hot spot injection and flow switching process. As these velocity perturbations pass through the nozzle, some noise may be generated. This phase of experimentation (See Figure D8) will measure this noise signal if it exists.

Configuration – Operation in this phase will be similar to Phase 1 but a nozzle will be used to produce a pressure drop at the end of the rig. The hot-spot heater will not be in operation.

Test Plan, Phase 3

Objective – The objective of this phase is to determine the character of the hot spots and to measure any extraneous noise caused by the hot-spot travelling through the valves and pipes. This noise must be distinguished from the noise generated in the controlled pressure drop of the nozzle. The test matrix for this checkout phase is shown in Figure D8.

Configuration – At this point, the hot-spot heater will be utilized for the first time; both with no nozzle, and then with the smallest exit area nozzle. First, the 10 inch hot-spot will pass through the piping without experiencing a static pressure drop at the end of the pipe. The small nozzle will then be used in conjunction with a reasonably small pressure ratio to slowly move the hot-spots through the pipe so they may be examined closely with the thermocouple probes.

Test Plan, Phase 4

Objective – The objective of this final phase of experimentation is to collect data which will evaluate the existing models of indirect combustion noise. Each of the relevent parameters will be varied independently, as shown in Figure D9.

Configuration – The rig will be operated utilizing two nozzles, three hot-spot lengths, three hot-spot temperatures, and three nozzle pressure ratios.

179

	1.2			1.4			1.6			
ΔT = 85°	X			X			X			0.003 ft²
							X			0.0015
ΔT = 170°	X			X			*X			0.003
										0.0015
ΔT = 340°	X	X	X	X	*X	X	X	*X	X	0.003
	X			X			*X			0.0015
	5	10	20	5	10	20	5	10	20	

Hot spot temp ~ deg above free str temp   Nozzle area ~ ft²

Hot spot length, lx ~ inches   *Denotes priority points

Figure D 9   *Test Program Matrix, Phase 4*

DATA REDUCTION

On-Stand Data Reduction — Phases 1, 2 and 3 are checkout phases, whereas Phase 4 is basic-ally aimed at gathering sufficient information for characterizing and verifying the prediction of indirect combustion noise. These goals will be most efficiently realized if Phases 1, 2 and 3 are conducted separately from Phase 4 with enough time between to analyze the be-havior of the rig and decide upon the best manner to proceed. Thus the analysis of the first three phases will be done on the stand, whereas the reduction of data from Phase 4 will be performed after the test program.

Post-Test Data Reduction — After the completion of the experimental work, the Phase 4 data will be reduced and analyzed. Signal enhanced time traces of selected farfield and in-ternal noise signals will be obtained. The resulting hot-spot noise characteristics will be analyzed as functions of nozzle pressure drop, hot-spot temperature and hot-spot length. The results will then be compared to predictions, and the accuracy of the predictions will be assessed.

ACKNOWLEDGMENTS

NOMENCLATURE

A	cross-sectional area, in^2
c	velocity of sound
C_1	constant defined in Eq. (3)
c_p	specific heat at constant pressure $(.28\ \frac{BTU}{lbm\,^\circ R}$ in typical reaction region)
D	outer diameter of turbine at combustor/turbine interface, ft
F	ratio of characteristic impedances across turbine, Eq. (46)
F_b	burner fuel-air ratio
F_{ST}	stoichiometric fuel-air ratio $\simeq .068$ for jet fuel and air
f_c	combustion noise peak frequency, Hz
H_f	fuel heating value $\simeq 18,500\ \frac{BTU}{lbm}$ for jet fuel
K_1, K_2, K_3	constants defined in Eqs. (10), (27), and (28), respectively
K_f	constant in peak frequency model, Eq. (11)
L	length defined in Figure 4.6-1, ft
L_b	burner length, ft
L_r	length of reaction region in burner, ft
L_r, L_θ, L_x	hot-spot correlation length scales
m	circumferential lobe number for spinning modes
N_f	number of fuel nozzles in burner
P	acoustic power
P_o'	acoustic pressure amplitude at burner exit
p	mean pressure, psia
$\dot{Q}$	volumetric heat release rate, $BTU/sec\text{-}ft^3$

R	gas constant $\simeq 53.35 \dfrac{\text{ft lbf}}{\text{lbm}^\circ\text{R}}$ for air
R_w	defined in Eq. (20) and Reference (3)
r	distance from source to observer, ft
T	temperature, $^\circ$R
T.L.	combustion noise transmission loss, dB
U_r	mean velocity through reaction region, ft/sec
V	volume
w_{a_b}	burner airflow, lbm/sec
w_{a_r}	airflow through reaction region, lbm/sec
w_f	fuel flow rate, lb/sec
γ	ratio of specific heats
ρ	density
τ_r	typical reaction time, Eq. (4), sec

Subscripts

4	burner entrance location
5	burner exit, turbine inlet location
7	turbine exit location
∞	denotes ambient conditions
b	denotes burner
corr	denotes correlated volume, area etc.
d	duct
ref	burner reference (or design) condition
ST	denotes stoichiometric condition
t	denotes stagnation value of pressure or temperature

REFERENCES

1. D. C. Mathews and A. A. Peracchio, "Progress in Core Engine and Turbine Noise Technology," AIAA Paper 74-948, August 1974.

2. S. B. Kazin, et. al., "Core Engine Noise Control Program," DOT/FAA Report No. FAA RD-74-125, Vols. I, II, and III, August 1974.

3. W. C. Strahle and B. N. Shivashankara, "Combustion Generated Noise in Gas Turbine Combustors," ASME Paper No. 75-GT-27, March 1975.

4. R. P. Gerend, H. P. Kumasaka, and J. P. Roundhill, "Core Engine Noise," AIAA Paper No. 73-1027, October 1973.

5. E. Grande, "Core Engine Noise," AIAA Paper No. 73-1026, October 1973.

6. E. G. Plett, H. H. Chiu, and M. Summerfield, "Research on Noise Generated by Ducted Air-Fuel Combustion Systems," Third Annual Report to the Office of Naval Research, ONR Contract N00014-67-A-0151-0029, June 1974.

7. E. A. Burdsall, F. P. Brochu, et. al., "Results of Acoustic Testing of the JT8D-109 Refan Engines, " NASA CR-134875, November 1975.

8. G. F. Pickett, "Core Engine Noise Due to Temperature Fluctuations Convecting Through Turbine Blade Rows, " AIAA Paper No. 75-528, March 1975.

9. N. A. Cumpsty, "Excess Noise from Gas Turbine Exhausts," ASME Paper No. 75-GT-61, March 1975.

10. W. C. Strahle, "The Convergence of Theory and Experiment in Direct Combustion Generated Noise," AIAA Paper No. 75-522, March 1975.

11. R. E. Motsinger and J. J. Emmerling, "Review of Theory and Methods for Combustion Noise Prediction," AIAA Paper No. 75-541, March 1975.

12. R. G. Huff, B. J. Clark, and R. G. Corsch, "Interim Prediction Method for Low Frequency Core Engine Noise," NASA TMX-71627, November 1974.

13. D. C. Mathews and N. F. Rekos, Jr., "Direct Combustion Generated Noise in Turbo-propulsion Systems-Prediction and Measurement," AIAA Paper No. 76-579, July 1976.

14. H. H. Chui and M. Summerfield, "Theory of Combustion Noise," Acta Astronautica, Vol. 1, pp. 967-984, 1974.

15. H. J. Shafer, E. G. Plett, and M. Summerfield, "Optical Evaluation of Combustion Noise Source Terms," AIAA Paper No. 76-38, January 1976.

REFERENCES (Cont'd)

16. P. M. Morse and K. U. Ingard, Theoretical Acoustics, McGraw-Hill Book Company, 1968.

17. B. M. Shivashankara, W. C. Strahle, and J. C. Handley, "An Evaluation of Combustion Noise Scaling Laws by an Optical Technique," AIAA Paper No. 74-7, AIAA 12th Aerospace Sciences Meeting, 1974.

18. R. R. Dils, "Dynamic Gas Temperature Measurements in a Gas Turbine Transition Duct Exit," ASME Paper 73-GT-7, 1973.

19. N. A. Cumpsty and F. E. Marble, "The Generation of Noise by the Fluctuations in Gas Temperature into a Turbine," University of Cambridge Report CUED/A TURBO/TR 57, 1974.

20. J. E. Ffowcs-Williams and M. S. Howe, "The Generation of Sound by Density Inhomogeneities in Low Mach Number Nozzle Flows," J. Fluid Mechanics, Vol. 70, Part 3, pp. 605-622, 1975.

21. T.G. Sofrin and N. Riloff, Jr., "Experimental Clean Combustor Program Noise Study," NASA CR-135106, October, 1976.

22. M. P. McMahon, "Static Noise Measurement of Full Scale Jet Engines," presented at 11th National Conference on Environmental Effects on Aircraft and Propulsion Systems, Trenton, N. J., May 1974.

23. L. E. Kinsler and A. R. Frey, Fundamentals of Acoustics, Second Edition, Wiley and Sons, Inc., New York, N. Y., 1962.